SPECTROELECTROCHEMICAL STUDIES OF BIPYRIDYLS AND RELATED SPECIES

by Jae-Inh Song

This thesis is submitted in part fulfillment
for the degree of Ph.D

Chemistry Department
University of Glasgow
Glasgow G12 8QQ

August 1989

For my parents

ACKNOWLEDGEMENTS

It is with great pleasure that I take this opportunity of thanking Dr. R.D. Peacock for his help and guidance throughout this work. I am also deeply indebted to Professor P.S. Braterman of University of North Texas, my supervisor from 1986 to 1988, for his constant enthusiasm, encouragement and assistance.

Thanks are due to Professor W. Kaim of Stuttgart Universität, Drs. F.L. Wimmer and S. Wimmer of CNRS at Toulouse, France, and Dr. G.B. Young of Imperial College of Science and Technology, London, for kind donation of their compounds: Mo-, Re-, Cu-bpym complexes from Professor Kaim; $[Pt(Me_2\text{-}bpy)_2]^{2+}$ and $[Pt(bpy)(Me_2N\text{-}py)_2]^{2+}$ from Drs. Wimmer and Wimmer; binuclear Pt(II) complexes from Dr. Young.

I am grateful to my parents without whose unfailing support this thesis would never have been completed.

Finally, I gratefully acknowledge the O.R.S. for financial support.

Jae-Inh Song

ABBREVIATIONS

adme	2-adamantylmethyl
BADPH	bromoaldehyde 2,4-nitrophenylhydrazone
bpy	2,2'-bipyridine
Me_2-bpy	4,4'-dimethyl-2,2'-bipyridine
bpyMe-H	1-methyl-2,2'-bipyridinium
bpym	2,2'-bipyrimidine
Ph	phenyl
phen	1,10-phenanthroline
dmp	2,9-dimethyl-1,10-phenanthroline
pn	1,2-diaminopropane
Me_2N-py	4-dimethylamino-pyridine
py	pyridine
terpy	2,2';6',2''-terpyridine
p-tol	toluene
DMF	N,N'-dimethylformamide
DMSO	dimethylsulphoxide
$TBABF_4$	tetrabutylammonium tetrafluoroborate
ε	extinction coeffient(dm^3 mol^{-1} cm^{-1})
$\bar{\upsilon}$	wavenumber(cm^{-1})
λ	wavelength(nm)
α(N)	Coulomb integral term at nitrogen
β	resonance integral

TABLE OF CONTENTS

SUMMARY

This thesis is devoted to the characterisation of redox-active ligand and metal-coordination complexes which contain the M-L chromophore, where M = metal and L = polypyridyls and their derivatives. The materials studied include simple and quaternised bipyridyls, and their complexes with Fe(II), Ru(II), and Pt(II), and bipyrimidine and its complexes.

The redox changes were generally achieved by controlled potential electrolysis using an optically transparent thin layer electrode (O.T.T.L.E.) cell and the required potentials can conveniently be determined by cyclic voltammetry. The O.T.T.L.E cell was placed in the spectrophotometer beam, and parent materials were electrolytically regenerated, so that the absorption spectra of the unstable low-oxidation state complexes could be unambiguously recorded.

The radicals formed by one-electron reduction of most of the free ligands show similar spectra, assignable in terms of a simple Hückel molecular orbital scheme, with strong bands for the $\pi \rightarrow \pi^*$ and $\pi^* \rightarrow \pi^*$ transitions. As required by theory, the positions of these bands are remarkably insensitive to the Coulomb energy at nitrogen. As expected, quaternisation and the incorporation of added nitrogens in the ring both lead to easier reduction. Thus N-methylation lowers the energy of the LUMO but does not alter its nature.

In all of the metal complexes examined, except the $[PtLL']^{2+}$ series, the reductions are based on the ligands and the oxidations are metal-based. The electronic absorption spectra of the reduced species show typical reduced ligand radical anion character. Furthermore, in the singly and doubly reduced $[M(L)_3]^{2+}$, it was found that the added electrons are localised on the individual bidentate ligands.

Spectrochemical and electrochemical data agree in showing that the first reduction of the $[PtLL']^{2+}$ species is metal-based, producing Pt(I) complexes. In this case, the MLCT transition from Pt(I) to ligand is available and this MLCT band should lie lower in energy than the corresponding transition from Pt(II). However, the first reduction of organometallic Pt(II) bipyridyl complexes is ligand-based.

Chapter 1 Introduction

Spectroelectrochemistry

Spectroelectrochemistry is the technique of generating species electrochemically inside the cell compartment of a spectrometer by controlled potential electrolysis and is the method of choice for highly reactive species such as radical ions, provided these can be specifically produced at the electrode and live long enough to be studied. The required potentials can conveniently be determined by cyclic voltammetry. The specific contribution of voltammetry provides intermolecular comparisons of the ionisation potentials and electron affinities, *viz*, the highest occupied molecular orbital (HOMO) and lowest unoccupied molecular orbital (LUMO) energies. In contrast, spectroelectrochemistry provides information on the relative intramolecular energy levels due to metal-to-ligand charge-transfer (MLCT) and ligand $\pi \rightarrow \pi^*$ and $\pi^* \rightarrow \pi^*$ transitions. In the case of metal coordination complexes, the highest occupied molecular orbital and lowest unoccupied molecular orbital are generally termed the 'frontier orbitals' and these frontier orbitals are directly involved in electronic transitions which should occur at discrete excitation energies. Together, the methods of spectroelectrochemistry and cyclic voltammetry can give information about the energies and the nature of frontier and near frontier orbitals. When applied to a series of related species, the results can be compared with theoretical expectations to build up a set of detailed assignments.

Spectroelectrochemistry was performed using a specially designed optically transparent thin-layer electrode (O.T.T.L.E.) cell mounted in a spectrophotometer beam. The general strategy of spectroelectrochemistry is described as follows;

1. Measurement of oxidation and reduction potentials of the parent compounds by cyclic voltammetry and checking for stability and reversibility of electrode products. If the cyclic voltammogram of a parent compound exhibits a reversible oxidation or reduction process, we can continue the rest of the experiments.

2. Running the spectrum of the starting material.

3. Controlled potential electrolysis inside the spectroscopic cell; collecting the spectra of any electrochemical products over time until a final spectrum is obtained.

4. Regeneration of the starting material; an essential precaution against unforeseen processes.

5. Assignments and interpretation in context.

Polypyridyl ligands

2,2'-Bipyridine **(1)** and 1,10-phenanthroline **(2)** are commonly employed as effective bidentate ligands which coordinate a large variety of metals. Both have a rich chemistry in which there is a growing interest. 2,2'-Bipyrimidine **(3)**

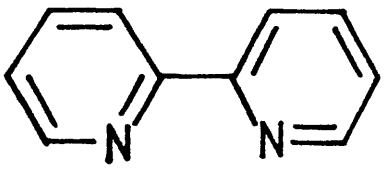

1. 2,2'-bipyridine

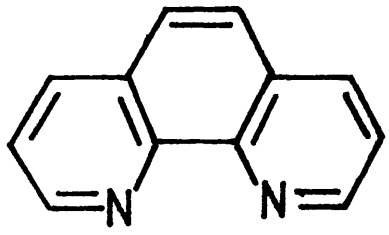

2. 1,10-phenanthroline

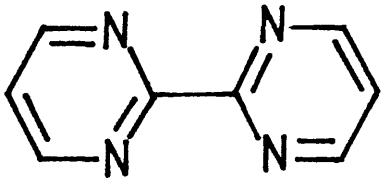

3. 2,2'-bipyrimidine

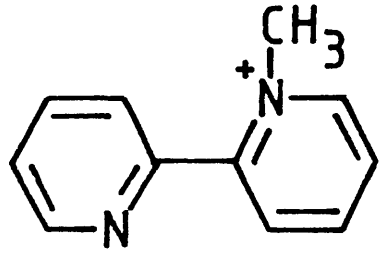

4. 1-methyl-2,2'-bipyridinium

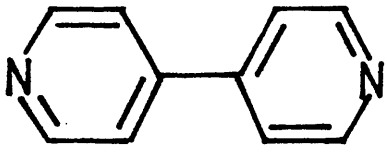

5. 4,4'-bipyridine

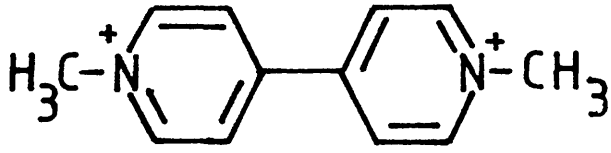

6. 1,1'-dimethyl-4,4'-bipyridinium (paraquat)

Figure 1,1. Schematic representations of aza-aromatic compounds.

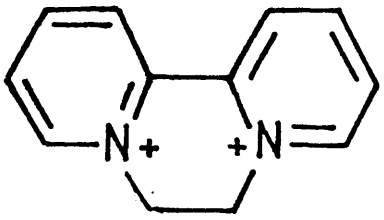

7. 6,7-dihydrodipyrido(1,2-a;2,1-c)-pyrazinedium (diquat)

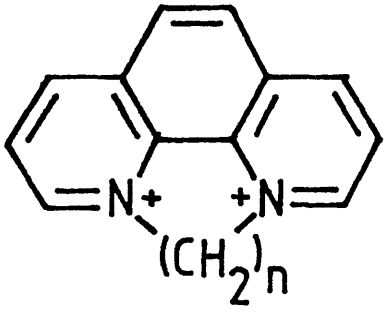

8.

a. n=2 5,6-dihydropyrazino(1,2,3,4-l,m,n)-1,10-phenanthrolinium

b. n=3 5H-6,7-dihydro-1,4-diazepino-(1,2,3,4-l,m,n)-1,10-phenanthrolinium

c. n=4 4H,5H-6,7-dihydro-1,4-diazino-(1,2,3,4-l,m,n)-1,10-phenanthrolinium

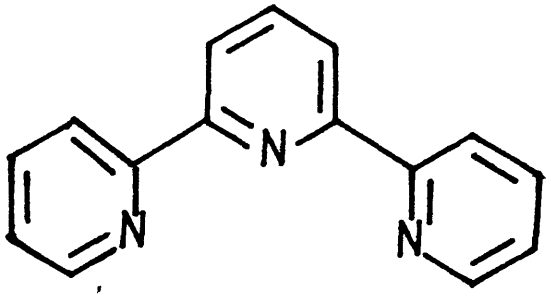

9. 2,2';6',2''-terpyridine

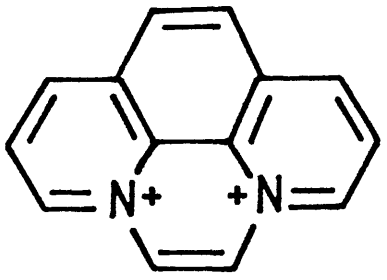

10. Pyrazino(1,2,3,4-l,m,n)-1,10-phenanthrolinium

Figure 1,1 continued

combines the chelating properties of the ligands such as 2,2'-bipyridine with the bridging function of ligands such as 1,4-diazine (pyrazine). These ligands function as typical bidentate chelate molecules. Bonding through the nitrogen atoms results in the formation of five membered rings. The first influential review of the coordination chemistry of the 2,2'-bipyridine (bpy) chelating ligand was published in 1954 by Brandt, Dwyer and Gyarfas[1]. Stable bpy complexes are formed with a wide variety of metals. In most cases a pseudo-octahedral or pseudo-square planar geometry is found.

The reaction between iron(II) salts and 2,2'-bipyridine with the formation of intensely red substances was first observed by Blau[2], who isolated a series of salts of the formula $[Fe(bpy)_3]X_2$ (where X= Cl, Br, etc.) and demonstrated that the colour resided in the common cation. The analogously constituted 1,10-phenanthroline[3] and 2,2'-bipyrimidine[4], were shown to form similarly coloured salts of the same type. The formation and reactions of $[Fe(L_3)]X_2$ (L = 2,2'-bipyridine, 1,10-phenanthroline, and 2,2'-bipyrimidine; X=Cl, Br, etc.) compounds were inexplicable by the then current Brömstrand-Jørgensen structure theory but were explained simply and naturally by Werner's octahedral model[5] for coordination compounds. Werner's model was initially received with widespread scepticism despite the vast array of chemical and spectroscopic evidence by which it was supported.

The resolution of these Fe(II) complexes cations into optically active forms was achieved by Werner[6]. However, interest in these chelate molecules then lapsed for nearly twenty

years. It was revived by the discovery of Walden, Hammet, and Chapman[7] that their iron(II) compounds could be used as valuable redox indicators. It is now recognised that chelating ligands such as 2,2'-bipyridine, 1,10-phenanthroline, and 2,2'-bipyrimidine rival in versatility the well-known ethylenediamine, not only in the stability of many of the metal derivatives and their frequently intense colours, but also in the number of different metals that can be chelated.

Bivalent platinum is almost invariably 4 coordinate and usually attaches one molecule of L to form the sparingly soluble $[Pt(L)X_2]$ (L= bpy, phen and bpym ; X = Cl, Br, I etc.). These substances are more soluble in the presence of excess aromatic ligand, and the existence of the ions $[Pt(L)_2]^{2+}$ in such solutions has been demonstrated by the isolation of the salt, $[Pt(L)_2]\ (ClO_4)_2$[8]. The substance $[Pt(bpy)Cl_2]$ exists in yellow and red dimorphous forms. The bis chloride complex cannot be isolated, but $[Pt(bpy)_2][PtCl_4]$ and $[Pt(bpy)_2]\ I_2 \cdot 2H_2O$ exist.[9]

2,2'-Bipyridine may be converted into a potentially monodentate ligand by quaternising one of the nitrogen atoms **(4)**. However, the resulting cation should still be capable of bidentate coordination using the carbon positioned at the 3-position of the same ring, since it has been shown that neither the presence of a positive charge on a ligand nor a bulky substituent in the 2-position of a pyridine prevent coordination to the appropriate metal ion. These zwitterionic platinum(II) complexes with quaternised 2,2'-bipyridine ligands such as $[Pt(bpyMe\text{-}H)(X)_2]^{2+}$ (where X_2= pyridines, 2,2'-bipyridine etc.) are of considerable interest.

The dimensions of 2,2'-bipyridine are such that a planar arrangement of two ligands about a metal atom will result in an impossibly close approach of the α-H atoms of the opposing ligands. Hence, the mutual steric influence of the hydrogen atoms on the 6,6'-positions of the 2,2'-bipyridine ligands causes them to show bowlike distortions. Hazell *et al.*[10] have reported that the $[Pt(bpy)_2]^{2+}$ complex cation was not planar, but the two halves of one bpy molecule were tilted by 22.7 ° with respect to each other, though symmetry requires the four nitrogens and the Pt atoms to lie exactly in a plane. Hence, the $[Pt(bpy)_2]^{2+}$ ion has two-fold symmetry, the N atoms being at the corners of a flattened tetrahedron. In the $[Pt(bpyMe\text{-}H)(bpy)]^{2+}$ complex, the Pt-N bond is probably longer than the Pt-C bond[11]; thus the $[Pt(bpyMe\text{-}H)(bpy)]^{2+}$ complex is even more distorted than $[Pt(bpy)_2]^{2+}$.

Placing substituents on parent bases might well be expected to change the stabilities of their metal complexes and so affect the redox potentials of the compounds. It is now well established that for a given metal there is a relationship between the proton-binding capacity of a ligand and the stabilities of the complexes.[12] For example, substitution of the electrophilic bromo or nitro groups in the 4,4'-positions in 2,2'-bipyridine or the 4,7-positions in 1,10-phenanthroline should lower the base strengths and hence reduce the stabilities of the metal complexes. In the same manner, methyl and phenyl substituents in these positions should increase the stabilities.

4,4'-Bipyridine **(5)**, diquaternised bipyridines **(6,7)** and diquaternised 1,10-phenanthroline **(8)** are used extensively as herbicides[13-16]. Homer and Tomlinson[17] first reported the preparation and physical properties of diquaternised bipyridines. They reported that the free radicals of diquaternised bipyridines are very stable, presumably owing to delocalisation of the odd electron over the whole molecule. The possibility of such delocalisation is illustrated by the eighteen possible resonance forms which can be written for the radical without postulation of charge separation. The stability of the diquaternary salt, however, is not dependent upon inter-ring conjugation; hence factors which tend to prevent ring coplanarity will tend to reduce the stability of the free radical relative to that of the unreduced salt.

2,2';6',2''-Terpyridine **(9)** was isolated[18] from the products of the dehydrogenation of pyridine with anhydrous iron(II) chloride in an autoclave at 500 °C. A substance described originally as 2,2';X'' - terpyridine, which also gave an intense colour with iron(II) salt solutions, was subsequently shown to be a dimorphous form of 2,2',2''-terpyridine[19]. 2,2';6',2''-terpyridine acts as a tridentate planar chelate ligand, and the formation of the platinum derivative [Pt(terpy)Cl]Cl has been advanced as evidence for the planar distribution of the bonds about bivalent platinum.[20] Since the bonds from the nitrogen atoms to the metal must lie in the plane of the pyridine ring and resonance requires coplanarity of the three rings, it follows that all the bonds from the chelate must be coplanar. Though the molecule can encompass three planar positions in octahedral coordination, it is apparent that there is some strain involved, the N-$\widehat{M}$-N being a little less than 90°. This would suggest, as actually is the case,

that the metal complexes would be somewhat less stable than would be anticipated for a tridentate chelate molecule.

Morgan and Burstall[19] considered the three possible arrangements of the two chelate molecules in an octahedral complex. Only one of three possible arrangements satisfies the condition of coplanarity of the pyridine rings. That is where the molecules of the base are arranged in two equatorial planes at right angles (see diagram below). Bis-terpyridine iron(II) salts are characterised by an intense purple colour, so intense that a definite colour reaction for iron(II) is observed at concentrations of one part in two million.[1]

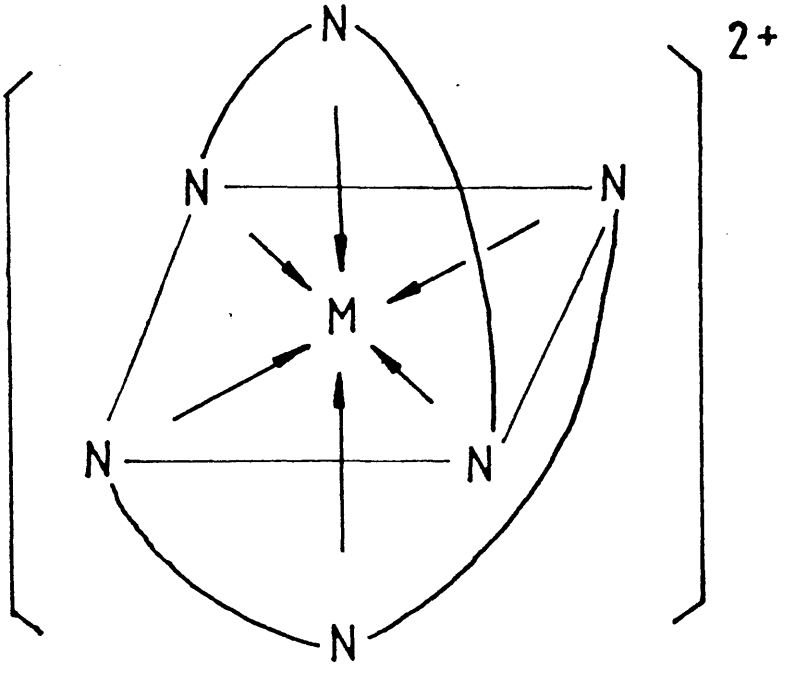

Recently, organoplatinum complexes such as $[PtR_2(L)]$ and $(\mu\text{-bpym})[PtR_2]_2$ (where R = aryl or alkyl groups such as CH_3 adamantylmethyl, phenyl and L = bidentate ligands such as bpy,

phen, bpym) have been of considerable interest[21,22-24]. In aryl platinum complexes, the platinum atom acts as a π- donor to the aryl groups. However, π interactions between platinum and aryl groups are weak and such π bonding is dependent on the nature of the other ligands bonded to platinum[25]. Spectra of most of these complexes are appreciably solvent dependent[23-25]. This effect is also shown by some octahedral mono- and binuclear complexes such as $[M(CO)_4(L)]$ and $(\mu\text{-bpym})[M(CO)_4]_2$ (where M = Mo, Cr, W, Re and L = bpy, bpym, phen)[26,27]. Usually, the negative solvatochromism displayed by these complexes, i.e. the hypsochromic shift of the MLCT absorption bands in polar solvents, is explained by assuming that the transfer of charge in the MLCT excited state occurs antiparallel to the ground-state dipole moment;[28,29] the higher transition energy in more polar solvents may thus be attributed to a dominating ground-stabilisation. In fact, nearly all of these studies were carried out with α-diimine complexes that have either idealised C_{2v} or C_s symmetry and should, therefore, possess a non-zero dipole moment; furthermore, the most frequently used ligands 1,10-phenanthroline[30], 2,2'-bipyridine[31,32] and 2,2'-bipyrimidine[23,24] also provide two identical or rather equivalent coordination sites.

In transition metal coordination compounds, we can categorise the electronic excitation as 'ligand-based' or 'metal-based' or 'charge transfer between metal and coordinated ligands'. The ligand-based transitions are transitions between molecular orbitals localised predominantly on the ligands and are almost invariably $\pi \rightarrow \pi^*$ excitations. The metal-based transitions are between molecular orbitals, largely localised on the metal centre

and are usually 'd → d' transitions. However, there is another important class of transitions in which the electron moves from a molecular orbital centred mainly on the ligands to one centred mainly on the metal atom, or *vice versa*. In these, the charge distribution is considerably different between the ground and the excited states. These are called charge-transfer transitions and more specifically can be distinguished into ligand-to-metal charge - transfer (LMCT) and metal-to-ligand charge-transfer (MLCT) transitions (Figure 1.2).

Metal-based d → d transitions of octahedral complexes have weak intensities because the transitions involved are from one centrosymmetric orbital to another (the sets of 'd-orbitals' that have been split apart by interactions with the ligands) and according to quantum theory such 'even-even' transitions should be electric dipole forbidden. However, for tetrahedral complexes the d → d transitions are slightly stronger because the entire complex is lacking a centre of symmetry. Nonetheless, the orbitals involved are largely metal d orbitals into which relatively small amounts of ligand orbitals have been mixed, and this means that the transitions are still strongly 'even-even', and so not as strong as the genuinely allowed 'even - odd' or 'odd - even' transitions such as intraligand transitions and charge-transfer transitions normally are. For an allowed charge-transfer transition to show appreciable intensity, it must also possess significant 'one-centre character'. Nearly all observed charge-transfer transitions are fully allowed, hence the charge- transfer transition bands are strong, showing that the nominally metal-based donor orbital should have some 'ligand-character'. Thus the intense absorption bands of coordinated metal complexes are highly characteristic of individual metal-ligand combinations.

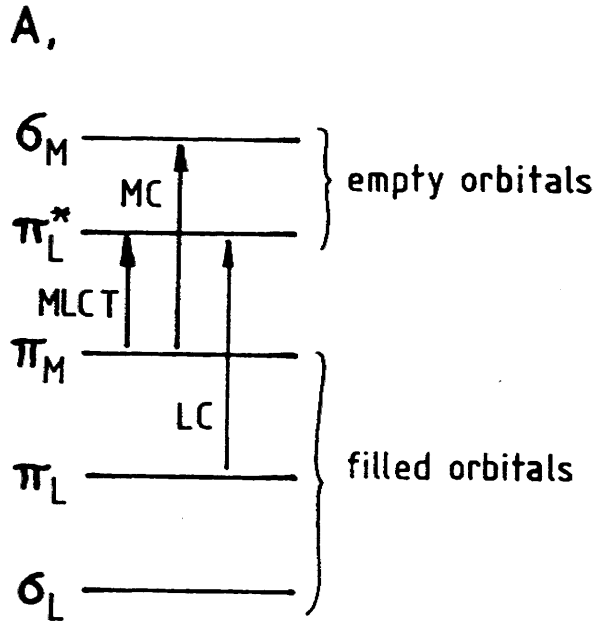

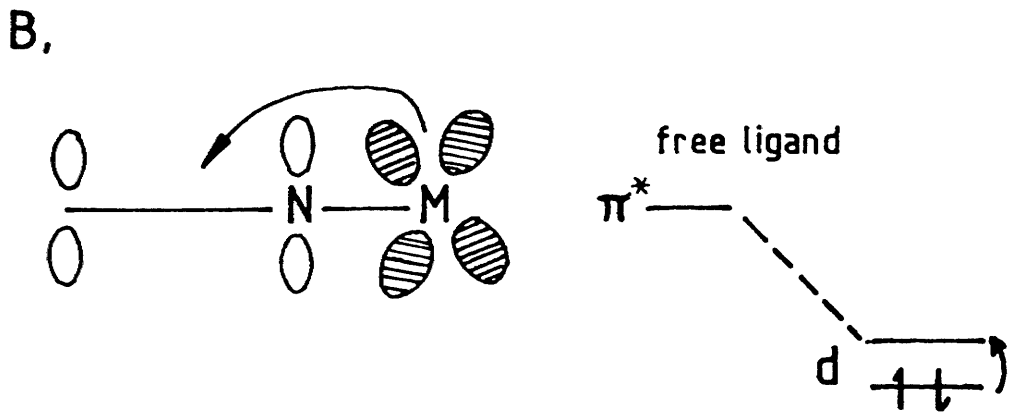

Figure 1.2 A, Simplified general molecular orbital diagram showing the three types of transition occuring at low energies.

B, Schematic diagram illustrating metal to ligand charge transfer.

$[Fe(L)_3]^{2+}$ possesses three consecutive, reversible one-electron reductions. The three reduction steps were assigned as ligand–based[33] and interest grew as to whether the electrons were localised on the individual bidentate ligands[34] (implying a symmetry lower than D_3 for the first two reduction products) or delocalised over all three. Evidence from electron spin resonance (e.s.r.)[35-37], ^1H. n.m.r[38], and resonance Raman spectroscopy[39,40], all suggested that the reduced compounds contained both L and L^- ligands so that the first reduction product was formulated as $[Fe(L)_2(L^-)]^+$, the second as $[Fe(L)(L^-)_2]^0$ and the third as $[Fe(L^-)_3]^-$. In particular, the e.s.r. spectra of the reduction products of $[Fe(L)_3]^{2+}$ suggested that the added electrons were localised on the individual ligands rather than delocalised over all three. In the singly and doubly reduced products it was found that the electrons hop from one ligand to another, broadening the e.s.r. line, whereas in the triply reduced species, one electron is on each ligand and no hopping was observed. π electron delocalisation between the ligands must therefore be small and the reduced ligands in the complex can be thought of as slightly perturbed 'free' reduced ligands. This implies that many of the properties of the free reduced ligand should be very similar to those of the reduced ligand in the complex.

The localised model of reduced mixed-ligand complexes is easier to understand as the π^* acceptor orbitals of each coordinated ligand are no longer identical. The one electron reduction product of $[Ru(bpy)_2(pn)]^{2+}$ (where pn=1,2-diaminopropane) and $[Ru(bpy)_2(NCS)_2]$ exhibit a weak and broad

intervalence absorption band centred at around 4000 cm^{-1} with an ε of 250 dm^3 mol^{-1} cm^{-1}. The spectrum of the two electron reduction product does not show any intervalence absorption band. The absence of this intervalence band for the two electron reduction product of the bis-bpy complex is consistent with the absence of this band for the three electron reduction product of the tris-complexes. Furthermore, resonance Raman spectra for the one electron reduction species of these complexes exhibit the vibrational patterns associated with both a bpy and a $[bpy]^-$ mode. This implies the simultaneous presence of discrete bpy and $[bpy]^-$ groups and as the IVCT band was weak in intensity, there cannot be much interaction between the different ligands in the complex. This is consistent with the electron localised model for the complexes.

Chapter 2. Experimental

GENERAL

Each compound was examined separately as a 0.005 mol dm^{-3} solution for cyclic voltammetry and 0.001 mol dm^{-3} for spectroelectrochemistry, and 0.1 mol dm^{-3} $TBABF_4$ was used as supporting electrolyte, except where stated otherwise. The chemicals which were used in this work, along with suppliers and grades of the materials, are listed in Table 2.1. Microanalyses were performed by David Wilson in this department.

2.1 INSTRUMENTATION

2.1.1 Cyclic voltammetry

All cyclic voltammetric experiments were performed under dried argon in a Metrohm cell equipped with a platinum wire in cross-section (0.01 mm^2) as working electrode, a 5 mm length of platinum wire as counter-electrode and a Ag/Ag^+ reference electrode. The reference electrode consisted of a silver wire in a 0.01 mol dm^{-3} solution of silver nitrate and in a 0.09 mol dm^{-3} solution of $TBABF_4$ in an air-tight compartment with a porous vycor frit, connected through second frit to the solution close to the working electrode. For work in acetonitrile or DMF, the working solvent was also the solvent in both reference electrode compartments. For work in CH_2Cl_2, acetonitrile was used in the inner compartment and CH_2Cl_2 in the outer compartment; no correction has been attempted for liquid-liquid junction potentials. The bottom part of the reference electrode was placed in a salt bridge compartment which was separated from the bulk electrochemical solution by a porous vycor frit. This salt bridge compartment

Table 2.1. Lists of Chemicals

Chemicals	Suppliers	Purities
Acetonitrile	Rathburn	HPLC Grade
Alumina	Hopkin & Williams	98 %
Amberlyte resin A-26	B.D.H.	Analar
Amberlyte resin IRA-400(Cl)	B.D.H.	Analar
Amberlyte resin IR-120(H)	B.D.H.	Analar
2-Aminopyridine	Lancaster synthesis	96 %
2,2-Bipyridine	Aldrich	Above 99 %
4,4-Bipyridine	Aldrich	98 %
2-Bromopyridine	Aldrich	99 %
Bromoacetaldehyde diethylacetal	Aldrich	97 %
n-Butyllithium	Aldrich	1.6 M
Calcium hydride	Aldrich	95 %
Copper powder 300 mesh	Lancaster synthesis	Pure
4,4-Dimethyl-2,2-bipyridine	Aldrich	99 %
1,2-Dibromoethane	Aldrich	98 %
1,3-Dibromopropane	Aldrich	98 %
1,4-dibromobutane	Aldrich	99 %
2,4-dinitrophenylhydrazine	Aldrich	98 %
N,N-Dimethylformamide	B.D.H.	Spectrol
Dimethylsulphoxide	Koch-Light	Above 99 %
Fluoroboric acid	B.D.H.	40 %
Ferrocene	Lancaster synthesis	Pure
Ferrous chloride tetrahydrate	Aldrich	Pure
Ferrous nitrite dihydrate	Hopkin & Williams	Pure
Hydrobromic acid	B.D.H.	42 %
Methyl viologen	B.D.H.	Pure

Chemicals	Suppliers	Purities
Methyl iodide	Aldrich	98 %
Molecular sieves	B.D.H.	Lab. Reg.
Neocuproine	Sigma	Pure
1,10-Phenanthroline	Aldrich	99 %
Propylene carbonate	Aldrich	99 %
Potassium nitrate	Koch-Light	Analar
Potassium hydroxide	B.D.H.	Analar
Potassium ferrocyanide	Hopkin & Williams	99 %
Potassium tetrachloroplatinate	J.M.C.	Analar
Silver nitrate	J.M.C.	99 %
Sodium nitrite	Riedel-de Haen	Above 99 %
Sodium bromide	M & G	Above 99 %
Tetrabutylammonium-tetrafluoroborate	Fluka	Puriss

Figure 2.1 Design of the O. T. T. L.E. cell

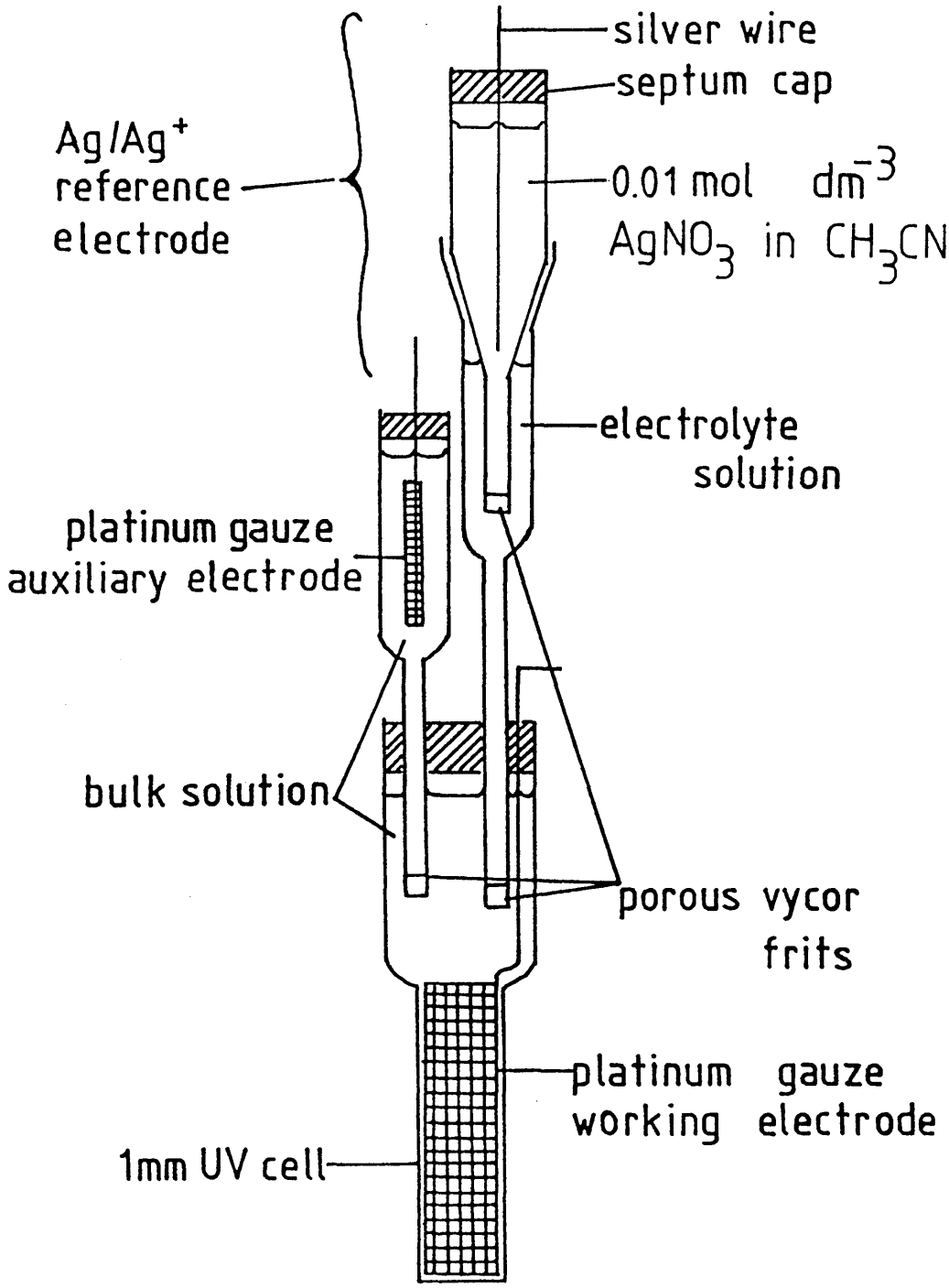

platinum gauze working electrode which was placed in the cell. Essential features of the experiment are that the working electrode covers the area sampled by the light beam and that the counter electrode compartment is isolated by a porous vycor frit from the main bulk of the solution to minimise reaction between reduced and non-reduced species. The reference electrode used was as the same as that used in the cyclic voltammetry work.

2.1.3 Low Temperature Cell

Low temperature (-40 °C) spectroelectrochemistry experiments were performed by mounting the optically transparent thin-layer electrode (O.T.T.L.E) cell in a Teflon block which was divided into three compartments by four strain-free quartz windows (Figure 2.2). The O.T.T.L.E. cell was inserted into the central compartment and cold, dry nitrogen which had been passed through a liquid nitrogen bath was blown through this compartment. Dry room temperature nitrogen was passed through the outer compartments to prevent ice forming on the quartz windows. The temperature inside the cell was monitored at all time using a thermocouple which was inserted into the cell.

2.1.3. Electronic Absorption Spectroscopy

Electronic absorption spectra were recorded on a Perkin Elmer Lambda 9 UV-vis.-near IR spectrophotometer, using standard 1 mm quartz cell or the 1 mm quartz O.T.T.L.E. cell.

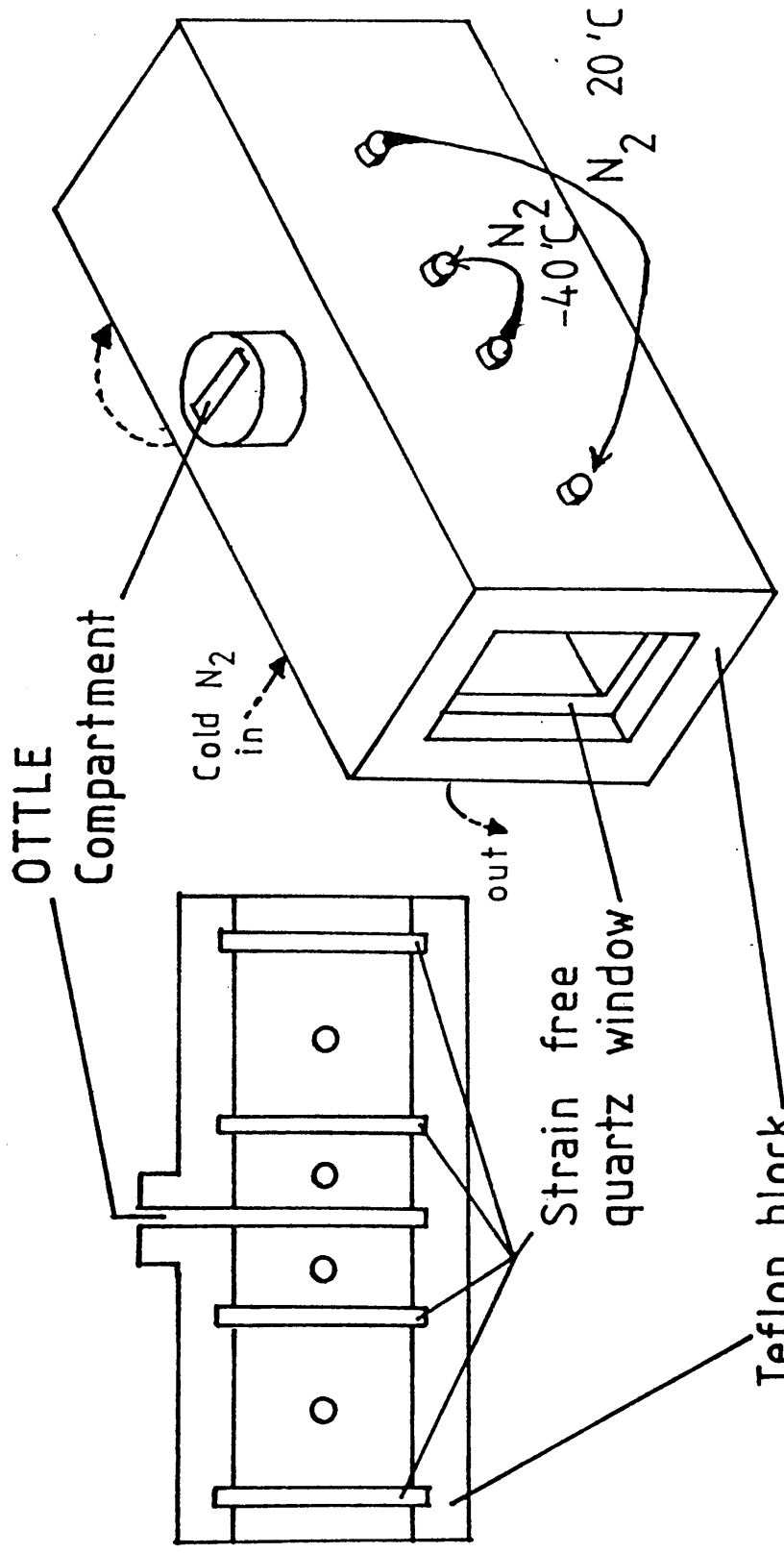

Figure 2.2
Schematic diagram of the low temperature cell

2.1.4 Ion Exchange Column Procedure from Chloride to Tetrafluoroborate.

The anion exchange resin used was Amberlyte IRA-400 (Cl), packed into a 50 cm column. To convert the resin from the chloride to the tetrafluoroborate form, the column was eluted with 4 litres of 0.2 mol dm^{-3} fluoroboric acid until testing with silver nitrate solution gave no precipitate (AgCl). Then the column was eluted with 1 litre of distilled water to remove excess tetrafluoroborate. A dilute aqueous solution (0.2 mol dm^{-3}) of the required compound as chloride was run down the column to convert it into the tetrafluoroborate salt

2.2 PURIFICATION OF CHEMICALS

2.2.1 Tetrahydrofuran (T.H.F.)

To a 500 ml round bottom flask was added 300 ml of tetrahydrofuran and 7 g of benzophenone and a little sodium-potassium alloy. The mixture was refluxed for approximately 1 hour. The tetrahydrofuran was distilled from calcium hydride, degassed and stored under nitrogen in brown bottles.

2.2.2. Acetonitrile

Acetonitrile was purified using the method of Winfield[41], then stored in a brown bottle over activated 3A molecular sieves.

2.2.3. Dichloromethane

Dichloromethane was dried over $CaCl_2$ for 2 days and then

distilled from P_2O_5. It was stored in a brown bottle over activated 3A molecular sieves.

2.2.4 Methyl iodide

Methyl iodide was purified by being shaken with aqueous $Na_2S_2O_3$ until colourless, washed with distilled water, aqueous $NaNO_3$, and more water, dried with $CaCl_2$ and distilled. It was stored in a brown bottle away from sunlight in contact with a small amount of mercury and copper powder.

2.2.5. Ethanol

Ethanol was refluxed over solid KOH and then over solid silver nitrate, then set aside overnight before filtering and distilling. The residual water was removed by standing the distillate over activated aluminium amalgam for one week, then filtering and distilling. It was stored in a brown bottle over activated 4A molecular sieves.

2.2.6. 1,2-Dichloroethane

1,2-Dichloroethane was washed with diluted aqueous sodium carbonate, then water, dried with $CaCl_2$ and fractionally distilled under reduced pressure.

2.2.7. Tetrabutylammonium tetrafluroborate ($TBABF_4$)

To a 50 ml beaker was added 10 g of $TBABF_4$ and the minimum amount of ethylacetate to dissolve the compound. After filtering a suitable quantity of isopentane was added dropwise to the solution until it became cloudy. The mixture was left for half an hour, and then filtered, and the solid dried under vacuum.

2.2.8. Petroleum ether

Into a separating funnel were added 250 ml of petroleum ether and 20 ml of concentrated sulphuric acid. After shaking, the sulphuric acid was removed, and the process repeated until the acid remained colourless. The petroleum ether was washed with distilled water several times, carefully shaken with dilute aqueous sodium carbonate solution, and washed again with water. After distillation it was kept in a brown bottle over sodium wire.

2.3. PREPARATIONS.

2.3.1. 2,2'-Bipyrimidine

2,2'-Bipyrimidine was prepared by a reverse diazotation reaction, using the procedure of Bly and Mellon[42], but using refluxing NaOH to decompose the intermediate Cu(I) complex instead of KCN-KOH solution.

(i) 2-bromopyrimidine;

Into a 500 ml three necked flask, equipped with a stirrer, equipressure dropping funnel, and thermometer was added 90 ml of distilled water, 90 g of sodium bromide, 30 g of sodium nitrite and 20 g of 2-aminopyrimidine. After the mixture was cooled to -10 °C, 48 ml of concentrated hydrobromic acid was added dropwise over a period of 3 hours (since the heat of reaction is very high and the temperature range must be kept between -3 °C and -11 °C). The mixture was left for approximately one hour to complete the reaction and then bromine and oxides of nitrogen

were removed by blowing through N_2 gas. The solution was made strongly alkaline with cold 40 % sodium hydroxide solution, filtered with suction and the filtrate and residue each extracted with four 100 ml portions of carbon tetrachloride. The extracts were combined and evaporated to dryness under reduced pressure at room temperature. The yield of crude 2-bromopyrimidine was 9.1 g (26.6 %). A double recrystallisation from purified petroleum ether (b.p. 60 - 80 °C) yielded 6.7 g of white crystals.
m.p. 55.5 - 57.0 °C, literature value 55 - 57 °C[42]

(ii) 2,2'-bipyrimidine;

All glassware was dried at 140 °C. Into a 150 ml three necked flask with a magnetic stirring bar, reflux condenser protected with $CaCl_2$ and blue silica gel, thermometer, and nitrogen inlet were added 20 g of activated copper, 10 g of 2-bromopyrimidine and 50 ml of dimethylformamide. The mixture was purged with nitrogen gas during the reaction, and the solution brought to reflux using an oil bath. After 3.5 hours 5 g of activated copper was added. After a total of 8.5 hours of reflux, the solution was gently cooled to 10 °C under nitrogen and filtered. The solid residue was placed in a 250 ml round bottom flask and refluxed for about one hour with 120 ml of 4 mol dm^{-3} sodium hydroxide solution. The hot mixture was filtered and was then extracted with four 200 ml portions of chloroform. The extracted chloroform was placed in an evaporating dish and evaporated in a high velocity hood. Enough ethylacetate was added to the tarry semicrystalline residue to dissolve it. A small amount of carbon black was added and the mixture was held at

reflux for 15 minutes. The hot mixture was filtered, then enough hot petroleum ether (b.p. 80 - 100 °C) was added to the ethylacetate solution until a permanent slight cloudiness occured at 80 °C. The mixture was slowly cooled to 0 °C with stirring and filtered again to yield 2.55 g of a tan crystalline solid. The purification was repeated to give 1.7 g (35 % yield) of white 2,2'-bipyrimidine, m.p. 114 - 115 °C after vacuum drying.

2.3.2. 2,2';6',2'' - Terpyridine

Method A [43,44];

Into a 500 ml three necked flask, equipped with an equipressure dropping funnel, and a thermometer were added 7.9 g of 2-bromopyridine and 100 ml of diethyl ether and the solution cooled to -65 °C. Then 32 ml of 1.6 mol dm^{-3} n-butyllithium in hexane was added dropwise over a period of 10 minutes and the red solution stirred for approximately 10 minutes to complete the conversion to 2-lithiopyridine. 5.2 g of 2,2'-bipyridine in 200 ml absolute diethyl ether was added dropwise over a period of 30 minutes while the temperature was kept below -40 °C. When most of the 2,2'-bipyridine had been added the red colour disappeared and a grey precipitate formed which gradually turned to light yellow by the end of 1 hour. The solution was slowly warmed to room temperature. After refluxing for about 30 minutes at 40 °C, the solution was hydrolysed with an ice-cold solution of ammonium chloride, and the ether layer was removed and dried over anhydrous sodium sulphate. Fractional distillation

gave a yellow oil. The oil was dissolved in 50 ml acetone and titrated with $KMnO_4$ in acetone until a dark violet colour just remained. After filtering off manganese dioxide, column chromatography [Al_2O_3; ether/petroleum ether(1;1)] gave 2.9 g of pale yellow terpyridine(39 %). m.p. 89 - 90 °C (Lit. 88 -89 °C)[45] and unreacted 2,2'-bipyridine.

Method B[46];

(i) [Fe(terpy)$_2$][PF_6]$_2$

Into a 100 ml three necked flask with thermometer, nitrogen inlet and reflux condensor was placed 2.5 g of 2-(2'-pyrrolidinopropionyl) pyridinium oxalate[47,48], 2.77 g of N-[1-(2'-pyridyl)-1-oxo-2-ethyl] pyridinium iodide[49], 8.5 g of ammonium acetate and 30 ml of aqueous methanol (1:1). After refluxing for 4 hours the solution, which had turned dark, was filtered hot. The filtrate was treated with 1.70 g of iron(II) chloride tetrahydrate to give a strong purple solution. This solution was treated with 3.40 g of ammonium hexafluoro-phosphate to give a purple microcrystalline precipitate of [Fe(terpy)$_2$][PF_6]$_2$ (3.4 g, 64 %)
Found; C,44.5; H, 2.7; N, 10.6 Calc.;C, 44.3; H, 2.7; N, 10.3

(ii) 2,2'-6',2'' -Terpyridine from [Fe(terpy)$_2$][PF_6]$_2$

One gram of [Fe(terpy)$_2$][PF_6]$_2$ was dissolved in 20 ml of aqueous acetonitrile (1:1) solution and to it was added dropwise 30 % aqueous hydrogen peroxide solution until the colour had been discharged. The solution was made alkaline by the addition of 4 ml of aqueous potassium hydroxide (1.2 mol dm^{-3}) solution. The suspension was filtered to remove iron oxides, and the filtrate

extracted with four 10 ml portions of chloroform. The extracts were concentrated and purified by column chromatography [Al_2O_3; ether/petroleum ether(1;1)] to give 0.46 g (81 %) of 2,2';6',2'' - terpyridine as a pale yellow solid. m.p. 88 - 89 °C.

Method C ; This procedure is a modified Ullmann reaction.

(i) N,N'-Dimethyl-2,2'-bipyridinium diiodide[17]

Twenty grams of 2,2'-bipyridine, 6.80 ml of methyl iodide, and 40 ml of methanol were placed in a 100 ml round bottom flask. The flask was sealed and heated behind a safety screen in a hot water bath at around 80 °C for 3 hours. The mixture was cooled in ice and filtered. Recrystallisation from acetone/toluene(1:1) gave 8.5 g of yellow crystalline N,N'-dimethyl-2,2'-bipyridinium diiodide. (15 %) m.p. 164-165 °C

(ii) N-methyl-2,2'-bipyridinium iodide[50]

The filtrate from the above reaction was evaporated to dryness under vacuum at 30 °C and a brown oil was obtained. Unreacted 2,2'-bipyridine was extracted with four 100 ml portions of hot toluene. The oily product was kept overnight in the refrigerator at 0 °C and N-methyl-2,2'-bipyridinium iodide crystallized. Recrystallisation from acetone/toluene(1:1) gave 24.8 g of light yellow N-methyl-2,2'-bipyridinium iodide. (65 %) m.p. 145-146 °C

(iii) N-Methyl-2,2'-bipyridinium chloride

N-Methyl-2,2'-bipyridinium chloride was prepared by ion-exchange of N-methyl-2,2'-bipyridinium iodide on a Dowex 1x8 cm

resin column. The resin was regenerated with 1 litre of 10 % sodium chloride solution and tested with silver nitrate. Then the column was eluted with 1 litre of distilled water. 20 g of N-methyl-2,2'-bipyridinium iodide were dissolved in 80 ml water and passed through the column. The solution obtained was evaporated under reduced pressure to give a pink oil which crystallized after 4 hours at 0 °C. Recrystallisation from 100 ml of acetone/toluene(1:1) solution gave 14.5 g of light yellow N-methyl-2,2'-bipyridinium chloride crystals. (85 %)

(iv) N-Methyl-2,2'-bipyridine-6-one[51]

One hundred grams of $K_3[Fe(CN)_6]$ was dissolved in 200 ml of water and the solution adjusted to pH 14 with 20 % sodium hydroxide solution. Then 11.3 g of N-methyl-2,2'-bipyridinium chloride dissolved in 70 ml of water were rapidly added to this solution, while maintaining the pH 14, following which the solution was heated at 80 °C for 1 hour. The hot solution was then cooled in ice and extracted with four 100 ml portions of chloroform. The chloroform fractions were evaporated in a high velocity hood and a brown oil was obtained. This brown oil was extracted with two 100 ml portions of hot heptane (80 °C). The combined organic fractions were evaporated under reduced pressure to give the crude product. Recrystallisation from heptane gave 7.0 g of N-methyl-2,2'-bipyridine-6-one. (68 %) m.p. 77 - 79 °C,

(v) 6- Bromo- 2,2'-bipyridine[52]

Five grams of N-methyl-2,2'-bipyridine-6-one, 7.8 g of $POCl_3$ and 122 g of PBr_3 were placed in a 250 ml round bottom flask and heated to 120 °C for approximately 3 hours. The solution

was gently cooled to room temperature and added to 150 g of ice. 600 ml of 20 % sodium hydroxide solution was added to the mixture giving a basic solution which was extracted with three 200 ml portions of chloroform. The extracted chloroform was placed in an evaporating dish and evaporated in a high velocity hood. The product was recrystallised from hexane and sublimed at 100 °C/0.01 mm Hg giving 4.6 g of 6-bromo-2,2'-bipyridine.(73 %) m.p. 74 - 75 °C.

(vi) 2,2';6',2''-Terpyridine[53]

A magnetic stirring bar, 1 g of 6-bromo-2,2'-bipyridine, 0.66 g of 2-bromopyridine and 580 mg of activated copper powder were placed in an evacuated tube and heated at 150 °C for 24 hours. The mixture was gently cooled to room temperature and treated with 50 ml of 20 % aqueous ammonia solution at 80 °C for approximately 4 hours. The cooled solution was extracted with three 70 ml portions of dichloromethane. The extracts were filtered and evaporated. The crude product was recrystallised from 50 ml ethanol/water(1:1) to give 0.72 g of pale yellow 2,2';6';2''-terpyridine.(72 %) m.p. 88 - 89 °C.

2.3.3. 6,7-Dihydrodipyrido[1,2-a;2,1-c]pyrazinedium dibromide (diquat)[17]

Five grams of 2,2'-bipyridine was stirred under reflux with 20 ml of dibromoethane for 16 hours. The mixture was cooled, and the solid filtered off. This solid was washed with acetone and diethyl ether to give the anhydrous diquaternary salt. Recrystallisation from aqueous acetone gave 6.2 g of yellow

6,7-dihydrodipyrido[1,2-a;2,1-c]pyrazinedium dibromide crystals. (70 %) m.p. 340 °C - decomp.

2.3.4. N - Methyl - 4,4'-bipyridinium iodide

One gram of 4,4'-bipyridine was stirred at room temperature with 0.4 ml of methyl iodide in 5 ml acetonitrile for 30 minutes and filtered. The solid was washed with acetone and diethyl ether to give the monoquaternary 4,4'-bipyridinium salt. Recrystallisation from aqueous acetone gave 1.15 g of N -methyl - 4,4'-bipyridinium iodide. (60 %)

2.3.5. 5,6-Dihydropyrazino[1,2,3,4-l.m.n]-1,10-phenanthrolinium dibromide[17]

One gram of 1,10-phenanthroline was stirred under reflux with a slight excess of 1,2-dibromoethane in acetonitrile for 1 hour. The mixture was cooled and the solid filtered off. This solid was washed with aqueous ethanol and diethyl ether to give the diquaternary salt. Recrystallisation from aqueous ethanol gave 1.68 g of brown 5,6-dihydropyrazino[1,2,3,4-l.m.n]-1,10-phenanthrolinium dibromide crystals. (65 %), m.p. above 390 °C.

2.3.6. 5H-6,7-dihydro-1,4-diazepino[1,2,3,4-l.m.n]-1,10-phenanthrolinium dibromide[17]

One gram of 1,10-phenanthroline was stirred under reflux with an excess of 1,3- dibromopropane for 1 hour. The mixture

was cooled and filtered. Recrystallisation from hot aqueous ethanol gave 1.24 g of the product as pale yellow 5H-6,7-dihydro-1,4-diazepino[1,2,3,4-l.m.n]-1,10-phenanthrolinium dibromide crystals. (47 %) m.p. 286 °C-decomp.

2.3.7. Pyrazino[1,2,3,4-l.m.n]-1,10-phenanthrolinium dibromide[54].

(i) Bromoaldehyde 2,4-dinitrophenylhydrazone

A solution of 5.0 g of 2,4-dinitrophenylhydrazine in 600 ml of 12 N hydrochloric acid was slowly added at room temperature to a rapidly stirred mixture of 5.05 g of bromoacetaldehyde diethylacetal in 100 ml of the same solvent. The yellow solid was filtered and washed with petroleum ether (b.p. 60 - 80 °C). The crude product was washed with methanol, leaving orange-yellow crystals of bromoaldehyde 2,4-dinitrophenylhydrazone. Recrystallisation was from anhydrous diethyl ether. (6.1 g; 64.2 %) m.p. 156 - 157 °C

(ii) 1-(β-2,4-dinitrophenylhydrazone) Ethyl-1,10'-phenanthrolinium bromide

Equimolar portions of 1,10-phenanthroline and bromoacetaldehyde-2,4-dinitrophenylhydrazone were heated in benzene solution at 60 °C for 1 hour. The yellow salts (92 %), m.p. 196 -198 °C with decomposition, were collected after 3 days and used in the next stage of the synthesis without further purification. Recrystallisation of a sample from aqueous methanol gave yellow crystals. m.p. 205 -206 °C with decomposition.

(iii) 5,6-Dihydro-5-hydroxypyrazino[1,2,3,4-l,m,n,]-1,10-phenanthrolinium dibromide.

Ten grams of 1-(β-2,4-dinitrophenylhydrazone)ethyl-1,10'-phenanthrolinium bromide and 50 ml of concentrated hydrobromic acid were placed in 100 ml round bottom flask and warmed on a steam bath for 40 minutes. The dark mixture was filtered and the cooled filtrate was diluted with acetone to give a precipitate of the product which after treatment with activated charcoal and recrystallisation from aqueous acetone gave brown crystals. (76 %) m.p. 300 °C.

(iv) Pyrazino[1,2,3,4-l,m,n,] - 1,10-phenanthrolinium dibromide

7.4 g of 5,6-dihydro-5-hydroxypyrazino[1,2,3,4-l.m.n.]-1,10-phenanthrolinium dibromide were heated with 37 ml of $SOCl_2$ under reflux for 1 hour. The $SOCl_2$ was removed in vacuo and the solid residue was treated with 25 ml of acetone. The precipitate which remained was crystallised from a mixture of acetone and hydrobromic acid to give the product as buff crystals. m.p. above 360 °C.

2.3.8. 2,2'-Bipyridyl-bis(chloro)platinum(II)[9]

To a 250 ml round bottom flask was added 1.03 g of potassium tetrachloroplatinate in 125 ml water, 0.39 g of 2,2'-bipyridine and 5 ml of 2N hydrochloric acid. After refluxing for 2 hours, a mass of filamentous yellow needles were precipitated from the solution. A further quantity of yellow needles was obtained by evaporating the filtrate.

Recrystallisation from dichloromethane gave 0.74 g of fine yellow [Pt(bpy)Cl_2]. (70 %)
Found; C, 28.6; H, 2.0; N, 6.5; Cl, 16.6 Calc.; C, 28.4; H, 1.9; N, 6.6; Cl, 16.8

2.3.9. Bis-2,2'-bipyridylplatinum(II) perchlorate[8]

One gram of sodium perchlorate and 1 g of 2,2'-bipyridine were dissolved in 20 ml of water. This solution was added to 1 g of [Pt(bpy)Cl_2] in 80 ml of water and heated to 90 °C. The filtrate from the undissolved salt (0.05 g) was then treated with a small amount of concentrated perchloric acid at the same temperature. Yellow crystals were obtained after filtering. Recrystallisation from dichloroethane gave 0.913 g of yellow bis-2,2'-bipyridylplatinum(II) perchlorate. (94 %)
Found; C, 40.1; H, 1.5; N, 8.0; Cl, 10.1 Calc.; C, 39.9; H, 1.4; N, 7.9; Cl, 10.0

Properties were similar to those of a sample donated by Drs. F.L. Wimmer and S. Wimmer.

2.3.10. 2,2'-Bipyridyl-bis(pyridyl)platinum(II) perchlorate[8]

A suspension of 0.5 g of [Pt(bpy)Cl_2] in 60 ml 17 % of aqueous pyridine was gently warmed at 45 °C on a water bath. 0.5 g of sodium perchlorate was added to this warm yellow solution

to give 0.84 g of pale yellow 2,2'-bipyridyl-bis(pyridyl)-platinum(II) perchlorate. (87 %)
Found; C, 40.2; H, 1.5; N, 8.0; Cl, 10.2 Calc.;C, 39.9; H, 1.4; N, 7.9; Cl, 10.0

2.3.11. N(1'),C(3)-dihapto(1-methyl-2,2'-bipyridinyl)-bis(chloro)platinum(II) [55]

1.03 g of potassium tetrachloroplatinate in 125 ml of water and 0.43 g of N-methyl-2,2'-bipyridinium nitrate were gently heated to a temperature of around 50 °C to give an orange microcrystalline precipitate. This solid was washed with dichloromethane to give 1.0 g of [Pt(bpyMe)Cl_3]. (84 %) m.p. above 270 °C-decomp.

One gram of [Pt(bpyMe-H)Cl_3] in 100 ml water was heated at 90 °C for 18 hours to give 0.88 g of orange needles of N(1'),C(3)-dihapto(1-methyl-2,2'-bipyridinyl)-bis(chloro)platinum(II). (81 %) m.p. above 270 °C -decomp.
Found; C, 30.3; H, 3.1; N, 6.3; Cl, 16.1 Calc.;C, 30.1; H, 3.0 ;N, 6.4; Cl, 16.2

2.3.12. N(1'),C(3)-dihapto(1-methyl-2,2'-bipyridinyl) 2,2'-bipyridylplatinum(II) perchlorate[55]

One gram of sodium perchlorate and 1 g of 2,2'-bipyridine were dissolved in 20 ml of water. This solution was added to 1 g

of N(1'),C(3)-dihapto(1-methyl-2,2'-bipyridinyl)-bis(chloro)-platinum(II) in 80 ml water and gently warmed to around 40 °C. Yellow crystals were obtained after filtering. Recrystallisation from dichloromethane gave 0.9 g of N(1'),C(3)-dihapto(1-methyl-2,2'-bipyridinyl)-2,2'-bipyridylplatinum(II) perchlorate. (94 %)
Found; C, 34.7; H, 1.5; N, 7.6; Cl, 9.9 Calc.;C, 34.9; H, 1.4 ;N, 7.8; Cl, 9.8

2.3.13. N(1'),C(3)-dihapto(1-methyl-2,2'-bipyridinyl)-bis(pyridyl)platinum(II) perchlorate[55]

A suspension of 0.5 g of N(1'),C(3)- dihapto(1-methyl-2,2'-bipyridinyl)-bis(chloro)platinum(II) in 60 ml 17 % aqueous pyridine were refluxed for 30 minutes to give a pale yellow crystals which were a mixture of [Pt(bpyMe-H)(py)Cl][ClO_4] and [Pt(bpyMe)$(py)_2$][ClO_4]$_2$. Recrystallisation from dichloromethane gave 0.74 g of pure N(1'),C(3)-dihapto(1-methyl-2,2'-bipyridinyl)-bis(pyridyl)platinum(II) perchlorate. (77 %)
Found; C, 34.7; H, 1.6; N, 7.6; Cl, 10.1 Calc.;C, 34.9; H, 1.4 ;N, 7.8; Cl, 9.8

2.3.14 cis-Diphenyl-bis(dimethylsulphoxide)platinum(II)[56]

Two grams of potassium tetrachloroplatinate was dissolved in 8 ml of dimethylsulphoxide and heated at 70 °C for 10 minutes. 1.16 g of $SnMe_3Ph$ was added to this solution and the mixture maintained at the same temperature for 6 hours. Evaporation of the solvent gave a white solid which was washed with dried

diethyl ether and dissolved in dichloromethane. The solution was treated with activated charcoal and filtered. Diethyl ether was added until the dichloromethane solution became cloudy. The solid was collected and washed with dried diethyl ether to give colourless needles of cis-diphenyl-bis(DMSO)platinum(II).(1.7 g, 70 %)

2.3.15 Diphenyl(2,2'-bipyrimidyl)platinum(II)[2 3]

0.9 g of $Pt(DMSO)_2Ph_2$ in 80 ml dichloromethane was slowly added over a period of 10 minutes to a rapidly stirred solution of 0.42 g of bipyrimidine in 80 ml dichloromethane. The reaction was complete after stirring for 2 hours at room temperature. The mixture was filtered to remove the small quantity of a binuclear product produced and the solvent removed under reduced pressure. Recrystallisation from warm acetone (35 °C) gave 0.54 g of red diphenyl(2,2'-bipyrimidyl)platinum(II). (71 %)

Found; C, 48.2; H, 3.3; N, 11.9 Calc.;C, 48.3; H, 3.3; N, 11.9

2.3.16. Tetraphenyl(μ-bipyrimidyl)diplatinum(II)[2 3]

0.159 g of 2,2'-bipyrimidine in 90 ml dichloromethane was added over a period of 1 hour to a rapidly stirred solution of 0.75 g of $Pt(DMSO)_2Ph_2$ in 90 ml dichloromethane. The mixture was allowed to stand overnight and the dark red microcrystals were filtered off. Washing with dichloromethane gave 0.60 g of dark red tetraphenyl(μ-bipyrimidyl)diplatinum (II). (88 %)

Found; C, 44.7; H, 3.0; N, 6.6 Calc.; C, 44.9; H, 3.1; N, 6.5

2.3.17. $[Fe(bpym)_3]\ (ClO_4)_2 \cdot 7H_2O$[4]

A solution of 0.16 g of iron(II) ammonium sulphate hexahydrate in 30 ml of water was added slowly to a rapidly stirred solution of 0.24 g of 2,2'-bipyrimidine in 30 ml of water. The colourless solution became dark red. 0.12 g of sodium perchlorate was added to this solution to give a dark red precipitate. The precipitate was filtered, washed twice with the minimum amount of cold water and dried in vacuo to give 0.34 g of $[Fe(bpym)_3]\ (ClO_4)_2 \cdot 7H_2O$ (81 %)
Found; C, 39.4;N, 23.6; H_2O, 17.5 Calc.;C, 39.6;N, 23.1; H_2O, 17.3

2.3.18. $[Fe(bpy)_3]\ (BF_4)_2$[57]

A solution of 0.16 g of iron(II) chloride dihydrate in 60 ml water was added slowly to a rapidly stirred solution of 0.47 g of 2,2'-bipyridine in 60 ml water. The colourless solution became a deep violet. Evaporation of the solvent produced violet crystals. The crystals were dissolved in 80 ml of water and passed through an ion-exchange column to give a solution of $[Fe(bpy)_3](BF_4)_2$. The solution obtained was evaporated under reduced pressure, washed with the minimum quantity of ice-cold water and dried in vacuo to give 0.51 g of violet needles of $[Fe(bpy)_3](BF_4)_2$. (74 %)
Found; C, 53.5; N, 12.2; H, 3.6 Calc.; C, 53.3; N, 12.0; H, 3.4

2.3.19. $[Fe(phen)_3]\ (BF_4)_2$

This complex was prepared by a similar method to that used for $[Fe(bpy)_3](BF_4)_2$.
Found; C, 55.9; N, 9.1; H, 3.2 Calc.; C, 55.7; N, 9.3; H, 3.1.

Chapter 3. Simple Hückel molecular orbital calculations of bipyridyl radical anions.

In this chapter, are presented molecular orbital calculations for planar 2,2'-bipyridine, 4,4'-bipyridine and 2,2'-bipyrimidine using an extension of the theoretical method that has been applied to biphenyl.[58-60] Each nitrogen atom provides the conjugated system with one π-electron, so that in the Hückel π-electron approximation this molecule presents a 12-electron problem as does biphenyl.[61] It is therefore justifiable to employ as a starting point the simple M.O.'s of biphenyl.

The ring system of pyridine is a slightly distorted hexagon because of the shorter C-N bond lengths in comparison to those of the C-C bonds. It can be represented by a cyclic structure containing one sp^2- hybridised nitrogen atom, each atom in the ring having a p-orbital orthogonal to the plane. The orbitals of pyridine have the same symmetry as benzene and the interaction of the six p-atomic orbitals of both compounds lead to six delocalised molecular orbitals; three bonding and three antibonding. The major difference between the two species is that the energies of the π-orbitals of pyridine are lowered relative to those of benzene because of the greater electronegativity of nitrogen. This is particularly so for π(2) which has a large coefficient on nitrogen, thus π(2) and π(3), which are degenerate in benzene, are no longer degenerate in pyridine. (Figure 3.1)

Differences in reactivity between benzene and pyridine might be expected since the π-bonding system in pyridine is of lower energy than that in benzene. In particular, the highest occupied orbitals in pyridine are of lower energy than those in benzene and are therefore less nucleophilic. The distribution of

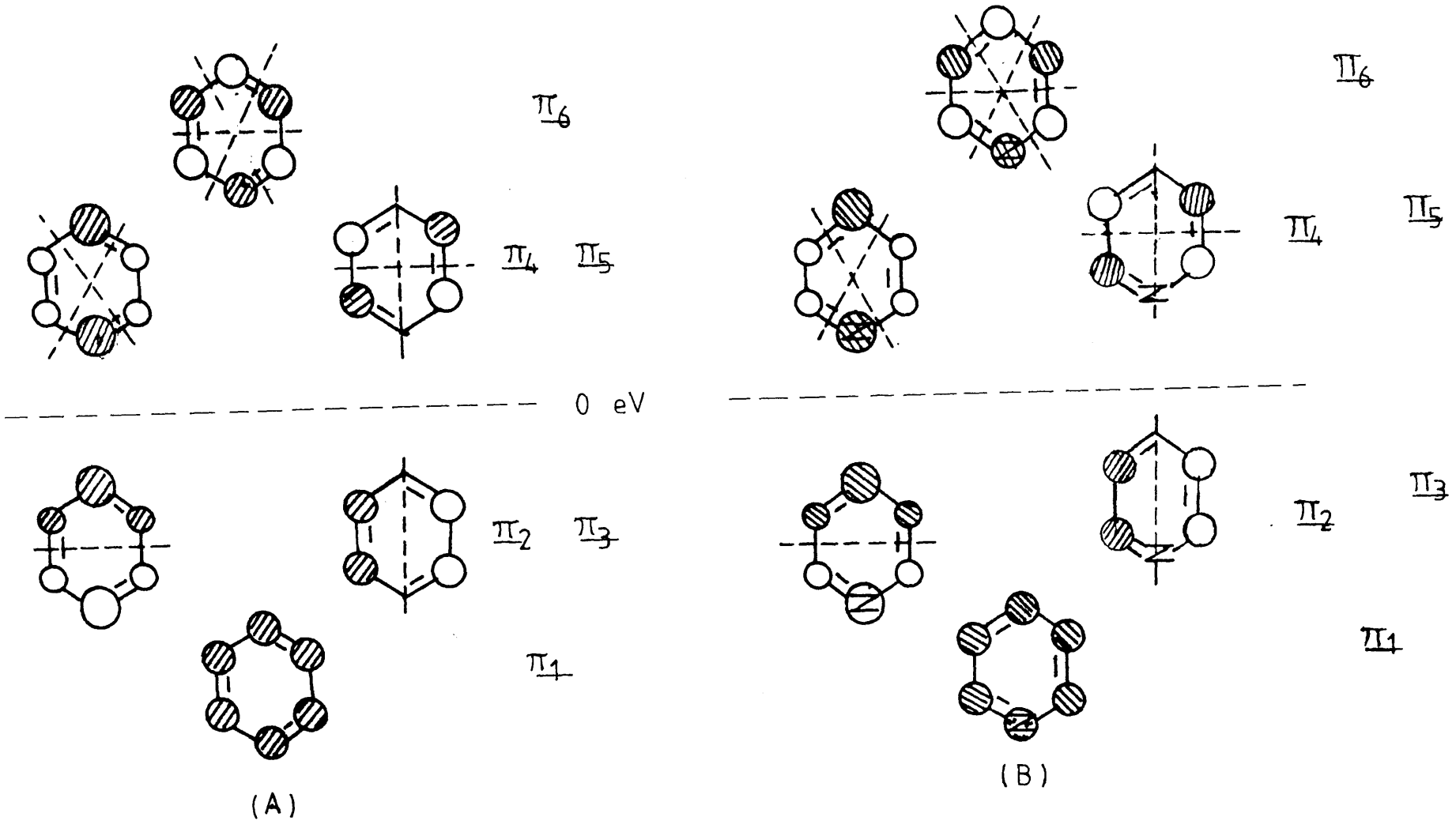

Figure 3.1 π-orbitals for benzene (A) and pyridine (B)

π-electron density around the ring is also distorted by the presence of the nitrogen atom.

A similar argument can be applied to 2,2'-bipyridine, 4,4'-bipyridine, 2,2'-bipyrimidine and biphenyl (Figure 3.2). The π-orbitals for the two-ring species are constructed from in-phase and out-of-phase combinations of orbitals on the corresponding one-ring species. π(7) is bonding between rings so that the anion, in which π(7) is singly occupied, will tend to be planar even when the parent is not.

The sets of π(4), π(5) and π(8), π(9) orbitals are degenerate (i.e. of equal energy) in biphenyl, 4,4'-bipyridine and 2,2'-bipyrimidine The orbitals are, however, nondegenerate in 2,2'-bipyridine. The $\pi^* \rightarrow \pi^*$ transitions $\pi(7) \rightarrow \pi(8)$ and $\pi(7) \rightarrow \pi(11)$ are forbidden in 4,4'-bipyridine, 2,2'-bipyrimidine and biphenyl molecules because they are u → u, but these transitions are electronically allowed in 2,2'-bipyridine.

Hückel theory

The M.O.'s are regarded as being made up of linear combinations of atomic orbitals (LCAO approach).

$$\Psi = \sum_i c_i \Phi_i. \qquad (3.1)$$

The coefficients and energies of these orbitals are obtained by solving the secular equation.

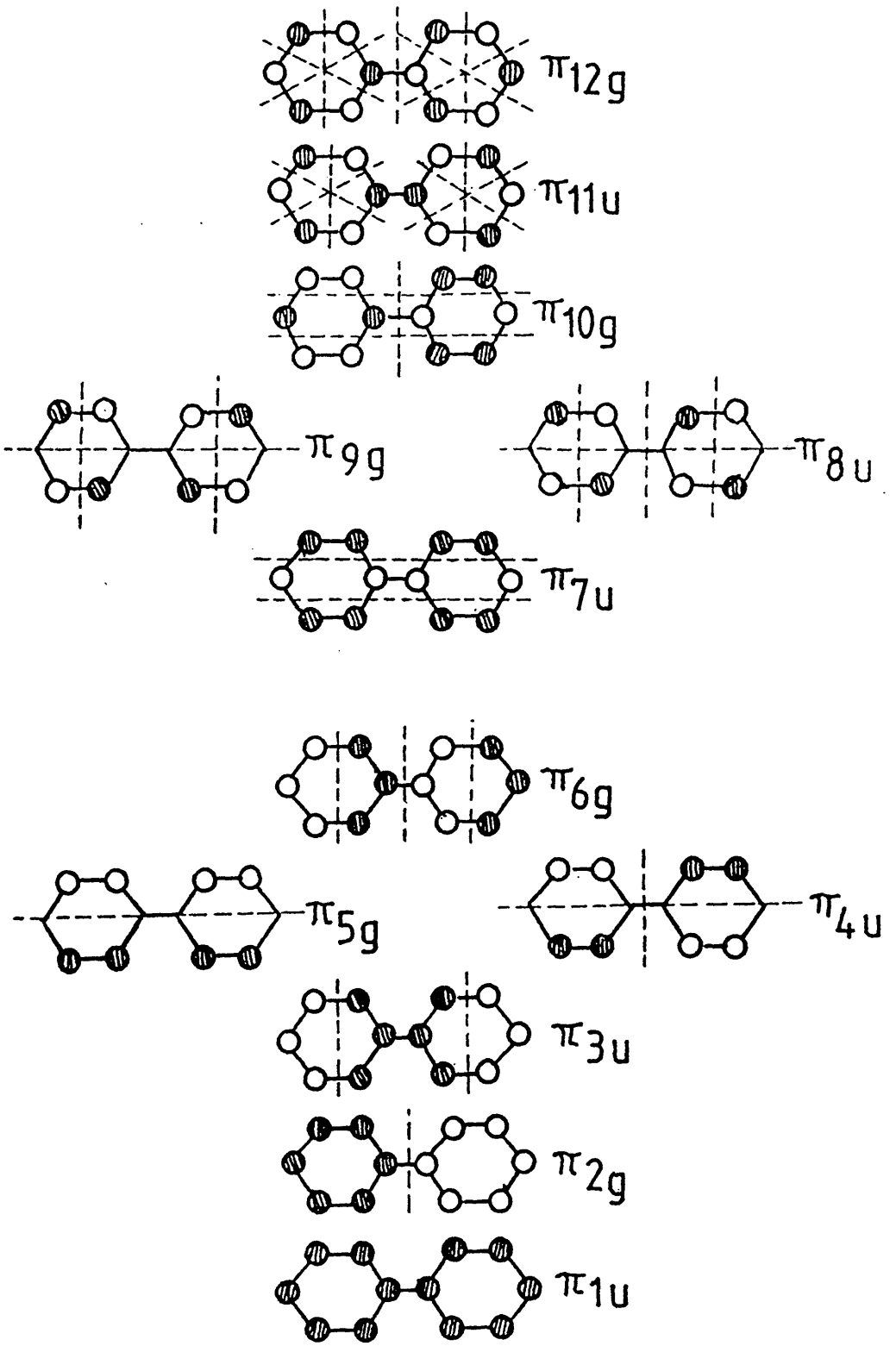

Figure 3.2 π-orbitals for biphenyl.

$$\sum_i c_j(H_{ij} - ES_{ij}) = 0 \qquad (3.2)$$

Then the best values for the energies are given by the roots (or eigenvalues) of the equation.

$$| H_{ij} - ES_{ij} | = 0 \qquad (3.3)$$

Where

$$H_{ij} = \int \phi_i H \phi_j d\tau \qquad (3.4)$$

$$S_{ij} = \int \phi_i \phi_j d\tau \qquad (3.5)$$

In the Huckel approximation, the following assumptions are made

i. Zero overlap between neighbouring A.O.'s,
   i.e. $S_{ij} = 1$ if $i = j$ or 0 if $i \neq j$.

ii. H_{ii} is assumed to be the same for each atom, it is given the symbol α and is called the 'Coulomb integral'.

iii. H_{ij} is given the symbol β and is called the 'resonance integral', if atom i is bonded directly to atom j, the $H_{ij} = 1$. If atom i is not bonded directly to atom j, the $H_{ij} = 0$.

With these approximations equation (3.2) becomes

$$c_j(\alpha - E) + \sum_{i \to j} c_i \beta = 0 \qquad (3.6)$$

Using ethylene as an example, if we label the two C atoms A and B, equation (3.6) simplifies to

$$\begin{vmatrix} \alpha - E & \beta \\ \beta & \alpha - E \end{vmatrix} = 0 \qquad (3.7)$$

which on expansion gives a quadratic equation with the solutions

$$E = \alpha \pm \beta \qquad (3.8)$$

We can determine the coefficients by substituting $E = \alpha \pm \beta$ back into the equations (3.6), and we have

$$c_A = \pm c_B. \qquad (3.9)$$

Applying the normalisation condition

$$\int \Psi^2 d\tau = 1, \qquad (3.10)$$

where Ψ are the un-normalised wavefunctions, i.e. $\Psi = c_A(\phi_A \pm \phi_B)$, gives

$$\Psi_{(A)} = 1/\sqrt{2}\cdot(\phi_{(A)} + \phi_{(B)}), \qquad E = \alpha + \beta \qquad (3.11)$$

$$\Psi_{(B)} = 1/\sqrt{2}\cdot(\phi_{(A)} - \phi_{(B)}), \qquad E = \alpha - \beta. \qquad (3.12)$$

The energies correspond to the two M.O.'s. There are no terms in $c_A c_B$ because of the zero-overlap approximation.

For bipyridyls, implicit in this treatment is the assumption that the two rings are coplanar; an assumption more likely to hold good for the anions (in which $\pi(7)$ is populated) than for the parents, in which dihedral angles of up to 40 ^{o} are known[60]. One major theoretical simplification arises for the singly reduced species. Since they consist of a closed shell to which one electron has been added, the transition energies can be treated to a good approximation as one-electron energy differences.

The π-orbitals for planar biphenyl derivatives can be constructed by fusing together in-phase and out-of-phase combinations of the appropriate orbitals taken over the two rings. Neglecting overlap and non-neighbour interactions, measuring energies relative to $\alpha(C)$, and assuming all resonance integrals β equal and resonance integral between rings as $\beta\cdot\cos\theta$, we can calculate the effect of substitution of C by the more electronegative N in terms of the parameter α. We then have (exactly within the rather severe limits of this model, for biphenyl, 4,4-bipyridine and its quaternised derivatives, and to first order in $\alpha(N)/\beta$ for 2,2'-bipyridine and its derivatives) the electron densities[62] and calculated orbital energies for the bipyridyls obtained from the basis set (Table 3.1).

For example,

$$\pi(1) = H_{11} = \int\Psi_{(1)} H\, \Psi_{(1)} d\tau \qquad (3.13)$$

$$= 1/12\cdot\int(\phi_1+\phi_2+\cdots\cdots+\phi_{12})\, H\, (\phi_1+\phi_2+\cdots\cdots+\phi_{12})d\tau \qquad (3.14)$$

$$= 13\cdot\beta(C)/6 + \alpha(N)/6. \qquad (3.15)$$

Table 3.1 The basis set of 2,2'-bipyridine.

$$\Psi_1 = 1/\sqrt{12}\cdot(\phi_1+\phi_2+\phi_3+\phi_4+\phi_5+\phi_6+\phi_7+\phi_8+\phi_9+\phi_{10}+\phi_{11}+\phi_{12})$$

$$\Psi_2 = 1/\sqrt{12}\cdot(\phi_1+\phi_2+\phi_3+\phi_4+\phi_5+\phi_6-\phi_7-\phi_8-\phi_9-\phi_{10}-\phi_{11}-\phi_{12})$$

$$\Psi_3 = 1/\sqrt{24}\cdot(\phi_1+2\phi_2+\phi_3-\phi_4-2\phi_5-\phi_6+\phi_7+2\phi_8+\phi_9-\phi_{10}-2\phi_{11}-\phi_{12})$$

$$\Psi_4 = 1/\sqrt{8}\cdot(\phi_1-\phi_3-\phi_4+\phi_6-\phi_7+\phi_9+\phi_{10}-\phi_{12})$$

$$\Psi_5 = 1/\sqrt{8}\cdot(\phi_1-\phi_3-\phi_4+\phi_6+\phi_7-\phi_9-\phi_{10}+\phi_{12})$$

$$\Psi_6 = 1/\sqrt{24}\cdot(\phi_1+2\phi_2+\phi_3-\phi_4-2\phi_5-\phi_6-\phi_7-2\phi_8-\phi_9+\phi_{10}+2\phi_{11}+\phi_{12})$$

$$\Psi_7 = 1/\sqrt{24}\cdot(\phi_1-2\phi_2+\phi_3+\phi_4-2\phi_5+\phi_6+\phi_7-2\phi_8+\phi_9+\phi_{10}-2\phi_{11}+\phi_{12})$$

$$\Psi_8 = 1/\sqrt{8}\cdot(\phi_1-\phi_3+\phi_4-\phi_6-\phi_7+\phi_9-\phi_{10}+\phi_{12})$$

$$\Psi_9 = 1/\sqrt{8}\cdot(\phi_1-\phi_3+\phi_4-\phi_6+\phi_7-\phi_9+\phi_{10}-\phi_{12})$$

$$\Psi_{10} = 1/\sqrt{24}\cdot(-\phi_1+2\phi_2-\phi_3-\phi_4+2\phi_5-\phi_6+\phi_7-2\phi_8+\phi_9+\phi_{10}-2\phi_{11}+\phi_{12})$$

$$\Psi_{11} = 1/\sqrt{12}\cdot(-\phi_1+\phi_2-\phi_3+\phi_4-\phi_5+\phi_6-\phi_7+\phi_8-\phi_9+\phi_{10}-\phi_{11}+\phi_{12})$$

$$\Psi_{12} = 1/\sqrt{12}\cdot(-\phi_1+\phi_2-\phi_3+\phi_4-\phi_5+\phi_6+\phi_7-\phi_8+\phi_9-\phi_{10}+\phi_{11}-\phi_{12})$$

Table 3.2 shows the calculated orbital energies of 2,2'-bipyridine and 4,4'-bipyridine. From these we can, for the singly reduced species, directly calculate transition energies, while the symmetries and forms of the wavefunctions lead to predictions of relative intensities.

For cis-2,2'-bipyridine derivatives, an elementary second-order treatment shows the general effects of the lowering of symmetry on energies and selection rules. These results are collected in Table3.3.

Figure 3.3, 3.4 and 3.5 show orbital energy correlations for each molecular orbital as a function of the Coulomb integral parameter $\alpha(N)/\beta$. The non-coordinating nitrogen atom centres are assigned $\alpha(N)/\beta = 0.75$. This value illustrates the situation for the free ligand. In agreement with the electronic absorption spectra of the singly reduced species, the energy sequences of the $\pi \rightarrow \pi^*$ and $\pi^* \rightarrow \pi^*$ transition are $\pi(6) \rightarrow \pi(7) > \pi(7) \rightarrow \pi(11) > \pi(7) \rightarrow \pi(10) > \pi(7) \rightarrow \pi(9) > \pi(7) \rightarrow \pi(8)$ at $\alpha(N)/\beta = 0.75$.

Table 3.2. The electron densities and orbital energies in 4,4'-bipyridine and 2,2'-bipyridine.

Orbital	Symmetry[a] $D_{2h}(C_{2v})(C_{2h})$	Density[b] Sites 1 etc.; 2etc.	Energy in 4,4'-bpy	Energy in 2,2'-bpy
$\pi(12)$	$b_{2g}(a_2)(a_g)$	$1/\sqrt{12};1/\sqrt{12}$	$-13\cdot\beta/6+\alpha/6$	$-13\cdot\beta/6+\alpha/6$
$\pi(11)$	$b_{1u}(b_1)(b_u)$	$1/\sqrt{12};1/\sqrt{12}$	$-11\cdot\beta/6+\alpha/6$	$-11\cdot\beta/6+\alpha/6$
$\pi(10)$	$b_{2g}(a_2)(a_g)$	$1/\sqrt{6}$; $1/\sqrt{24}$	$-4\cdot\beta/3+\alpha/3$	$-4\cdot\beta/3+\alpha/12$
$\pi(9)$	$b_{3g}(b_2)(b_g)$	$0;1/\sqrt{8}$	$-\beta$	$-\beta+\alpha/4$
$\pi(8)$	$a_u(a_2)(a_u)$	$0;1/\sqrt{8}$	$-\beta$	$-\beta+\alpha/4$
$\pi(7)$	$b_{1u}(b_1)(b_u)$	$1/\sqrt{6};1/\sqrt{24}$	$-2\cdot\beta/3+\alpha/3$	$-2\cdot\beta/3+\alpha/12$
$\pi(6)$	$b_{2g}(a_2)(a_g)$	$1/\sqrt{6};1/\sqrt{24}$	$2\cdot\beta/3+\alpha/3$	$2\cdot\beta/3+\alpha/12$
$\pi(5)$	$b_{3g}(b_2)(b_g)$	$0;1/\sqrt{8}$	β	$\beta+\alpha/4$
$\pi(4)$	$a_u(a_2)(a_u)$	$0;1/\sqrt{8}$	β	$\beta+\alpha/4$
$\pi(3)$	$b_{1u}(b_1)(b_u)$	$1/\sqrt{6};1/\sqrt{24}$	$4\cdot\beta/3+\alpha/3$	$4\cdot\beta/3+\alpha/12$
$\pi(2)$	$b_{2g}(a_2)(a_g)$	$1/\sqrt{12};1/\sqrt{12}$	$11\cdot\beta/6+\alpha/6$	$11\cdot\beta/6+\alpha/6$
$\pi(1)$	$b_{1u}(b_1)(b_u)$	$1/\sqrt{12};1/\sqrt{12}$	$13\cdot\beta/6+\alpha/6$	$13\cdot\beta/6+\alpha/6$

[a]Assuming rings are coplanar and (for 2,2'-bipyridine) (cisoid) (transoid)

[b]Sites 1 etc.; 1,1', 4,4'. Sites 2 etc.; 2,2', 3,3', 5,5', 6,6'

Table 3.3.The one-electron transition energies in 4,4'-bipyridine and 2,2'-bipyridine.

Transition	Energy (Strength)[a] in 4,4'-bpy	Energy (Strength) in (cis; trans) 2,2'-bpy	Comments[b]
$\pi(7) \rightarrow \pi(8)$	$-\beta/3 - \alpha/3$ (f)	$-\beta/3 - \alpha/3$ (w;f)	r
$\pi(7) \rightarrow \pi(9)$	$-\beta/3 - \alpha/3$ (vw)	$-\beta/3 - \alpha/3$ (w;w)	r
$\pi(7) \rightarrow \pi(10)$	$-2\cdot\beta/3$ (s)	$-2\cdot\beta/3$ (s;s)	r
$\pi(7) \rightarrow \pi(11)$	$-7\cdot\beta/6 - \alpha/6$ (f)	$-7\cdot\beta/6 + \alpha/12$ (w;f)	
$\pi(7) \rightarrow \pi(12)$	$-3\cdot\beta/2 - \alpha/6$ (s)	$-3\cdot\beta/2 + \alpha/12$ (s;s)	
$\pi(6) \rightarrow \pi(7)$	$-4\cdot\beta/3$ (s)	$-4\cdot\beta/3$ (s;s)	l
$\pi(6) \rightarrow \pi(8)$	$-5\cdot\beta/3 - \alpha/3$ (s)	$-5\cdot\beta/3 + \alpha/6$ (s;s)	l
$\pi(6) \rightarrow \pi(9)$	$-5\cdot\beta/3 - \alpha/3$ (f)	$-5\cdot\beta/3 + \alpha/6$ (w;f)	r
$\pi(5) \rightarrow \pi(7)$	$-5\cdot\beta/3 + \alpha/3$ (s)	$-5\cdot\beta/3 - \alpha/6$ (s;s)	l

(a) f; forbidden w; weak s; strong v; very strong vw; very weak

(b) l; lowered and r; raised in cis-2,2'-bipyridine.

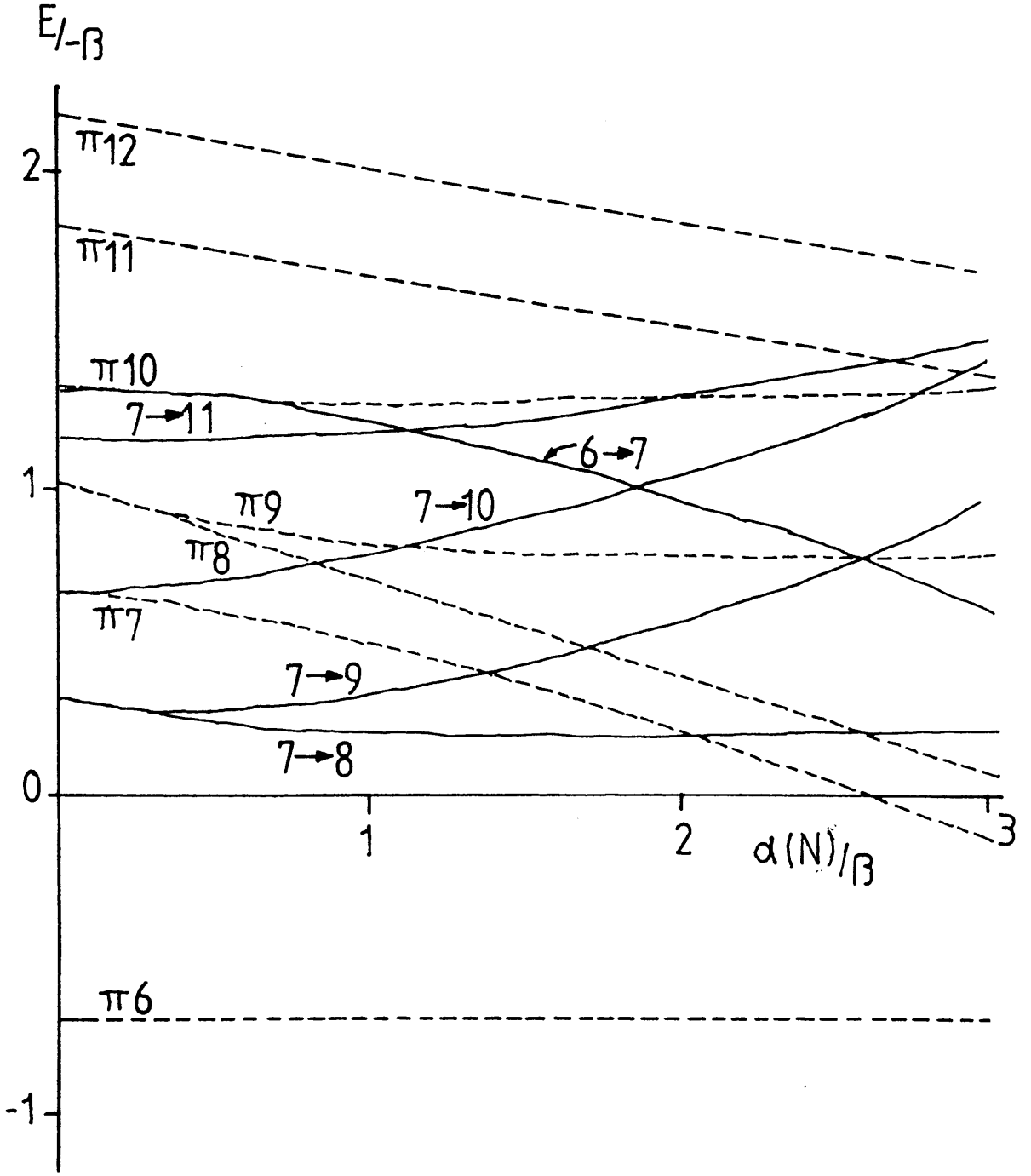

Figure 3.3 Plot of the Hückel orbital energies (----) and differences between Hückel orbital energies (——) against $\alpha(N)/\beta$ for 2,2'-bpy.

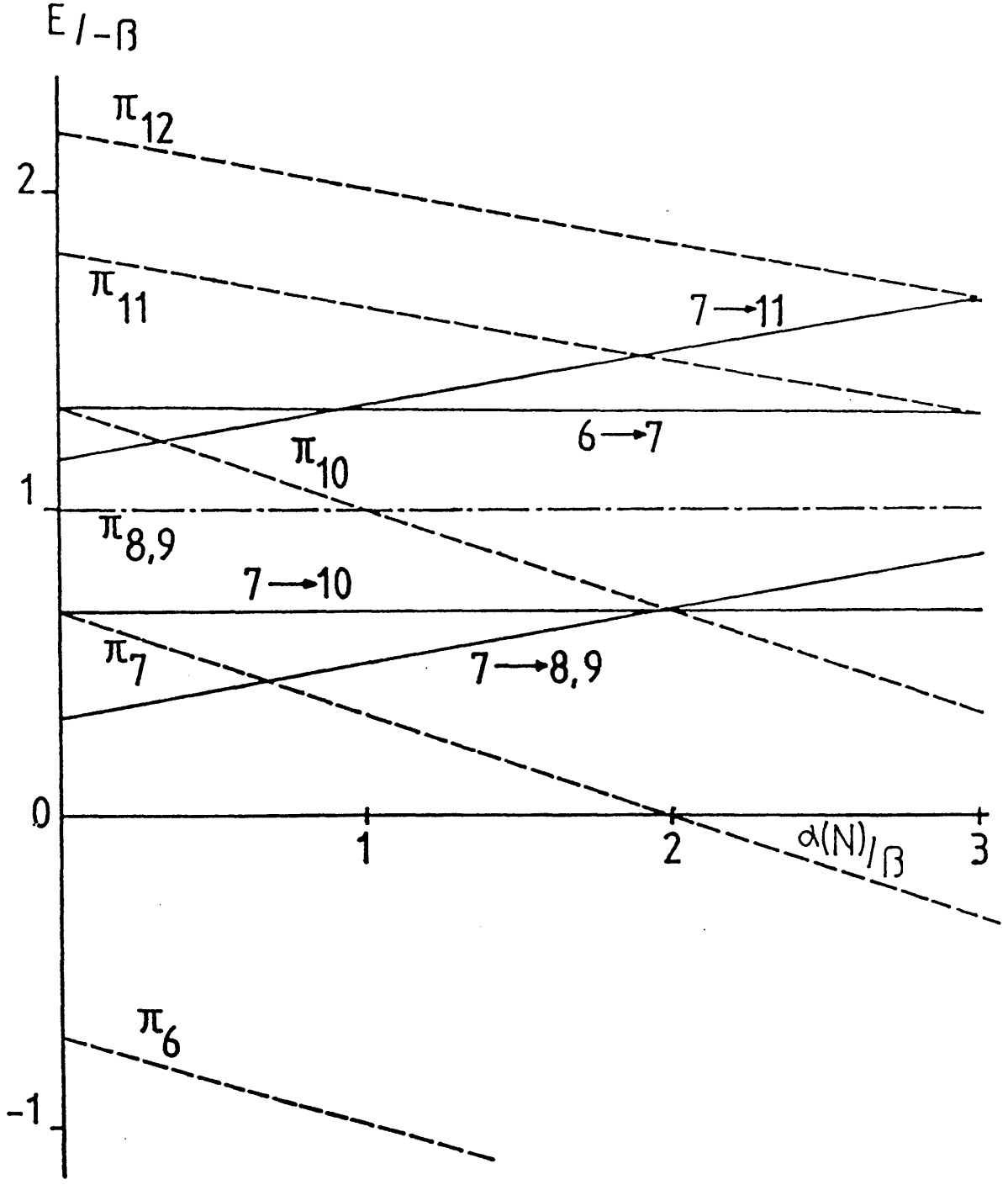

Figure 3.4. Plot of the Hückel orbital energies (----) and differences between Hückel orbital energies (——) against $\alpha(N)/\beta$ for 4,4-bpy.

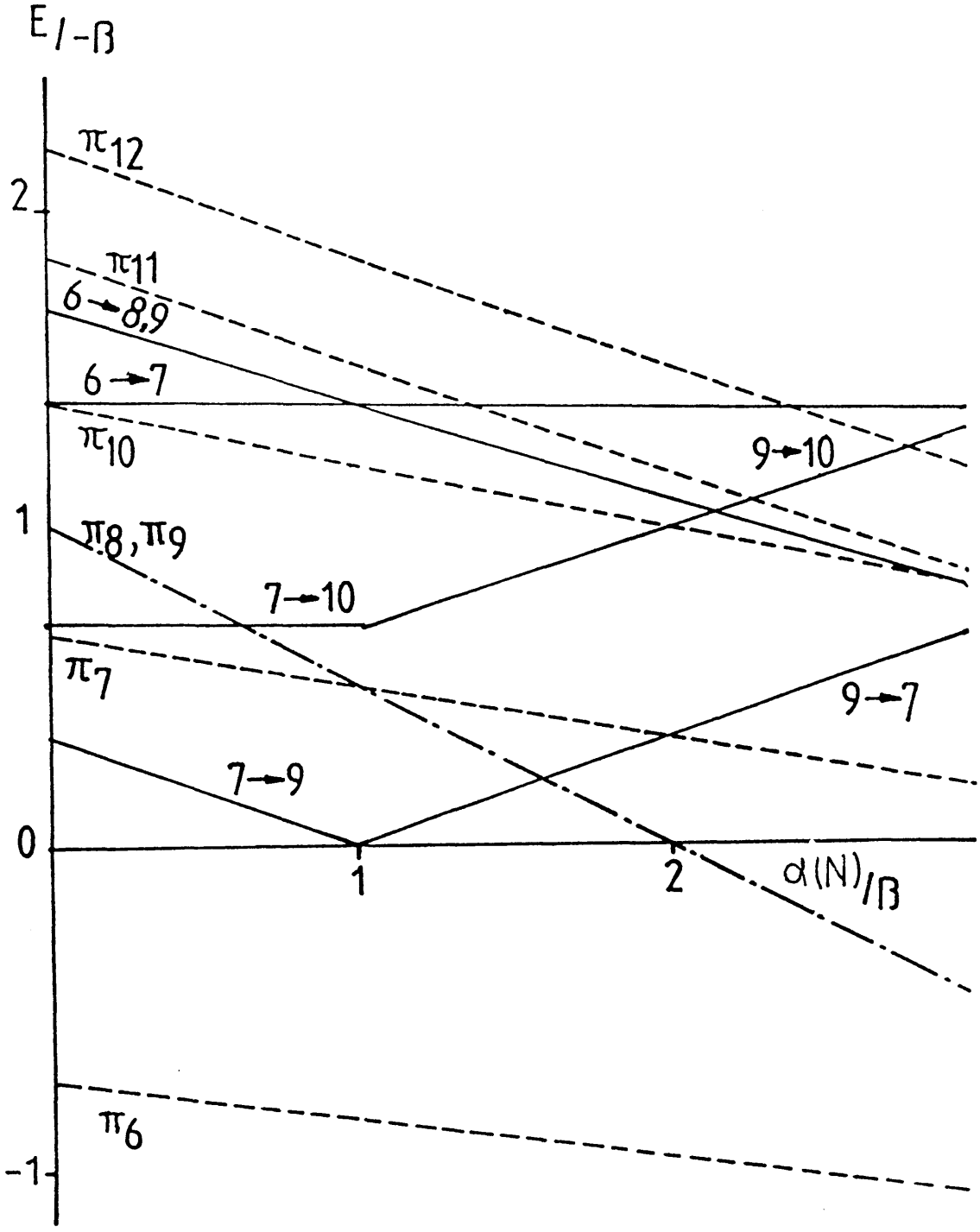

Figure 3.5 Plot of the Hückel orbital energies (----) and differences between Hückel orbital energies (——) against $\alpha(N)/\beta$ for 2,2'-bpym.

Chapter 4. Electrochemistry and Spectroelectrochemistry of Free Ligands and Organic Derivatives

4.1 REDUCTION POTENTIALS OF FREE LIGANDS AND ORGANIC DERIVATIVES.

The bpy anion M[bpy] has been made by reaction of sodium metal (or lithium metal) and 2,2'-bipyridine in tetrahydrofuran[63,64]. It was assumed that the lithium and sodium cations were coordinated to both nitrogen atoms of $[bpy]^-$ and that unpaired electrons resided in the π^* orbitals of the aromatic compound. However, one of the most generally applicable preparative methods for aromatic radical anions is electrochemical reduction. One electron reduction of bpy and related species form the appropriate radical anion.

In general, the free ligands examined show two accessible reductions, the first being chemically and electrochemically reversible (equation 1). However, the second one electron reduction is chemically irreversible except in the case of diquat and paraquat which both show reversible reductions.

$$I \rightarrow (I)^{\cdot -} \rightarrow (I)^{2-} \qquad (1)$$

Where I is bpy or related species

The measured reduction potentials of the free ligands are collected in table 4.1. The reduction potentials of the compounds are sensitive to the substituents. The relative orientation of the two pyridine rings (planar or twisted) may affect the degree of delocalisation of the added electron in the bpy radical anion. The peak separation (E_{pa}-E_{pc}) between the corresponding anodic and

Table 4.1. Reduction potentials of the free ligands and organic derivatives[A].

Compounds	$E_{red}^{(0/-1)}$	$E_{red}^{(-1/-2)}$
2,2'-bipyridine	-2.428 (0.074)[a]	-3.063 (0.116)
4,4'-dimethyl-2,2'-bipyridine	-2.651 (0.074)	
4,4'-bipyridine	-2.259 (0.069)	-2.740 (irr)[b]
2,2'-bipyrimidine	-2.287 (0.063)[i]	-2.804 (irr)
	-2.395 (0.040)[ii,c]	
1-methyl-2,2'-bipyridinium	-1.257 (irr)	
1,1'-dimethyl-2,2'-bipyridinium	-0.765 (qua)[c,d]	
1-methyl-4,4'-bipyridinium	-1.113 (0.065)	-1.621 (irr)
diquat (7, See Figure 1.1)	-0.504 (0.064)	-0.915 (0.074)
paraquat (6, See Figure 1.1)	-0.445 (0.065)	-0.821 (0.076)
	-0.740 (0.062)[i,e]	-1.120 (0.074)
	-0.670 (0.039)[ii,c,e]	

[A]Data from cyclic voltammetry, potentials in volts vs Ag/Ag^+ in DMF-$TBABF_4$ solution at room temperature. [a]E_{pa}-E_{pc} (V) [b]Denote (chemically) irreversible redox processes with peak potentials given (scan rate 200 mV/sec)

[c]Two-electron reduction process [d]Denotes a quasi-reversible redox process

[e]Solvents; water-KNO_3/KOH solution (0.1 mol dm^{-3})

[i]Concentration 0.005 mol dm^{-3} [ii]Concentration 0.02 mol dm^{-3}

cathodic peaks of each redox pair slightly exceeded the theoretical value for a one electron reversible reduction; 59 mV [(Fc/Fc^+) vs Ag/Ag^+ at room temperature]. The discrepancy was probably the result of slight ohmic loss or overvoltage.

4.1.1. Electrochemistry of 2,2'-bipyridine and its derivatives

Free 2,2'-bipyridine undergoes a reversible one-electron reduction at -2.428 V vs Ag/Ag^+ in dimethylformamide solution (Figure 4.1). The bpy-$[bpy]^-$ couple gives a typical one-electron cyclic voltammogram in such media. However, after holding at position A for 30 seconds, the second anodic peak (a) of 2,2'-bipyridine increased without changing position. The peak which appeared at position B could be explained by reaction products of 2,2'-bipyridine radical anion and DMF-$TBABF_4$ solution. It may be that the dianion can extract protons from the tetrabutylammonium cation, with the formation of butene and tributylamine[65].

Methyl substitution causes a shift to more cathodic potentials because the methyl group increases the electron density in the pyridine ring. Presumably for this reason, the second reduction of 4,4'-dimethyl-2,2'-bipyridine was not observed.

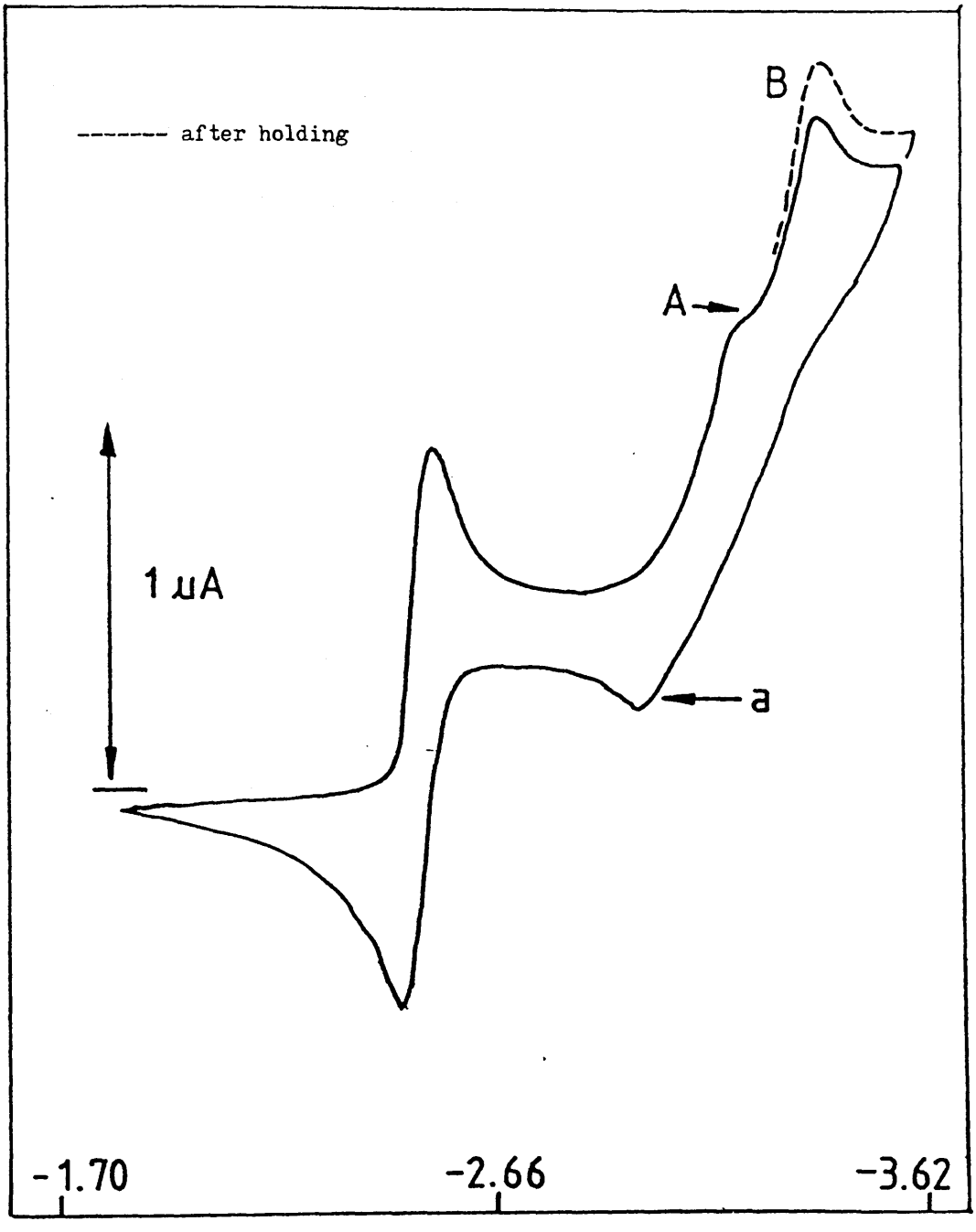

Figure 4.1 Cyclic voltammogram of 2,2'-bipyridine in DMF at room temperature.
V vs Ag/Ag^+, 200 mV/sec.

According to the cyclic voltammogram of diquat, both pairs of redox waves exhibit distintive reversible one-electron processes (Figure 4.2a) attributed to the electron delocalisation effect of the two pyridine rings when the diquat becomes reduced[17]. The free radical is stable, owing to delocalisation of its odd electron over the whole molecule. The probability of such delocalisation is illustrated by eighteen possible resonance forms which can be written for the radical without postulation of charge separation. Some of these structures do not involve conjugation between the ring (A), but six of the structures (B) involve conjugation *via* a double bond between the rings

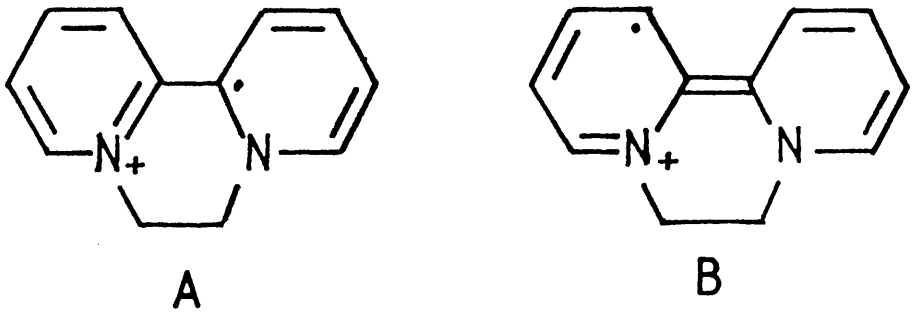

A B

The reduction stages of diquat are described in Figure 4.3.

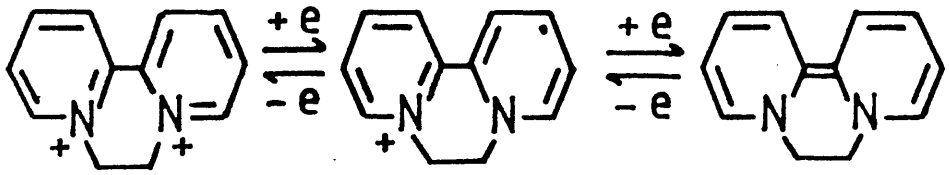

Figure 4.3. The two reduction stages of diquat.

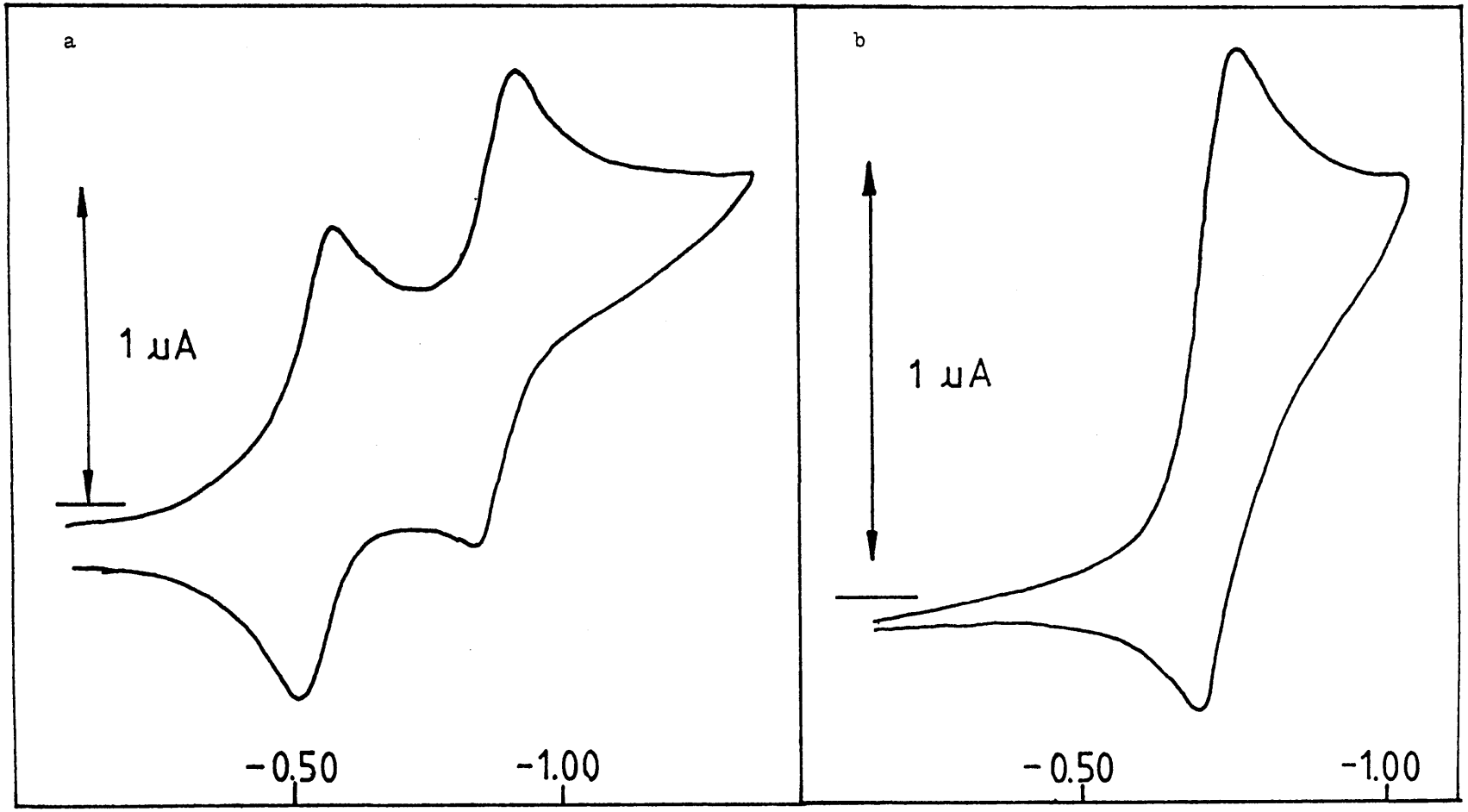

Figure 4.2. Cyclic voltammograms of diquat (a) and 1,1'-dimethyl-2,2'-bipyridinium (b) in DMF-$TBABF_4$ solution at room temperature. V vs Ag/Ag^+ 200 mV/sec

The stability of the original quaternary salt, however, is not dependent upon inter-ring conjugation; hence factors which tend to prevent ring coplanarity will tend to reduce the stability of the free radical relative to that of the unreduced salt. When compared with the 1,1'-dimethyl-2,2'-bipyridinium dication, diquat should be better conjugated, because the two pyridine rings can adopt a near planar conformation. The 1,1'-dimethyl-2,2'-bipyridinium dication is less conjugated than diquat because the methyl quaternising groups sterically hinder the adoption of a coplanar conformation by the two pyridine rings[66]. High resolution X-ray diffraction analysis of the diquat dication confirms that the two pyridine rings are nearly coplanar with a dihedral angle between the planes of the pyridine ring of about 20° [67]. The dihedral angle of the 1,1'-dimethyl-2,2'-bipyridinium dication, as expected, is much larger at about 75° [68]. Electrochemical studies of the 1,1'-dimethyl-2,2'-bipyridinium dication (Figure 4.2b) have revealed that the diquaternised bipyridinium, unlike paraquat, undergoes a one step reduction in which the single step involves two electrons and is quasi-reversible at a scan rate of 200 mV/sec. This two-electron reduction process may be explained by intermolecular radical-radical coupling at the 4,4'-positions, which are sterically unhindered. The reduction potential of diquat (-0.504 V) is less negative than that of the 1,1'-dimethyl-2,2'-bipyridinium dication (-0.765 V). This is attributed to the high degree of conjugation between the rings in the diquat radical, which is related to the amount of steric hindrance in the molecule.

4.1.2. Electrochemistry of 4,4'-bipyridine and its derivatives.

The reduction potentials of 2,2'-bipyridine and 4,4'-bipyridine are -2.428 and -2.259V respectively, thus the reduction of 4,4'-bipyridine is some 170mV easier than that of 2,2'-bipyridine. This is consistent with the simple theoretical treatment, in which the electron density in the reduction orbital is lower when the N atom is in the para position rather than the ortho position to the ring-ring bond. 4,4'-Bipyridine, monoquat and paraquat are all well established two step reversible redox systems[65,69-70], whose redox potentials lie in a convenient range for electrochemical measurements.

As was the case with the diquaternary 2,2'-bipyridinium, the reduction of the paraquat dication by one-electron reducing agents in a solvent system gives rise to an intense violet colour because of the stable radical cation. The one electron transfer is completely reversible and the radical cation can take up the second electron to form the neutral, doubly reduced, species. The stability of the radical cation is due to the ability of the odd electron to be located at any of the nuclear positions because of the coplanarity of the two pyridine rings. The reduction stages of 4,4'-bipyridine and paraquat are described in Figure 4.4. Paraquat exists in three main reduction states, the first reduction step is chemically and electrochemically highly reversible and can be cycled many times without significant side reactions. Further reduction to the fully reduced state, however, is less completely electrochemically reversible.

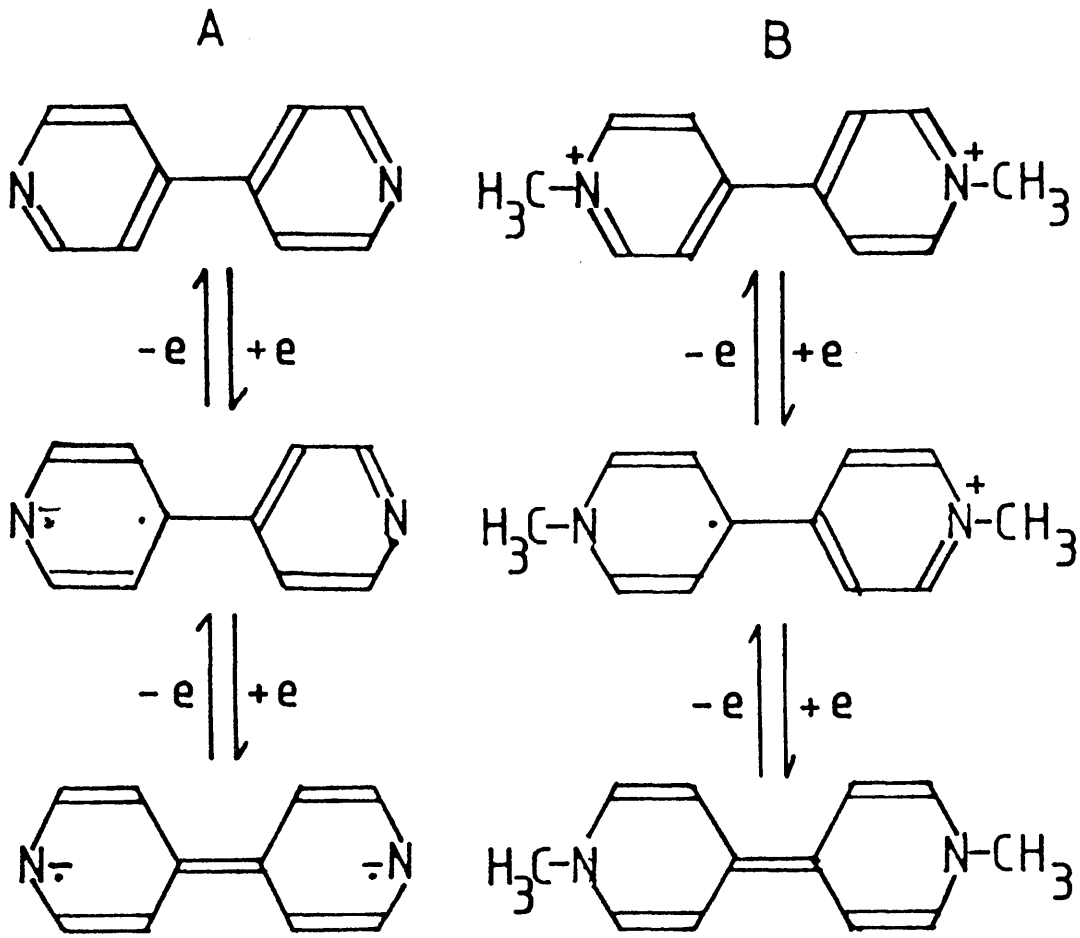

Figure 4.4. Schematic diagram of the reduction steps of 4,4'-bipyridine and paraquat.

Taking the reaction, we may measure the reversible potentials for each step for a given paraquat and may formulate here the so-called 'conproportionation' and 'disproportionation' reactions. These reactions can take place both in solution and at the surface of the electrode[71]. In the latter case, the

$$2V^{\cdot+} \rightarrow V^{2+} + V^{\cdot} \qquad \text{(disproportionation)}$$

$$V^{0} + V^{2+} \rightarrow 2V^{\cdot+} \qquad \text{(conproportionation)}$$

process may be a combination of the homogeneous reaction and coupled anodic and cathodic reactions on the platinum electrode surface at especially high concentration.

$$V^0 - e \rightarrow V^{\cdot+} \quad \text{(anodic)}$$

$$V^{2+} + e \rightarrow V^{\cdot+} \quad \text{(cathodic)}$$

$$V^0 + V^{2+} \rightarrow 2V^{\cdot+} \quad \text{(overall)}$$

The cyclic voltammograms of paraquat in DMF and water are shown in Figure 4.5. The first reduction potential of paraquat in DMF occurs at -0.445 V and further reduction of the radical forms the sparingly soluble, neutral species at -0.821 V. These redox potentials are explained on the basis of the degree of resonance stabilisation due to the delocalisation of the free electron in the radical cation when the dication is reduced by one electron[72,73]. In dilute aqueous solution (5×10^{-3} mol dm^{-3}), the corresponding values are -0.740 and -1.120 V, reflecting the stabilisation of the dication by the more polar solvent. However, in relatively concentrated aqueous solution such as (1×10^{-2} mol dm^{-3}) the cyclic voltammogram of paraquat shows a reversible two-electron reduction process at -0.624 V which presumably is due to formation of a dimer. This argument can be applied to the conproportionation reaction between the parent paraquat and the doubly reduced paraquat. At low concentration

$$MV^{2+} + MV^0 \rightleftharpoons 2MV^{\cdot+}$$

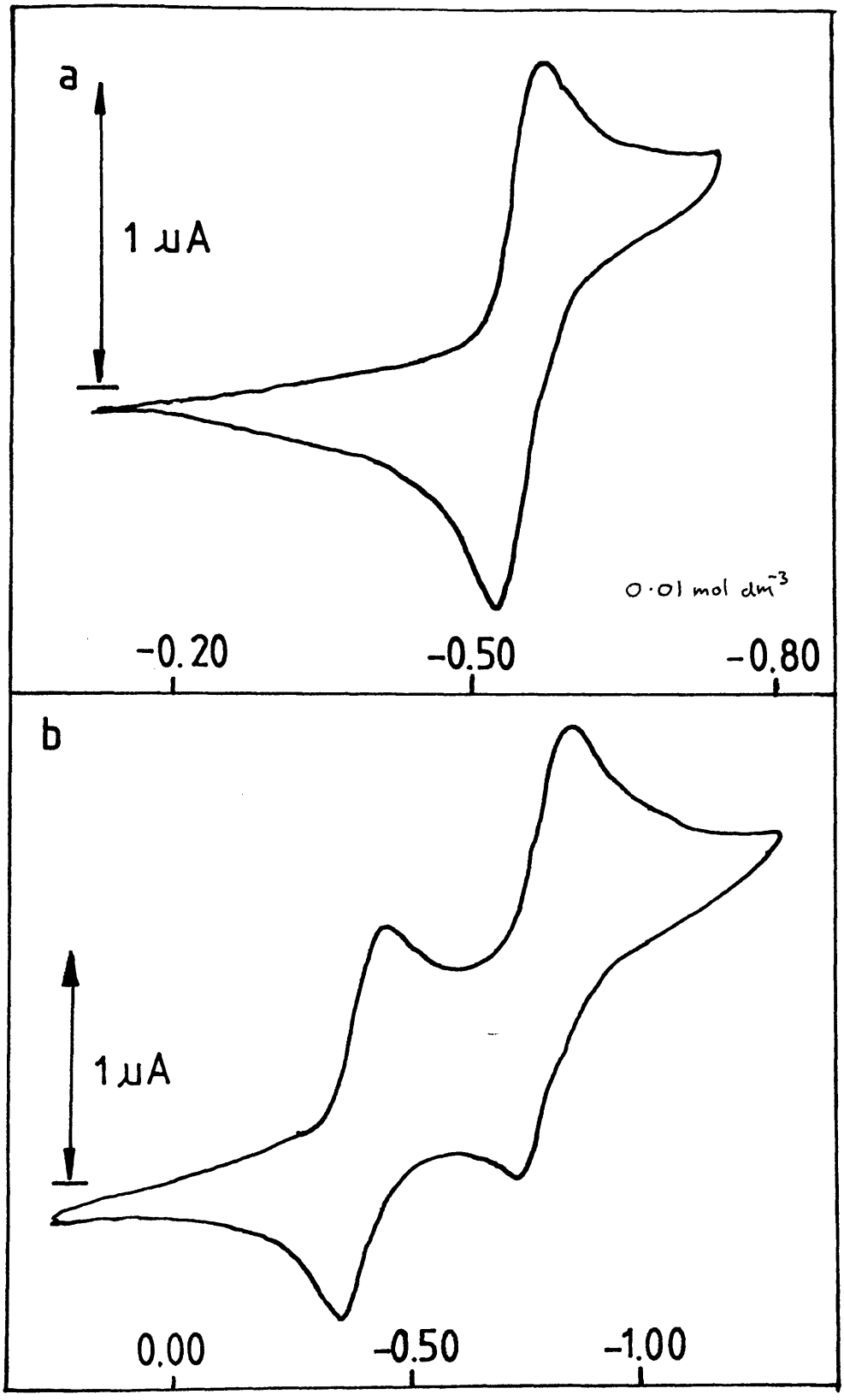

Figure 4.5 Cyclic voltammograms of paraquat in water-KNO_3/KOH (a) and DMF-$TBABF_4$ (b) at room temperature. V vs Ag/Ag^+ 200 mV/sec.

such as $1x10^{-3}$ mol dm^{-3} in aqueous media or any concentrations in non-aqueous media such as acetonitrile or dimethylformamide, the cyclic voltammogram shows no evidence of dimerisation. This means the dimerisation is dependent upon the concentration of paraquat in water solution, and probably ion-pair formation or charge repulsion in DMF or acetonitrile preclude dimerisation. As a result, the typical electrochemical characteristics of paraquat are as follows. (in dilute aqueous and non-aqueous solutions)

1. It undergoes reversible, simple electron transfer steps.

2. Redox states are chemically and electrochemically stable and undergo no structural or bonding changes[74].

4.1.3. Electrochemistry of 2,2'-bipyrimidine and 1,10-phenanthroline derivatives.

2,2'-Bipyrimidine undergoes a reversible one-electron reduction at -2.287 V vs Ag/Ag^+ in DMF-$TBABF_4$ solution. The redox potential is shifted to a less negative value compared to that of 2,2'-bipyridine, because nitrogen is more electronegative than the carbon it replaces, and the π^*-orbitals would be expected to be lower in energy for the 2,2'-bipyrimidine than for 2,2'-bipyridine[75]. The second reduction is an irreversible one-electron process with no electrochemical reaction similar to that of 2,2'-bipyridine after completion of the second reduction. The cyclic voltammogram of the 2,2'-bipyrimidine free ligand is shown in Figure 4.6. At the relatively high concentration of 0.01 mol dm^{-3}, the first redox wave of 2,2'-bipyrimidine was shifted to a more

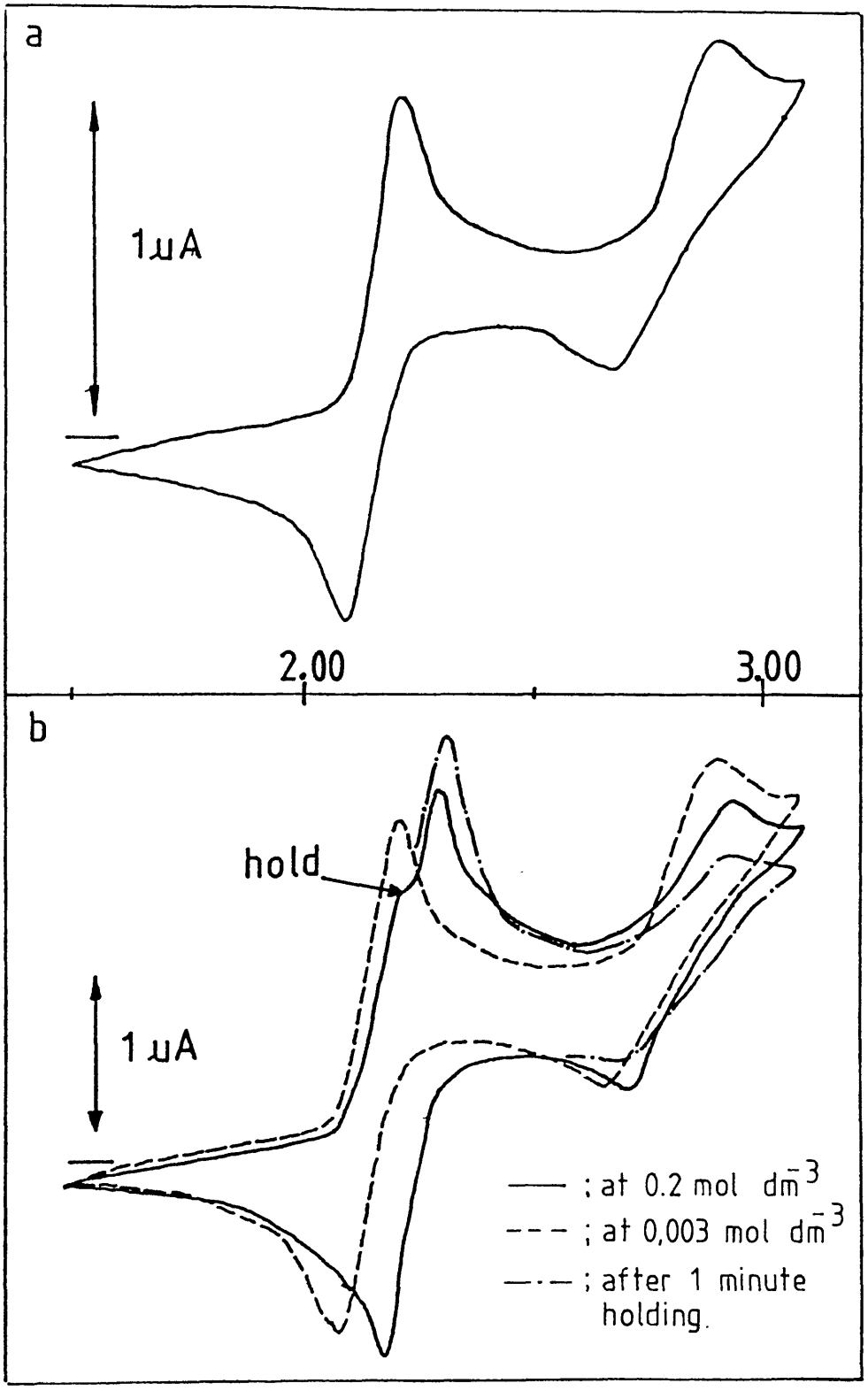

Figure 4, 6 Cyclic voltammograms of 2,2'-bipyrimidine (a: 0.003 mol dm^{-3}, b: 0.2 mol dm^{-3}) in DMF at room temperature. V vs Ag/Ag^{+}, 200 mv/sec.

negative potential (-2.395 V) and a shoulder appeared around -2.29 V. After holding at -2.287 V for 1 minute, the first reduction wave became more intense and the second reduction peak almost disappeared. The shifted reduction potential which appeared at -2.395 V had a reduced peak to peak separation (from 63 mV to 40 mV). This is strong evidence for a one step two-electron reduction. This two electron reduction process is presumably due to the dimerisation during the electrolysis.

The polarographic behaviour of 1,10-phenanthroline has been studied in aqueous solution, but interpretation of the reduction waves is not always certain because of complications due to adsorption and catalytic hydrogen waves. There are two clear reduction waves obtained with 1,10-phenanthroline and its derivatives in DMF[76]. The reduction potentials are listed in Table 4.2. 1,10-Phenanthroline and its derivatives show a irreversible one-electron reduction process for the first reduction which is due to a rapid chemical protonation reaction. Hoijtink *et al.*[77] have reported that hydrogenation occurs at the 5,6 positions. The first reduction of 1,10-phenanthroline at -40 °C shows a small return wave while the second wave is reduced in relative intensity.

5-Chloro-1,10-phenanthroline gives three redox waves. The first and second redox waves resemble the reduction of 1,10-phenanthroline itself. The gap between the reversible second and third reduction potentials is only about 200 mV, making assignment difficult.

It is not possible to obtain the simple methyl diquaternary 1,10-phenanthrolinium ion because of steric difficulties.

Table 4.2. Redox potentials of 1,10-phenanthroline and its derivatives[a]

Compounds	$E_{red}^{(0/-1)}$	$E_{red}^{(-1/-2)}$
1,10-phenanthroline	-2.190 (irr)[b]	-2.406(0.084)[c]
neocuproine (2,9-dimethyl-1,10-phenanthroline)	-2.295 (irr)	-2.491 (0.091)
5-chloro-1,10-phenanthroline[d]	-1.980 (irr)	-2.170 (0.080)
5,6-dihydropyrazino[1,2,3,4-l.m.n]-1,10-phenanthrolinium (8a, Figure 1.1)	-0.406 (0.107) qua[e]	-0.850 (irr)
5H-6,7-dihydro-1,4-diazepino [1,2,3,4-l.m.n]-1,10-phenanthrolinium (8b)	-0.400 (0.101) qua	-0.795 (irr)
4H,5H-6,7-dihydro-1,4-diazino-[1,2,3,4-l.m.n]-1,10-phenanthrolinium (8c)	-0.575 (irr)	
Pyrazino[1,2,3,4-l.m.n]-1,10-phenanthrolinium (10)	-0.304 (irr)	

[a]Data from cyclic voltammetry, potential in volts vs Ag/Ag^+ in DMF-$TBABF_4$ solution at room temperature. [b]Denotes irreversible redox processes with peak potentials given (scan rate 200 mV/sec) [c]E_{pa}-E_{pc} (V)
[d]A third reduction wave appeared at -2.367 V (reversible; E_{pc}-E_{pa} = 0.083 V)
[e]Denotes a quasi-reversible redox process.

However, some diquaternised compounds were obtained, using 1,2-bromoethane, 1,3-bromopropane etc. like the analogous compounds from 2,2'-bipyridine. Summers[78] has reported, that similarly to diquaternised 2,2'-bipyridinium, diquaternised 1,10-phenanthroline becomes a radical cation in water when it is treated with Zn powder, and shows a reversible reduction wave at around -0.30 V.

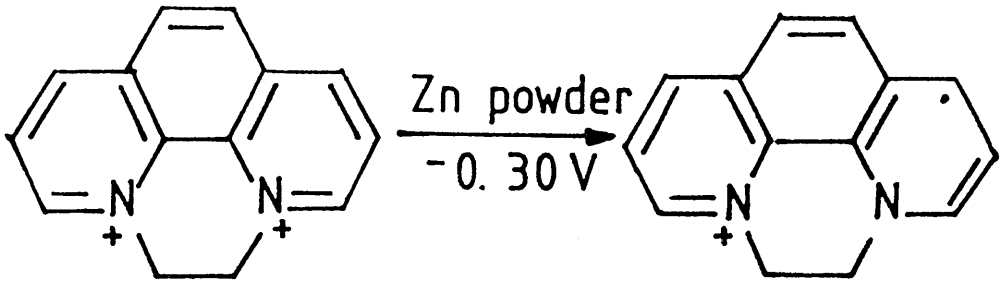

As expected, for the derivatives of the very rigid planar phenanthroline ring system, the redox potentials of 5,6,-dihydropyrazino[1,2,3,4-l.m.n]-1,10-phenanthrolinium and 5H-dihydro-1,4-diazepino[1,2,3,4-l.m.n]-1,10-phenanthrolinium were almost identical, but 4H,5H-6,7-dihydro-1,4-diazino-[1,2,3,4-l.m.n]-1,10-phenanthrolinium moved to a more cathodic potential causing the loss of its rigidity compared to the former two compounds. The reduction potential of Pyrazino[1,2,3,4-l.m.n]-1,10-phenanthrolinium appeared at -0.314 V. This more negative potential was due to the full aromaticity of the molecule.

4.2. Electronic absorption spectra of free ligands.

Bipyridine and bipyrimidine can be considered to have twelve Hückel molecular π-orbitals[79]. The first six of these orbitals are bonding orbitals and will be completely filled in the neutral molecule. In the neutral ligand, the lowest energy π to π* transition is π(6) (HOMO) to π(7) (LUMO) and occurs in the range 260 - 300 nm. This transition still occurs in the reduced species, in which π(7) is half full, but lower energy transitions from π(7) to π(8-11) are now possible. The occupancies of the π-orbitals of both bpy, bpym and their radical anions are shown in Figure 4.7[80].

There are strong resemblances between the spectra reported by Kalyanaraman, Rao, and George for the alkali metal reduction of 4,4'-bipyridine[81], the transient spectra found by Simic and Ebert after pulse radiolysis of 4,4'-bipyridine in water at pH 3.7 or 5[82] and our spectra for singly reduced 4,4'-bipyridine, monoquat and paraquat. The main difference is that we observe the relatively weak π(7) → π(9) transition, which is symmetry allowed in planar biphenyl although the transition with which it correlates in benzene is forbidden. As required by D_{2h} symmetry, however, π(7) → π(8) is very weak or absent. We infer that, as required by our simple theory, the relative energies of π(7), π(9) and π(10) are insensitive to the effective electronegativity of nitrogen. All these spectra can be accommodated by the same molecular orbital scheme, with N-methylation lowering the energies of the LUMO and near-LUMO orbitals without changing their nature.

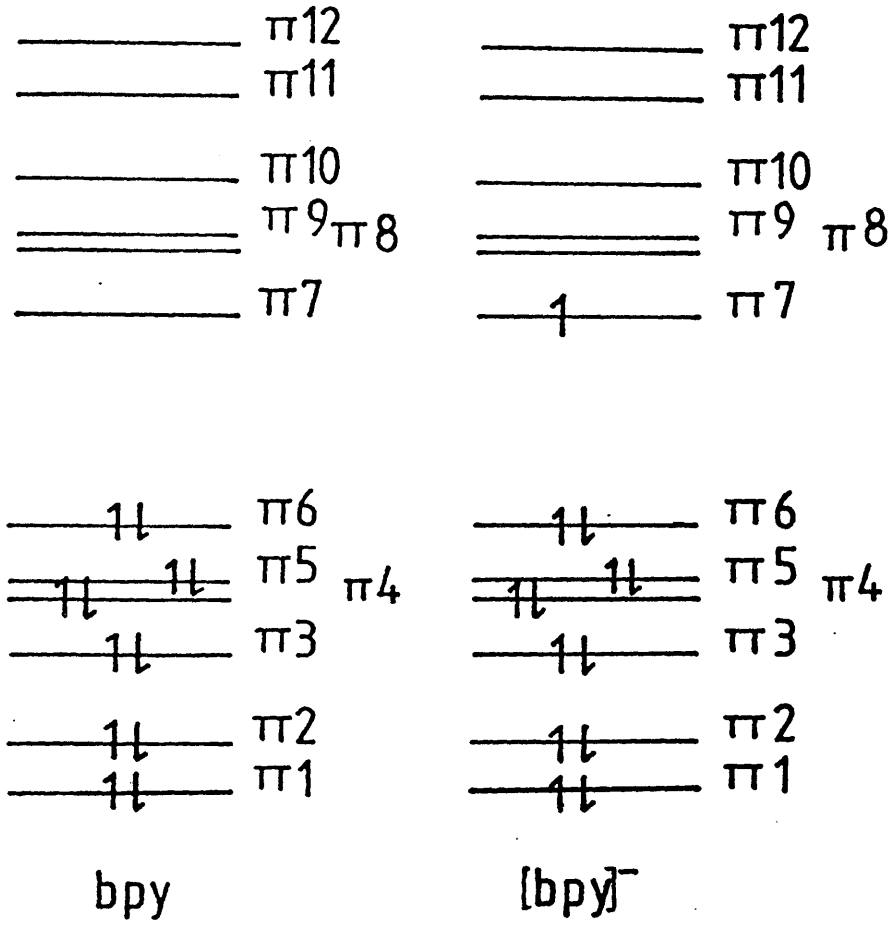

Figure 4.7 The occupancies of π-orbitals of bpy and related species

The spectra of the 4,4'-bipyridine anion and its N-protonated conjugated acid should also be very similar, thus accounting for the insensitivity of the pulse radiolysis results to pH. The shift of $\pi(7) \rightarrow \pi(9)$ to higher energy on methylation is also in accord with theory, since $\pi(7)$ is more localised than $\pi(9)$ on the para positions of the rings.

4.2.1 Spectroelectrochemistry of 2,2'-bipyridine and its derivatives.

(a) 2,2'-Bipyridine

The absorption spectra of singly and doubly reduced 2,2'-bipyridine have been assigned by König and Kremer[64]. The spectrum of $[bpy]^-$ was assigned as follows. The strongest band at 397 nm was assigned as the $\pi(6) \rightarrow \pi(7)$ transition and the band centered at 580 nm was assigned as a $\pi(7) \rightarrow \pi(10)$ transition . The bands between 800 nm and 1000 nm were assigned as $\pi(7) \rightarrow \pi(8,9)$ transitions. The high energy bands in the UV region, which could not be individually assigned, were collectively assigned as $\pi(6) \rightarrow \pi(8,9)$, $\pi(4) \rightarrow \pi(7)$ and $\pi(5) \rightarrow \pi(7)$ transitions. The absorption spectra of bpy and $[bpy]^-$ (obtained in a 1mm O.T.T.L.E. cell at potential of -2.460 V vs Ag/Ag^+) is shown in Figure 4.8. A diagram of all the possible transitions of the 2,2'-bipyridine anion radical and dianion radical is shown in Figure 4.9.

The most intense band occuring at around 397 nm was assigned to the $\pi(6) \rightarrow \pi(7)$ transition. This shows an irregular

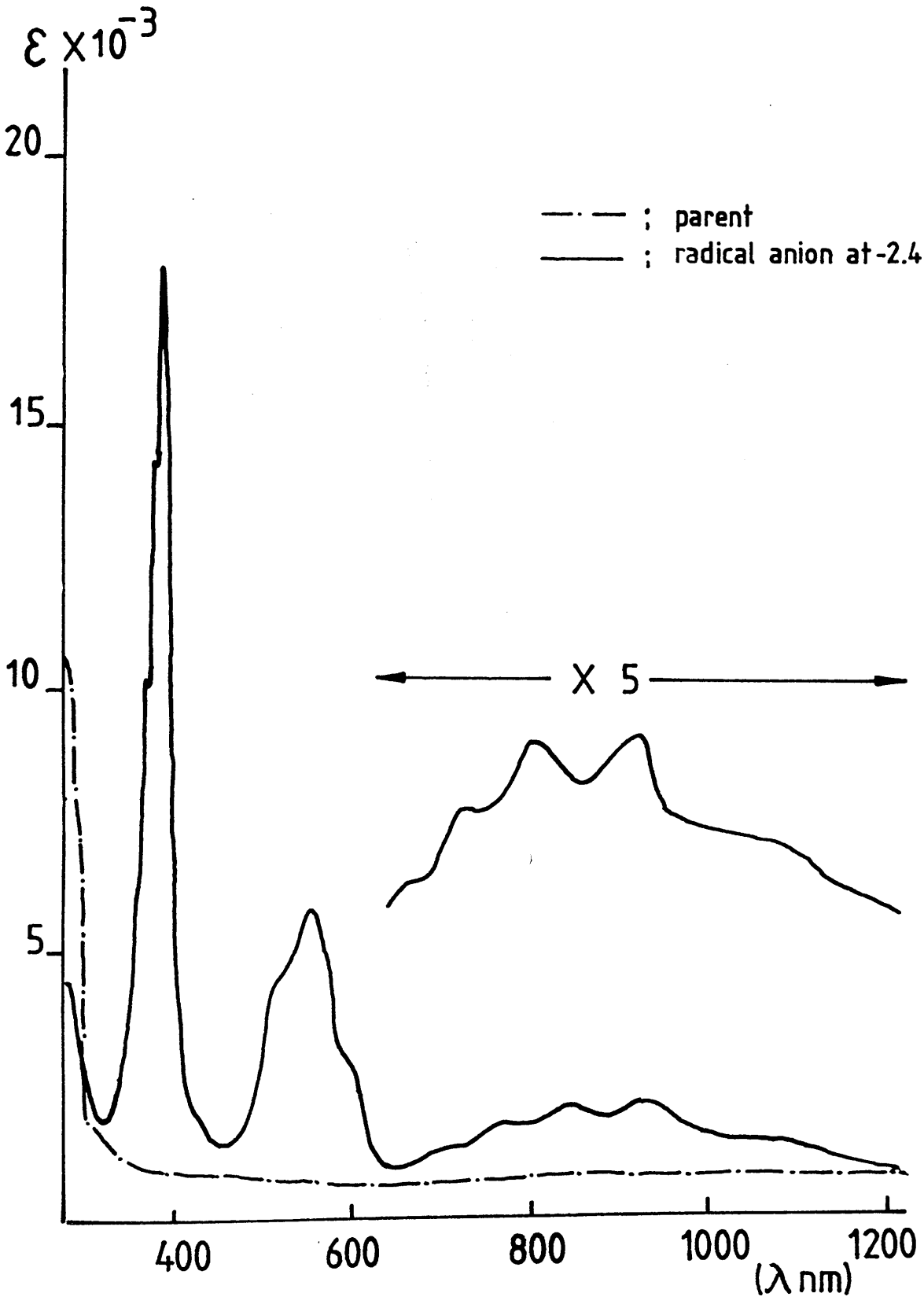

Figure 4.8 Absorption spectra of bpy and $[bpy]^-$ in DMF at room temperature.

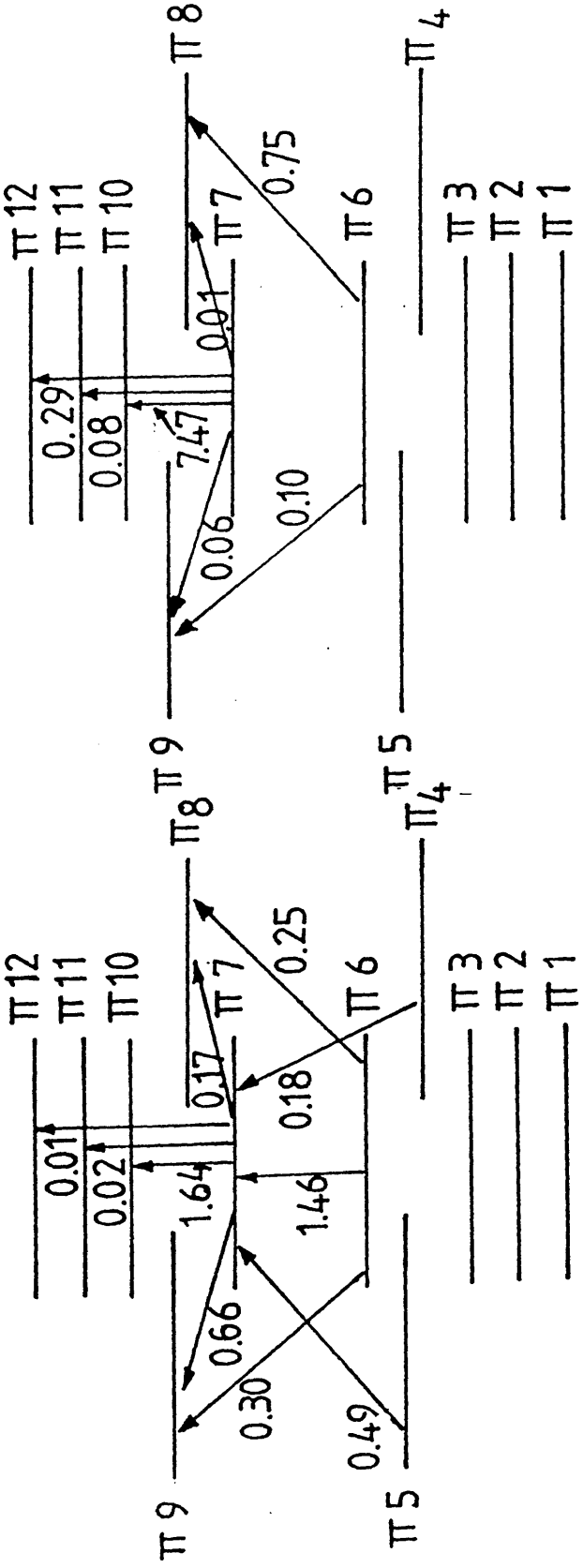

Figure 4.9 Schematic diagrams of possible transitions of 2,2'-bipyridinium anion radical and dianion radical and their dipole strengthes (in $Å^2$) 64

vibrational pattern from 800 cm^{-1} to 1100 cm^{-1} [80], which is presumably due to ortho C-H bending modes. The general shift of the $\pi(6) \rightarrow \pi(7)$ transition to lower energy on reduction might be due to a structural change from the twisted 2,2'-bipyridine parent molecule to a planar 2,2'-bipyridine anion radical. This is because the electron added to the $\pi(7)$ orbital of 2,2'-bipyridine confers some double bond character across the bond between the two pyridine rings and the rings will orientate themselves to become planar with respect to each other in order to maximise the π-overlap across the bond.

According to the calculations of König and Kremer[64], the $\pi(7) \rightarrow \pi(11)$ transition of the 2,2'-bipyridine radical anion should appear in the same region as the $\pi(6) \rightarrow \pi(7)$ transition. However, the $\pi(7) \rightarrow \pi(11)$ transition band could not be detected. This is probably due to its very weak dipole strength (0.02 $Å^2$) relative to that of the $\pi(6) \rightarrow \pi(7)$ transition (1.46 $Å^2$), and so it must be masked by the strong absorption band of the $\pi(6) \rightarrow \pi(7)$. transition

The lowest energy transitions between 650 nm to 1300 nm have been assigned to the $\pi(7) \rightarrow \pi(8,9)$ transitions[64]. Noble[80] reported that these two transitions could be distinguished by measuring the vibrational intervals. When the vibrational intervals were measured between 1000 nm and 1300 nm the interval was approximately 1360 cm^{-1}, but between 650 nm and 1000 nm the interval was 1390 cm^{-1}. Hence the band at higher energy which has a vibrational progression of 1390 cm^{-1} and which has relatively high intensity was assigned as the

$\pi(7) \rightarrow \pi(9)$ transition, and the band at lower energy which has vibrational progression of 1360 cm^{-1} and which has relatively low intensity was assigned as the $\pi(7) \rightarrow \pi(8)$ transition. Both the MNDO[80] and the simple one-electron molecular orbital calculations place the orbital energy of $\pi(8)$ below that of $\pi(9)$; thus the transition from $\pi(7)$ to $\pi(8)$ requires less energy than the transition from $\pi(7)$ to $\pi(9)$. (Figure 4.10)

The $\pi(7)$ and $\pi(10)$ orbitals have a significant double bond character in both of the rings, although the $\pi(10)$ orbital has no double bond character between the rings. However, the $\pi(9)$ and $\pi(8)$ orbitals appear to have very little double bond character, either in the rings or between the rings. Both the $\pi(7) \rightarrow \pi(9)$ and the $\pi(7) \rightarrow \pi(8)$ transitions should therefore have similar characteristic vibrational progressions. Finally, the vibrational progression of 1450 cm^{-1} in the $\pi(7) \rightarrow \pi(10)$ transition is possibly due to the symmetric inter-ring stretching mode of the 2,2'-bipyridine radical anion.

(b) 4,4'-Dimethyl-2,2'-bipyridine

The electronic absorption spectrum of the 4,4'-dimethyl-2,2'-bipyridinium radical anion is shown in Figure 4.11 and is similar to that of singly reduced 2,2'-bipyridine except that all the $\pi^* \rightarrow \pi^*$ transitions are shifted to slightly higher energy. This is because the methyl substituents on the nitrogen atoms increase the electron density in the pyridine ring, thus the $\pi \rightarrow \pi^*$ and $\pi^* \rightarrow \pi^*$ transitions of this molecule require more energy than those of the 2,2'-bipyridine radical anion.

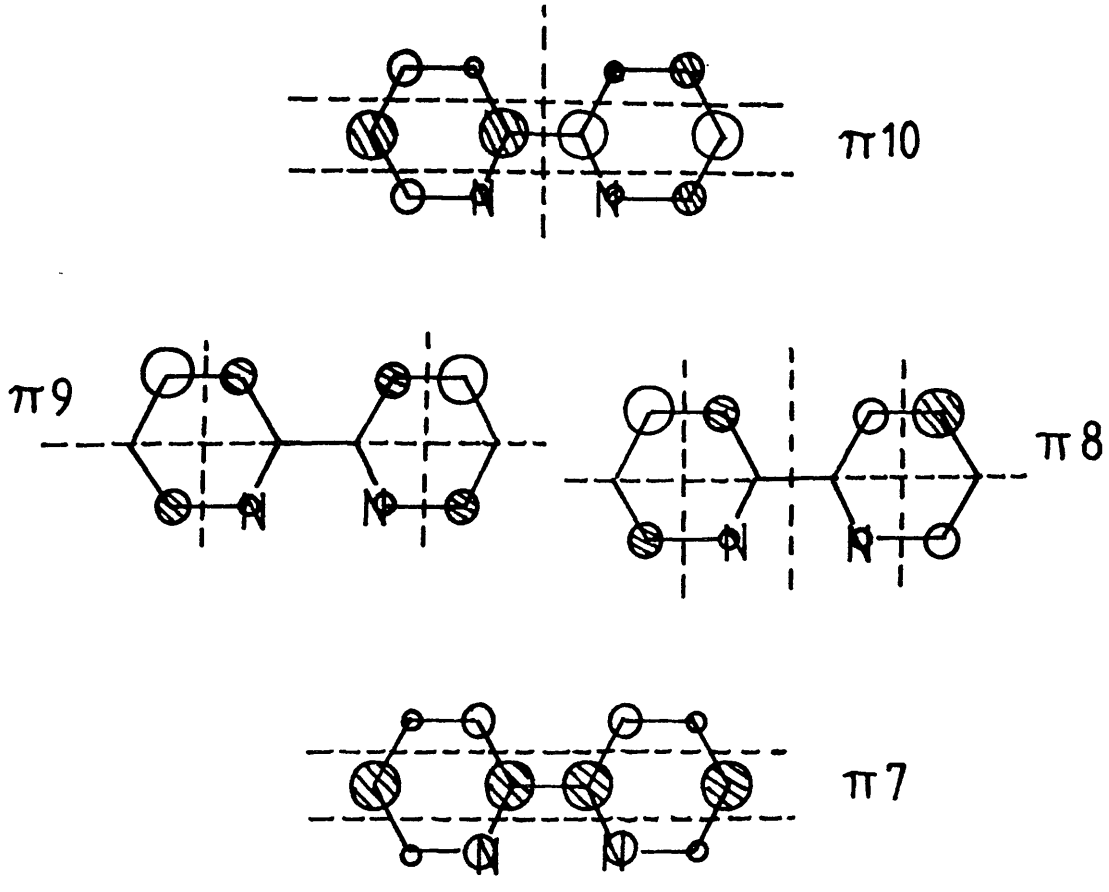

Figure 4.10 Schematic diagram of the molecular orbitals of 2,2'-bipyridine calculated by MNDO and simple one electron models.

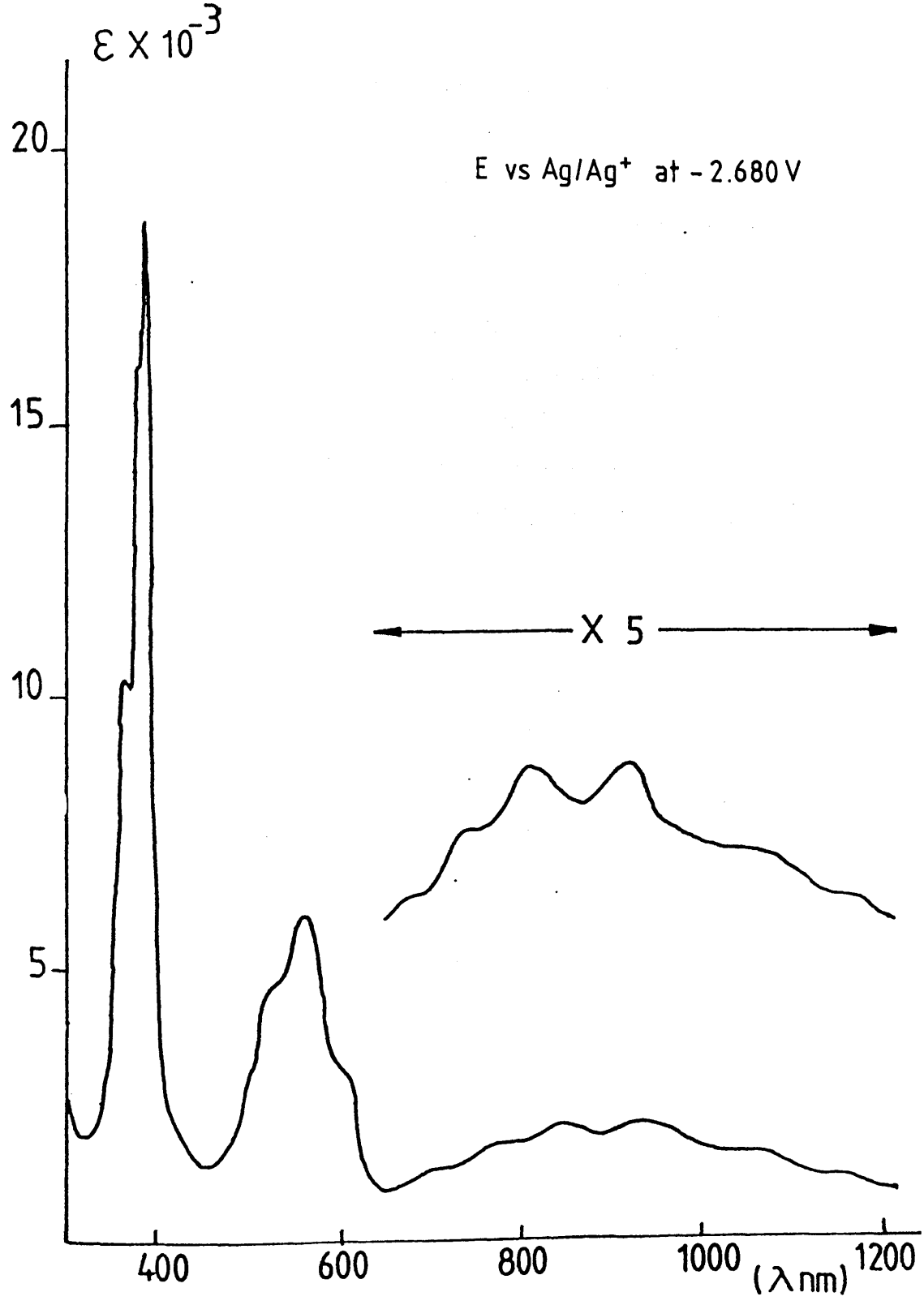

Figure 4.11. The electronic absorption spectrum of 4,4'-dimethyl-2,2'-bipyridinium radical anion in DMF at room temperature.

(c) Diquat

The interpretation of the electronic absorption spectra of the diquat radical cation and doubly reduced diquat are quite complicated (Figure 4.12). In singly reduced diquat, the band at 313 nm is assigned to the $\pi(6) \rightarrow \pi(7)$ transition. However, this transition does not shift to lower energy compared to that of the parent molecule, unlike the $\pi(6) \rightarrow \pi(7)$ transition of the 2,2'-bipyridinium radical cation. This is presumably due to the fact that the inter-ring angle is similarily constrained in diquat and its reduced species[83]. The band centred at 425 nm is assigned to the $\pi(7) \rightarrow \pi(10)$ transition and the bands between 800 nm and 1100 nm are assigned to the $\pi(7) \rightarrow \pi(8,9)$ transitions. The principle bands of 2,2'-bipyridine and its derivatives are shown in Table 4.3. Compared to singly reduced 2,2'-bipyridine, all the $\pi^* \rightarrow \pi^*$ transitions of the diquat radical cation appear at higher energies, presumably due to the structural difference between the molecules. The two aromatic rings can not twist because of the ethylene bridge, as they can in 2,2'-bipyridine. Hence, after one electron is added, the dihedral angle of the diquat cation radical does not change much. The spectrum of doubly reduced diquat is less easily understood, since the species is no longer aromatic and the transitions are from closed shell to open shell. In doubly reduced diquat, a new band with strong intensity appears at 392 nm and a very broad, wide band with vibrational structure appears between 600 nm and 1100 nm. This spectrum is similar to that which Creutz[84] attributed to singly reduced diquat in neutral aqueous solution. Erhard *et al.*[85] reported that reduced diquat formed a polymer in aqueous solution when the diquat solution was very concentrated, and Mullazzani *et al.*[86]

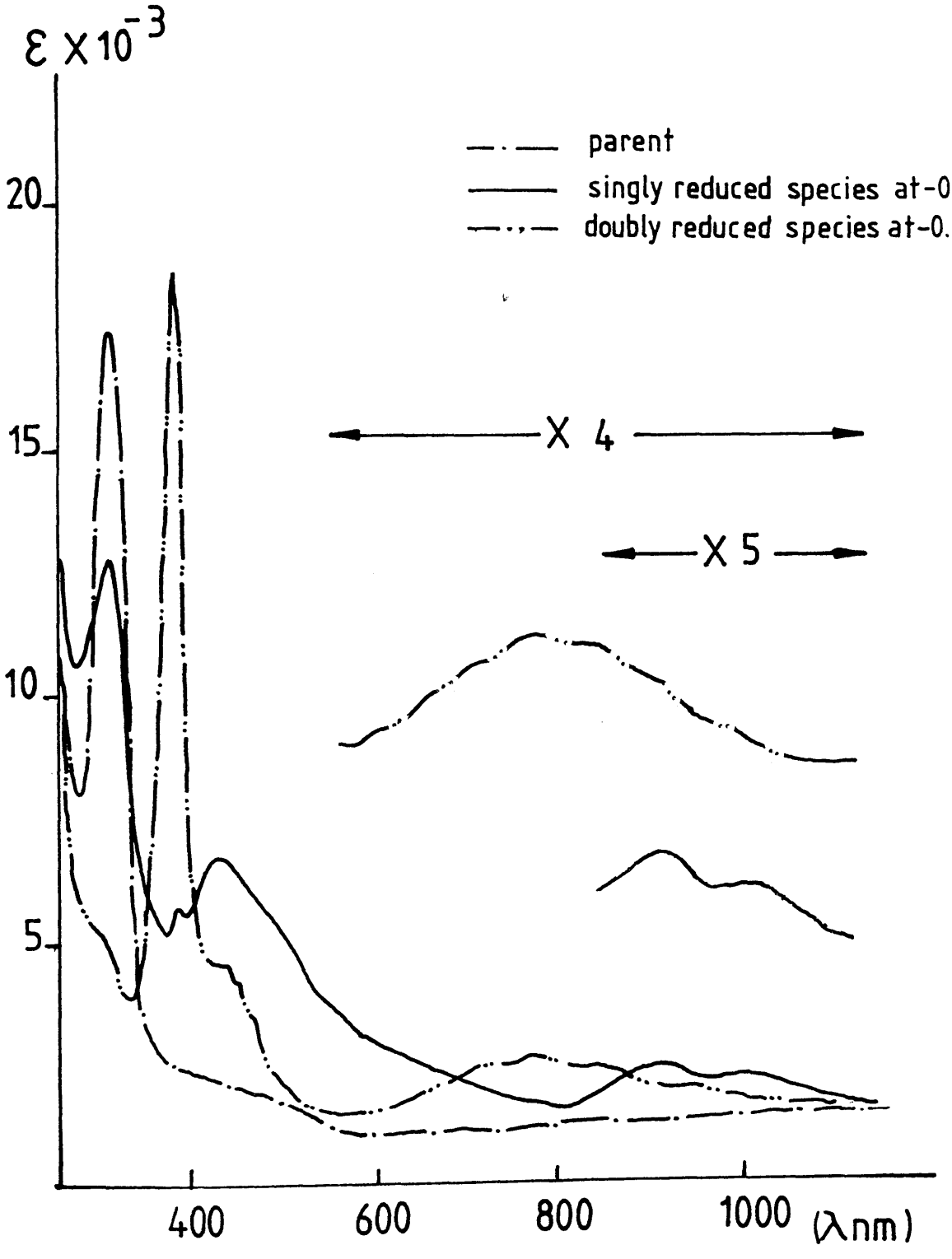

Figure 4.12 Absorption spectra of parent, singly and doubly reduced diquat in DMF at room temperature.

Table 4.3. The main bands of reduced 2,2'-bipyridine and its derivatives in DMF-$TBABF_4$ solution at room temperature.[λnm ($\bar{\upsilon}$ cm^{-1})]

	2,2'-bipyridine	4,4'-dimethyl 2,2'-bipyridine	diquat
	368 (27173)w[a]	357 (28011)w	313 (31948)vs[b]
	380 (26315)vw[c]	368 (27173)vw	
	397 (25188)vs	384 (26041)vs	
singly	501 (19960)sh[d]	493 (20283)sh	395 (25316)w
reduced	539 (18552)w	530 (18867)w	425 (23529)
species	582 (17182)	571 (17513)	
	635 (15748)	621 (16103)	
	712 (14044)vw	699 (14306)vw	807 (12391)sh
	788 (12690)w	773 (12936)w	905 (11049)
	882 (11337)	863 (11587)	1036 (9653)
	1002 (9970)	977 (10235)	
	1167 (8569)w	1131 (8842)w	
	1394 (7174)vw	1342 (7452)vw	
			395 (25316)vs
doubly			432 (23148)w
reduced			450 (22222)
species			473(21141)w
			590 (16949) --
			1030 (9709)

[a]weak [b]very strong [c]very weak [d]shoulder

described this as a trimer with associated water. In the doubly reduced species, $\pi(6) \rightarrow \pi(7)$ is of course absent. I assign the observed bands to $\pi(7) \rightarrow \pi(10)$ and $\pi(7) \rightarrow \pi(8,9)$, moved to higher frequencies because of enhanced double bond character between the rings in the doubly reduced species.

4.2.2. Spectroelectrochemistry of 4,4'-Bipyridine and its Derivatives.

(a) Paraquat

In singly reduced paraquat (Figure 4.13), the strong band which has its origin at 248.8 nm has a vibrational progression of 1040 cm^{-1} (Table 4.4). However, the absorption band assigned to the $\pi(6) \rightarrow \pi(7)$ transition[64] occurring at approximately 370 nm shows vibrational structure, with a spacing from 710 cm^{-1} to 1240 cm^{-1} that has an extremely irregular pattern, which we attribute to ortho C-H bending modes. The general shift of $\pi(6) \rightarrow \pi(7)$ to lower energy on reduction is consistent with the onset of coplanarity, although the use of a one-electron model for the parent is questionable. The band between 514.4 nm and 735.3 nm was assigned to the $\pi(7) \rightarrow \pi(10)$ transition which shows a more regular progression of 1380 cm^{-1}, consistent with a transition whose main effect is to weaken the inter-ring bond. The lowest energy absorption is assigned to the $\pi(7) \rightarrow \pi(9)$ transition [the $\pi(7) \rightarrow \pi(8)$ transition is forbidden because it is a u→u transition] which has a vibronic interval of 1510 cm^{-1}. The vibrational progression in the $\pi(7) \rightarrow \pi(9)$ transition is

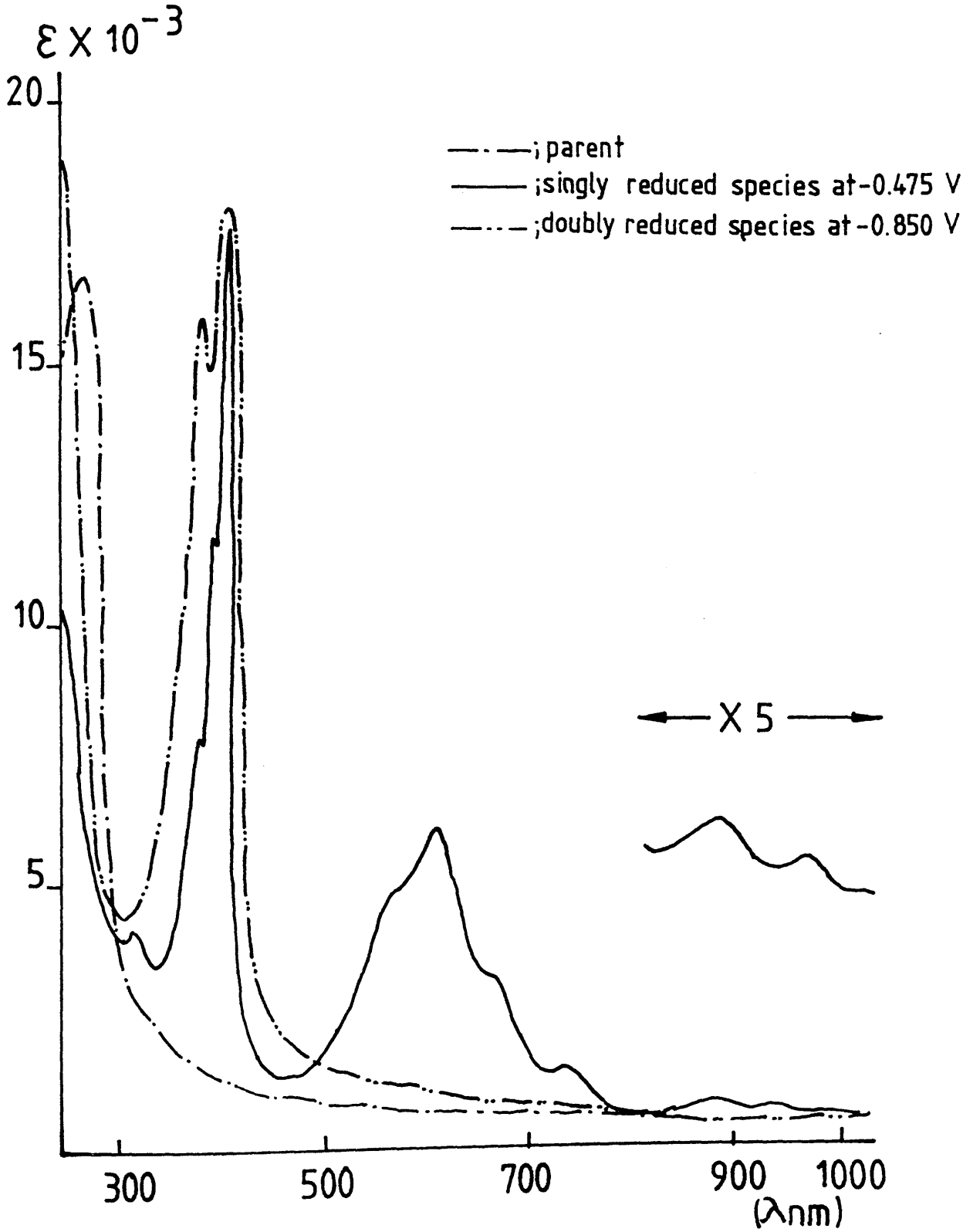

Figure 4.13 Absorption spectra of parent, singly and doubly reduced paraquat in DMF at room temperature.

Table 4.4 Experimental observed wavelengths and energies of the electronic transition and vibronic lines and the assignments for paraquat. Data here and elsewhere are given to more figures than are significant, to avoid rounding errors.

Wavelengths (λnm)	Energies ($\bar{\upsilon}$ cm^{-1})	Progression ($\bar{\upsilon}$ cm^{-1})	Assignments ($\bar{\upsilon}$ cm^{-1})
242.2	41186	994	Average; 1036
248.9	40192	1212	$\pi(5) \rightarrow \pi(7)$
256.5	38986	1007	$\pi(6) \rightarrow \pi(8)$
263.3	37979	997	
270.4	36982	1011	
310.6	32200		dimer band
340.6	29411	1242	Average; 1017
355.5	28169	877	$\pi(6) \rightarrow \pi(7)$
366.4	27292	1237	origin
383.8	26055	713	
394.6	25342		
517.4	19327	1406	Average; 1376
558.0	17921	1277	$\pi(7) \rightarrow \pi(10)$
600.8	16644	1404	
656.2	15239	1419	
723.6	13819		
845.2	11831	1506	$\pi(7) \rightarrow \pi(9)$
968.5	10325		

significantly higher in frequency than that of $\pi(7) \rightarrow \pi(10)$. To help reconcile these differences, the molecular orbital diagrams and the schematic bonding diagram have been combined and simplified for the $\pi(7)$, $\pi(9)$ and $\pi(10)$ orbitals of the paraquat radical cation in Figure 4.14. The $\pi(7)$ and the $\pi(10)$ orbitals are found to have significant double bond character in both the rings, though the $\pi(10)$ orbital has little double bond character between the rings. However, the $\pi(9)$ orbital appears to have extremely little double bond character, either in the ring or between the rings. Therefore the vibration of 1380 cm^{-1} in the $\pi(7) \rightarrow \pi(10)$ transition is possibly due to the symmetric inter-ring stretching mode.

The spectrum of doubly reduced paraquat is less easily understood, since the species is no longer aromatic and the transitions are from a closed shell to an open shell configuration. However, we can use the same theory as was applied to doubly reduced 2,2'-bipyridine. The calculated values of the dipole strengths of each of the transitions of 2,2'-bipyridinium dianion[64] were as follows: the $\pi(7) \rightarrow \pi(10)$ transition had the highest value of 7.47 $Å^2$ and the values of both the $\pi(7) \rightarrow \pi(9)$ and $\pi(7) \rightarrow \pi(8)$ transitions were extremely low (0.06 $Å^2$ for the $\pi(7) \rightarrow \pi(9)$ transition and 0.01 $Å^2$ for the $\pi(7) \rightarrow \pi(8)$ transition). It is therefore clear that only one strong absorption band should be observed between 260 nm to 1300 nm. A strong peak is observed around 400 nm in our experiment which has a vibrational progression of 1395 cm-1. This may be tentatively assigned as the $\pi(7) \rightarrow \pi(10)$ transition, now shifted to higher energy by the full double bond connecting the rings in the ground state.

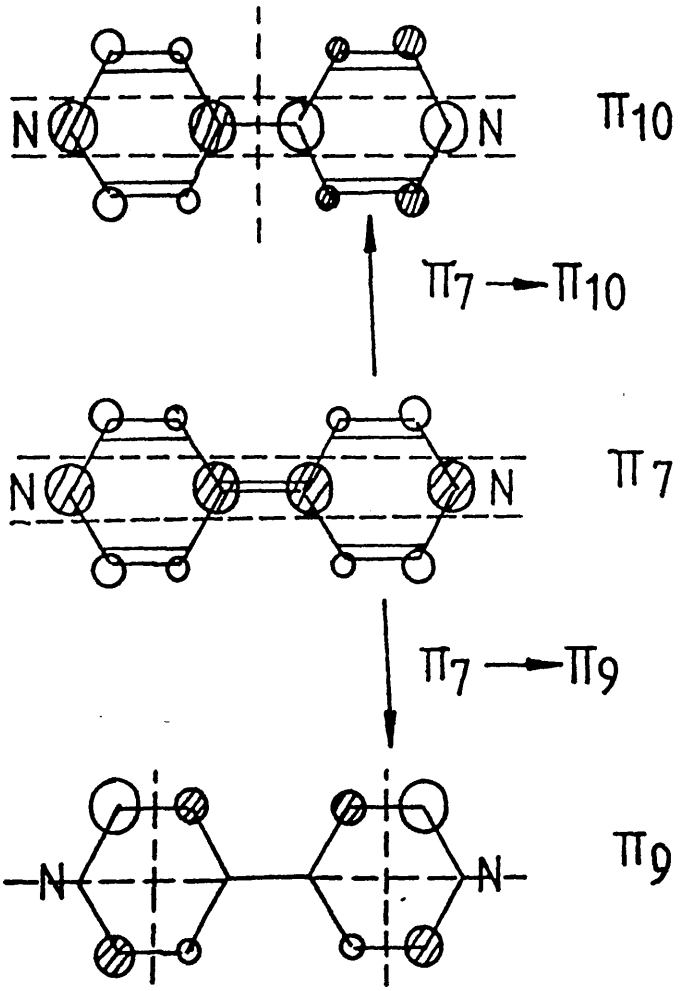

Figure 4.14 Schematic bonding orbitals and molecular orbital diagram for the π^*-orbitals of the paraquat radical cation and 4,4'-bipyridinium radical anion.

Müller and Bruhn[87] reported that the colour of reduced aqueous paraquat solutions ranges from blue to purple depending upon the concentration. They examined the spectrum of a solution of the paraquat radical over the concentration range in which an obvious colour change occurs and confirmed the idea that a monomer-dimer equilibrium is involved, with $k_{diss} = 2.6 \times 10^{-3}$ mol dm^{-3} (at 1 mol dm^{-3} salt concentration). The spectroscopic changes are striking and are reproduced in Figure 4.15. The equilibrium is expressed in following scheme, with $V^{\cdot +}$ = paraquat radical cation. The differences between the absorption

$$(V^{\cdot +})_2 \rightleftharpoons 2V^{\cdot +}$$

spectrum of the dimer and the monomer include a new band at 860 nm, a shift in the visible absorption to shorter wave-lengths, and a shift of the near ultraviolet absorption to shorter wavelengths with some loss in fine structure (Table 4.5)

The gross appearances of the spectra suggest that the transitions responsible for absorption in the 450 nm to 665 nm regions are the same in the dimer as in the monomer, excluding a gross difference in structure between the monomer and dimer. The dimer is thus not a complex of the oxidised and reduced forms of the paraquat cation radical. The dimer is presumably a diradical and the 860 and 560 nm bands are probably related to the corresponding transitions of the monomer. We have observed the dimerisation in water but not in acetonitrile nor in DMF.

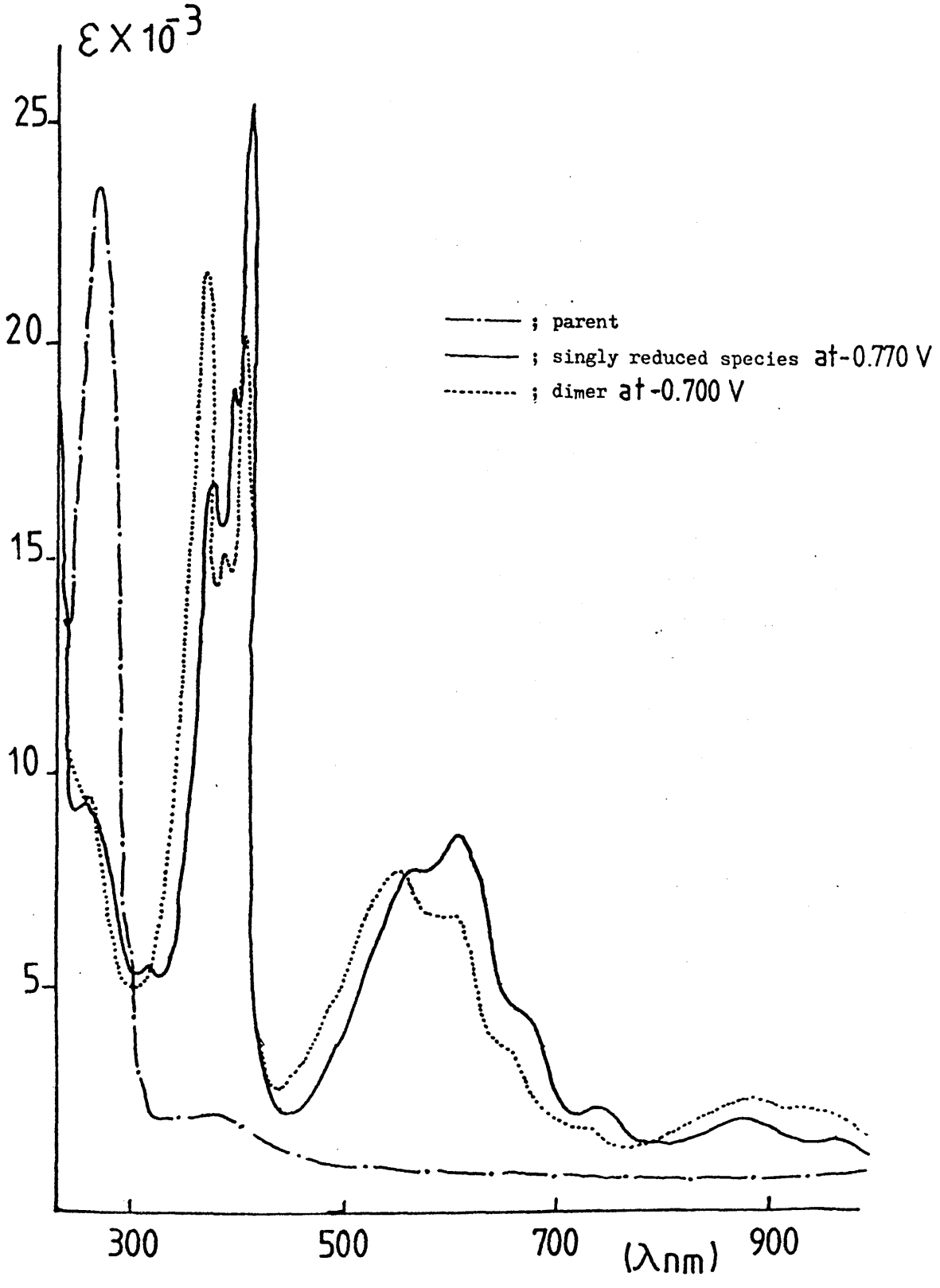

Figure 4.15. The spectroscopic changes between the paraquat radical cation and its dimer in water at room temperature

Table 4.5. A comparison of the main absorption bands for the paraquat radical cation monomer and dimer in water/KNO_3 solution.

monomer		dimer	
λnm	ε x 10^{-3} $dm^3\ mol^{-1}\ cm^{-1}$	λnm	ε x 10^{-3} $dm^3\ mol^{-1}\ cm^{-1}$
366.4	16.1	355.1	21.4
383.8	18.0	371.5	14.5
394.6	25.6	391.7	18.7
558.0	7.5	548.1	7.6
600.8	9.2	597.7	6.6
656.6	4.8	655.0	4.1
800 - 900	1.8 (max)	750 - 1050	2.7 (max)

It is likely that ion-pair formation or charge repulsion in acetonitrile or DMF preclude dimerisation[88].

(b) 4,4'-Bipyridine and monoquat

The electronic absorption spectra of singly reduced 4,4'-bipyridine and monoquat resemble that of paraquat (Figure 4.16, 4.17). In singly reduced 4,4'-bipyridine, the most intense band appears at 375 nm which is assigned to the $\pi(6) \rightarrow \pi(7)$ transition, the band centered at 570 nm is assigned to the $\pi(7) \rightarrow \pi(10)$ transition and the band between 800 nm and 1000 nm is assigned to the $\pi(7) \rightarrow \pi(9)$ transition.

The main structural difference between monoquat and paraquat is that monoquat has two different kinds of pyridine rings. The vibrational progression due to the symmetric inter-ring stretching mode does not appear in the $\pi^* \rightarrow \pi^*$ transitions of singly reduced monoquat. Hence, the electronic absorption spectrum of singly reduced monoquat is diminished in vibrational patterns compared to that of the paraquat radical cation. The strong band at 365 nm is assigned to the $\pi(6) \rightarrow \pi(7)$ transition, the band at 545 nm is assigned to the $\pi(7) \rightarrow \pi(10)$ transition and the band between 650 nm and 870 nm is assigned to the $\pi(7) \rightarrow \pi(9)$ transition. However, a band due to the dimer appeared around 420 nm in highly concentrated solution (eg. 0.01 mol dm^{-3}) for a similar reason to that given for paraquat. The main bands from 260 nm to 1000 nm of 4,4'-bipyridine and its derivatives are presented in Table 4.6.

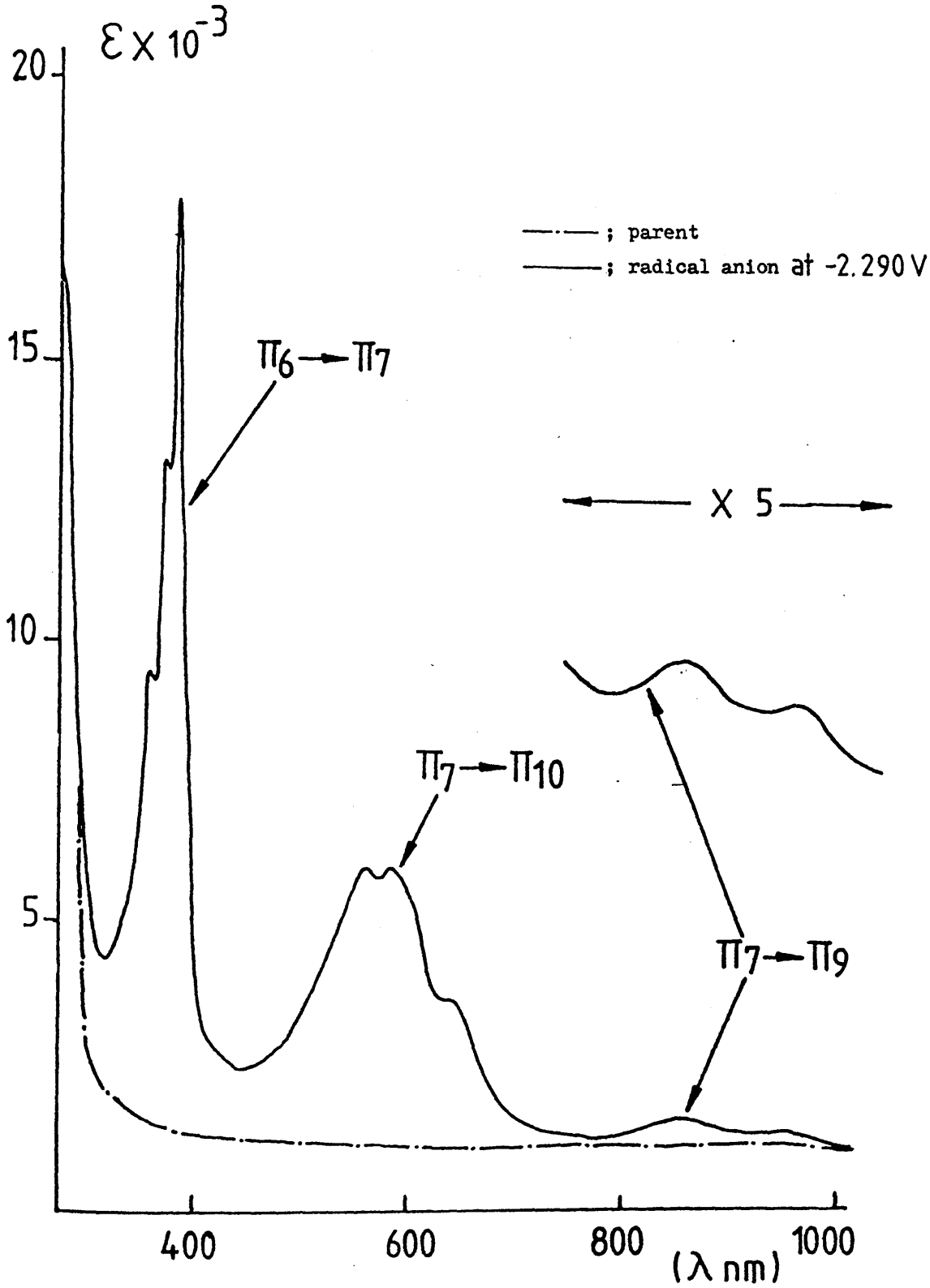

Figure 4.16. Absorption spectra of 4,4'-bipyridine and 4,4'-bipyridinium radical anion in DMF at room temperature.

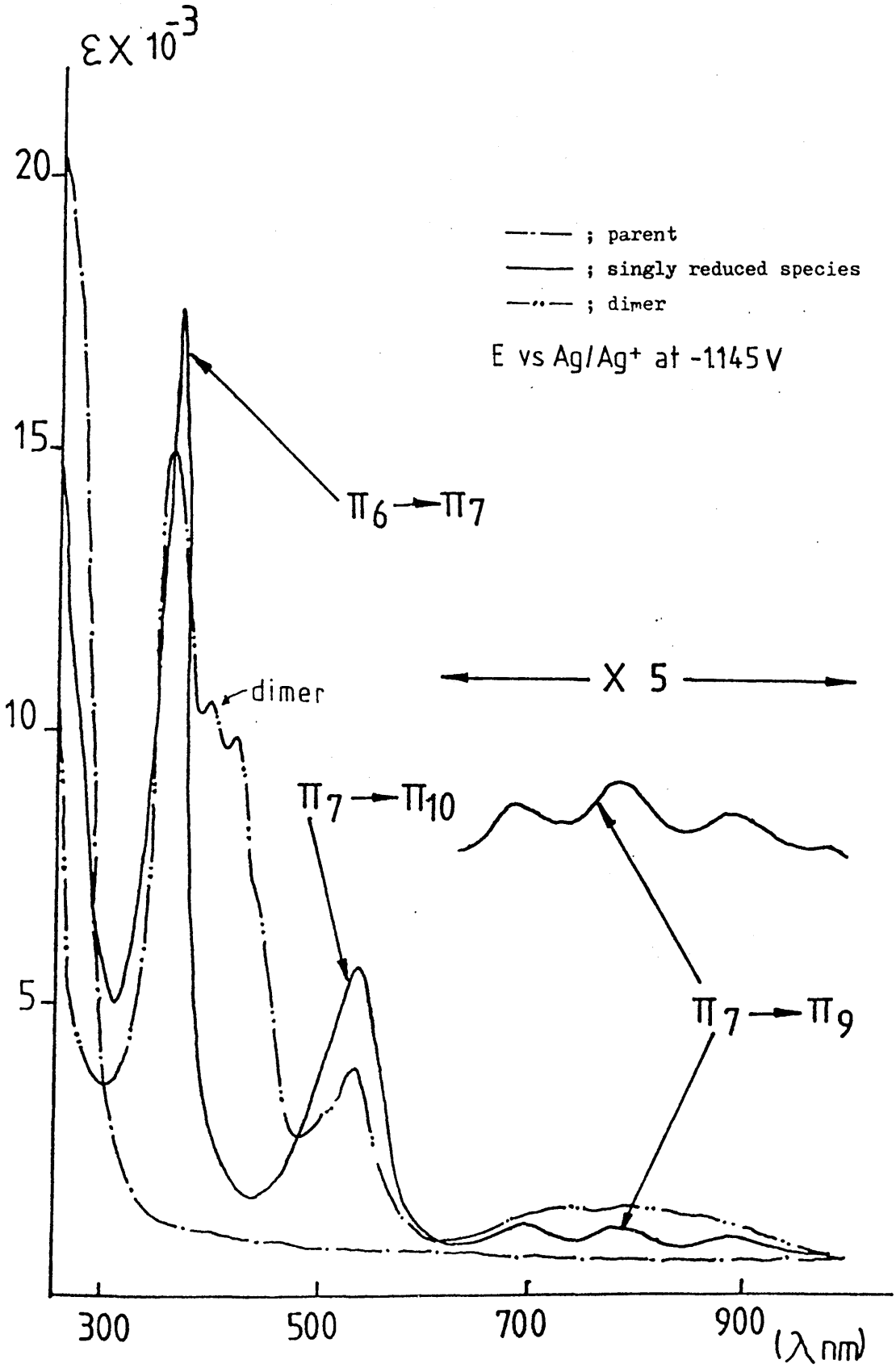

Figure 4.17 Absorption spectra monoquat neutral radical and its dimer in DMF at room temperature.

Table 4.6. The main bands of singly reduced 4,4'-bipyridine and its derivatives in DMF- $TBABF_4$ solution at room temperature.[λnm($\bar{\upsilon}$ cm^{-1})]

	4,4'-bipyridine	monoquat	diquat
	351 (28490)sh[a]	354 (28248)sh	340 (29411)sh
	363 (27548)w[b]	365 (27397)vs[c]	355 (28196)sh
	380 (26315)w		366 (27322)w
	393 (25510)vs		395 (25316)vs
singly	509 (19646)sh	506 (19762)sh	517 (19342)sh
reduced	549 (18214)	545 (18348)	558 (17921)w
species	595 (16806)		601 (16638)
	649 (15408)		656 (15242)
			724 (13812)
	834 (11990)	713 (14025)	845 (11834)
	954 (10482)	790 (12658)	969 (10319)w
		889 (11248)	
		A	**B**
		368 (27173)vs	373 (26809)s
		395 (25316)	394 (25386)vs
		422 (23696)	
		511 (19569)vw[d]	
		551 (18148)	

[a]shoulder [b]weak [c]very strong [d]very weak

A; dimerisation **B**; doubly reduced species of paraquat

4.2.3. Spectroelectrochemistry of 2,2'-Bipyrimidine

The electronic absorption spectra of the 2,2'-bipyrimidinium radical anion at different concentrations are shown in Figure 4.18. As in 4,4'-bipyridine, the orbital energies can be derived from those of biphenyl, described by Maier and Turner[60], by applying a correction in terms of α, the excess coulombic stabilisation at nitrogen, and the electron densities as calculated by a naive Hückel treatment. $\pi(7)$ is bonding between the rings and the strength of this bond is proportional to the cosine of the dihedral angle. For this reason we can assume that the 2,2'-bipyrimidinium radical anion is planar in contrast to the parent species, in which there is no first order inter-ring π-bonding, and the dihedral angle is known to be 40 °[89]. In the 2,2'-bipyrimidinium radical anion, we are dealing with the behaviour of a single electron moving in the field of a closed shell, so that we can approximate the transition energies by one-electron energy differences. The assignment of the $\pi^* \rightarrow \pi^*$ transitions of singly reduced 2,2'-bipyrimidine were based on those of König and Kremer[64] for the 2,2'-bipyridinium radical anion with the exception that our case is conceptually simpler, and the selection rules more rigid, because of the higher symmetry. The lowering in energy of the $\pi(6) \rightarrow \pi\ (7)$ transition at 361 nm on going from the parent to the anion is attributed to the change in dihedral angle, which raises the $\pi(6)$ and lowers the $\pi(7)$ orbital simultaneously. The absence of any vibrational structure in this band is in contrast the situation in the 2,2'-bipyridine system where the vibronic structure was attributed to C-H deformation modes. The band centered at approximately 500 nm is assigned to the $\pi(7) \rightarrow$

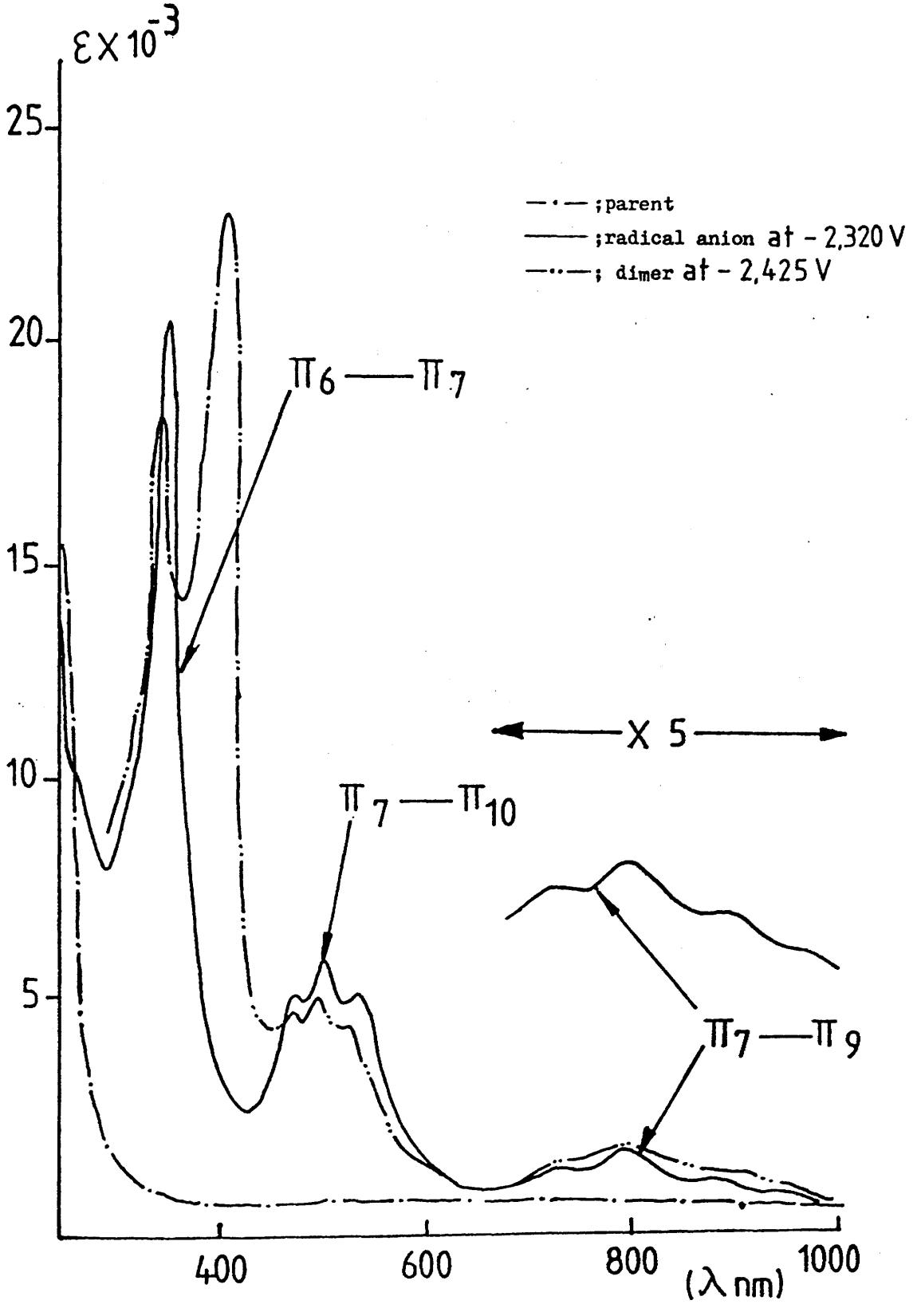

Figure 4.18. Absorption spectra of 2,2'-bipyrimidinium radical anion and its dimer in DMF at room temperature.

$\pi(10)$ transition which shows a short progression with spacing around 1400 cm^{-1}, as expected for a transition which reduces the order of the inter-ring carbon-carbon bond, but does not affect bonding within the rings. The band between 650 nm and 950 nm is assigned to the $\pi(7) \rightarrow \pi(9)$ transition. The $\pi(7) \rightarrow \pi(9)$ transition is forbidden because it is a u $\rightarrow$ u transition which has somewhat longer spacing around 1510 cm^{-1}. This can be related to the associated changes in intra-ring bonding. The main bands are collected in Table 4.7. To derive these intensities, we used the selection rules for D_{2h}, and the forms of the relevant wave-functions.

As shown in Figure 4.18, at concentrations higher than 0.003 mol dm^{-3} a new band appears at 416 nm. This we attribute to a transition, related to the $\pi(6) \rightarrow \pi$ (7) transition in the monomeric species, associated with dimer formation. Such dimerisation is known to occur in the one-electron reduction products of the paraquat radical cation. If we take the extinction coefficient in the dimer to be about twice that of the corresponding monomer band, this would imply a formation constant of around 3 x 10^2 mol^{-1} dm^3. This dimerisation reaction is, however, without apparent effect on the electrochemistry of 2,2'-bipyrimidine, from which we infer that the dimerisation reaction is slow on the timescale of up to several seconds of a normal cyclic voltammetry experiment.

Table 4.7. The main bands of singly reduced 2,2'-bipyrimidine and its dimer in DMF-$TBABF_4$ solution [$\lambda nm(\bar{\upsilon}\ cm^{-1})$]

monomer		dimer	
λnm	ε x 10^{-3} $dm^3\ mol^{-1}\ cm^{-1}$	λnm	ε x 10^{-3} $dm^3\ mol^{-1}\ cm^{-1}$
361 (27700)	20.5	357 (28011)	18.0
		416 (24038)	23.0
467 (21413)	5.0	463 (21598)	4.5
500 (20000)	6.5	496 (20161)	5.0
538 (18587)	5.0	533 (18761)	4.0
719 (13908)		700 (14285)	max; 2.5
800 (12500)	max; 2.0	-- 1000 (10000)	
901 (11098)			
1029 (9718)			

Chapter 5. The Electronic Absorption Spectra of Fe(II) Complexes.

The ground state, ^5D, appropriate for the d^6 configuration of high spin Fe(II) complexes is split by octahedral and tetrahedral ligand fields into $^5T_2$ and ^5E states; all tetrahedral complexes of Fe(II), such as $[Fe(dmp)Cl_2]$ (where dmp= 2,9-dimethyl-1,10-phenanthroline), are high spin, while some octahedral complexes are low spin such as $[Fe(CN)_6]^{4-}$ and $[Fe(L)_3]^{2+}$,[90]. (where L= 2,2'-bipyridine, 1,10-phenanthroline and 2,2'-bipyrimidine)

2,2'-bipyridine, 1,10-phenanthroline and 2,2'-bipyrimidine have been widely used as 'Classical' ligands for metal ions. Apart from their good σ-donor complexing properties, due to the bidentate coordination, these systems are distinguished because of their relatively low lying π^* orbitals. As a result of this particular combination of electronic properties, these ligands often form highly coloured coordination compounds because of a low energy charge transfer transition[91-93]. They can stabilise labile inorganic species, including metals in low oxidation states by accepting excess negative charge[94,95], and can form easily reducible complexes with the additional electrons residing often in the ligand π^* orbital.

The nature of the intense coloured complexes which iron(II) ions form with these ligands has received much attention and has been extensively studied[4,34-40,57]. The π-bonding formed between the central metal atom and these ligand molecules seems to play an important role in the nature of these complexes. 2,2'-Bipyrimidine is far more reactive towards nucleophilic attack when coordinated to Fe(II) than 2,2'-bipyridine and 1,10-phenanthroline in the corresponding complexes[95].

Distortion in tetrahedral Fe(II) complexes has been discussed by Gill et al[96], in the critical evaluation of ligand field and other theories in the prediction and interpretation of the stereochemistry of Fe(II) complexes, and they have drawn attention to factors which are potentially important structure determinants[97]. It was pointed out that four-covalent high spin tetrahedral Fe^{2+} (d^6), where the Fe^{2+} has the electronic configuration $e_g^3\ t_{2g}^3$, complexes should be considerably distorted.

5.1. Electrochemistry of Fe(II) Complexes.

The uncoordinated free ligands (bpy, phen, bpym) undergo a one-electron reduction process at just over -2 V vs Ag/Ag^+, but no oxidations are observed (see chapter 4). However, the reversible one-electron oxidations of metal complexes $[Fe(L)_3]^{2+}$ are observed around +1.0 V which is due to metal based $d^6 \rightarrow d^5$ oxidation, whereas the reduction steps of $[Fe(L)_3]^{2+}$ are still based on the ligands. The order of decreasing ease of reduction in the complexes is bpym > bpy ≥ phen, and the potential differences are roughly parallel to the reduction potential differences of the free ligands. The effect of the metal is to stabilise the energy of the $[bpy]^-\ \pi^*$ level by approximately 0.6 V. This stabilisation is caused by the mixing of a charge transfer configuration into the ground state. In other words, π-bonding is formed between the iron atom and the ligand molecules. This large stabilisation is undoubtedly responsible for the high stability of these complexes. The oxidation-reduction potentials of Fe(II) complexes studied are shown in Table 5.1 and the cyclic voltammogram of each

Table 5.1. The oxidation and reduction potentials of Fe(II) complexes[A]

Compounds	$E_{oxi}^{(III/II)}$	$E_{red}^{(2+/+)}$	$E_{red}^{(+/0)}$	$E_{red}^{(0/-1)}$
$[Fe(bpym)_3]^{2+}$ [a]	+1.036(0.070)[b]	-1.411(0.069)	-1.570(0.079)	-1.752(0.102)
$[Fe(bpy)_3]^{2+}$	+0.802(0.065)	-1.672(0.062)	-1.855(0.067)	-2.035(0.082)
$[Fe(phen)_3]^{2+}$	+0.785(0.067)	-1.735(0.065)	-1.924(0.070)	-2.105(0.091)
$[Fe(terpy)_2]^{2+}$	+0.737(0.069)	-1.650(0.066)	-1.797(0.070)	
$[Fe(dmp)Cl_2]$[c]				-1.678(0.059)

[A]Data from cyclic voltammetry, Potentials in Volts vs Ag/Ag^+ in DMF-$TBABF_4$ solution at room temperature. [a]Results at -40 °C. [b]Epa-Epc (V).

[c]Reduction from $[Fe(dmp)Cl_2]^0 \rightarrow [Fe(dmp)Cl_2]^{-1}$.

complex in DMF using a platinum working electrode is shown in Figure 5.1. All reduction and oxidation processes are confirmed to be reversible one-electron steps and solvents (e.g. propylene carbonate, dimethylsulphoxide, acetonitrile) do not significantly affect the peak potentials. Replacing the platinum electrode with gold makes no difference to the electrochemistry.

The cyclic voltammograms establish an extended sequence of narrowly spaced reversible reduction potentials (around 175 mV for $[Fe(L)_3]^{2+}$ and 147 mV for $[Fe(terpy)_2]^{2+}$ (Figure 5.2) (where terpy = 2,2';6',2''- terpyridine). The species $[Fe(L)_3]^{2+}$ show three closely spaced reductions, while $[Fe(terpy)_2]^{2+}$ shows only two. This is as expected if the reduction orbitals are located on the ligands.

In the cyclic voltammogram of $[Fe(bpym)_3]^{2+}$ at room temperature, no reversible steps were observed besides one for the liberated ligand molecules. (Figure 5.3) The crystal structure[98] of the $[Fe(bpym)_3]^{2+}\cdot 7H_2O$ shows that hydrogen bonds are formed between the uncoordinated nitrogen atoms of the ligands and three water molecules; the remaining $4H_2O$ being outer-sphere coordinated. Hence, a substitution reaction in which the ligands are replaced by water molecules on the Iron(II) centre presumably occurs during the electrolysis. However, at -40 °C, a series of three narrowly spaced reversible reductions appeared as in $[Fe(bpy)_3]^{2+}$. Thus this substitution reaction is dependent upon the temperature.

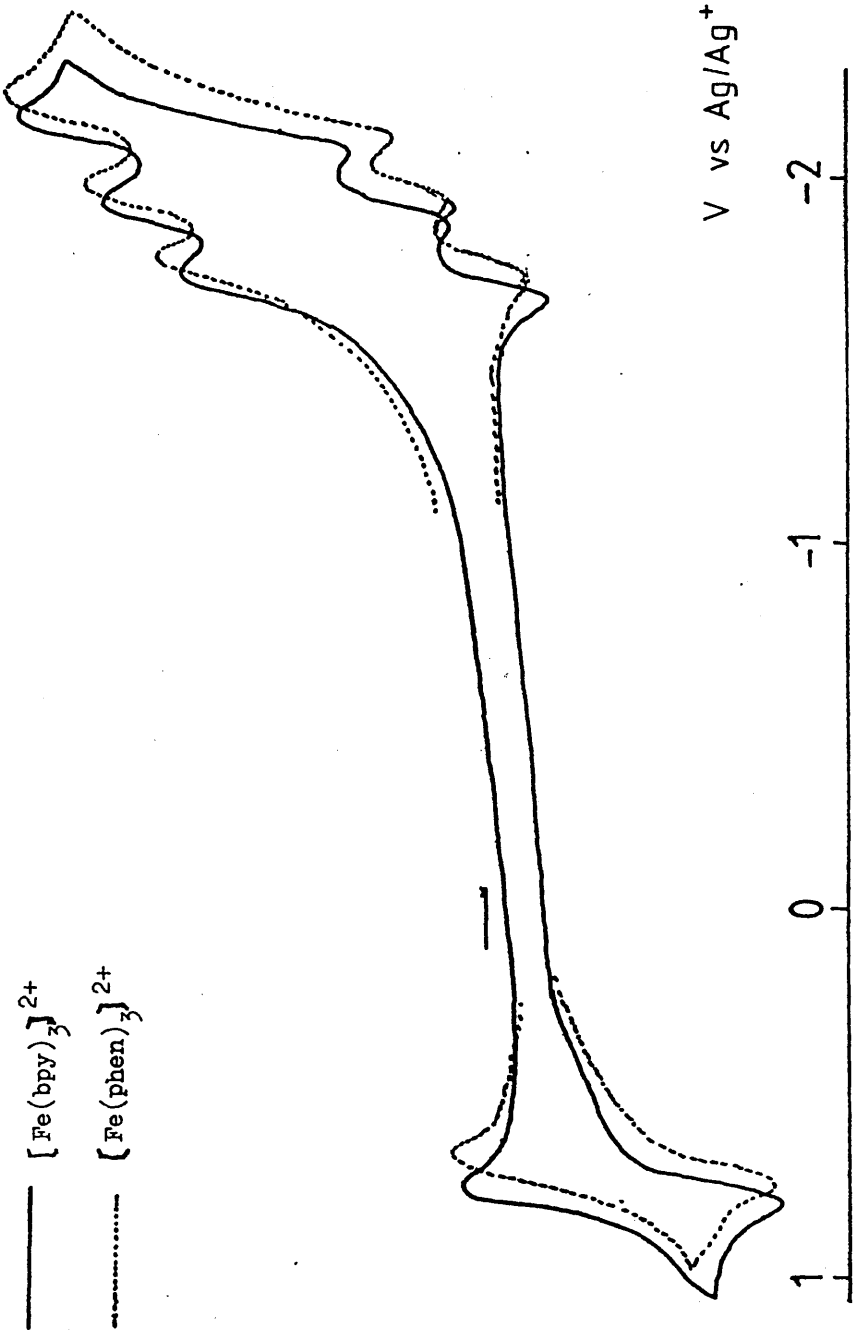

Figure 5.1. Cyclic voltammograms of $[Fe(bpy)_3]^{2+}$ and $[Fe(phen)_3]^{2+}$ in DMF at room temperature.

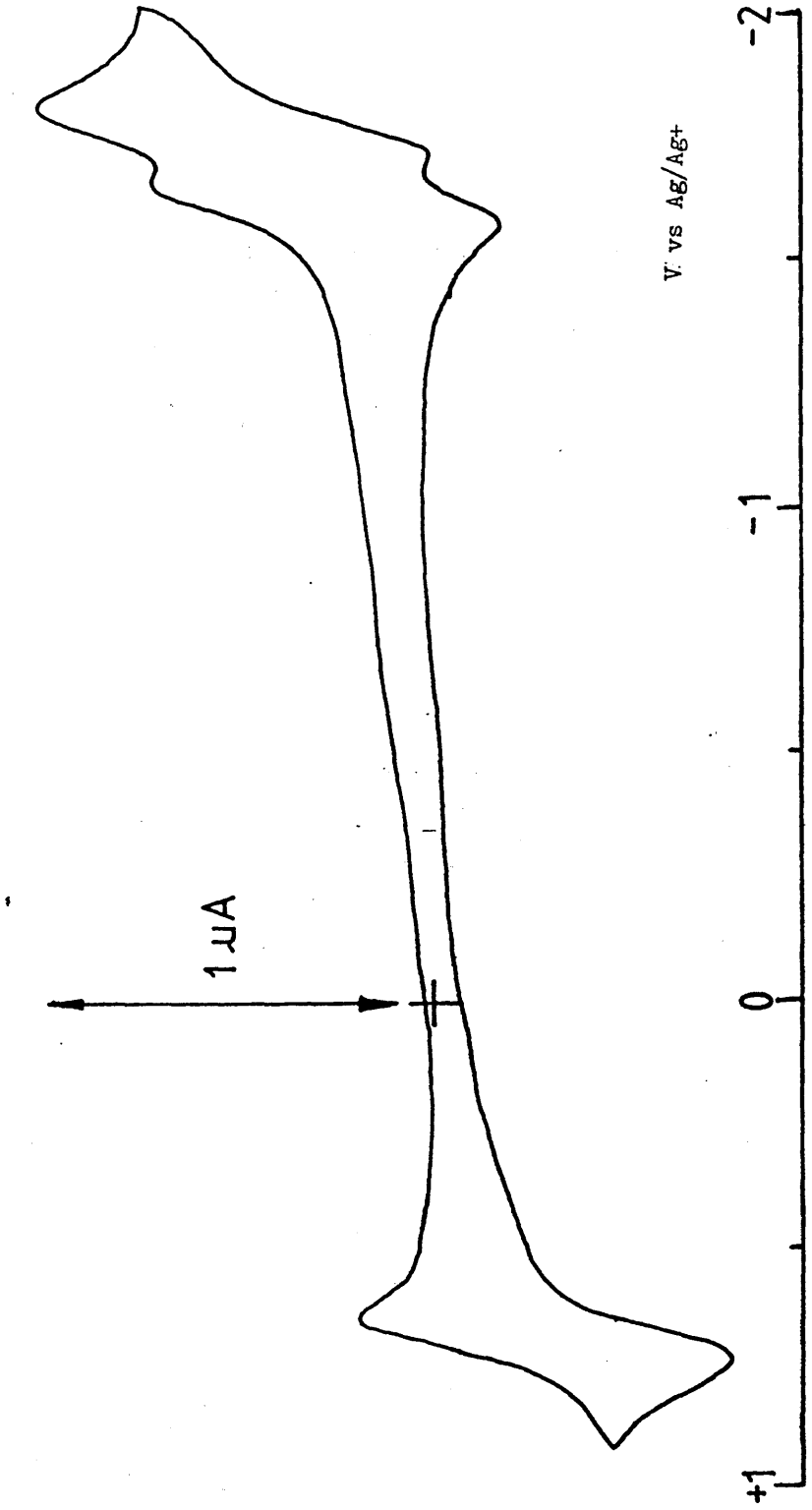

Figure 5.2. Cyclic voltammogram of $[Fe(terpy)_2]^{2+}$ in DMF at room temperature.

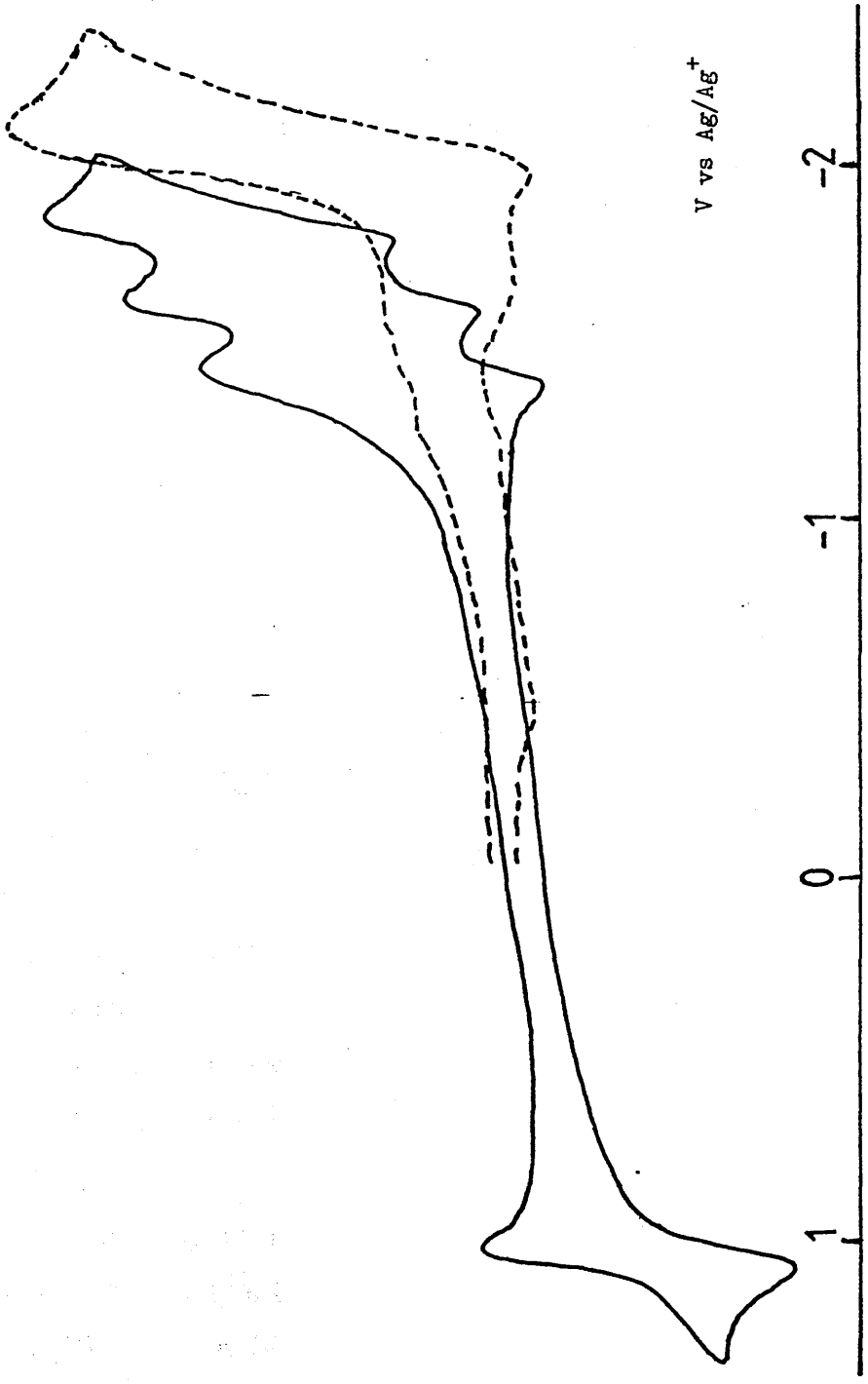

Figure 5.3. Cyclic voltammograms of $[Fe(bpym)_3]^{2+}$ in DMF at room temperature (------) and - 40 °C (———)

As shown in Table 5.1, the reduction potentials of $[Fe(bpym)_3]^{2+}$ are less negative than those of $[Fe(bpy)_3]^{2+}$ and $[Fe(phen)_3]^{2+}$. This is because, in bpym, nitrogen is more electronegative than the carbon it replaces. The π^* orbitals would therefore be expected to be lower in energy for the bpym ligands than bpy or phen which could result in greater mixing of the lower energy redox orbitals with the metal through π-backbonding. Hence, the bpym complex redox orbitals are lower in energy than those of the bipyridine and phenanthroline complexes. The lower basicity of 2,2'-bipyrimidine has been shown to result in weaker metal-ligand bonding and to negate the tendency toward increased π-backbonding for the unreduced complexes[99].

The lower redox potentials of $[Fe(bpym)_3]^{2+}$ vs $[Fe(bpy)_3]^{2+}$ and $[Fe(phen)_3]^{2+}$ suggests that the $d\pi[Fe(II)] \rightarrow \pi^*(bpym)$ transition of bpym is lower in energy than that for bpy or phen. Qualitatively, this fits into the previously established pattern of lowering the MLCT transition energy as electron-withdrawing groups are incorporated into the aromatic heterocyclic ring[100]. These results are not surprising since molecular orbital calculations indicate the bpym π^* LUMO lies lower in energy than the corresponding phen or bpy π^* LUMO. Thus, the net result of the lower energy bpym LUMO is to decrease the energy of the $d\pi \rightarrow \pi^*$ transition[101].

Assuming constant bpy, phen and bpym π^* and σ^* orbital energy for interaction with the metal $d\pi$ orbitals, the metal $d\pi[Fe(II)] \rightarrow \pi^*(ligand)$ interaction should stabilise the $d\pi$ molecular orbitals for Fe(II) complexes. (Figure 5.4) As expected from this argument, the metal based oxidation of $[Fe(bpym)_3]^{2+}$ occurs at a more positive potential than that of $[Fe(bpy)_3]^{2+}$.

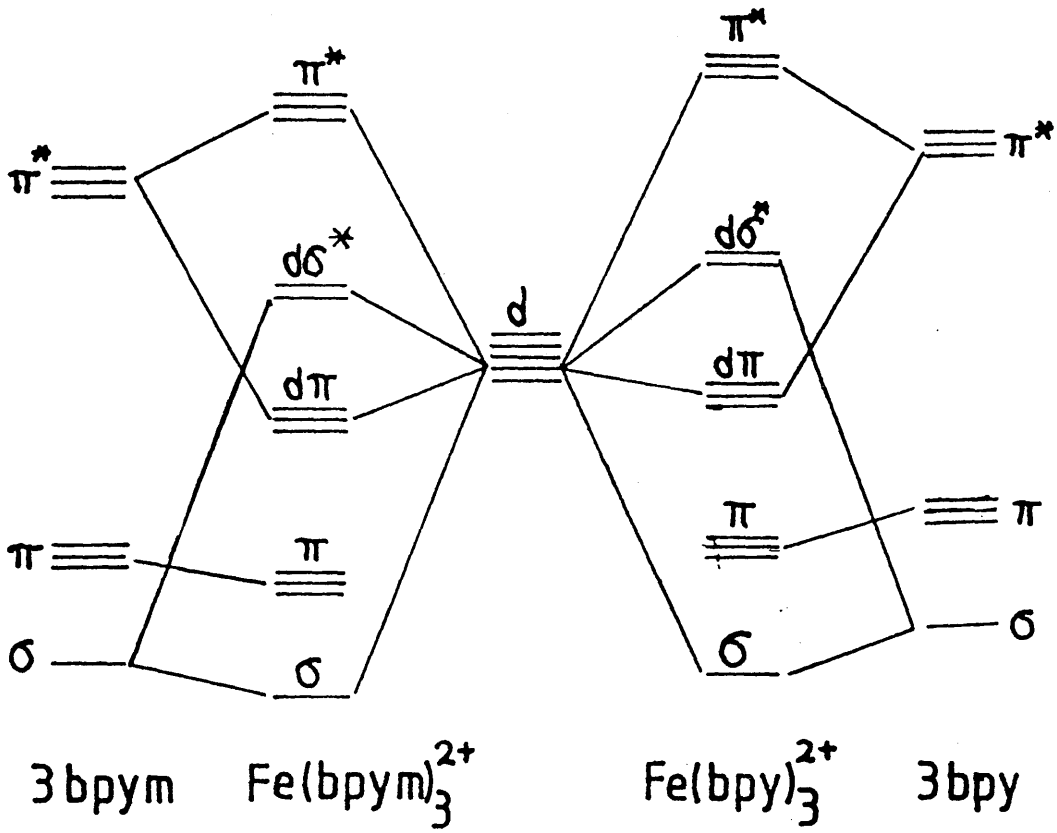

Figure 5.4. General molecular orbital diagram for bpym-Fe and bpy-Fe interactions.

Dimethyl substitution of 1,10-phenanthroline at the 2,9-positions is expected to increase the ligand's σ-donation basicity through positive (electron releasing) inductive and resonance effects and this should increase the ligand field strength. On the other hand, 2,9- substitution is expected to have maximum, steric effect on the metal-N ligation, increasing this distance and decreasing the metal-ligand π-interaction. Fe(II) complexes of

the bidentate ligand 2,9-dimethyl-1,10-phenanthroline(dmp) are well documented[102] and mono complexes of the type $[Fe(dmp)X_2]$ have been studied (where X= Cl, Br, I), in particular by Fox *et al.*[103]. Of these, the chloro-complexes have been found to be monomeric, with a distorted tetrahedral geometry, whereas, similar complexes such as $[Fe(phen)Cl_2]$ and $[Fe(bpy)Cl_2]$ have chloro-bridged polymeric structure containing six-coordinated iron (II)[97]. Complexes where X = Br or I are of a similar molecular structure. The cyclic voltammogram of $[Fe(dmp)Cl_2]$ is shown in Figure 5.5. Only one reversible reduction is observed at -1.678 V which is due to ligand based reduction (59 mV; E_{pa}-E_{pc}).

5.2. Electronic Absorption Spectra of Fe(II) Complexes

The visible-UV-NIR spectra of the parent complexes $[Fe(L)_3]^{2+}$ contain three main absorption bands. The highest energy absorption (at approximately 300 nm) of each complex is associated with a ligand-localised $\pi \rightarrow \pi^*$ transition due to the coordinated diimine ligand. There are also intense bands around 500 nm which have been assigned to $d\pi[Fe(II)] \rightarrow \pi^*$(ligand) charge-transfer transition. These $d\pi[Fe(II)] \rightarrow \pi^*$(ligand) charge-transfer transition bands are dependent upon the LUMO energy of the coordinated diimine ligands. For example, the MLCT energy of $[Fe(bpym)_3]^{2+}$ is relatively lower in energy compared to complexes of $[Fe(bpy)_3]^{2+}$ and $[Fe(phen)_3]^{2+}$. However, the observed MLCT band in $[Fe(phen)_3]^{2+}$ appears very wide and shows vibrational structure. This band may be assigned to the

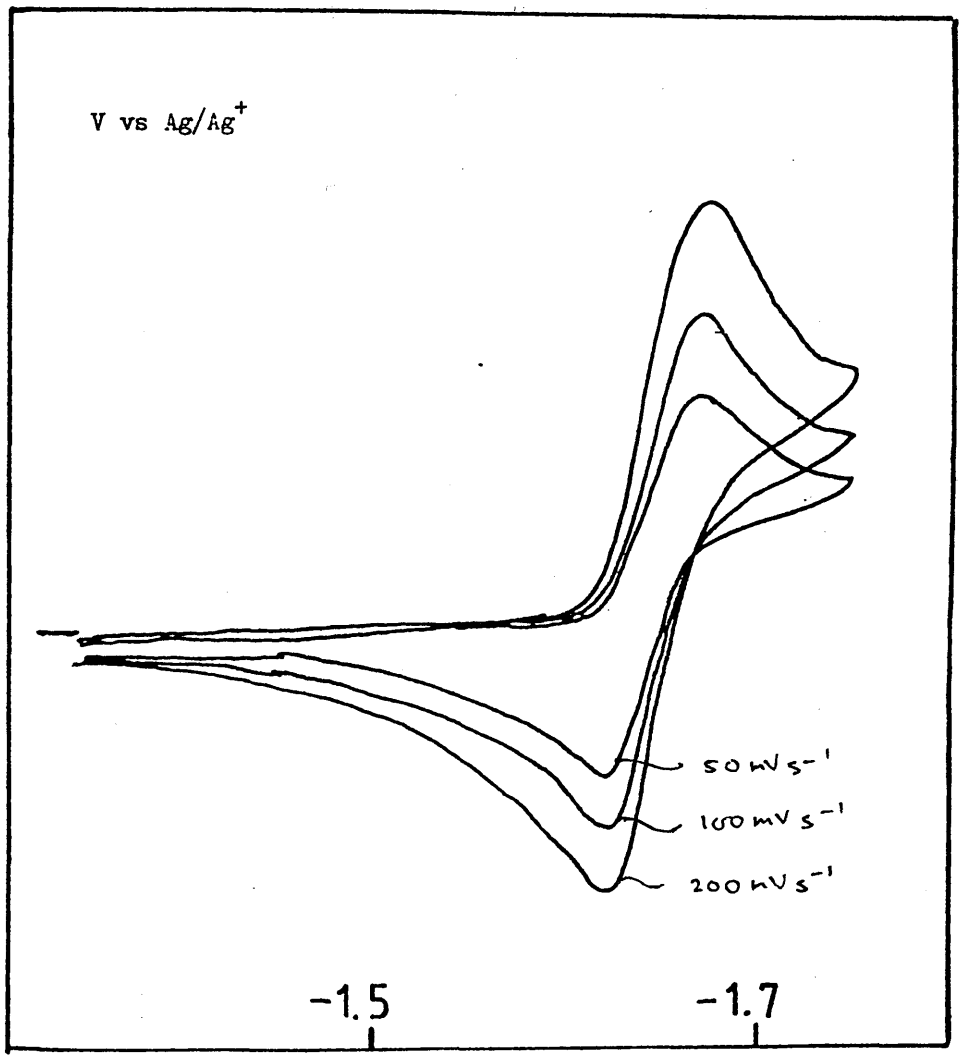

Figure 5.5. Cyclic voltammogram of [Fe(dmp)Cl_2] in DMF at room temperature.

overlapping of a second charge transfer band involving the second lowest unoccupied molecular orbital[104]. Figure 5.6 shows the charge transfer band shapes of the $[Fe(bpym)_3]^{2+}$, $[Fe(bpy)_3]^{2+}$ and $[Fe(phen)_3]^{2+}$ ions.

The energy of electron transfer from the 3d AO of iron to the vacant ligand π-MO depends strongly on the formal charge on the iron; in other words, the σ-electron distribution in the metal complex. The spectrum of a coordinated phen is similar to that of

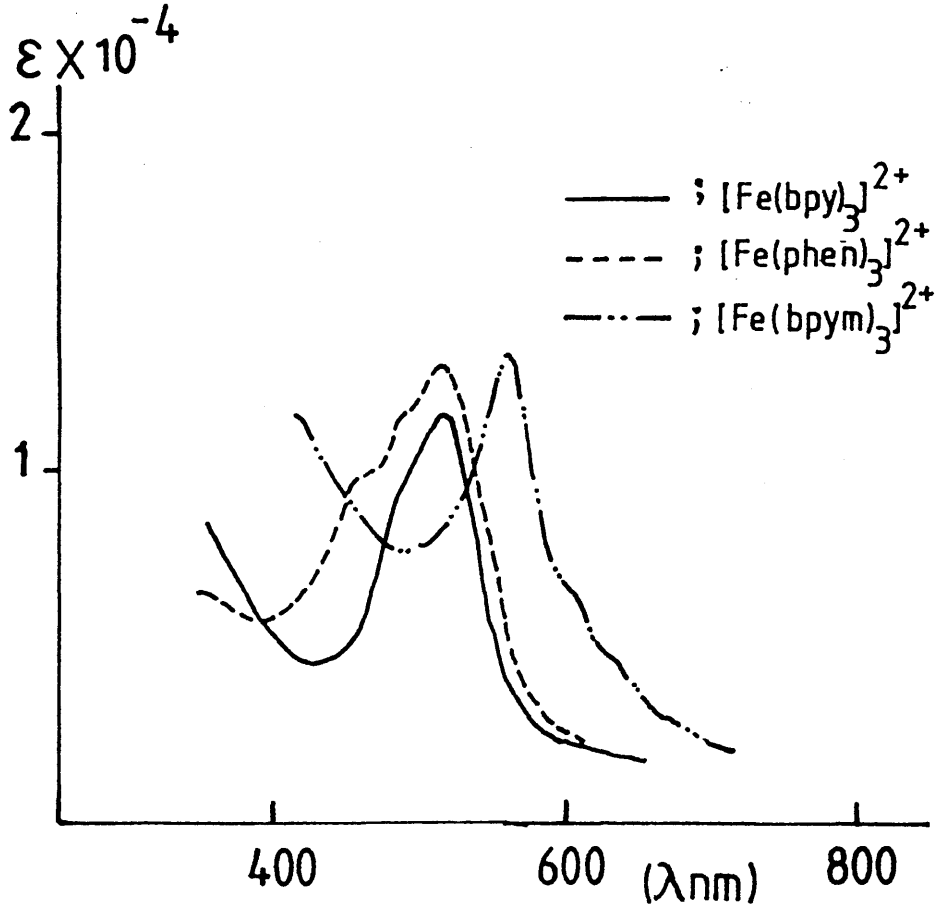

Figure 5.6. The charge transfer band shapes of $[Fe(bpym)_3]^{2+}$, $[Fe(bpy)_3]^{2+}$ and $[Fe(phen)_3]^{2+}$ in DMF.

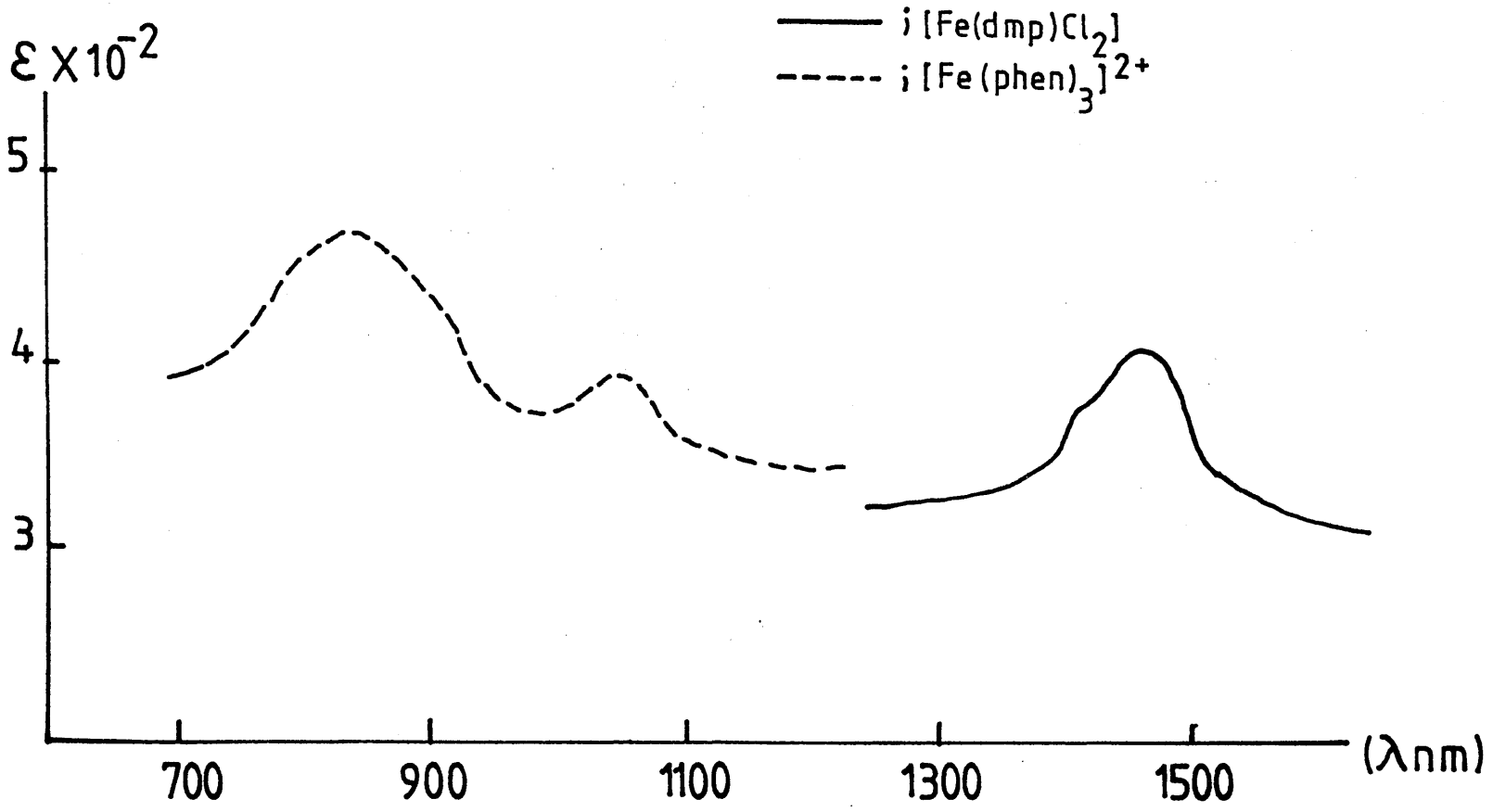

Figure 5, 7 Absorption spectra of d→d transition of $[Fe(dmp)Cl_2]$ and $[Fe(phen)_3]^{2+}$

state[106] (presumably the SLUMO i.e. the second lowest unoccupied molecular orbital). The shift of λmax to longer wavelength for $[Fe(terpy)_2]^{2+}$ than $[Fe(bpy)_3]^{2+}$ is attributed to the greater electron acceptor character of the terpyridine ligands. Finally a very weak absorption around 830 nm could be assigned to a d $\rightarrow$ d transition of central metal ion.

The electronic absorption spectrum of reduced $[Fe(bpy)_3]^{2+}$ shows characteristic $[bpy]^-$ intraligand $\pi \rightarrow \pi^*$ and $\pi^* \rightarrow \pi^*$ transitions in the near-infrared visible and ultraviolet regions, with stepwise growth of the ultraviolet and near-infrared bands and a stepwise shift of the visible band from $[Fe(bpy)_3]^+$ to $[Fe(bpy)_3]^{-1}$. (Figure 5.8)

The high energy band in the ultraviolet region(304 nm) is assigned to the intraligand $\pi(6) \rightarrow \pi(7)$ transition of coordinated neutral bipyridine ligands, giving an absorption coefficient per neutral bpy ligand of 19700 $dm^3\ mol^{-1}\ cm^{-1}$, compared to 15000 $dm^3\ mol^{-1}\ cm^{-1}$for $[Ir(bpy)_3]^{3+}$ [107]. This band shifts slightly to lower energies on reductions and shows the expected progressive loss of intensity. In the partly reduced species, bpy and $[bpy]^-$ ligands coexist, within what could be regarded as a hetero-tris-chelated complex.

The new band around 360 nm is assigned to the $\pi(6) \rightarrow \pi(7)$ transition of coordinated $[bpy]^-$ and the intensity of this band grows stepwise on going from $[Fe(bpy)_3]^+$ to $[Fe(bpy)_3]^{-1}$. It is, however too intense, compared to $\pi(6) \rightarrow \pi(7)$ of the free $[bpy]^-$ radical anion, for this alone to be a satisfactory assignment, and

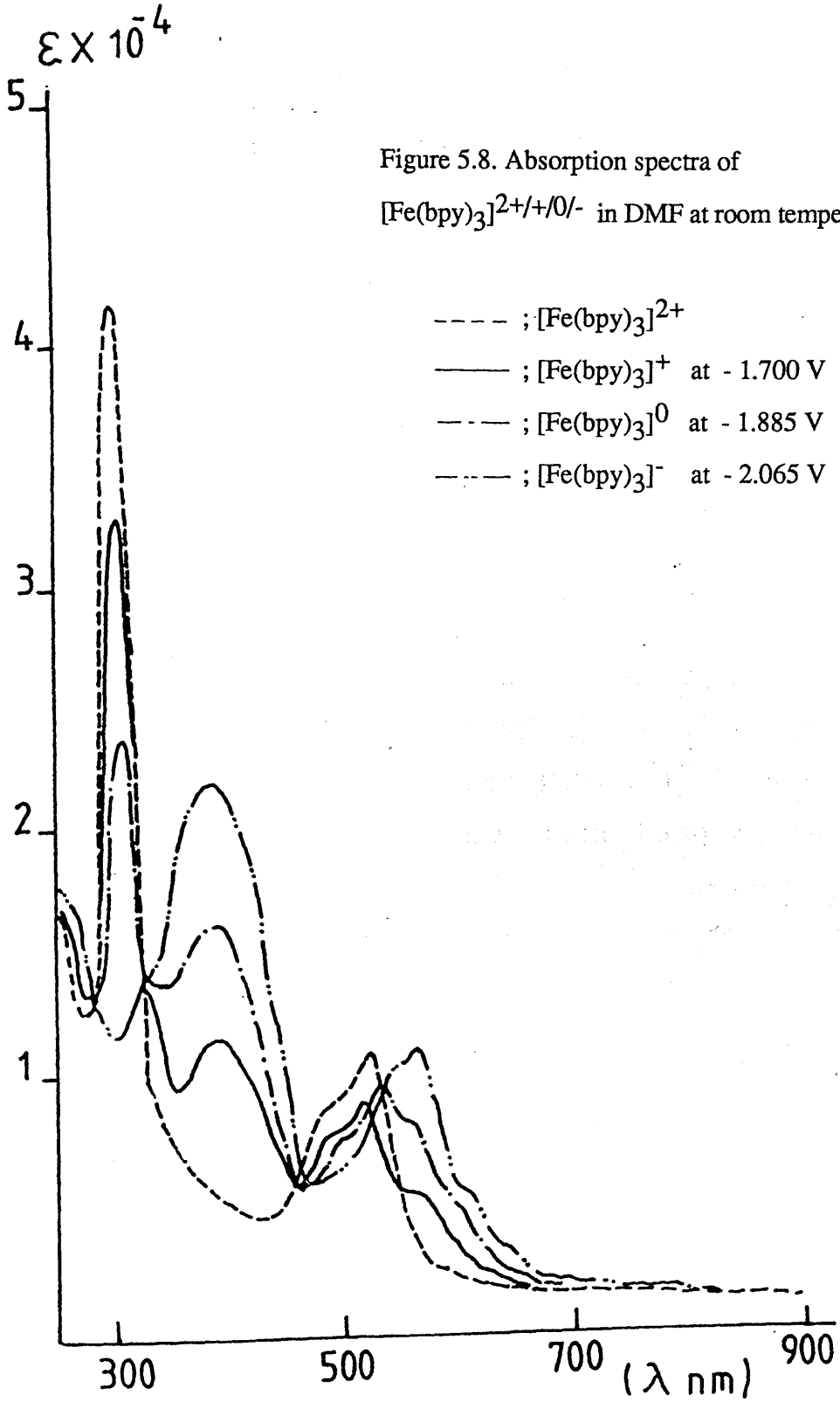

Figure 5.8. Absorption spectra of $[Fe(bpy)_3]^{2+/+/0/-}$ in DMF at room temperature.

- - - - ; $[Fe(bpy)_3]^{2+}$

——— ; $[Fe(bpy)_3]^{+}$ at - 1.700 V

— · — ; $[Fe(bpy)_3]^{0}$ at - 1.885 V

— ·· — ; $[Fe(bpy)_3]^{-}$ at - 2.065 V

we suggest that M[Fe(II)] → L([bpy]$^-$) CT is also contributing. Also the expected π(7) → π(11) transition of [bpy]$^-$ is presumably masked by the π(6) → π(7) transition of [bpy]$^-$ because of the very weak dipole strength of the π(7) → π(11) transition compared to that of the π(6) → π(7) transition[64].

The band at 522 nm of the $[Fe(bpy)_3]^{2+}$ complex is assigned to the dπ[Fe(II)] → π*[π(7) orbital of bpy] charge-transfer(MLCT) transition band (Table 5.2). However, $[Fe(bpy)_3]^{-1}$ does not have this MLCT transition band because there is no neutral bpy in this molecule. Presumably, in all the reduced species, dπ[Fe(II)] → π*(π(8) orbital of [bpy]$^-$) charge-transfer transition may occur at higher energy than dπ[Fe(II)] → π*(bpy) charge-transfer transition.

The band at around 550 nm is assigned to the π(7) → π(10) transition of [bpy]$^-$ and the predicted π(7) → π(8,9) transition of coordinated [bpy]$^-$ appears at around 950 nm. The weak d → d transition ($^1A_{1g} \rightarrow {}^3T_{1g}$) of the central Fe(II) ion should still remain around 820 nm in reduced $[Fe(bpy)_3]^{2+}$ species, but this d → d transition is masked by the relatively intense π(7) → π(8,9) transitions of coordinated [bpy]$^-$.

The assignments of the electronic absorption spectra of reduced $[Fe(phen)_3]^{2+}$ (Figure 5.9) are more difficult than those of $[Fe(bpy)_3]^{2+}$, because the 1,10-phenanthroline system is characterised by two low-lying unoccupied molecular orbitals of comparable energies. Although this fact had been reported in a Pariser-Parr-Pople M.O. study[104] of phen and was successfully used to interpret the electronic absorption spectra of

Table 5.2a. The main absorption bands and assignments of reduced $[Fe(bpy)_3]^{2+}$ species in DMF-$TBABF_4$ solution.[λnm ($\bar{\upsilon}$ cm^{-1})]

	$\pi \rightarrow \pi^*(L)$	$\pi \rightarrow \pi^*(L^-)$	MLCT [Fe(II) $\rightarrow$ ligand]	$\pi \rightarrow \pi^*(L^-)$	$\pi \rightarrow \pi^*(L^-)$
$[Fe(bpy)_3]^{2+}$	304(32895)		522(19157)		
$[Fe(bpy)_3]^{+}$	307(32573)	361(27701)	514(19455)	549(18215)	935(10695)
$[Fe(bpy)_3]^{0}$	311(32154)	365(27027)	498(20080)sh	550(18182)	956(10460)
$[Fe(bpy)_3]^{-1}$		379(27027)		562(17794)	979(10215)
Assignments	$\pi(6) \rightarrow \pi(7)$ of bpy	$\pi(6) \rightarrow \pi(7)$ of $[bpy]^-$	$d\pi$[Fe(II) $\rightarrow \pi^*(\pi(7)$ of bpy)]	$\pi(7) \rightarrow \pi(10)$ of $[bpy]^-$	$\pi(7) \rightarrow \pi(10)$ of $[bpy]^-$

Table 5.2b. The main absorption bands and assignments of reduced $[Fe(phen)_3]^{2+}$ species in DMF-$TBABF_4$. [λnm ($\tilde{\upsilon}$ cm^{-1})]

	$\pi \rightarrow \pi^*(L^-)$	MLCT [Fe(II) → ligand]		$\pi \rightarrow \pi^*(L^-)$	$\pi \rightarrow \pi^*(L^-)$
$[Fe(phen)_3]^{2+}$		435(22988)	515(19471)		
$[Fe(phen)_3]^{+}$	385(25974)	415(24096)sh	509(19646)	592(16892)	782(12788)
$[Fe(phen)_3]^{0}$	391(25575)		503(19880)sh	598(16722)	804(12438)
$[Fe(phen)_3]^{-1}$	398(25125)			605(16529)	829(12062)
Assignments	$\pi(7) \rightarrow \pi(8)$ of $[phen]^-$	$d\pi[Fe(II)] \rightarrow \pi^*$ of phen[π(9)]	$d\pi[Fe(II)] \rightarrow \pi^*$ of phen[π(8)]	$\pi^* \rightarrow \pi^*$ of $[phen]^-$	$\pi^* \rightarrow \pi^*$ of $[phen]^-$

Figure 5.9 Absorption spectra of $[Fe(phen)_3]^{2+/+/0/-}$ in DMF at room temperature.

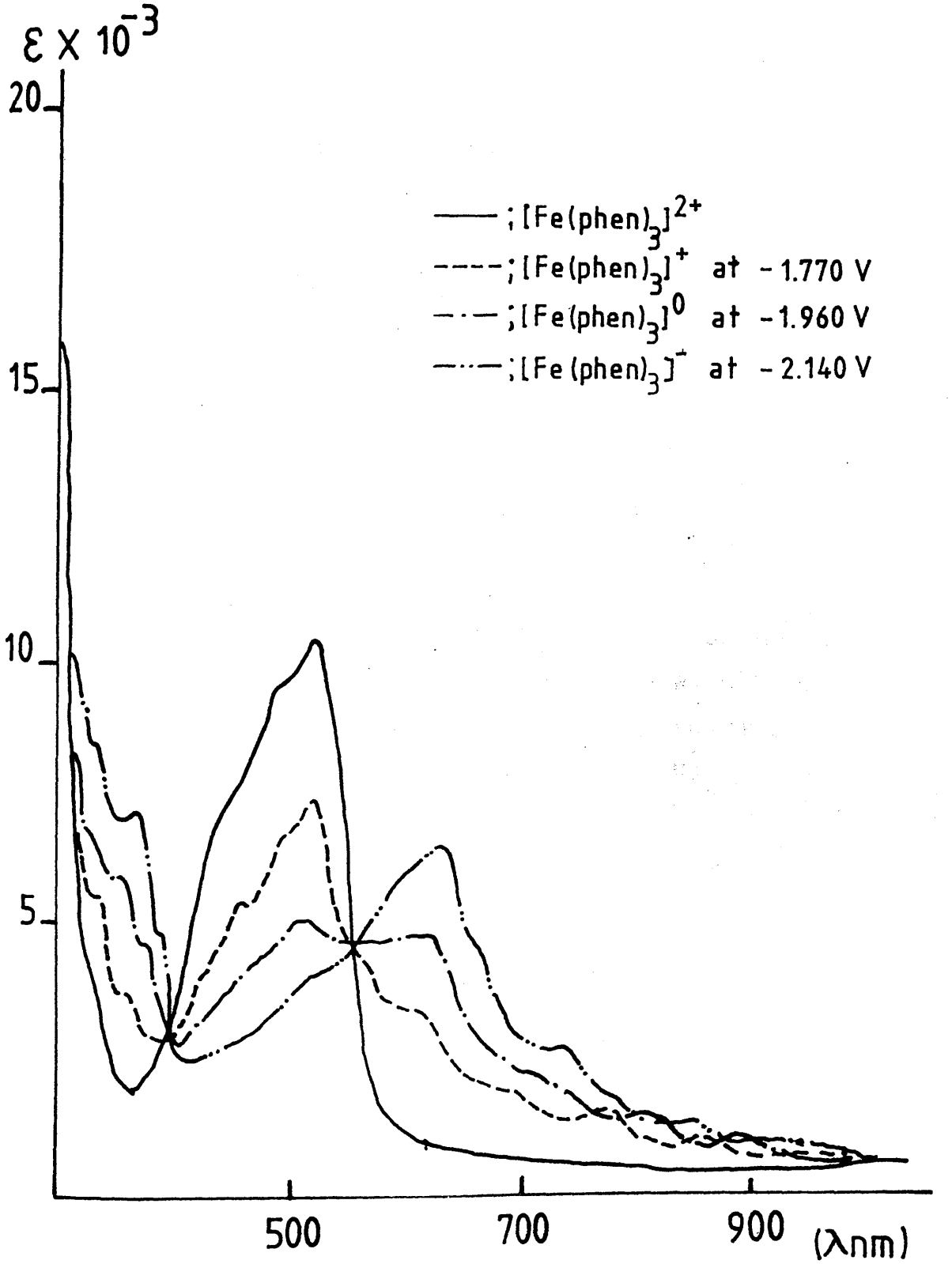

$[Fe(phen)_3]^{2+}$, no effort has been made to determine the nature of the LUMO experimentally. Surprisingly, the question as to which of the two orbitals is occupied on reduction of the compound has not yet been unequivocally determined. Even though numerous M.O. calculations have been performed for the 1,10-phenanthroline system[108-111], in those cases where the nature of the LUMO was stated either explicitly[104] or implicitly[112], it was identified as a $\pi(8)$ orbital. However, this is obviously an invalid assumption because even in the solvent separated ion pair $K^+/[phen]^-$, it is the $\pi(9)$ M.O. that is singly occupied[113]. This is more surprising since a standard Hückel M.O. calculation predicts a crossing of the two lowest unoccupied molecular orbitals of phen within the normal range of the Coulomb integral parameter term $\alpha(N)/\beta$ for the two nitrogen centres[114]. A closer look at the HMO calculation results, shows that the relative energies of the two pertinent orbitals depend on the $\alpha(N)/\beta$ term. For $\alpha(N)/\beta < 0.83$, the lowest unoccupied molecular orbital is the $\pi(8)$ orbital and its representation for $\alpha(N)/\beta \leq 0.4$ exhibits a small HMO coefficient at the nitrogen centre. Only for relatively high values of $\alpha(N)/\beta > 0.83$ is the $\pi(9)$ orbital calculated to be the LUMO.

Figure 5.10 shows the two LUMOs for phen and bpy to which an electron is transferred. The molecules are considered to have similar electronic structure, but the lowest two levels are very close to each other for 1,10-phenanthroline and moderately separated for 2,2'-bipyridine. Hence, the charge transfer from metal to ligand is composed of one kind of charge transfer for the 2,2'-bipyridine complexes, whereas it is composed of two kinds of very closely located metal-to-ligand charge-transfer transitions for the 1,10-phenanthroline complexes.

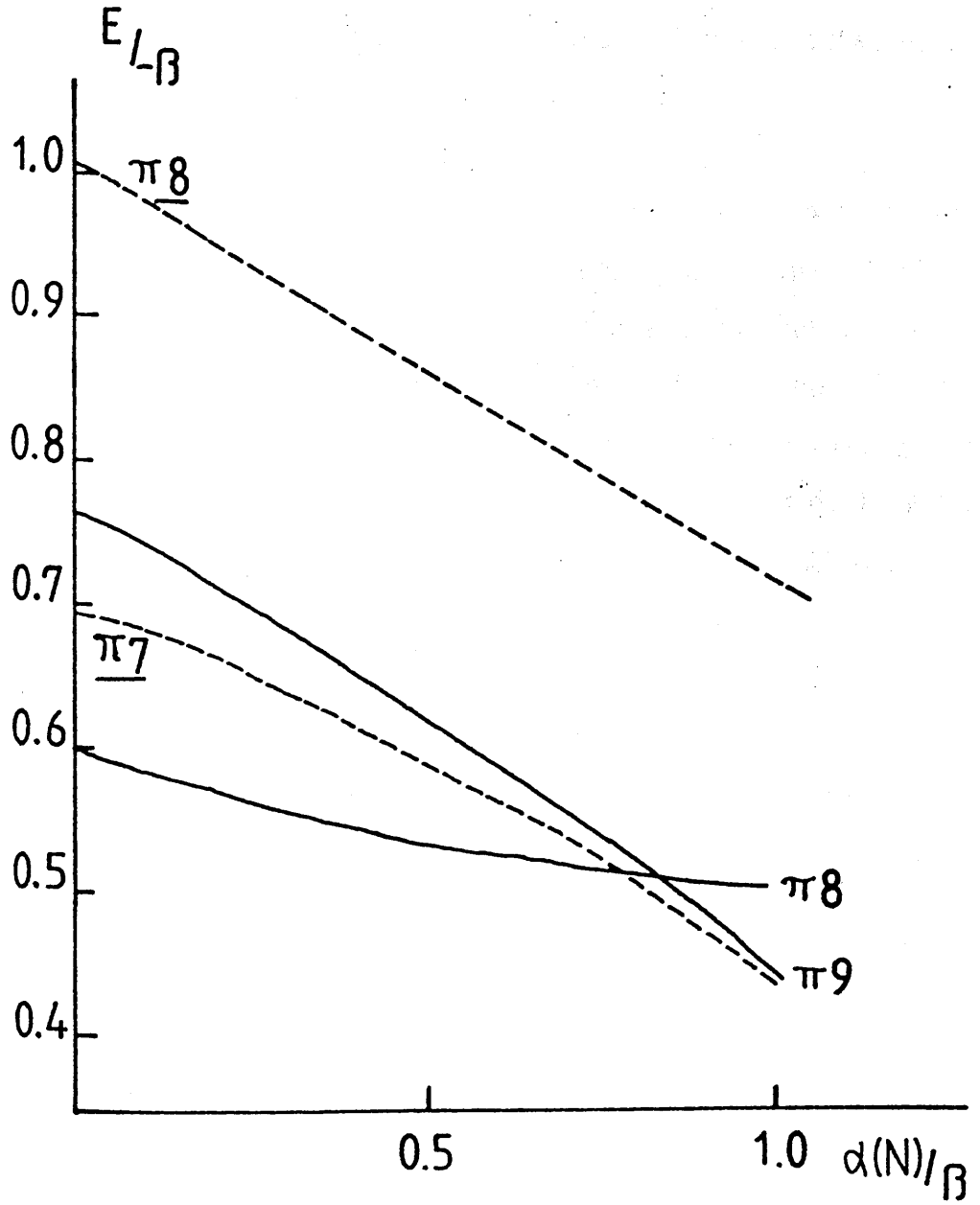

Figure 5.10. Correlation diagram showing the Hückel MO energies E/-β for the two lowest unoccupied molecular orbitals of 1,10-phenanthroline (solid line) and 2,2'-bipyridine (broken line).

An electronic absorption spectrum has been reported without assignments for the species generated by pulse radiolysis of 1,10-phenanthroline[86], and attributed to the phen-H radical. McCaffery *et al.*[115] described the LUMO of the 1,10-phenanthroline free ligand as the $\pi(8)$ orbital(a_2 type) at $\alpha(N)/\beta$ = 0.5, even though the orbital energy difference between $\pi(8)$ and $\pi(9)$ is very small (approximately 0.1 eV)

In reduced [Fe(dmp)Cl_2], the extra electron is based on the dmp ligand. The main absorption bands are shown in Table 5.3. The absorption bands centered at 370 nm and 540 nm are assigned to the $\pi \rightarrow \pi^*$ and $\pi^* \rightarrow \pi^*$ transitions of $[dmp]^-$ repectively. These two bands seem to relate to the main absorption bands of Mulazzani's reduced 1,10-phenanthroline[86], but each of the bands of the reduced Fe(II) species are lowered in energy by around 1100 cm^{-1} compared to the bands of $[phen]^-$. The band centered at 540 nm has a vibrational progression at around 1460 cm^{-1}, consistent with a transition whose main effect is to weaken the C - C bond which is positioned between C(12) and C(13) on the $[dmp]^-$ (Figure 5.11).

According to the MO calculation carried out by Kaim[116], the C - C bond between C(12) and C(13) has non-bonding character in the $\pi(12)$ orbital, bonding character in $\pi(8)$, anti-bonding character in $\pi(9)$. The vibrational structure of the bands is consistent with changes in bond order between ground and exited state, but more detailed assignments are not yet possible, since even the ground state assignment is uncertain.

Table 5.3. The observed bands of [phen]$^-$ and [Fe(dmp)Cl_2]$^-$ in DMF-TBABF$_4$ [λnm ($\bar{\upsilon}$ cm^{-1})]

[phen]$^-$ [a]	[Fe(dmp)Cl_2]$^-$	Average Energy differences (υ cm^{-1})
355 (18169)	370 (27027)	
	403 (24813)	
	435 (22989)	1584
	462 (21645)	
489 (20449)	516 (19380)	1459
	558 (17921)	
	701 (14265)	
	783 (12771)	1459
	881 (11351)	

[a]Data from Mulazzani *et al.*[86]

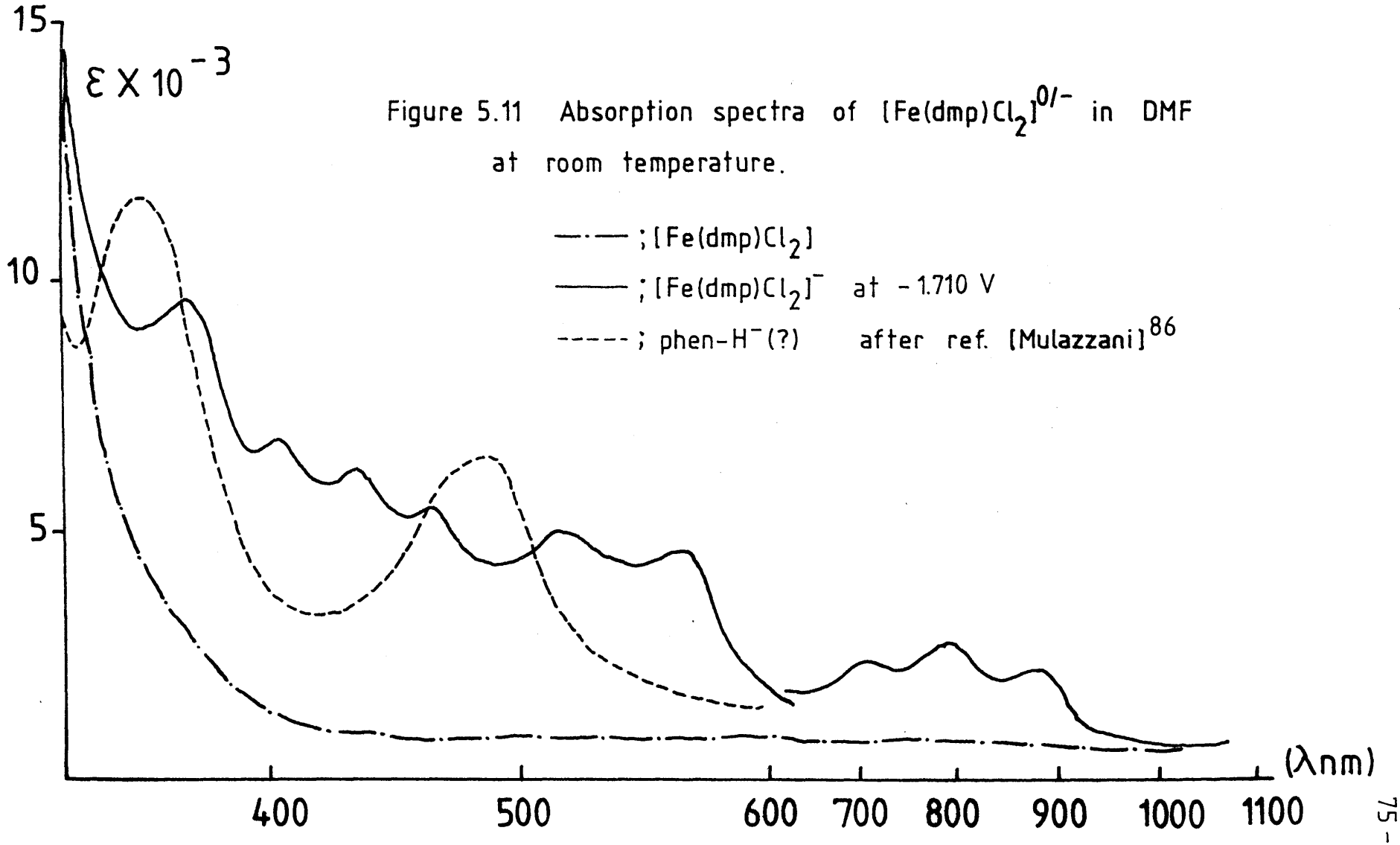

Figure 5.11 Absorption spectra of $[Fe(dmp)Cl_2]^{0/-}$ in DMF at room temperature.

—·— ; $[Fe(dmp)Cl_2]$

——— ; $[Fe(dmp)Cl_2]^-$ at -1.710 V

----- ; phen-H^-(?) after ref. [Mulazzani][86]

The triply split absorption band which appeared unexpectedly between 403 nm and 462 nm has a vibrational progression of around 1584 cm^{-1}. This absorption band may be associated with transitions to higher orbitals, such as $\pi(13)$ or $\pi(14)$.

The absorption spectra of reduced $[Fe(phen)_3]^{2+}$ show bands at around 800 nm, 600 nm and 390 nm. These increase in intensity with the degree of reduction and are therefore assigned to the reduced 1,10-phenanthroline ligand (Figure 5.9). For the reasons given above, more detailed assignments seem premature.

Figure 5.12 shows the electronic absorption spectra of the 2,2';6',2''- terpyridine anion which was synthesised as the lithium salt by direct reaction in ether at room temperature using an ultrasonic bath. Repulsions among the non-bonding and anti-bonding electrons on the three nitrogen atoms of terpyridine keep them far apart. This situation holds with regard to the conformation of the free terpyridine anion. We predict that the lithium cation is coordinated between the three nitrogen atom of $[terpy]^-$ and that the unpaired electron resides in the π-orbitals of the aromatic compound. The 2,2';6',2''- terpyridine has eighteen Hückel π-molecular orbitals [designated $\pi(1)$ to $\pi(18)$], but the exact assignments of the $\pi \rightarrow \pi^*$ and $\pi^* \rightarrow \pi^*$ transitions of both terpy and $[terpy]^-$ are unidentified. The observed absorption bands of the $[terpy]^-$ anion are collected in Table 5.4.

Figure 5.12 Absorption spectrum of $Li^{+}(terpy)^{-}$ in ether.

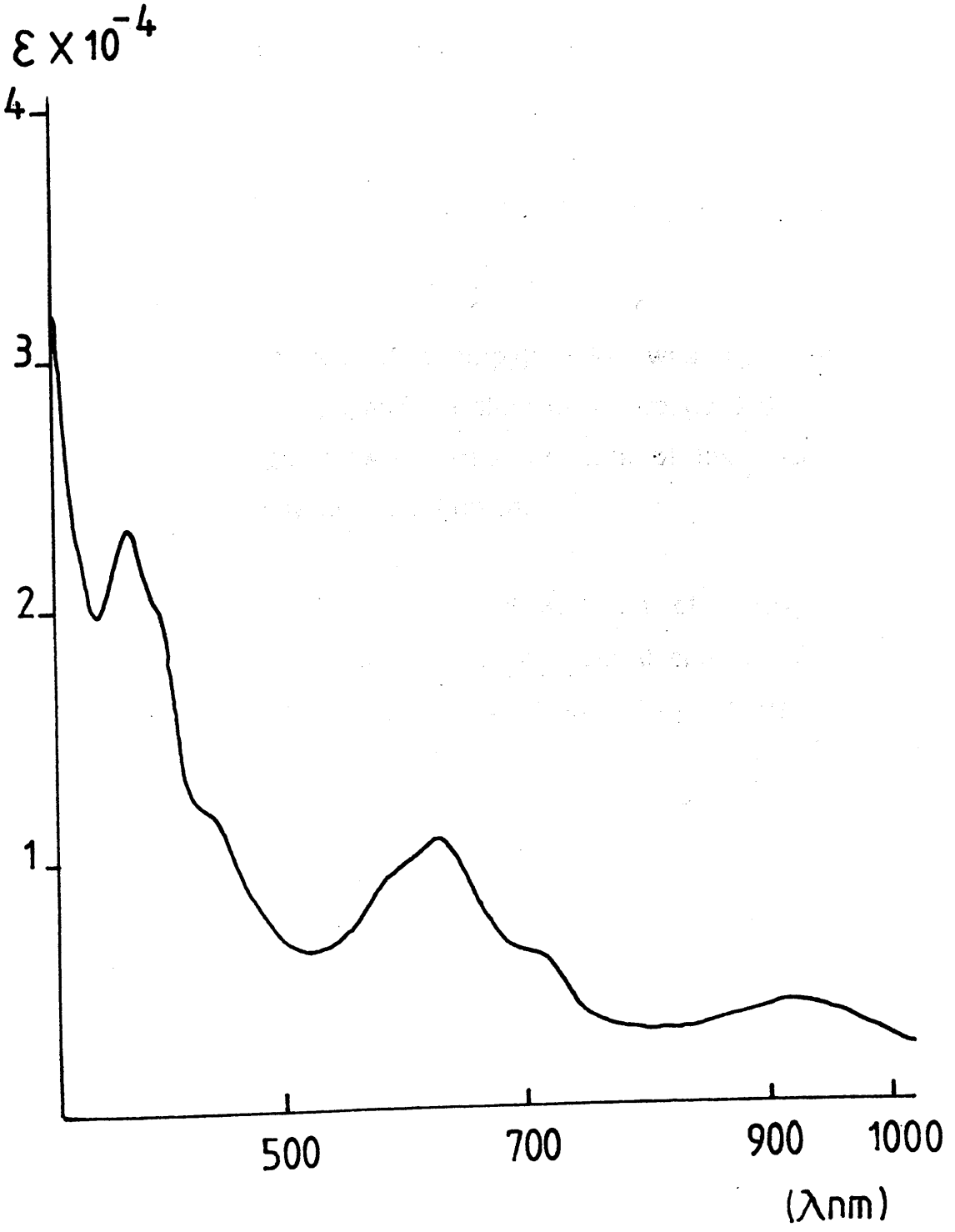

Table 5.4. The observed absorption bands of $[Li]^+[terpy]^-$ in ether [λnm ($\bar{\upsilon}$ cm^{-1})]

378	(26445)	402	(24876)sh[a]		
445	(22472)				
567	(17636)sh	621	(16103)	705	(14184)
942	(10616)				

[a]shoulder

The visible spectrum of a $[terpy]^-$ anion was first reported by Nakamura[117] who assigned the shoulder at around 560 nm to a conformational change. However, the structure of the absorption bands is more probably due to vibrations.

The strong absorption band at 378 nm of $[terpy]^-$ may correlate with the band at 310 nm in the neutral species. We can find quite a few intramolecular $\pi \rightarrow \pi^*$ and $\pi^* \rightarrow \pi^*$ transitions in the spectrum of $[terpy]^-$. According to our simple one electron model, the three lowest unoccupied molecular orbitals, which are $\pi(10)$, $\pi(11)$ and $\pi(12)$, have comparable energies; furthermore two higher orbitals [$\pi(13)$ and $\pi(14)$] are also pseudo-degenerate. Hence, there are various possible HOMO to π^* orbital transitions and also there are many $\pi^* \rightarrow \pi^*$ transitions that may occur in the reduced species; thus to understand this spectrum would be impossible without further study.

The electronic absorption spectra of the singly and doubly reduced $[Fe(terpy)_2]^{2+}$ show five main absorptions in the regions from 260 nm to 1100 nm with two isosbetic points at 301 nm and 341 nm. Figure 5.13 shows the electronic absorption spectra of the parent and reduced $[Fe(terpy)_2]^{2+}$ and the observed absorption bands are shown in Table 5.5. The bands at 274 nm and 318 nm are assigned to the intraligand $\pi \rightarrow \pi^*$ transitions of the coordinated neutral terpy and the energy difference between these two bands is approximately 5000 cm^{-1} (0.63 eV). The band at 318 nm has slightly shifted to lower energies and has lost its intensity on going to the reduced species. The loss of intensity in this absorption band is presumably due to the loss of neutral terpyridine function.

The new band at approximately 280 nm with stepwise shift on going to $[Fe(terpy)_2]^0$ is assigned to the intraligand $\pi \rightarrow \pi^*$ transition of coordinated $[terpy]^-$.

The band at 561 nm of $[Fe(terpy)_2]^{2+}$ complex is assigned to the $d\pi[Fe(II)] \rightarrow \pi^*(terpy)$ charge-transfer (MLCT) transition band. The MLCT band is moved to higher energy when the complex becomes singly reduced. More $\pi^* \rightarrow \pi^*$ transitions appear at around 590 nm, 740 nm and 910 nm having shifted to lower energy on going to the more reduced species.

When the $[Fe(terpy)_2]^{2+}$ complex becomes reduced, the added electrons are localised in the reduced $[Fe(L)_2]^{2+}$ system. From the electronic absorption spectrum, singly reduced $[Fe(terpy)_2]^{2+}$ shows $\pi \rightarrow \pi^*$ transitions of both neutral terpy and $[terpy]^-$ ligands in the same complex ion because the terpy and $[terpy]^-$

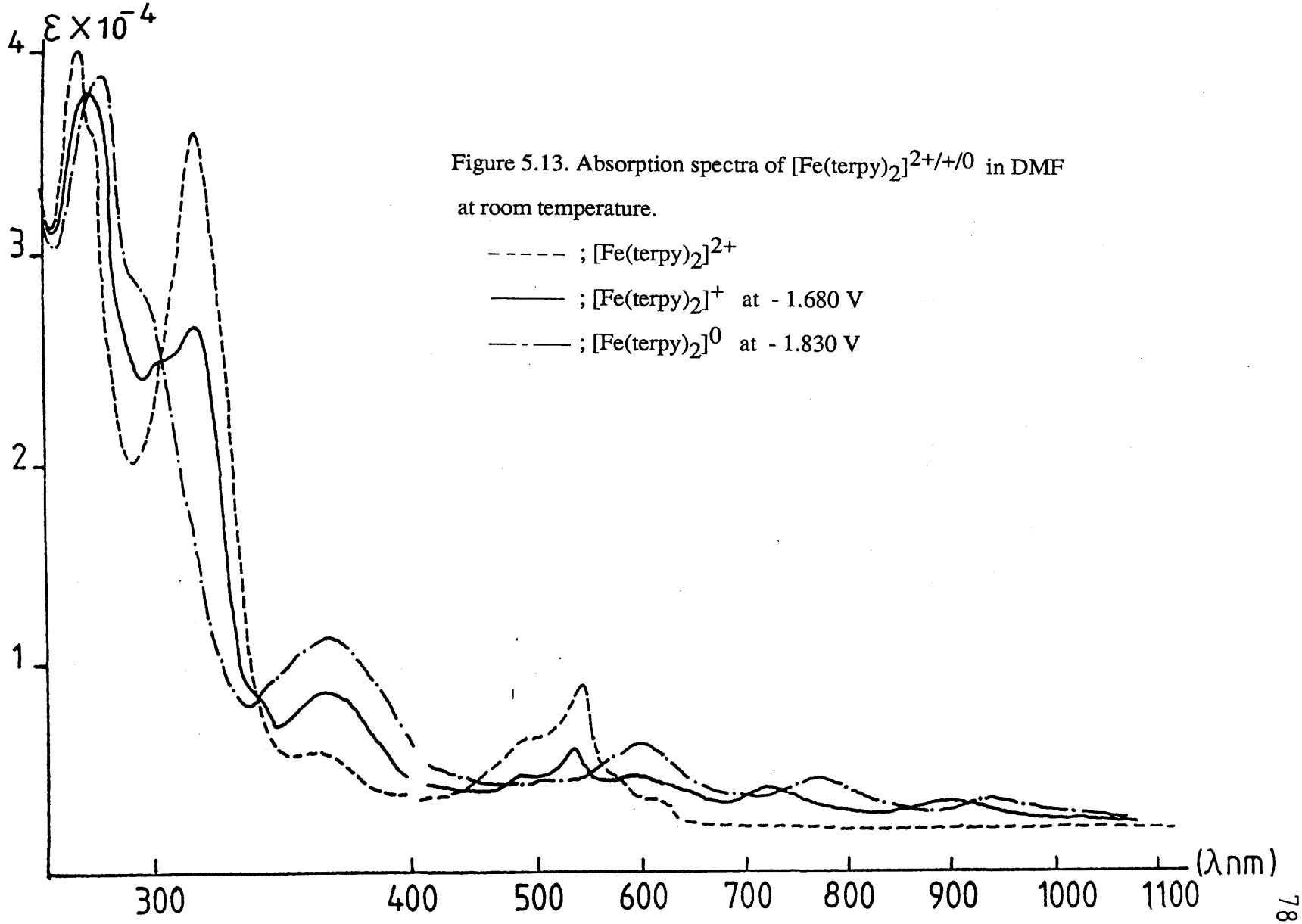

Figure 5.13. Absorption spectra of $[Fe(terpy)_2]^{2+/+/0}$ in DMF at room temperature.

- - - - - ; $[Fe(terpy)_2]^{2+}$

——— ; $[Fe(terpy)_2]^{+}$ at - 1.680 V

—·—— ; $[Fe(terpy)_2]^{0}$ at - 1.830 V

Table 5.5. The main absorption bands of reduced $[Fe(terpy)_2]^{2+}$ species in DMF-$TBABF_4$ solution. [λnm ($\bar{\upsilon}$ cm^{-1})]

	$\pi \rightarrow \pi^*(L)$	$\pi \rightarrow \pi^*(L^-)$	$\pi \rightarrow \pi^*(L)$	$\pi \rightarrow \pi^*(L^-)$	MLCT[Fe(II)] $\rightarrow \pi^*$ of terpy	$\pi \rightarrow \pi^*(L^-)$
$[Fe(terpy)_2]^{2+}$	274(36496)		318(31447)		561(17825)	
$[Fe(terpy)_2]^{+}$		278(35971) 293(34130)sh	321(31153)	366(27322)	553(18083)	585(17094) 727(13755) 896(11160)
$[Fe(terpy)_2]^{0}$		284(35211) 300(33333)sh		371(26954)		593(16863) 755(13245) 927(10787)

ligands are non-degenerate; the $\pi \rightarrow \pi^*$ transitions of neutral terpy are of higher energy than the $\pi \rightarrow \pi^*$ transitions of the $[terpy]^-$ anion. Furthermore, Morris *et al.*[118] reported that the g factors and frozen spectra for one- and two-electron reduced $[Fe(terpy)_2]^{2+}$ require only an S=1/2 spin Hamiltonian, i.e. no evidence for an S=1 state is observed for the two electron product. Such behaviour is consistent with single chelated ring localisation of the reduced electrons.

Chapter 6. Spectroelectrochemistry of ruthenium(II) mixed-ligand complexes.

The central metal ion of the Ru(II) complexes in this series has a diamagnetic electronic configuration represented by low spin $d\pi^6$ and a wealth of information is available on the electrochemical behaviour of the Ru(II)-mixed ligand family[119-121]. Reduction of Ru(II) complexes may, in principle, either be metal-based or ligand-based, depending on the relative energy ordering. When the ligand field is sufficiently strong and/or the ligands can be easily reduced, reduction takes place on a ligand π^* orbital. In this case, the reduced forms, which retain the low-spin $4d^6$ configuration of Ru(II), are inert and the reduction processes are reversible[122]. The localisation of the acceptor orbitals in the reduction processes is often particularly clear in mixed-ligand complexes with different energies of the π^* orbitals. In such a case the first and subsequent reduction steps can be attributed to the various ligands in the complexes.

When the ligand field is weak and/or the ligands cannot be easily reduced, the lowest unoccupied orbital in the reduction process could be metal based. In this case reduction would lead to an unstable low spin d^7 system, which should give rise to a fast ligand dissociation making the electrochemistry irreversible[122].

6.1. Electrochemistry of Ru(II) mixed-ligand complexes.

The reduction of ruthenium(II) mixed-ligand complexes studied here are ligand based. The effect of the metal is to lower the energy of the ligand π^* level by approximately 0.6 V. The cyclic voltammograms of each complex in DMF at room

temperature on a platinum working electrode are shown in Figure 6.1 and 6.2. Peak potentials for different waves are given in Table 6.1. All processes were confirmed to be reversible one-electron steps and solvents (e.g. propylene carbonate, dimethylsulphoxide, acetonitrile) do not affect the peak potentials. Replacing the platinum working electrode with gold makes no difference to the electrochemistry.

$[Ru(phen)(bpy)_2]^{2+}$ undergoes three reversible one-electron reductions similar to $[Ru(bpy)_3]^{2+}$ [123] and the sequence of steps is best interpreted as stepwise reduction of each ligand π^* system. However, the potential gap between the second and the third redox waves is larger (approximately 260 mV) than the potential difference between the first and second redox waves (approximately 175 mV). By comparison with the reduction potential gaps of $[Ru(bpy)_3]^{2+}$ which are 175 mV between two redox waves[123], the third reduction of $[Ru(phen)(bpy)_2]^{2+}$ is presumably due to reduction of the coordinated 1,10-phenanthroline ligand.

The cyclic voltammogram of cis-$[Ru(bpy)_2(NCS)_2]$ at room temperature shows one reversible and one irreversible one-electron reduction process (Figure 6.2). However, at -40 °C, the second reduction wave become a reversible process and appears at -1.980 V because the temperature dependent substitution reaction on the metal centre becomes very slow. At low temperature, both reduction potentials of $[Ru(bpy)_2(NCS)_2]$ are shifted to more negative potentials (about 35 mV). This can be safely attributed to the temperature induced junction potential since the oxidation potential of ferrocene is found to move by the

Table 6.1. The observed oxidation and reduction potentials of Ru(II) mixed-ligand complexes in DMF-$TBABF_4$ solution at room temperature.

Compounds	$E_{oxi}^{(III/II)}$	1st Red.	2nd red	3rd red
$[Ru(bpy)_2(phen)]^{2+}$	+0.980(0.062)	-1.667(0.065)[a]	-1.854(0.071)	-2.117(0.086)
$[Ru(bpy)_2(pn)]^{2+}$	+0.810(0.065)	-1.735(0.069)	-1.928(0.077)	
$[Ru(bpy)_2(NCS)_2]$	+0.668(0.072)	-1.829(0.072)	-1.980(0.084)[b]	

[a] $E_{pa} - E_{pc}$ (V) [b] At -40 °C

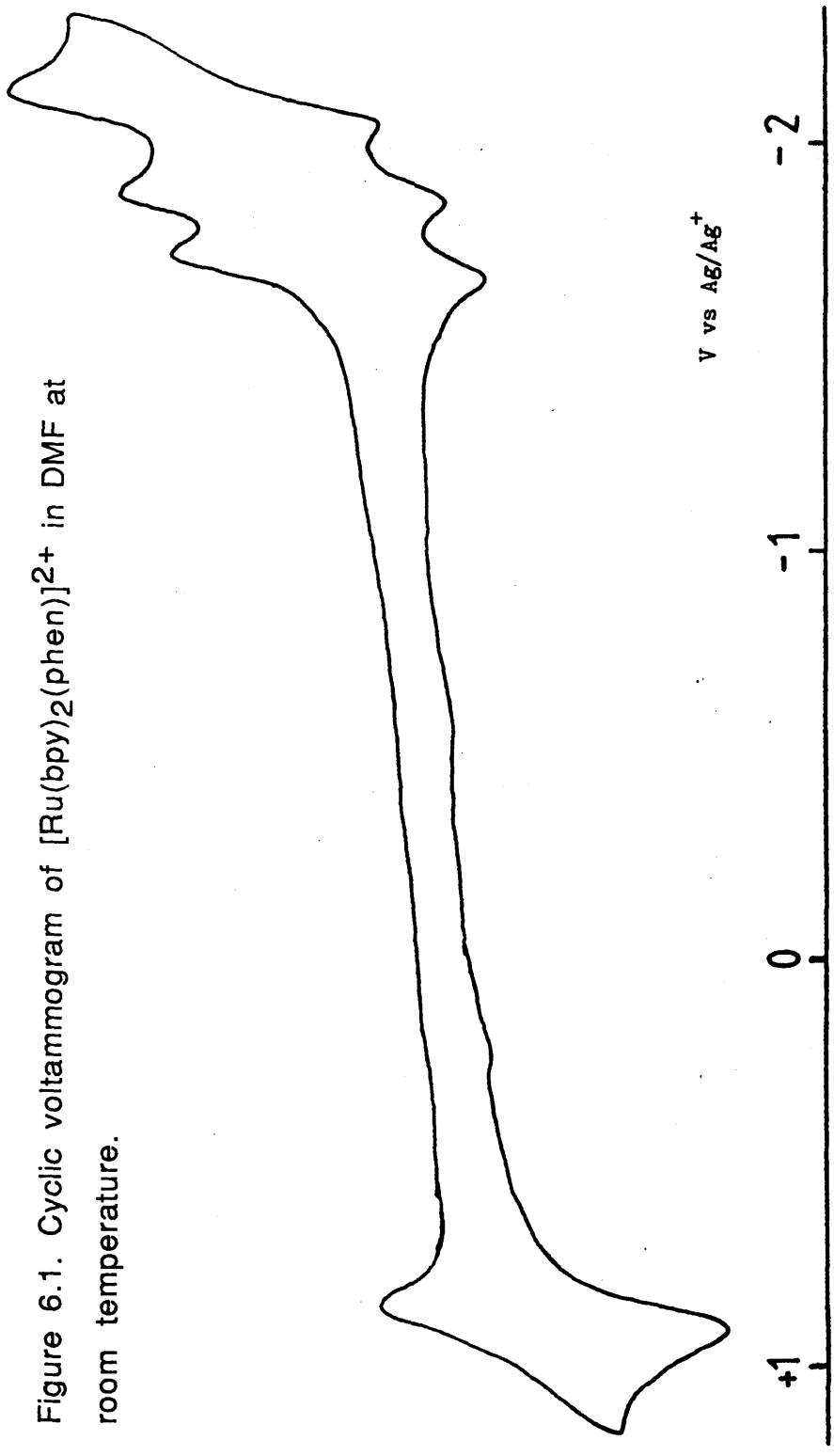

Figure 6.1. Cyclic voltammogram of $[Ru(bpy)_2(phen)]^{2+}$ in DMF at room temperature.

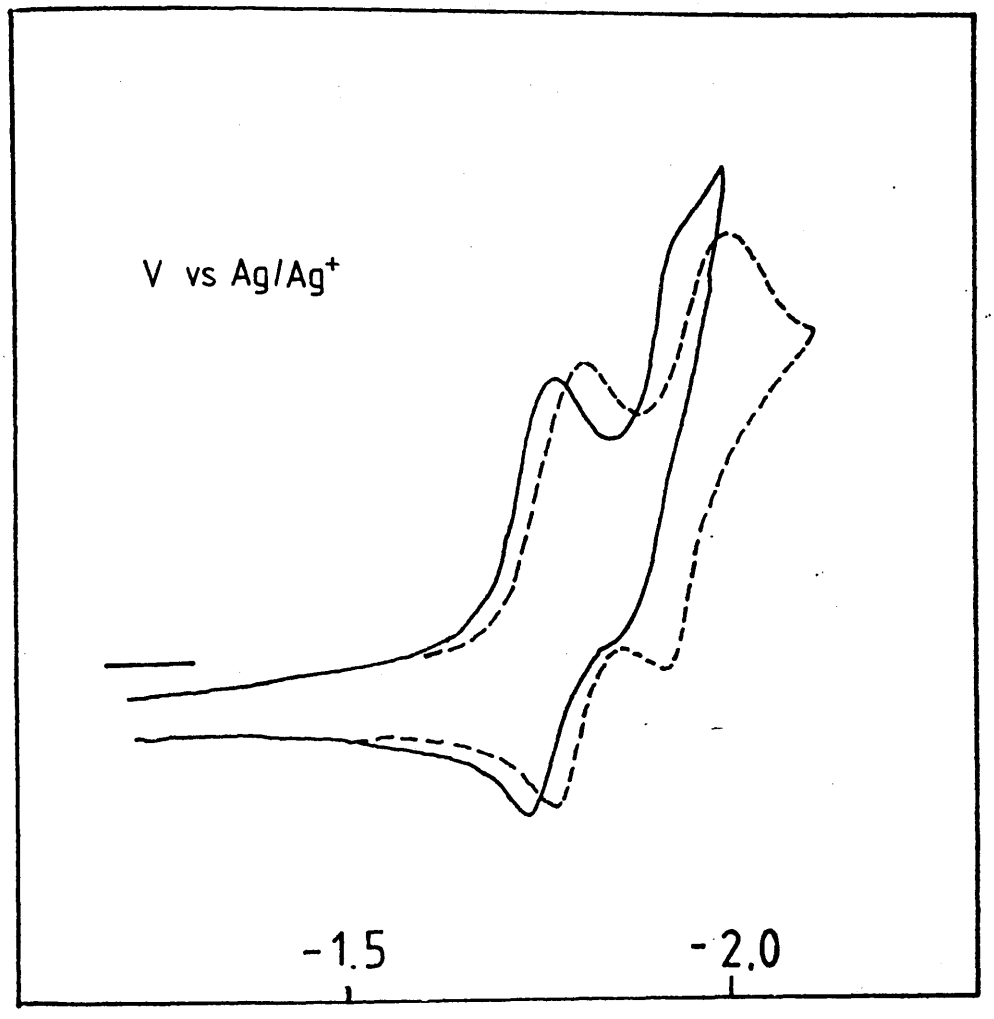

Figure 6.2. Cyclic voltammogram of $[Ru(bpy)_2(NCS)_2]$ in DMF at room temperature (————) and -40 °C (------).

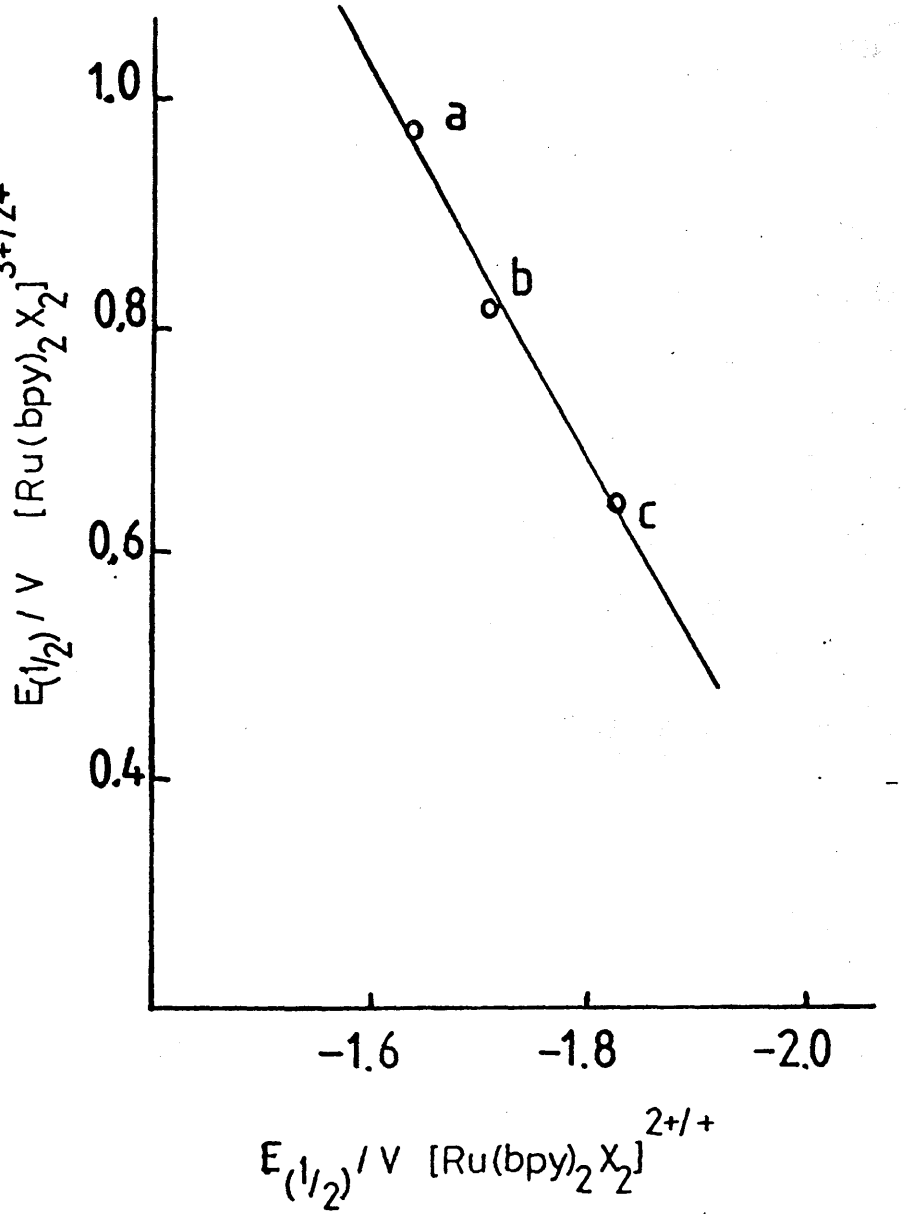

Figure 6.3. Free energy correlation for the first oxidation and the first reduction (V vs Ag/Ag^+) for ruthenium mixed-ligand complexes studied here. Slope was 2.2 for this series. a; $[Ru(bpy)_2(phen)]^{2+}$ b; $[Ru(bpy)_2(pn)]^{2+}$ c; $[Ru(bpy)_2(NCS)]$

removed from the complete metal d_π^6 sub-shell of the Ru(II) core to give a Ru(III)/neutral bpy complex.

$$[Ru^{2+}(bpy)_2X_2]^{2+} \rightarrow [Ru^{3+}(bpy)_2X_2]^{3+} + e$$

Where X_2= phen, 1,2-diaminopropane and $(NCS)_2^{2-}$

Thus, we expect, in this case, the [Ru(III)]$d\pi \rightarrow \pi^*$(bpy) charge transfer (MLCT) (at higher energy than MLCT in the Ru(II) parent) as well as the (bpy)$\pi \rightarrow$ dπ[Ru(III)] charge transfer (LMCT). Also we expect an intraligand $\pi \rightarrow \pi^*$ transition of the neutral bipyridyl ligand to occur as in the parent species. However, this transition should be shifted to lower energy because of the higher central metal charge.

The split absorption bands between 270 nm and 310 nm are clearly assigned to the $\pi \rightarrow \pi^*$ transition which involves neutral bipyridine ligands. (Figure 6.4, Table 6.2) The splitting of these bands is possibly due to the asymmetry of the t_{2g}^5 configuration.

Yellowlees has reported[123] that the π^* orbital of bpy in Ru(III) complexes is approximately 3200 cm^{-1} (0.4eV) lower than in Ru(II) complexes which causes easy reduction. However, the Ru(III) complexes also have lower bipyridine π orbitals, making the theoretical shift approximately 2200 cm^{-1} to lower energies in Ru(III) complexes. In the complexes we studied, the $\pi \rightarrow \pi^*$ transition of the Ru(III) complexes is shifted by approximately 2000 cm^{-1} to lower energies compared to Ru(II)-bpy complexes which is in satisfactory agreement with Yellowlees' results.

Table 6.2. The observed absorption bands of Ru(III) mixed-ligand complexes.[λnm($\bar{\upsilon}$ cm^{-1})

Compounds	$\pi \rightarrow \pi^*$	MLCT Ru(III) $\rightarrow$ bpy	MLCT Ru(III) $\rightarrow X_2$	LMCT $X_2 \rightarrow$ Ru(III)	LMCT bpy(π) $\rightarrow$ Ru(III)
$[Ru(bpy)_2(pn)]^{3+}$	295(33823) 307(32573)	459(21786)			583(17152)
$[Ru(bpy)_2(NCS)_2]^{+}$	296(33783) 306(32679)	462(21645)	501(19960)?		589(16977)
$[Ru(bpy)_2(phen)]^{3+}$		463(21598)	495(20202)	701(14265)	638(15673)

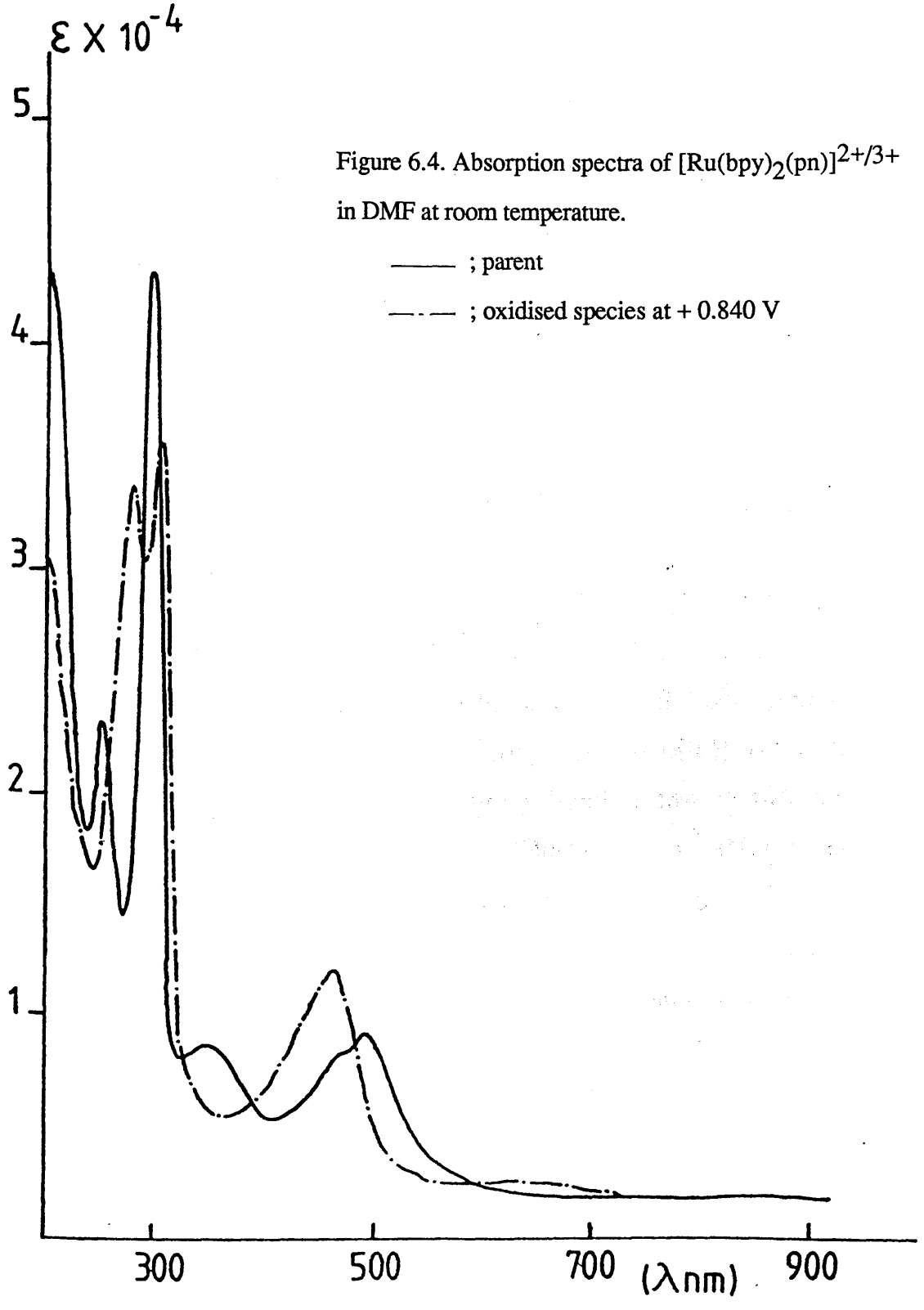

Figure 6.4. Absorption spectra of $[Ru(bpy)_2(pn)]^{2+/3+}$ in DMF at room temperature.

——— ; parent

—·— ; oxidised species at + 0.840 V

The weak and broad bands which appear in the region between 575 nm and 720 nm are assigned to ligand-to-metal charge transfer (bpy)$d\pi \rightarrow d\pi$[Ru(III)] (Figure 6.5). The $\pi \rightarrow t_{2g}$ transition of $[Ru(bpy)_2(NCS)_2]^+$ has a higher energy than that of $[Ru(bpy)_2(phen)]^{3+}$ and the band of $[Ru(bpy)_2(pn)]^{3+}$ is positioned at a similar energy to that of $[Ru(bpy)_2(NCS)_2]^+$. Hence the required energy of the LMCT may be related to the relevant π electron populations of ligand X_2.

Two ligand-to-metal charge-transfer transitions are possible in principle, i.e. $\pi \rightarrow t_2$ and $\pi \rightarrow e^*$[128]. However, the latter transition[129] should lie at around 20000 cm^{-1} to higher energy and should be less intense. Such a transition would be obscured by ligand bands.

It is suggested that the visible spectrum of $[Ru(bpy)_2(phen)]^{3+}$ (Figure 6.5) consists of two overlapping transitions; the [Ru(III)]$d\pi \leftarrow \pi$ (bpy) and [Ru(III)] $\leftarrow \pi$ (phen) charge-transfer transitions. The strong band between 440 nm and 480 nm is tentatively assigned to [Ru(III)]$d\pi \rightarrow \pi^*$(bpy) charge transfer, although the energy difference between this band and the MLCT band of the corresponding Ru(II) species is surprisingly small. Absorption spectra of the Ru(III) complexes between 440 nm and 550 nm are shown in Figure 6.6. The spectrum of $[Ru(bpy)_2(phen)]^{3+}$ shows two transitions and the band at 495 nm is assigned to the [Ru(III)]$d\pi \rightarrow \pi^*$(bpy) charge-transfer transition and the band at 463 nm is assigned to the [Ru(III)]$d\pi \rightarrow \pi^*$(phen) charge-transfer transition because of their relative energies.

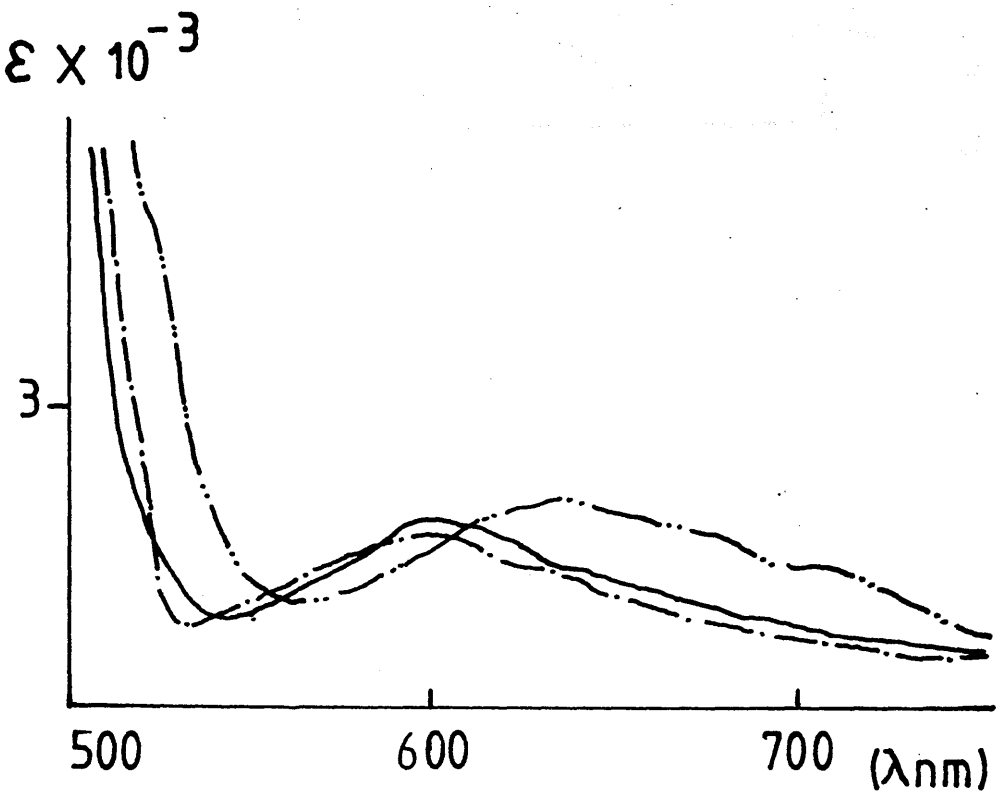

Figure 6.5 The LMCT bands of $[Ru(bpy)_2X_2]^{3+}$ in DMF at room temperature.

——— ; $[Ru(bpy)_2(pn)]^{3+}$ at +0.840 V
—·— ; $[Ru(bpy)_2(NCS)_2]^{+}$ at +0.700 V
—··— ; $[Ru(bpy)_2(phen)]^{3+}$ at +1.010 V

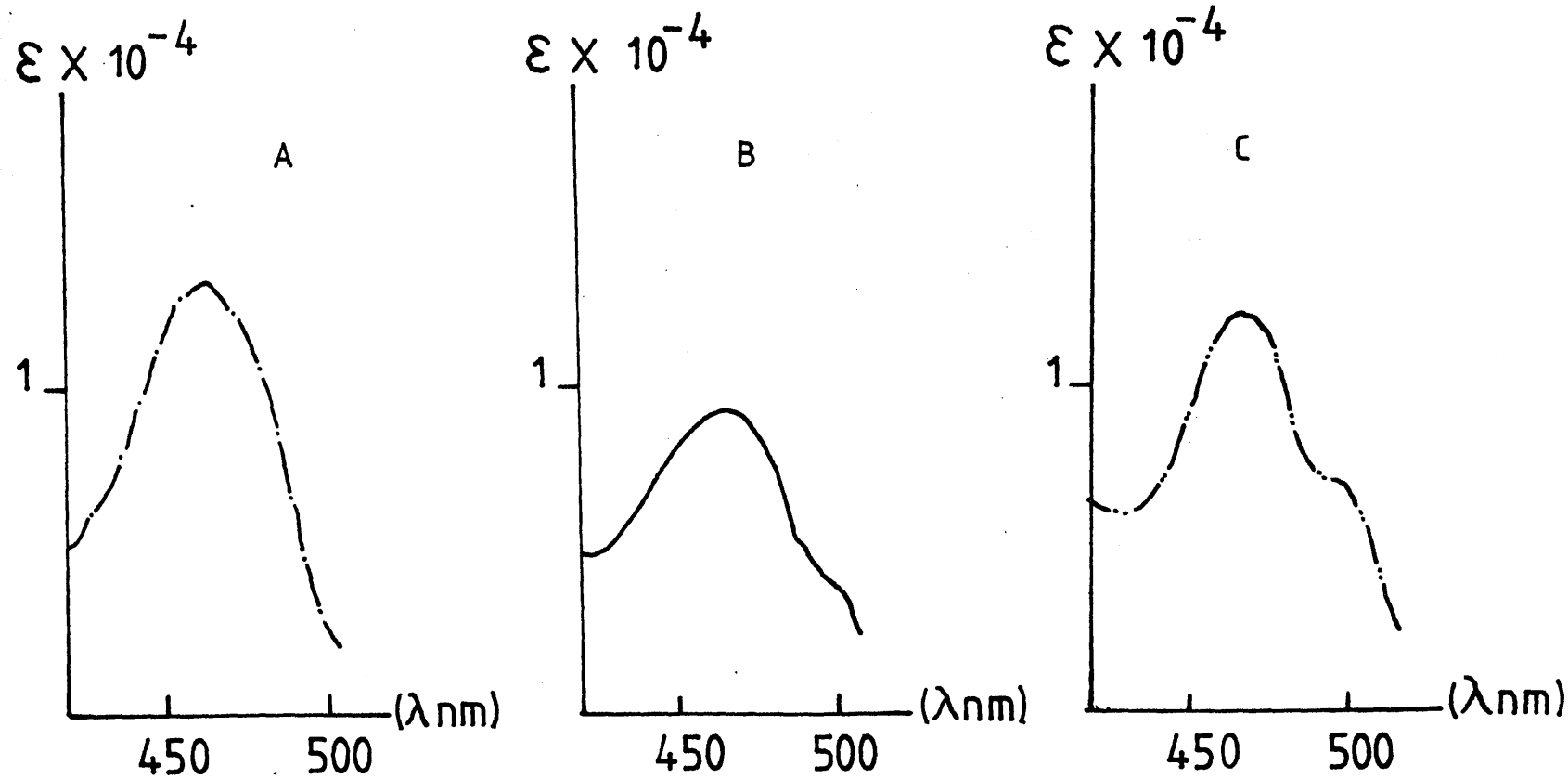

Figure 6.6 Absorption spectra of $[Ru(bpy)_2X_2]^{3+}$ in DMF at room temperature. (400nm - 500nm)

A ; $[Ru(bpy)_2(NCS)_2]^{+}$ at +0.700 V B ; $[Ru(bpy)_2(pn)]^{3+}$ at +0.840 V

C $[Ru(bpy)_2(phen)]^{3+}$ at +1.010 V

6.3. Electronic Absorption Spectra of the Reduced Ru(II) Mixed-Ligand Complexes.

The UV-visible spectra of $[Ru(bpy)_2(pn)]^{2+}$ and $[Ru(bpy)_2(NCS)_2]$ both show the characteristic absorption bands of M-bpy complexes. The high energy absorption band of each complex in the region between 240 nm and 310 nm is associated with the ligand-localised $\pi \rightarrow \pi^*$ transition which is due to coordinated bpy ligands. However, in $[Ru(bpy)_2(phen)]^{2+}$, the extremely intense intraligand $\pi \rightarrow \pi^*$ transitions of coordinated phen occur at similar energies to that of bpy and they apparently mask the expected $\pi \rightarrow \pi^*$ transition of coordinated bpy.

The energies of the HOMO and LUMO orbitals of the two ligands are similar, but the other orbitals are of considerably different energies. The differences are to be expected since phen has two more π-orbitals than does bpy and so there cannot be one-to-one correspondence of orbitals[130]. The similarities between the HOMO and LUMO orbitals explain the many parallels typically found between the chemistry of bpy and phen metal complexes.

Another strong band appears at around 500 nm which is assigned to the $d\pi[Ru(II)] \rightarrow \pi^*$(ligand) charge-transfer (MLCT) transition. This MLCT band energy responds in a consistent and systematic way to changes in the remaining ligands, X_2. If X_2 is a

good π acceptor ligand, back-bonding from Ru(II) to X_2 results in stabilisation of the dπ levels relative to π*(bpy) and in an increase in the MLCT band energy[131]. A decrease in the MLCT band energy is observed when X_2 is a relatively good π-donor ligand. Accordingly, the λmax of the MLCT absorption bands of the ruthenium mixed-ligand complexes are slightly red-shifted compared to that of $[Ru(bpy)_3]^{2+}$. As a result, charge transfer from metal to higher ligand π* levels can also be observed[132].

The characteristic $[bpy]^-$ intraligand $\pi \rightarrow \pi^*$ transitions can be seen in the near-infrared, visible and ultraviolet regions, with the stepwise growth of the ultraviolet and near infrared bands, and stepwise shift to lower energies of the visible band. Thus the complexes must be formulated in terms of a Ru(II) core with $[bpy]^0$ and $[bpy]^-$ ligands for $[Ru(bpy)_2(X)_2]^{2+}$ and $[Ru(bpy)_2(X)_2]^0$ respectively, and both ligands present in $[Ru(bpy)_2(X)_2]^+$. In each of these, the two reductions which are of primary interest here correspond to formation of radical anions, as electrons are added to the π* orbitals of the bipyridyl ligands[133].

$$\textbf{cis-}[Ru(bpy)_2(X)_2]^{2+} = \textbf{cis-}[Ru^{2+}(bpy^0)_2(X)_2]^{2+}$$
$$\textbf{cis-}[Ru(bpy)_2(X)_2]^{+} = \textbf{cis-}[Ru^{2+}(bpy^-)(bpy^0)(X)_2]^{+}$$
$$\textbf{cis-}[Ru(bpy)_2(X)_2]^{0} = \textbf{cis-}[Ru^{2+}(bpy^-)_2(X)_2]^{0}$$

However, the third reduction of $[Ru(bpy)_2(phen)]^{2+}$ is due to an one-electron addition to the π* orbital of the 1,10-phenanthroline ligand.

$$[Ru(bpy)_2(phen)]^- = [Ru^{2+}(bpy^-)_2(phen^-)]^-$$

The electronic absorption spectra of the reduced Ru(II) mixed-ligand complexes are shown in Figure 6.7 and 6.8. The main bands of the reduced cis-$[Ru(bpy)_2(X)_2]^{2+}$ complexes are collected in Table 6.3. The absorption spectra of these Ru(II) mixed-ligand complexes are not solvent dependent in dimethylsulphoxide, dichloromethane or acetonitrile.

The high energy band around 250 nm is assigned to the overlapping $\pi(6) \rightarrow \pi(8),\pi(9)$ transitions of $[bpy]^-$ although no individual assignment is possible. The band at approximately 300 nm is assigned to the intraligand $\pi(6) \rightarrow \pi(7)$ transition of neutral bpy. This band shifts to slightly lower frequency in the reduced species. The intensity loss on going from the parent to the reduced species in this region is due to the loss of the neutral bipyridine function.

The new band at around 350 nm is assigned to the $\pi(6) \rightarrow \pi(7)$ transition of coordinated $[bpy]^-$. The extinction coefficient of this band is proportional to the number of coordinated $[bpy]^-$ ligands.

The band at 495 nm is assigned as a $d\pi[Ru(II)] \rightarrow \pi^*(bpy)$ charge-transfer transition band. The band at around 520 nm is assigned to the $\pi(7) \rightarrow \pi(10)$ transition of coordinated $[bpy]^-$. The singly reduced species in this energy region, which has co-existing $[bpy]^0$ and $[bpy]^-$ ligands, has a two-fold structure due to the superposition of a Ru-bpy charge transfer and $[bpy]^-$ intraligand charge transfer.

Table 6.3. The absorption bands and assignments of cis-$[Ru(bpy)_2X_2]^{n+}$ complexes. [λnm($\bar{\upsilon}$ cm^{-1})]

	MLCT Ru(II) → bpy	π(6)→π(8,9) of [bpy]⁻	π(6)→π(7) of bpy	π(6)→π(7) of [bpy]⁻	MLCT Ru(II) → bpy	π(7)→π(10) of [bpy]⁻	π(7)→π(9,8) of [bpy]⁻
$[Ru(bpy)_2(pn)]^{2+}$	242(41332)		294(34013)		490(20408)		
$[Ru(bpy)_2(pn)]^{+}$		245(40816)	298(33557)	358(27932)	467(21413)sh	507(19723)	908(11013)
$[Ru(bpy)_2(pn)]^{0}$		249(40160)		365(27397)		518(19305)	924(10822)
$[Ru(bpy)_2(NCS)_2]$	238(42016)		288(34722)		465(21505)		
$[Ru(bpy)_2(NCS)_2]^{-}$		242(41322)	292(34246)	351(28490)	463(21598)sh	499(20040)	894(11185)
$[Ru(bpy)_2(NCS)_2]^{2-}$		246(40650)		357(28011)		511(19569)	911(10976)
$[Ru(bpy)_2(phen)]^{2+}$					503(19880)		
$[Ru(bpy)_2(phen)]^{+}$				369(27100)		515(19417)	921(10857)
$[Ru(bpy)_2(phen)]^{0}$				372(26881)		527(18975)	945(10582)

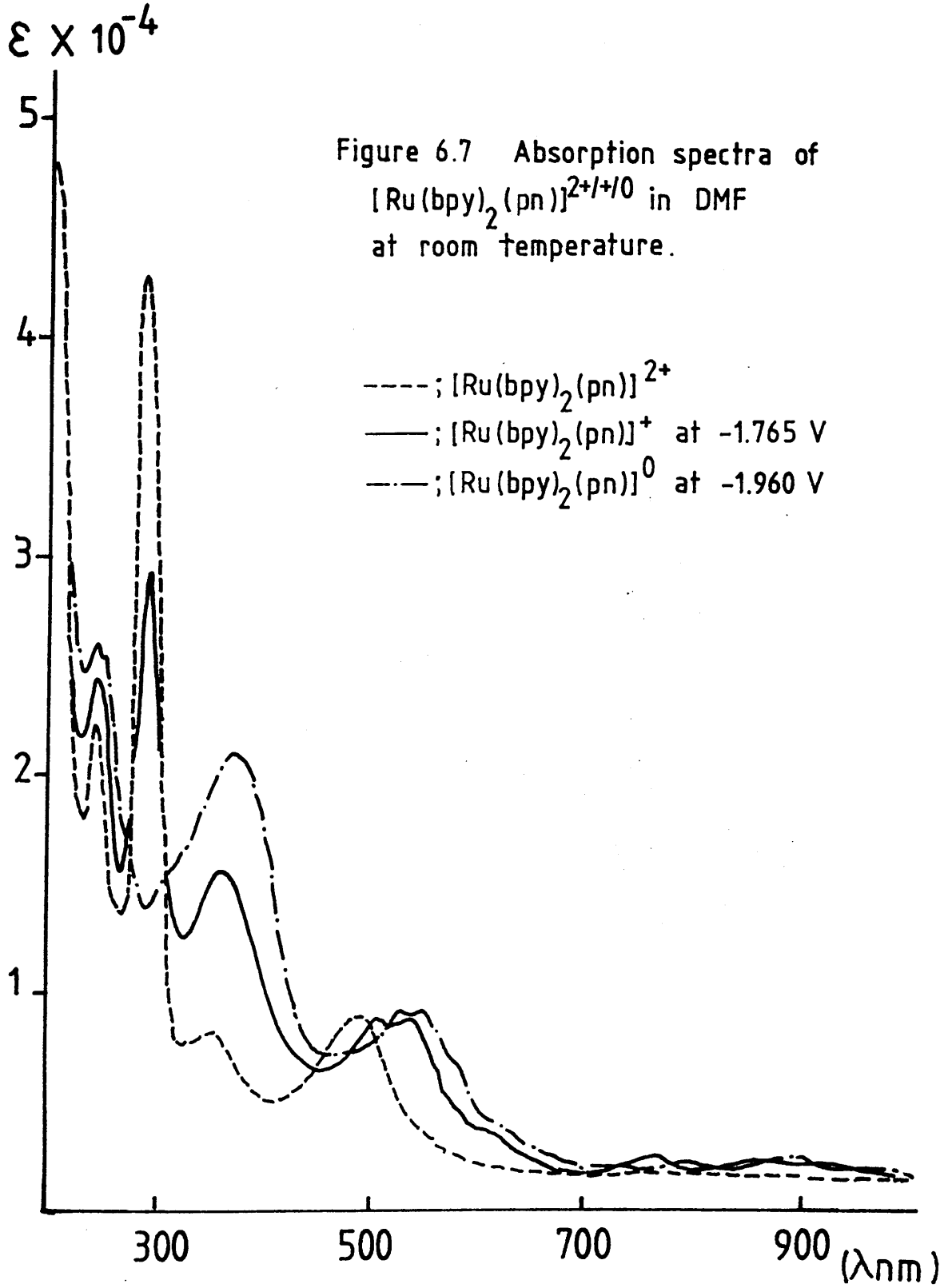

Figure 6.7 Absorption spectra of $[Ru(bpy)_2(pn)]^{2+/+/0}$ in DMF at room temperature.

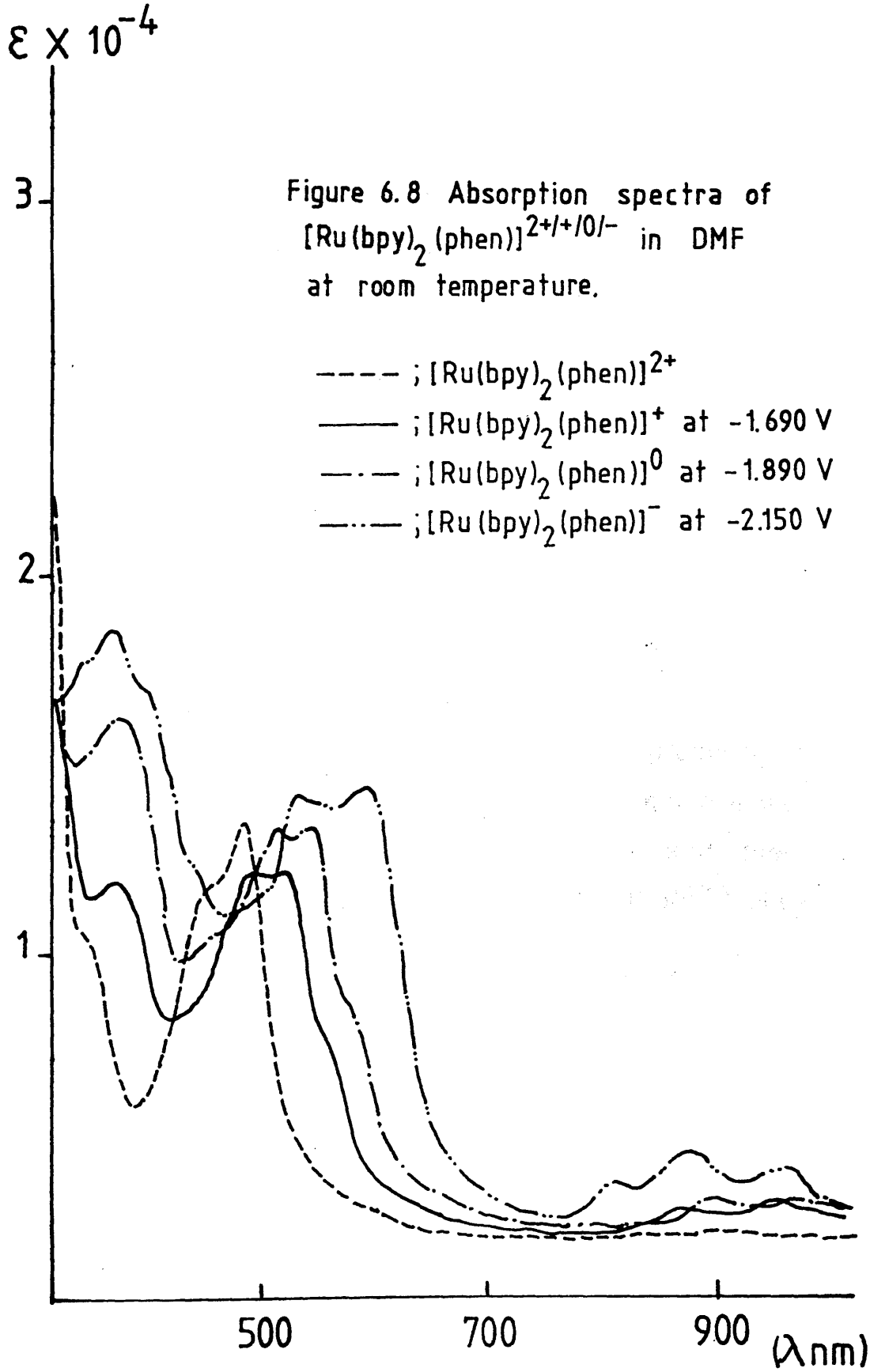

Figure 6.8 Absorption spectra of $[Ru(bpy)_2(phen)]^{2+/+/0/-}$ in DMF at room temperature.

---- ; $[Ru(bpy)_2(phen)]^{2+}$

——— ; $[Ru(bpy)_2(phen)]^{+}$ at -1.690 V

—·— ; $[Ru(bpy)_2(phen)]^{0}$ at -1.890 V

—··— ; $[Ru(bpy)_2(phen)]^{-}$ at -2.150 V

The $\pi(7) \rightarrow \pi(8)$, $\pi(9)$ transitions of coordinated $[bpy]^-$ appear in near-infrared region, and these can be seen to grow in a progressive fashion with the increasing number of $[bpy]^-$ ligands.

The electronic absorption spectrum of the triply reduced $[Ru(bpy)_2(phen)]^{2+}$ shows a similar feature to that of the spectrum of $[Fe(phen)_3]^-$ (Figure 6.8 and Table 6.4). The new band centered at 375 nm may be assigned to the $\pi \rightarrow \pi^*$ transition (HOMO $\rightarrow$ LUMO) of $[phen]^-$. The bands around 550 nm and 900 nm may be assigned to $\pi^* \rightarrow \pi^*$ transitions, but more precise assignments cannot be given.

Bosnich[134] described mixed ligand complexes of ruthenium(II) such as $[Ru(bpy)_2(phen)]^{2+}$ and $[Ru(bpy)(phen)_2]^{2+}$ as having C_2 symmetry, whereas the symmetry of $[Ru(bpy)_3]^{2+}$ is D_3. There is considerable similarity between the c.d spectra of the mixed $[Ru(bpy)_n(bpy^-)_{3-n}]^{2+}$ species and the mixed $[Ru(bpy)_n(phen)_{3-n}]^{2+}$ complexes[80]. Heath *et al.*[134] observed a weak absorption band between 4000 cm^{-1} and 5000 cm^{-1} in singly and doubly reduced $[Ru(bpy)_3]^{2+}$ which they attributed to a ligand $\rightarrow$ ligand intervalence charge-transfer transition (IVCT). This implies the simultaneous presence of discrete bpy and $[bpy]^-$ groups and as the IVCT band was weak in intensity, there cannot be much interaction between the different ligands in the complex. This could be predicted by the electron localised model for the complexes. McCaffery *et al.*[115] and Noble[80] have calculated the exciton interaction energy of which average energies are 970 cm^{-1} for bpy with bpy, 1400 cm^{-1} for $[bpy]^-$ with $[bpy]^-$ and

Table 6.4. The observed main bands of $[Ru(bpy)_2(phen)]^-$ in DMF-$TBABF_4$ at room temperature.

λmax		$\varepsilon \times 10^{-4}$
λnm	$\tilde{\upsilon}\ cm^{-1}$	$dm^3\ mol^{-1}\ cm^{-1}$
375	26666	1.89
536	18656	1.31
582	17182	1.43
807	12391	0.43
899	11123	0.58
1006	9940	0.50

1200 cm^{-1} for bpy with $[bpy]^-$. These results are easily reproduced and confirm without doubt the localised electron model for the complexes.

Chapter 7. Spectroelectrochemistry of Binuclear Transition Metal (Re, Cu, Mo) Complexes of 2,2'-Bipyrimidine.

Binuclear transition metal complexes of 2,2'-bipyrimidine (bpym) have received increasing attention in recent years[136-139]. Because 2,2'-bipyrimidine can act as a doubly bidentate, bridging ligand with delocalised π bonding it combines the chelating properties of ligands such as 2,2'-bipyridine with the bridging function of ligands such as the 1,4-diazines[139]. In particular, it is noteworthy that bpym can hold together two metal atoms at a distance of approximately 5 Å ; this is very short compared to metal-metal distances in other molecule-bridged systems[136,140]. In this chapter, we have undertaken spectroelectrochemical studies of binuclear { $[Mo(CO)_4]_2(\mu\text{-bpym})$, $[Re(CO)_3Cl]_2(\mu\text{-bpym})$ and $\{[Cu(PPh_3)_2]_2(\mu\text{-bpym})\}^{2+}$} complexes of bpym.

7.1 Electrochemistry of binuclear complexes of bpym

The electrochemistry of the binuclear complexes was investigated in dimethylformamide with $TBABF_4$ as the supporting electrolyte. The Cu(I) complex was examined in the presence of 0.01 mol dm^{-3} triphenylphosphine because a rapid exchange occurs between solvent and coordinated triphenylphosphine. The reduction potentials of the binuclear bpym complexes are collected in Table 7.1 and cyclic voltammograms of each complex in DMF on a platinum working electrode are shown in Figure 7.1 and 7.2. All reductions were reversible one-electron processes except the second reduction of the Re(I) complex.

Table 7.1. Reduction potentials of 2,2'-bipyrimidine and its binuclear complexes in DMF[a]

Compounds	1st red.	2nd red.
2,2'-bipyrimidine	-2.287[b](0.063)[c]	-2.804(irr)[d]
$\{[Cu(PPh_3)_2]_2(\mu\text{-bpym})\}^{2+}$ [e]	-1.275(0.064)	-1.915(0.079)
$[Mo(CO)_4]_2(\mu\text{-bpym})$	-1.182(0.064)	-1.826(0.070)
$[Re(CO)_3Cl]_2(\mu\text{-bpym})$	-0.865(0.072)	-1.540(irr)

[a] Cyclic voltammetric results in $TBABF_4$-DMF at room temperature [b] $E_{(red)}$/ V vs Ag/Ag^+ [c] $E_{pa} - E_{pc}$ (V)
[d] Denotes a irreversible one-electron reduction process.
[e] With 0.01 mol dm^{-3} of triphenylphosphine.

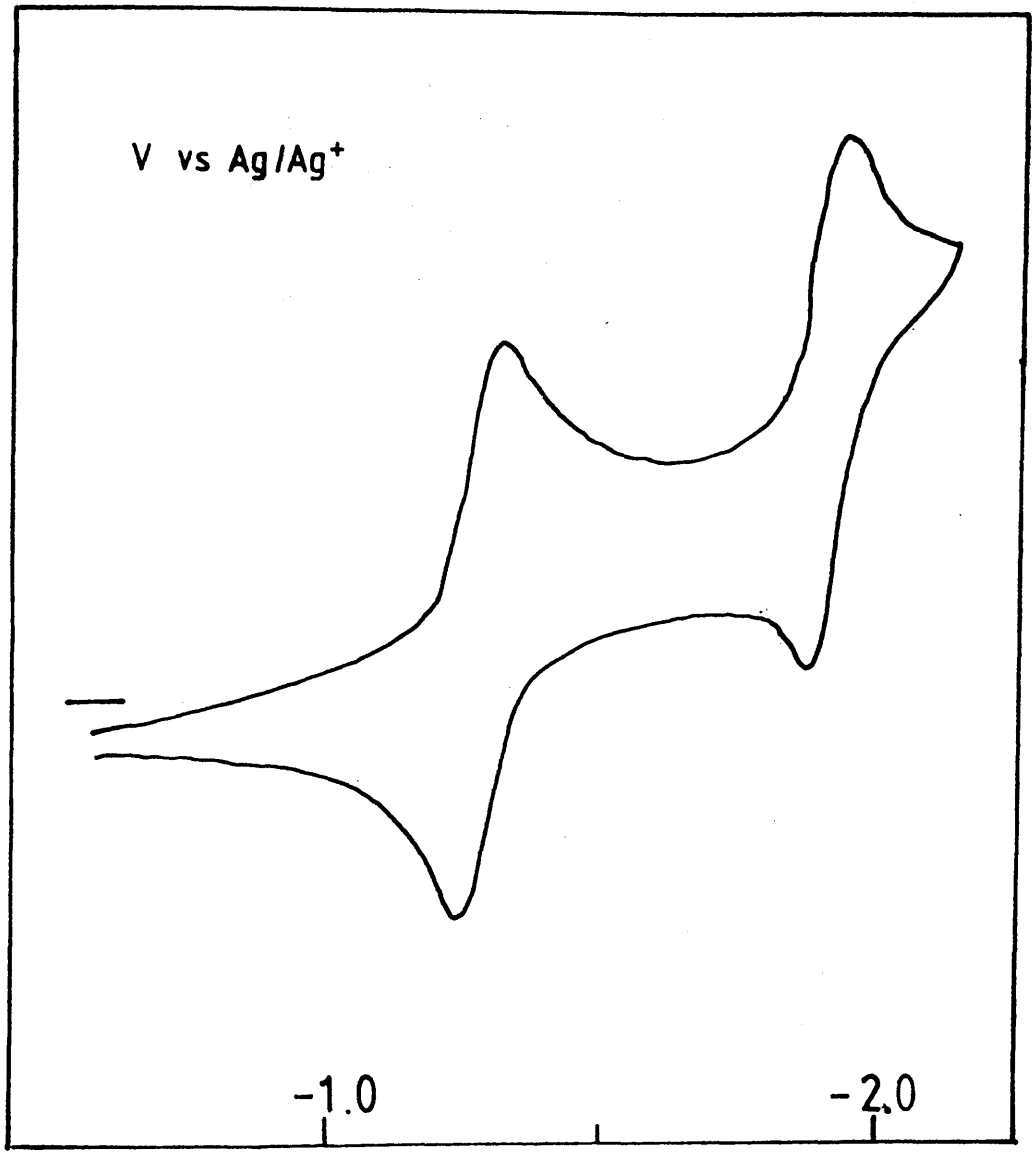

Figure 7.2 Cyclic voltammogram of $\{[Cu(PPh_3)_2]_2(u\text{-}bpym)\}^{2+}$ in DMF with 0.01 M mol dm^{-3} of triphenylphosphine at room temperature. 200 mV / sec

The differences $\Delta = E_{red}(2nd) - E_{red}(1st)$ are only slightly different in the three complexes and are close to the free ligand value of around 650 mV. Hence the reductions of these binuclear complexes are undoubtably based on the ligand (2,2'-bipyrimidine), and the redox orbital should be $\pi(7)$, the lowest π^* orbital of bpym. The lowest unoccupied molecular orbital in these complexes can be populated through addition of an electron to yield the corresponding radical anion. For a ligand centered LUMO, stable π radicals may be expected, especially since the ligand itself undergoes reversible reduction. After being singly or doubly reduced, each of the binuclear complexes contains a very stable anion or dianion ligand and this high stability is possibly due to a hyperconjugative interaction between the LUMO (π^*) of 2,2'-bipyrimidine and the anti-bonding metal-carbonyl or metal-phosphine σ^* orbitals[75].

The binuclear complexes are more easily reduced than the corresponding mononuclear complexes[26]. The dramatic shift to less negative potentials for the binuclear complexes indicates that the remote metal centre increases the electron withdrawing ability of bpym by acting as a Lewis acid. This may be why the metal-to-ligand charge-transfer absorption bands appear at longer wavelength in the binuclear complexes.

Unlike the reductions, the electrochemical oxidation of the Mo complex in DMF is irreversible at around +0.58 V. This process probably corresponds to a loss of one electron from a metal centred orbital. In particular, it is well known that the +1 oxidation state of molybdenum is labile[141]. Neither the increase of the scan rate up to 500 mV/sec nor the use of a weak

nucleophilic solvent such as CH_2Cl_2 improved this situation. Solubility problems prevented studies at low temperature.

7.2. Spectroelectrochemistry of binuclear complexes of bpym.

The electronic absorption spectrum of the parent $[Mo(CO)_4]_2(\mu\text{-bpym})$ in the region between 260 nm and 1000nm exhibits three main absorption bands. The band at 301 nm is associated with the HOMO $\rightarrow$ LUMO ($\pi \rightarrow \pi^*$) transition of the bridged 2,2'-bipyrimidine ligand. However, another two transitions appear in the visible region at approximately 390 nm and 545 nm. Both are assigned to metal-to-ligand charge-transfer transitions from the $d\pi$ orbital of molybdenum to the π^* orbitals of the bridged 2,2'-bipyrimidine ligand. Compared to the corresponding mononuclear complexes[136], the MLCT absorption bands are shifted to longer wavelength in the binuclear complexes. Such a red-shift is generally observed when ligands such as pyrazine or bipyrimidine undergo coordination to a second metal centre and form binuclear complexes[142]. In the $[Re(CO)_3Cl]_2(\mu\text{-bpym})$ complex, the two MLCT transition bands also appear in the visible region at approximately 370 nm and 490 nm tailing out at about 570 nm. Hence, these two complexes are distinguished by long-wavelength metal-to-ligand charge-transfer absorption bands, compared to the corresponding mono-nuclear complexes, resulting from transitions between the electron rich metal and the very low-lying π^* orbitals of the 2,2'-bipyrimidine. The two bands correspond to transfer of an electron to $\pi(7)$ and $\pi(8,9)$ respectively.[75]

This assignment gives a separation of around 7000 cm^{-1} between the two MLCT bands which is in moderate agreement with the 11000 cm^{-1} energy of $\pi(7) \rightarrow \pi(9)$ in the singly reduced species (see below). Absorption around 390 nm could also arise from M $\rightarrow$ CO charge transfer, as in $[(Ph_2P)_2MeN]Mo(CO)_4$[143] or in trans-$(R_3P)_2Mo(CO)_4$[144].

The electronic absorption spectra of the reduced bi-metallic complexes show characteristic $[bpym]^-$ intraligand $\pi \rightarrow \pi^*$ and $\pi^* \rightarrow \pi^*$ transitions in the region between 260 nm and 1000 nm. The main absorption bands and assignments are shown in Table 7.2 and the electronic absorption spectra of the reduced binuclear complexes are shown in Figure 7.3, 7.4 and 7.5.
Kaim[139] has reported radical formation of similar mono- and bi-nuclear complexes and has proved by e.s.r. studies that the electron is localised in the π^* orbital of the coordinated 2,2'-bipyrimidine ligand.

The band at around 350 nm which appears with high intensity in each complex is assigned to the intraligand $\pi(6) \rightarrow \pi(7)$ transition of the bridged $[bpym]^-$ ligand. The transition in the reduced species appears lower in energy than the corresponding $\pi(6) \rightarrow \pi(7)$ transition of neutral bpym in these complexes. A similar effect was found in the free ligand. (see chapter 4)

The visible band with a vibronic structure of approximately 1480 cm^{-1} is assigned to the $\pi(7) \rightarrow \pi(10)$ transition of $[bpym]^-$. The vibrational progression of 1480 cm^{-1} is presumably due to the weakening of the C - C bond between the two pyrimidine

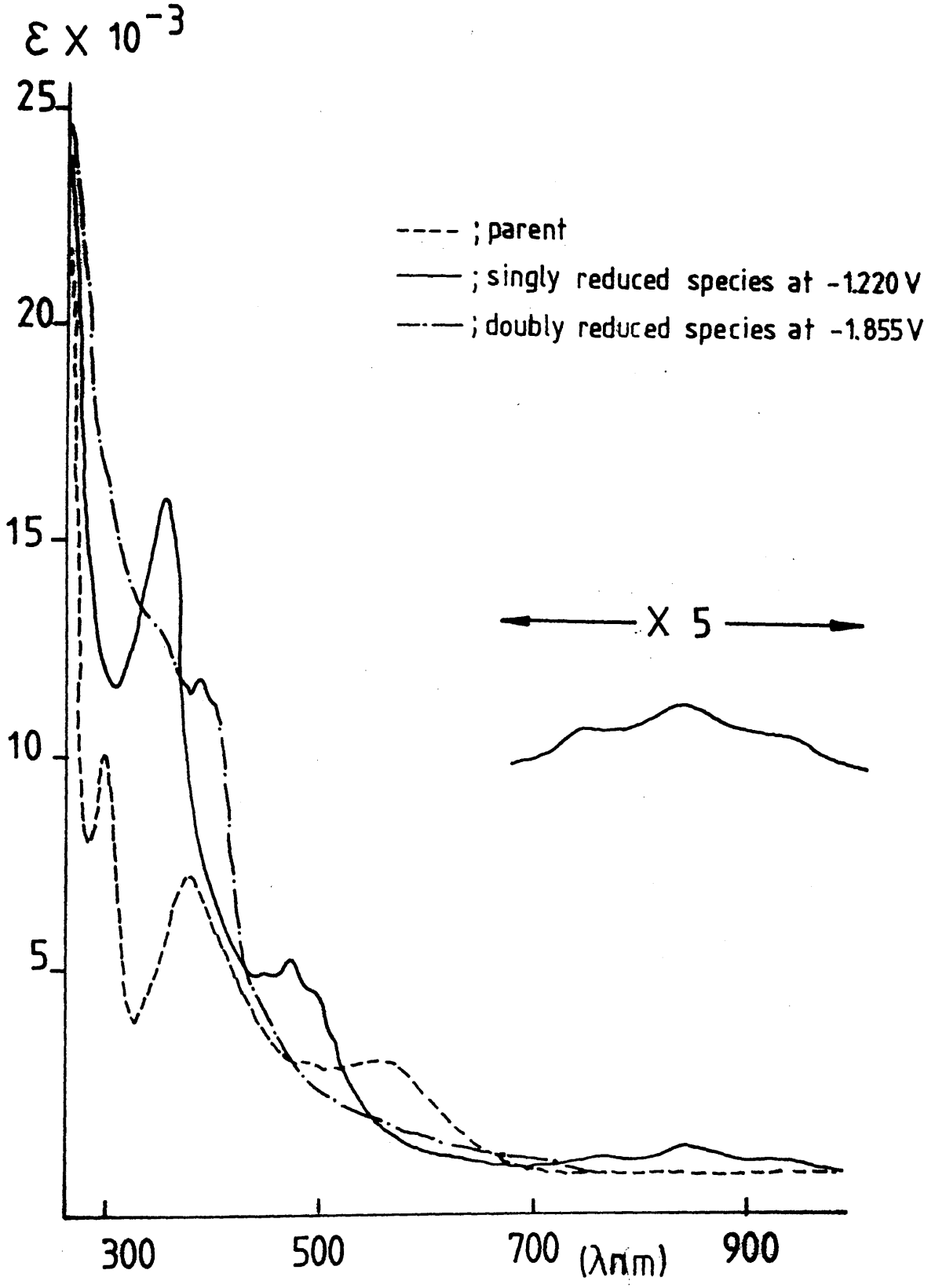

Figure 7.3 Absorption spectra of $\{[Mo(CO)_4]_2(\mu\text{-bpym})\}^{0/-/2-}$ in DMF at room temperature.

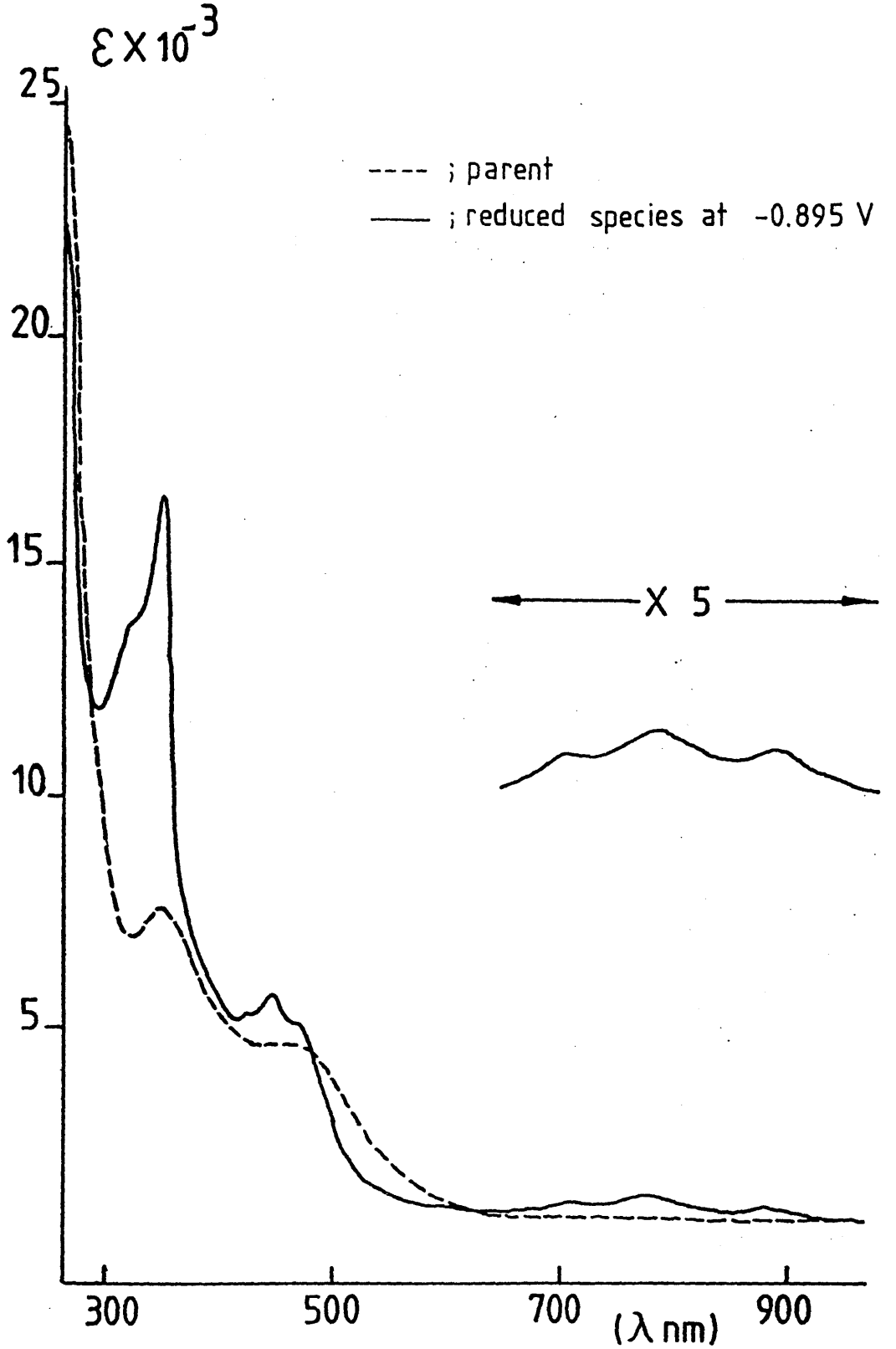

Figure 7.4 Absorption spectra of $\{[Re(CO)_3Cl]_2(\mu\text{-bpym})\}^{0/-}$ in DMF at room temperature

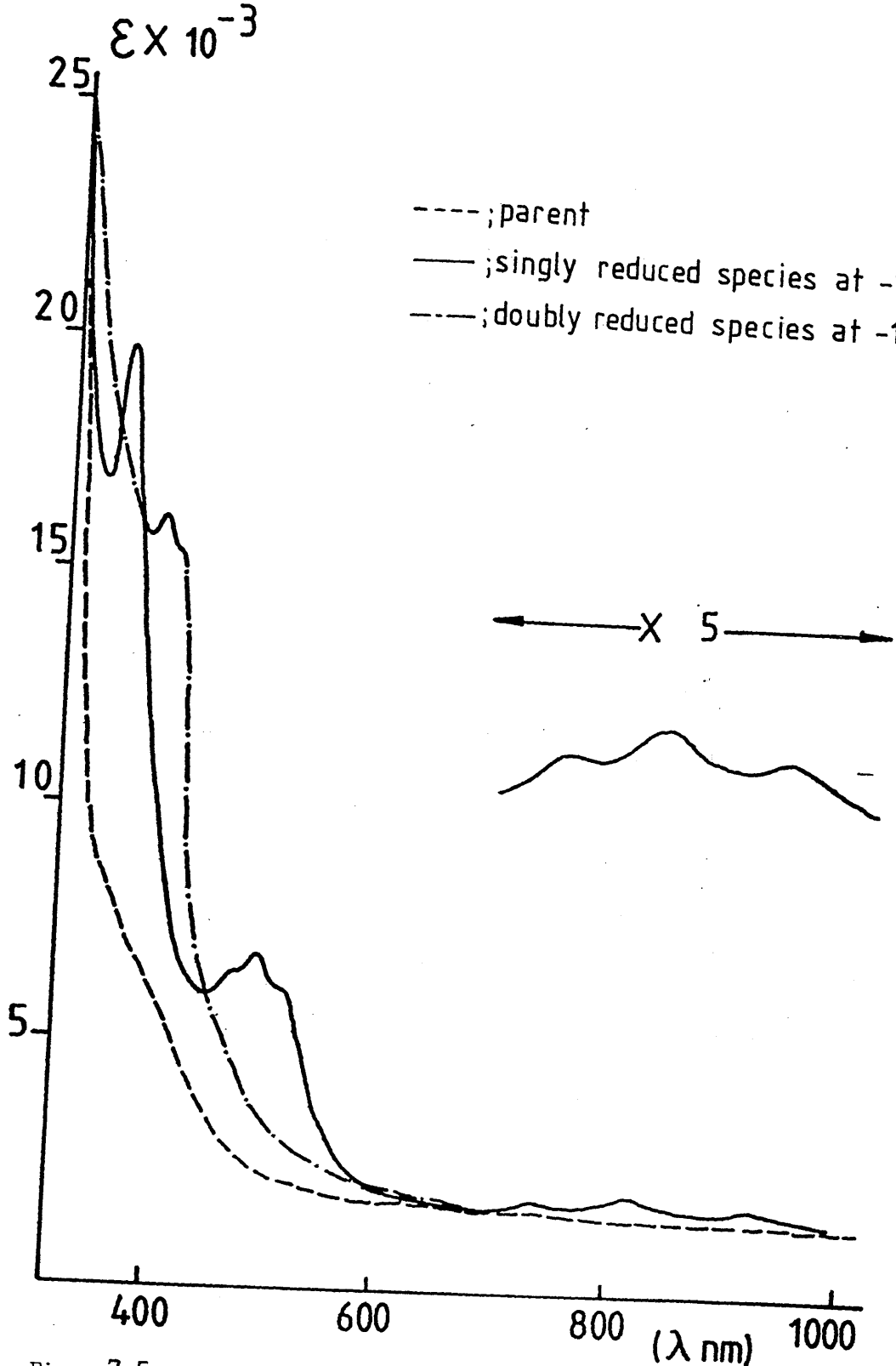

Figure 7.5 Absorption spectra of $\{[Cu(PPh_3)_2]_2\ (\mu\text{-bpym})\}^{2+/+/0}$ in DMF -triphenylphosphine(0.01 mol dm^{-3}) at room temperature.

rings. Another expected vibronic low energy band appears in the region between 700 nm and 900 nm and is assigned to the $\pi(7) \rightarrow \pi(9)$ transition of $[bpym]^-$. The $\pi(7) \rightarrow \pi(8)$ transition of $[bpym]^-$ is forbidden.

These are the first reported UV-visible spectra of the doubly reduced binuclear complexes of 2,2'-bipyrimidine. We can again apply the theory appropriate to a 12-centre biphenyl-like system. The absorption bands of the doubly reduced species centered at around 390 nm (Mo complex) and 404 nm (Cu complex) are presumably assigned to the $\pi(7) \rightarrow \pi(10)$ transition of $[bpym]^{2-}$. We also expect another $\pi^* \rightarrow \pi^*$ transition of $[bpym]^{2-}$, but as in doubly reduced paraquat it is weak and is hidden under the $\pi(7) \rightarrow \pi(10)$ transition.

Chapter 8. Spectroelectrochemistry of Pt(II) Complexes.

Complex compounds of Pt(II) occupy a central position in the development of coordination chemistry, and much of their behaviour had been clearly charted by the end of the 1930s. The discovery that even the simplest of such compounds, such as cis-$[Pt(NH_3)_2Cl_2]$, may interfere with cell-division has further stimulated interest in them. Complexes of 2,2'-bipyridine with platinum were first prepared by Morgan and Burstall[9] who mentioned that the compound $[Pt(bpy)Cl_2]$ was very stable. The bipyridine base is tightly bound and is not readily displaced by other bases, such as 1,2-diaminoethane, pyridine etc., and since the two chlorides occupy adjacent positions in the coordination sphere, both can be replaced by two monodentate ligands or a bidentate ligand. The ligand 2,2'-bipyridine, which (due to the possibility of rotation about the 2,2'-bond) can be considered to be intermediate in flexibility between 1,2-diaminoethane and 1,10-phenanthroline generally displays bidentate behaviour, except when it acts as a bridging ligand[145].

2,2'-Bipyridine can also be converted into a potentially monodentate ligand by quaternising one of nitrogens and the resulting cation can undergo ortho-metallation at the C(3) position of the ring carrying the quaternised nitrogen to generate the bidentate zwitterionic ligand Mebpy-H[56].

Hence, the Me bpy -H ligand can be considered to be similar to 2-phenylpyridine and benzoquinoline which readily form cyclometallated complexes with platinum. Especially, [Pt(bpyMe-H)Cl_2] is an unusual type of compound in that the ligand itself is

acting as a zwitterion as a result of orthometallation. Thus blocking one of the nitrogens of 2,2'-bipyridine by an alkyl group does not prevent the resulting cation from acting as a chelate.

There has been considerable interest recently in the nature of the platinum to carbon σ-bond in alkyl and aryl platinum complexes[23-25]. After some controversy, recent reports suggest that, in aryl platinum complexes, the platinum atom acts as a π-donor to the aryl groups, but that the π-bonding is weaker than was originally thought and that the extent of such π-bonding is independent of the other ligands bonded to platinum.

8.1 ELECTROCHEMISTRY OF Pt(II) COMPLEXES

8.1.1. Electrochemistry of $[PtLL']^{2+}$ complexes

Bis-bipyridine platinum(II) $[Pt(bpy)_2]^{2+}$ and related species are pale yellow, d^8, complexes.

The electronic configuration[146] of the platinum(II) ion is $d\pi^6 d\sigma^2$.

The electrochemical behaviour of Pt(II) complexes can broadly be divided into two types;

i, metal-based oxidations and reductions; and
ii, ligand-based reductions

Uncoordinated bpy and bpym undergo reversible one-electron reduction at over -2.0 V vs Ag/Ag^+ but no oxidation processes are

Table 8.1. Reduction potentials of $[PtLL']^{2+}$ complexes in DMF[a]

	$E_{red}(2+/+1)$	$E_{red}(+/0)$	$E_{red}(0/-1)$
$[Pt(bpy)(py)_2]^{2+}$	-1.181 (0.063)[b]	-1.871 (0.074)	
$[Pt(bpy)(Me_2N\text{-}py)_2]^{2+}$	-1.205 (0.064)	-1.921 (irr)[c]	
	-1.215[d] (0.067)	-1.906[d] (0.085)	
$[Pt(bpy)_2]^{2+}$	-1.174 (irr)	-1.662 (0.066)	-1.838 (0.072)
$[Pt(4,4'\text{-}Me_2\text{-}bpy)_2]^{2+}$	-1.114 (irr)	-1.778 (0.066)	-1.942 (0.079)
$[Pt(bpyMe\text{-}H)(py)_2]^{2+}$	-1.326 (0.063)	-1.690 (0.073)	
$[Pt(bpyMe\text{-}H)(bpy)]^{2+}$	-1.262 (0.074)	-1.492 (0.062)	-1.868 (0.071)

[a]Data from cyclic voltammetry, potentials in volts vs Ag/Ag^+ in $TBABF_4$-DMF solution at room temperature. [b]$E_{pa} - E_{pc}$ (V) [c]Denotes irreversible redox process with peak potentials given (Scan rate 200 mV/sec) [d]At -40 °C

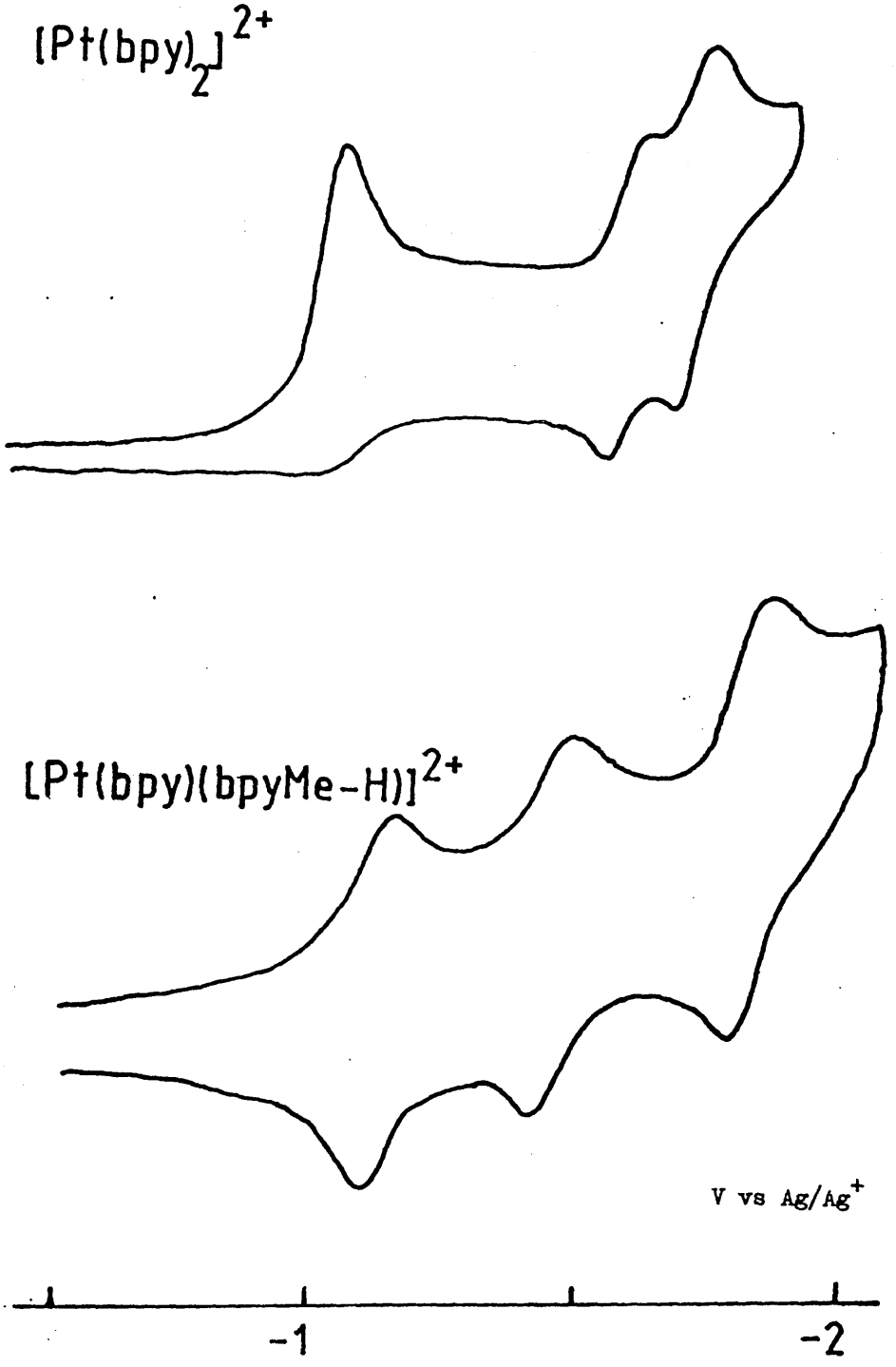

Figure 8.1. Cyclic voltammograms of $[Pt(bpy)_2]^{2+}$ and $[Pt(bpy)(bpyMe\text{-}H)]^{2+}$ in DMF at room temperature.

Scheme I

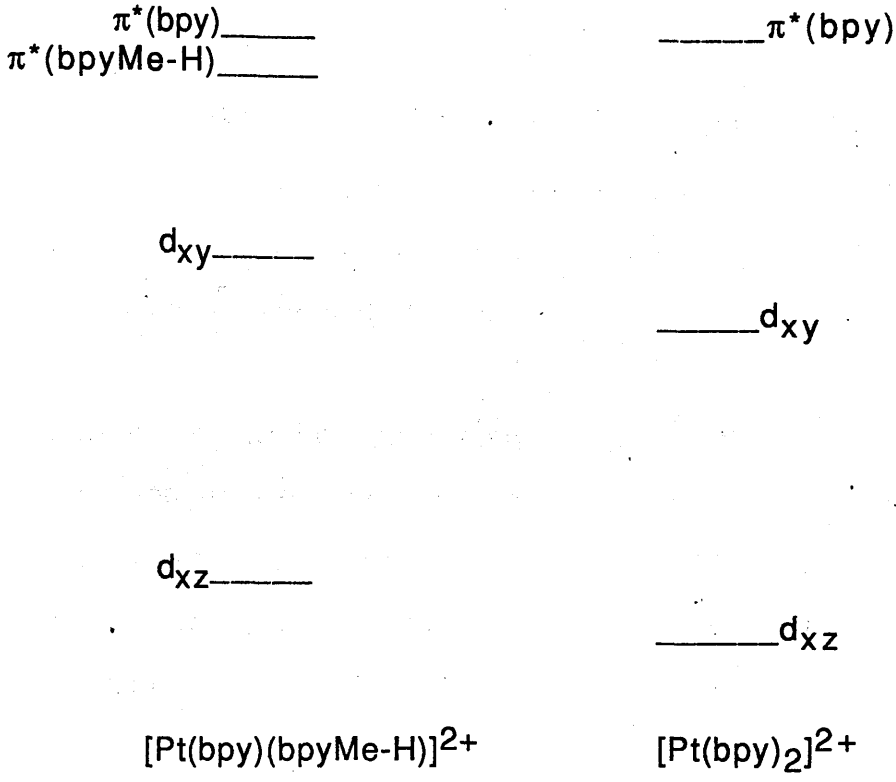

Scheme II.

$$[Pt(bpy)(bpyMe\text{-}H)]^{2+} \underset{-e}{\overset{+e}{\rightleftharpoons}} [Pt(bpy)(bpyMe\text{-}H)]^{+} \quad \text{at } -1.262 \text{ V}$$

$$[Pt(bpy)(bpyMe\text{-}H)]^{+} \underset{-e}{\overset{+e}{\rightleftharpoons}} [Pt(bpy)(bpyMe\text{-}H)]^{0} \quad \text{at } -1.492 \text{ V}$$

$$[Pt(bpy)(bpyMe\text{-}H)]^{0} \underset{-e}{\overset{+e}{\rightleftharpoons}} [Pt(bpy)(bpyMe\text{-}H)]^{-} \quad \text{at } -1.868 \text{ V}$$

In both $[Pt(bpy)(py)_2]^{2+}$ and $[Pt(bpyMe\text{-}H)(py)_2]^{2+}$ (Figure 8.2) a reversible one-electron metal based reduction is observed.

The second reductions of the $[Pt(bpy)(py)_2]^{2+}$ and $[Pt(bpyMe\text{-}H)(py)_2]^{2+}$ are assigned as the reduction of coordinated bpy or bpyMe-H ligands. From table 8.1, the order of decreasing ease of reduction in the complexes is (bpyMe-H) > bpy > 4,4'-Me_2-bpy, and this sequence is consistent with the order of decreasing ease of reduction of the free ligands.

Figure 8.3 show the cyclic voltammograms of $[Pt(bpy)(Me_2N\text{-}py)_2]^{2+}$ (where Me_2N-py is 4-dimethylamino-pyridine) at room temperature (a) and at -40° C (b). At room temperature, the second reduction is irreversible. This is presumably due to an EC process where Pt(I)-bound aromatic ligands react in a fast, irreversible step, most probably with the solvent. However, at -40 °C, the forward and reverse peaks of the second reduction wave become narrowly separated (E_{pa}-E_{pc} = 0.085 V) indicating a reversible one-electron reduction of the coordinated bpy ligand. Hence, the reaction between Pt(I)-reduced bpy ligands and solvent is dependent upon the temperature.

In the $[Pt(bpy)(bpyMe\text{-}H)]^{2+}$ complex, there are two ligand based reductions which involve both bpy and (bpyMe-H). This means that ortho-metallated (bpyMe-H) is interchangeable with ordinary bpy in the Pt complex and is able to accept an added electron.

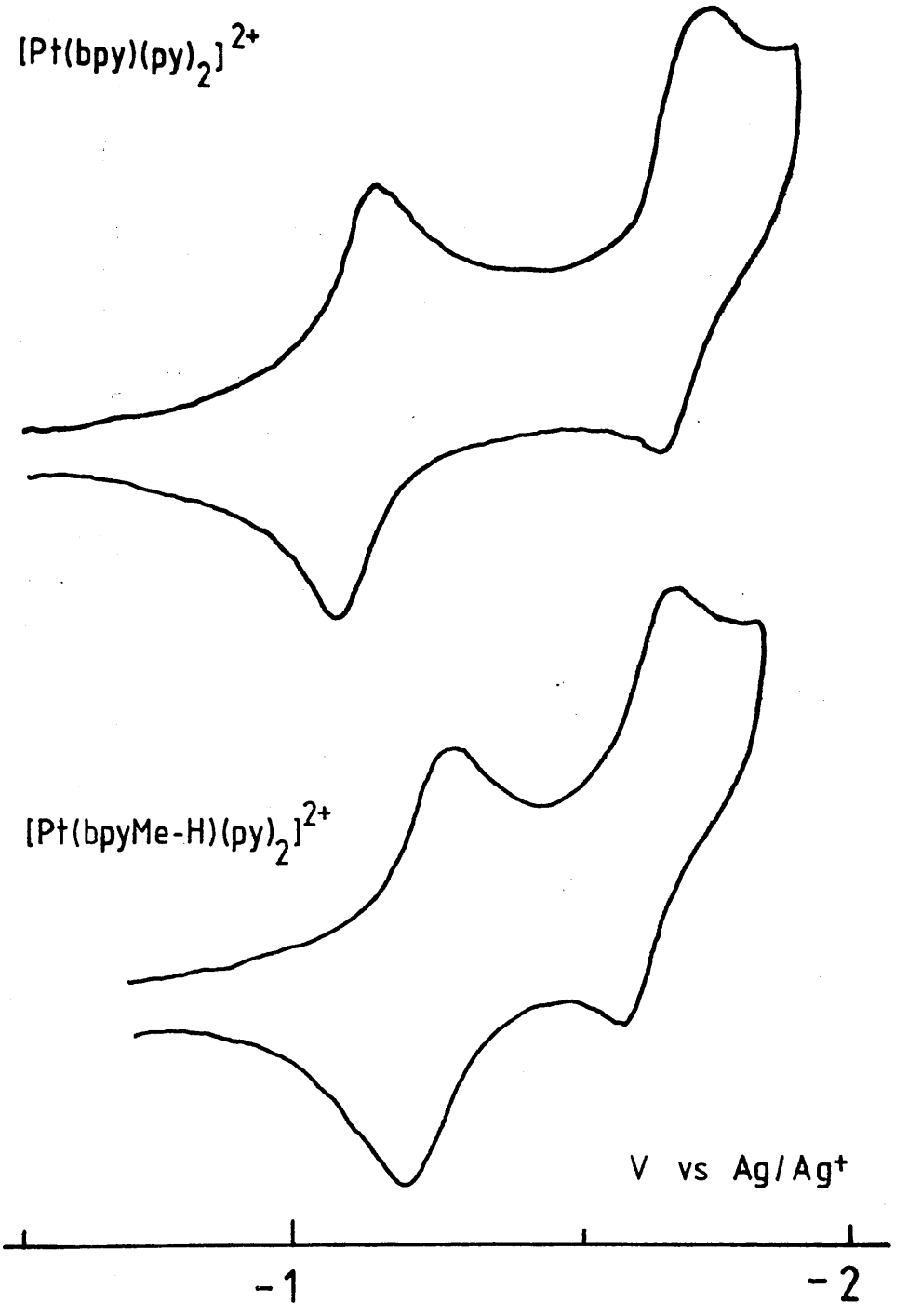

Figure 8, 2 Cyclic voltammograms of $[Pt(bpy)(py)_2]^{2+}$ and $[Pt(bpyMe-H)(py)_2]^{2+}$ in DMF at room temperature.

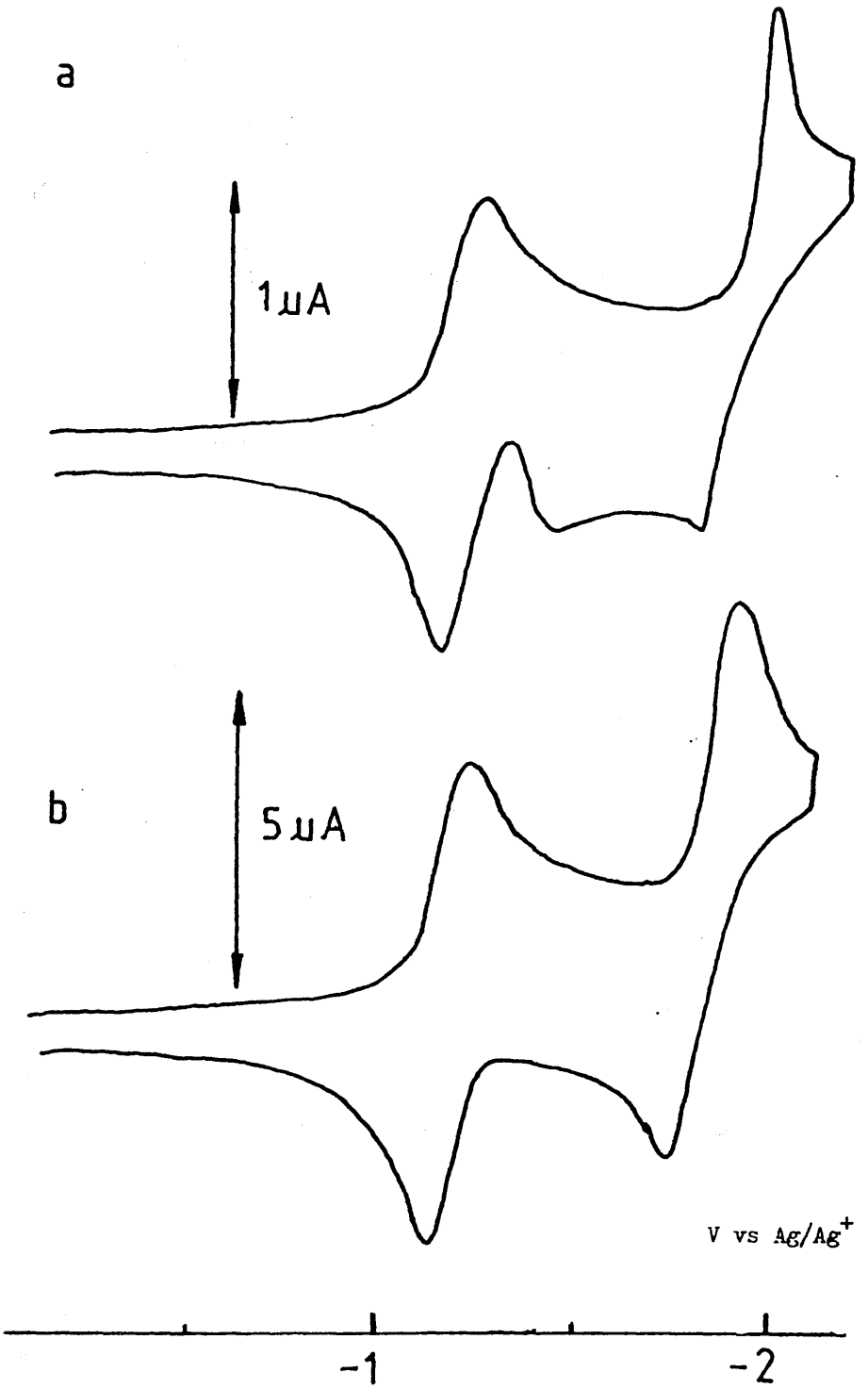

Figure 8.3 Cyclic voltammograms of $[Pt(bpy)(Me_2N\text{-}py)_2]^{2+}$ in DMF at room temperature (a) and at -40 °C (b).

We can now explain the electrochemistry of $[Ir(bpy)_2(bpy\text{-}H)]^{2+}$ [123] (where bpy-H is N,C(3)'-dihapto-2,2'-bipyridinyl), which shows a similar pattern to those of bis-bpy Ru(II) complexes with two closely spaced waves, 175 mV apart, then a gap of 650 mV before two further waves 290 mV apart. Thus the complex contains two regular bpy ligands and one unique bpy-H ligand which is redox-inert in an unprecedented fashion. Presumably this is due to the formal negative charge on the ligand. If the bpy-H ligand were methylated, this would give Mebpy-H which would show a reduction wave in the same region as coordinated bpy. Since methylation shifts reduction potentials in bipyridyls by up to 1.2 V (see chapter 4) it is not surprising that bpy-H is so difficult to reduce.

8.1.2. Electrochemistry of organoplatinum complexes.

The organoplatinum complexes discussed in this section are more difficult to reduce than the cations discussed above. Presumably the σ-bonds between Pt(II) and the two coordinated aryl groups destabilise the d orbitals of the platinum. The first reduction is in the region characteristic of coordinated bpy, and it is suggested that the LUMO is now the ligand π^* [π(7)] orbital (Scheme III). The reduction is therefore assigned to a ligand-centered process. The reduction potentials of the organoplatinum(II) complexes are given in Table 8.2.

Table 8.2 Reduction potentials of organoplatinum(II) complexes in Dichloromethane[a]

compounds	$E_{red}^{(2+/+)}$	$E_{red}^{(+/0)}$
$[Pt(bpy)(Ph)_2]$	-1.641 (0.064)[b]	-2.252 (irr)[c]
$[Pt(4,4'\text{-}Me_2\text{-}bpy)(Ph)_2]$	-1.748 (0.065)	-2.383 (irr)
$[Pt(bpym)(Ph)_2]$	-1.263 (0.061)	-1.798 (irr)
$[(adme)_2Pt]_2(\mu\text{-}bpym)$	-1.058 (0.062)	-1.516 (0.075)
$[(p\text{-}tol)_2Pt]_2(\mu\text{-}bpym)$	-0.753 (0.068)	-1.290 (0.079)

[a]Data from cyclic voltammetry, potentials in volts vs Ag/Ag^+ in $TBABF_4$-DMF solution at room temperature. [b]$E_{pa} - E_{pc}$ (V) [c]Denotes irreversible redox process with peak potentials given (Scan rate 200 mV/sec)

Scheme III

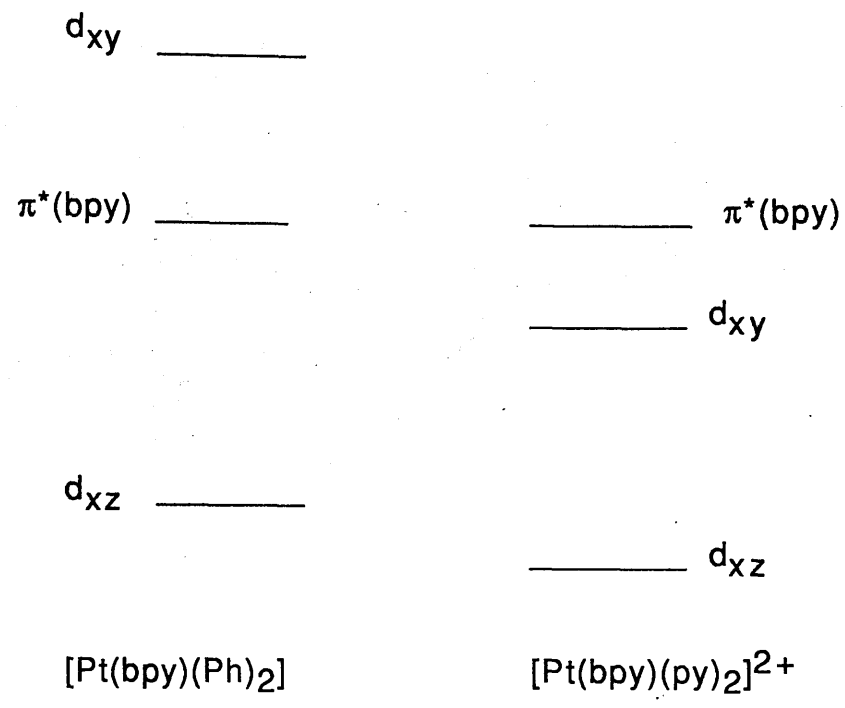

The cyclic voltammogram of [Pt(bpym)(Ph)$_2$] in dichloromethane shows two one-electron reduction processes at -1.263 V and -1.798 V vs Ag/Ag$^+$. The first reduction is reversible, giving a stable product, while the second is irreversible. (Figure 8.4) However, binuclear Pt complexes such as [(p-tol)$_2$Pt]$_2$(μ-bpym) show two reversible one-electron reductions at less negative potentials (-0.753 V and -1.290 V vs Ag/Ag$^+$) than in the corresponding mononuclear complexes.

The completely irreversible anodic wave at E_p varying from +1.06 to +1.38 V [vs Ag/Ag$^+$] is assigned to a Pt-centred oxidation, followed by a very fast chemical process. This process probably involves a reaction with the solvent.

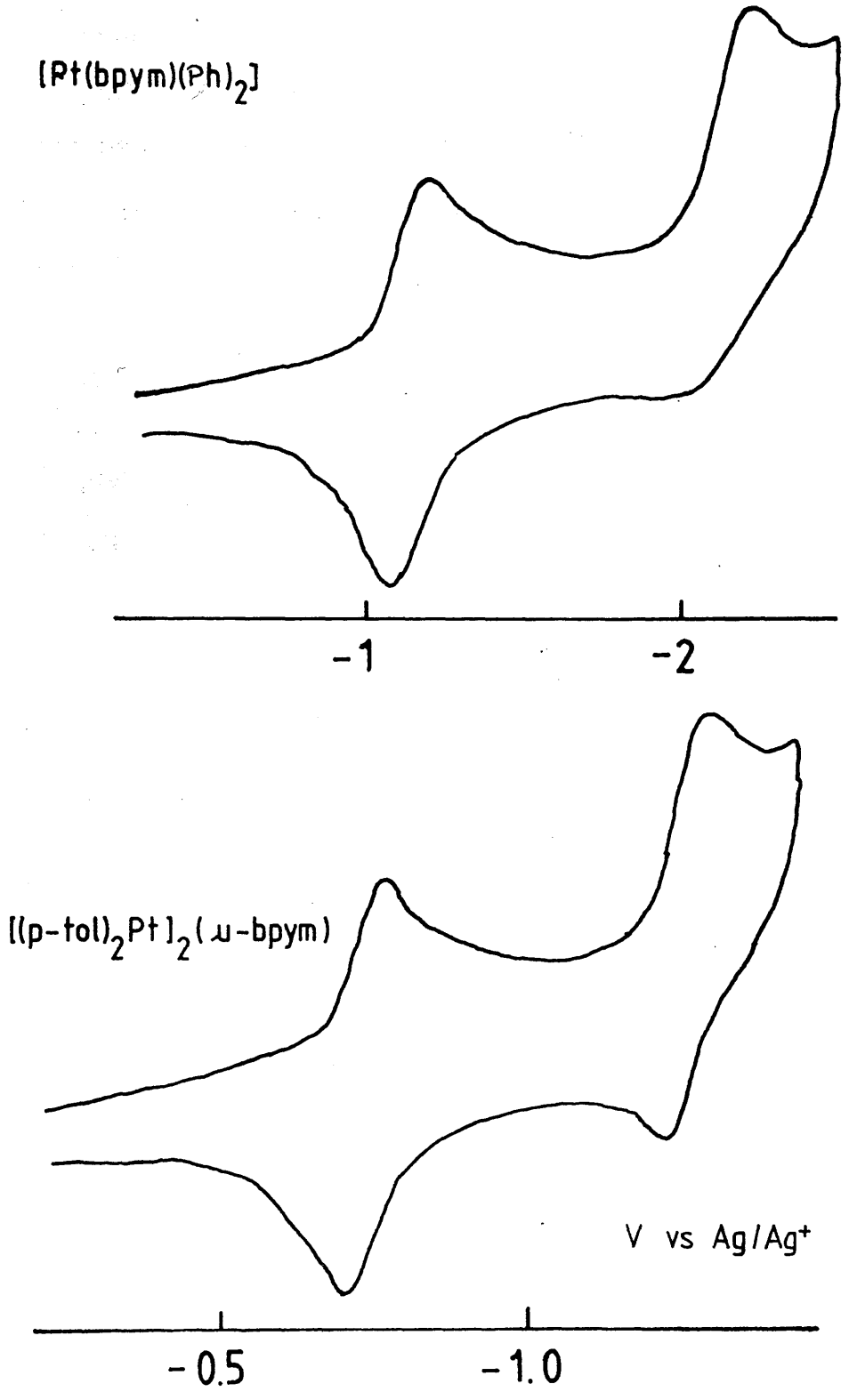

Figure 8.4 Cyclic voltammograms of $[Pt(bpym)(Ph)_2]$ and $[Pt(p\text{-}tol)_2]_2(\mu\text{-}bpym)$ in CH_2Cl_2 at room temperature.

8.2. ABSORPTION SPECTRA OF PARENT Pt(II) COMPLEXES

The electronic absorption spectra of dihalogeno(2,2'-bipyridine)platinum(II) complexes have been studied previously and four distinct bands were detected[147,148]. Two of these, in the regions 260 - 250 nm and 330 - 305 nm, were assigned to the $\pi \rightarrow \pi^*$ transitions within the 2,2'-bipyridine ligand shifted slightly from similar bands observed in the free ligand[132]. Two extra bands in the regions 415 - 335 nm and 295 - 270 nm were assigned as the metal-to-ligand charge transfer transitions (MLCT) from platinum d-orbitals to π^*-orbitals of 2,2'-bipyridine. The energies of the MLCT transition bands were strongly dependent on the solvent while the others were not.

8.2.1. Absorption Spectra of Parent $[PtLL']^{2+}$ Complexes.

The electronic absorption spectra of the parent $[PtLL']^{2+}$ complexes in acetonitrile in the region between 200 nm and 1000 nm contain three main absorptions (Table 8.3). The lowest energy absorption, seen as a shoulder at 343 nm in $[Pt(bpy)(py)_2]^{2+}$, is associated with the first metal to ligand charge transfer transition from the platinum d-orbitals to the $\pi^*[\pi(7);LUMO]$ orbital of the 2,2'-bipyridine ligand. However, the MLCT transition from Pt(II) to quaternised bpyMe-H in $[Pt(bpyMe-H)(py)_2]^{2+}$ is placed some 2700 cm^{-1} lower in energy than that of $[Pt(bpy)(py)_2]^{2+}$. As shown in scheme IV, the separation of the π and π^* orbitals of $[Pt(bpyMe-H)(py)_2]^{2+}$ is approximately 1600 cm^{-1} less when the ligand bpyMe-H replaces bpy. Hence, the

Table 8.3 The main absorption bands of $[PtLL']^{2+}$ complexes in acetonitrile at room temperature.

	MLCT		$\pi \rightarrow \pi^*$		MLCT	
compounds	Pt→bpy	Pt→(bpyMe-H)	$\pi \rightarrow \pi^*$(bpy)	$\pi \rightarrow \pi^*$(bpyMe-H)	Pt→bpy	Pt→(bpyMe-H)
$[Pt(bpy)(py)_2]^{2+}$	245[a](40816)[b]		306(32680)		343(29155)	
$[Pt(Me_2\text{-}bpy)(py)_2]^{2+}$	248(40322)		309(32362)		345(28986)sh	
$[Pt(bpy)_2]^{2+}$	251(39840)		313(31949)		352(28410)sh	
$[Pt(Me_2\text{-}bpy)_2]^{2+}$	246(40650)		325(30769)		359(27855)sh	
$[Pt(bpyMe\text{-}H)(py)_2]^{2+}$		260(38461)		309(32362)		379(26385)
				323(30959)		
$[Pt(bpyMe\text{-}H)(bpy)]^{2+}$	246(40650)	261(38314)	295(33898)	312(32051)	357(28011)	381(26246)
				324(30864)		

[a]wavelength (λnm) [b]energies ($\tilde{\upsilon}$ cm^{-1})

$\pi(6)$ (HOMO) orbital of bpy and the d_{xz} orbital of Pt(II) in $[Pt(bpyMe\text{-}H)(py)_2]^{2+}$ are further separated in energy than in $[Pt(bpy)(py)_2]^{2+}$. The MLCT transition absorption of the former complex can be clearly observed in the lower energy region of the spectrum.

Scheme IV

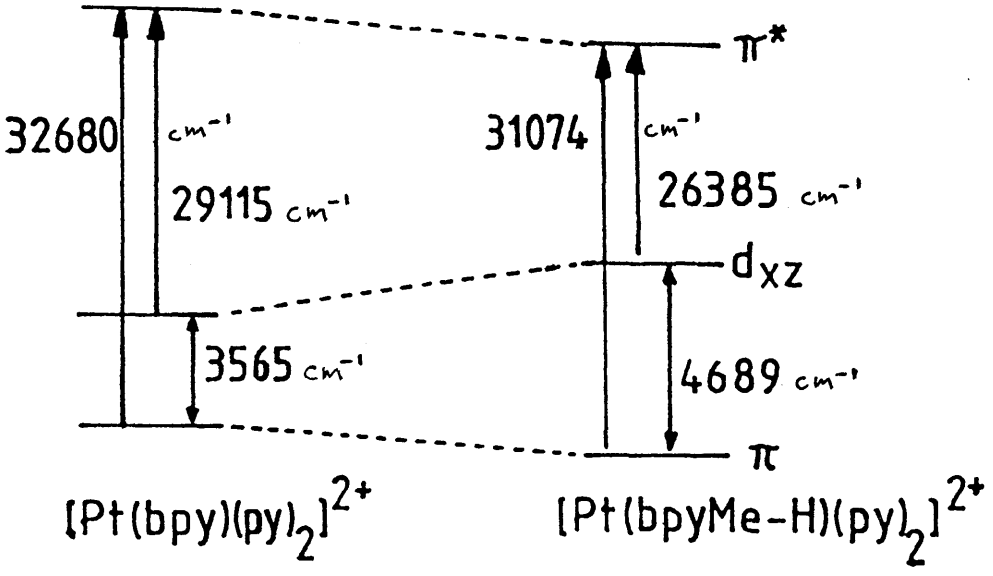

The highest energy absorption, at approximately 250 nm in each complex, is assigned to the second metal-to-ligand charge-transfer transition, $d\pi[Pt(II)] \rightarrow \pi^*[(SLUMO;\pi(8)]$. The value of Δ = 9,000 cm^{-1} found for these complexes is in reasonable agreement with that of the LUMO/SLUMO gap of the bpy system (around 1.2 eV).

The most intense bands appearing in the region between 305 nm and 325 nm of each of the complexes are assigned to the $\pi(6) \rightarrow \pi(7)$ transitions of coordinated bpy and bpyMe-H. (Figure 8.5)

The bands between 290 nm and 324 nm in $[Pt(bpyMe\text{-}H)(bpy)]^{2+}$ are collectively assigned to the $\pi \rightarrow \pi^*$ transitions of both bpy and bpyMe-H. The lower energy bands at 312 and 324 nm with a separation of 1420 cm^{-1}, are assigned to coordinated bpyMe-H. The higher energy band at 295 nm is assigned to the coordinated bpy.

8.2.2. Absorption spectra of the parent organoplatinum(II) complexes

The spectra of these organoplatinum(II) complexes are characterised by two absorptions which are due to MLCT transitions (Table 8.4). The higher of the two in energy, λ_2, is often obscured by the more intense intraligand $\pi \rightarrow \pi^*$ transitions. The lower energy absorption, λ_1, can be observed at 130 - 160 nm to longer wavelength of λ_2.

The energy of this transition is considerably lower for $[Pt(bpym)(Ph)_2]$ than the corresponding $[Pt(bpy)(Ph)_2]$. This is consistent with the general observation that energies of MLCT absorptions in complexes of N-bonded heterocyclic ligands are lowered by introduction of electronegative ring atoms or substituents[137,149].

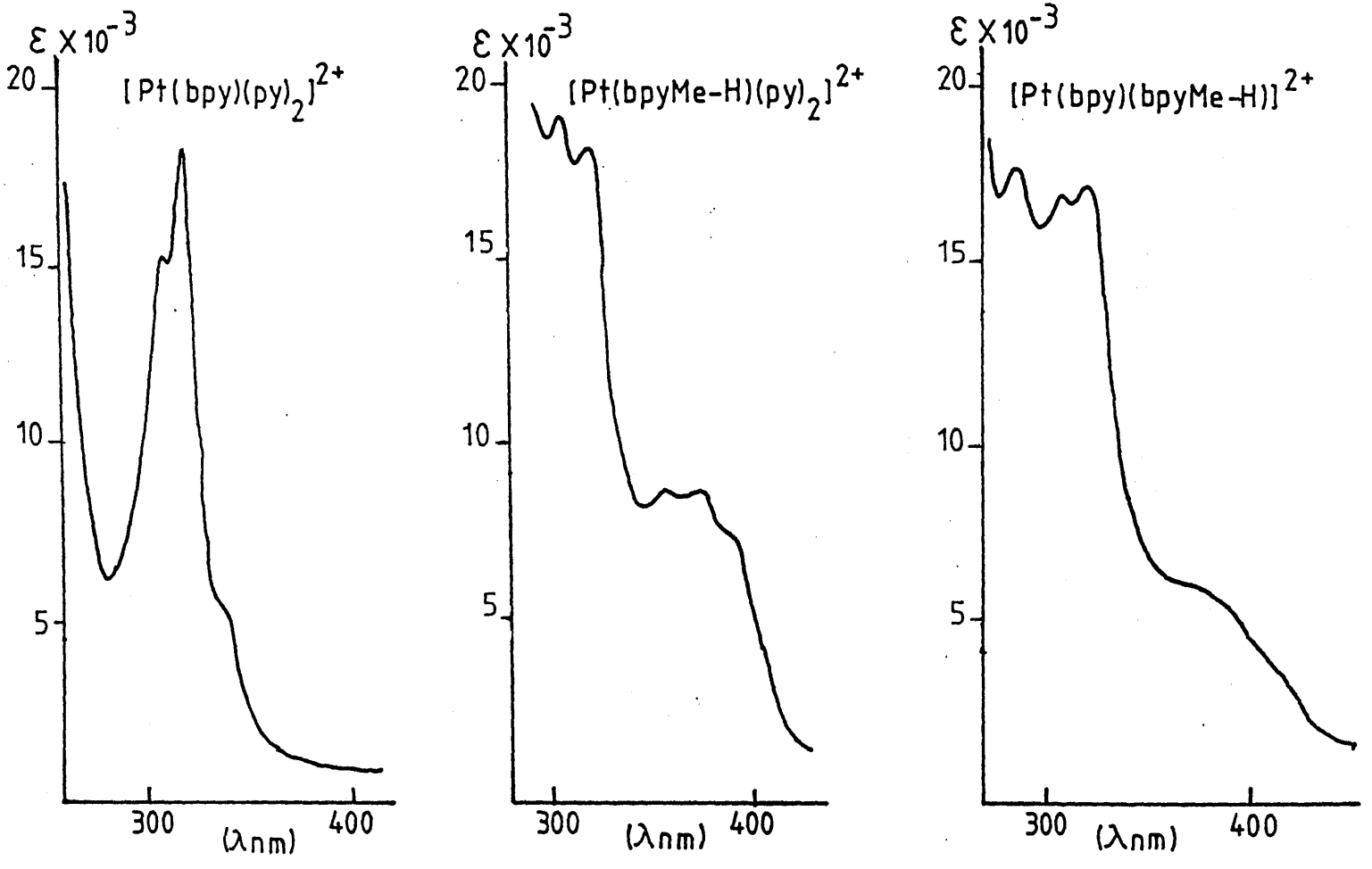

Figure 8.5 Absorption spectra of Pt(II) complexes (300 nm -- 400 nm) in DMF at room temperature.

Table 8.4 The observed MLCT transition bands of organoplatinum(II) complexes in CH_2Cl_2. [λnm($\tilde{\upsilon}$ cm^{-1})]

compounds	$\pi \rightarrow \pi^*$	MLCT (λ_2)	MLCT (λ_1)
[Pt(bpy)$(Ph)_2$]	292(34247)	309(32362)sh	441(22676)
[Pt(4,4'-Me_2-bpy)$(Ph)_2$]	289(34602)	a	422(23697)
[Pt(bpym)$(Ph)_2$]	301(33223)	326(30674)sh	462(21645)
[$(adme)_2$Pt]$_2$(μ-bpym)	309(32362)	410(24390)	595(16807) 535(18692)
[$(p\text{-}tol)_2$Pt]$_2$(μ-bpym)	301(33222)	395(25316)	576(17361) 520(19231)

[a]obscured

For the binuclear complexes, the first MLCT absorption occurs at longer wavelength than in the corresponding mononuclear complexes. The λ_1 band (Table 8.4) comprises two peaks of about equal intensity with 40 - 60 nm separation between the maxima (Figure 8.6). The bathochromic shift is most marked for adamantylmethyl derivatives which give green solutions. The lower energy of this transition could be due to further stabilisation of the LUMO on the ligand by the electron withdrawing influence of the second metal centre and/or to the presence of a relatively high energy, less stable, largely non-bonding HOMO spanning both metals in the binuclear Pt(II) complexes[150].

8.2.3. Solvent effects on the electronic absorption spectra.

Strong solvent effects on the energy of the MLCT bands in a number of bpy complexes of the transition elements have been observed[29]. In particular, Burgess[151] showed that the MLCT bands of $[Fe(bpy)(CN)_2]$ were solvent dependent, while those of $[Fe(bpy)_3]^{2+}$ were not, and suggested that the solvent effect operated through the cyanide groups. A similar effect was proposed[152] for some octahedral complexes $[M(CO)_4(bpy)]$, where M = Mo, W, Cr. However, Yamamoto and co-workers[150] showed that the energies of the MLCT bands of square-planar complexes $[Ni(bpy)R_2]$, where R = Et, Me, were not solvent-dependent, and suggested that direct solvation of nickel in the square planar

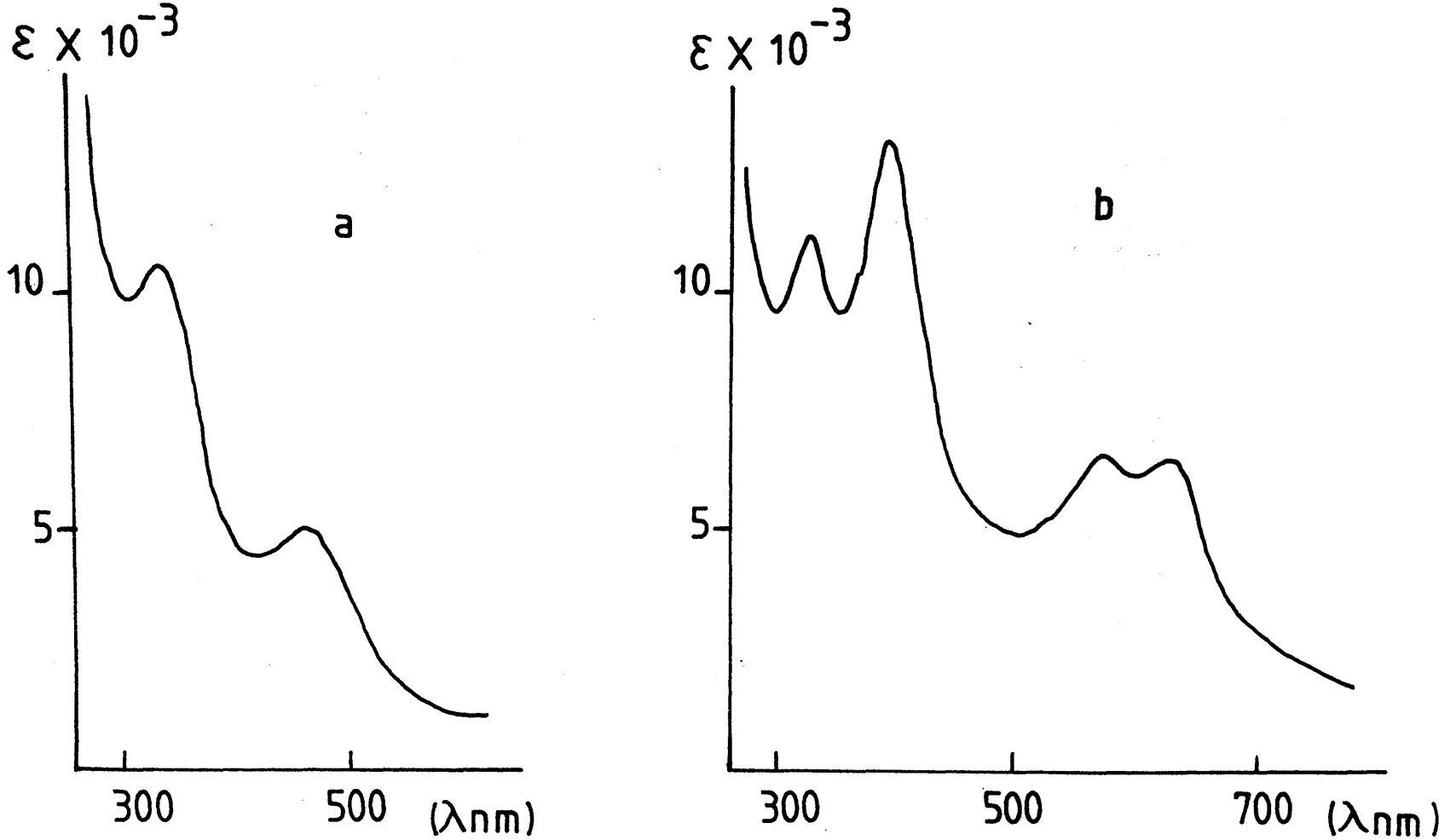

Figure 8.6 Absorption spectra of (a) $[Pt(bpym)(Ph)_2]$ and (b) $[(adme)_2Pt]_2(\mu\text{-bpym})$ in CH_2Cl_2 at room temperature.

complexes was responsible for the effect. Similar solvent effects on the MLCT bands were observed for a variety of platinum(II) complexes. (Table 8.5, 8.6)

According to Table 8.6, the $[(adme)_2Pt]_2(\mu\text{-bpym})$ complex shows lower solvent effects than the other organoplatinum(II) complexes, presumably because of steric hindrance to the approach of solvent molecules to the platinum centre. However, the MLCT bands of most organoplatinum complexes are more strongly affected by solvents than those of $[Pt(bpy)L]^{2+}$, L = bpy, $(py)_2$, perhaps because of greater charge asymmetry.

A similar argument can be applied to the ortho-metallated Pt(II) complexes where the ortho-metallated bpy ligand is a better σ-donor and π-acceptor than the ordinary bpy ligand. Thus $[Pt(bpyMe\text{-}H)L]^{2+}$ shows a stronger solvatochromic effect than the $[Pt(bpy)L]^{2+}$ complexes.

8.3 Electronic Absorption Spectra of the Reduced Pt(II) Complexes.

8.3.1. Absorption spectra of the reduced $[PtLL']^{2+}$ complexes.

As stated before in this chapter, the first reduction of each $[PtLL']^{2+}$ is based on the Pt(II) ion to produce Pt(I), because the d_{xy} orbital lies lower in energy than the π^*(bpy) LUMO orbital.

Table 8.5 Solvent effects on the first MLCT band in the electronic absorption spectra of $[PtLL']^{2+}$ complexes. (λnm)

	$CH_3CN(E_t=46.0)^a$	DMF(E_t=44.9)	$CH_2Cl_2(E_t=41.1)$
$[Pt(bpy)(py)_2]^{2+}$	355	356	358
$[Pt(bpy)(Me_2N\text{-}py)_2]^{2+}$	366	369	368
$[Pt(bpy)_2]^{2+}$	370	369	367
$[Pt(Me_2\text{-}bpy)_2]^{2+}$	359	361	363
[Pt(bpyMe-H)$(py)_2]^{2+}$	379	386	391
[Pt(bpyMe-H)(bpy)$]^{2+}$	366	372	386

Table 8.6 Solvent effects on the first MLCT band in the electronic absorption spectra of organoplatinum complexes (λnm)

	$CH_3CN(E_t=46.0)$	DMF(E_t=44.9)	$CH_2Cl_2(E_t=41.1)$
$[Pt(bpy)(Ph)_2]$	441	446	435
$[Pt(Me_2\text{-}bpy)(Ph)_2]$	422	427	416
$[Pt(bpym)(Ph)_2]$	462	471	456
$[(adme)_2Pt]_2(\mu\text{-}bpym)$	595	596	b
	535	537	
$[(p\text{-}tol)_2Pt]_2(\mu\text{-}bpym)$	576	581	b
	520	526	

[a]solvent polarity [b]insufficiently soluble

Hence, the MLCT transitions from the Pt(I)(d_{xy}) orbital to ligand orbital must appear lower in energy than those from the Pt(II)(d_{xz}) orbital.

The electronic absorption spectrum of singly reduced $[Pt(bpy)(py)_2]^{2+}$ in the region between 250 nm and 1300 nm contains five main absorptions in DMF, and careful measurements of the energy differences between the main absorptions give an important clue to the assignment (Figure 8.7). The energy difference between the band at 400 nm and 492 nm is approximately 4700 cm^{-1} and the gap between the band at 348 nm and 492 nm is approximately 8500 cm^{-1}. Yellowlees[123] has reported that charge transfer from Ru(II) to py requires some 4800 cm^{-1} more energy than charge transfer from Ru(II) to bpy. Hence, the strong band at 400 nm can be assigned to the Pt(I) $\rightarrow$ py charge-transfer transition and the band centered at 492 nm can be assigned to the Pt(I) $\rightarrow$ bpy charge-transfer transition; both MLCT bands are approximately 9000 cm^{-1} lower in energy than the corresponding absorptions in the parent species. The near UV band at 348 nm which lies approximately 8500 cm^{-1} higher in energy than the Pt(I) $\rightarrow$ bpy charge-transfer transition band, but is approximately 9000 cm^{-1} shifted to lower energy compared to that of $[Pt(bpy)(py)_2]^{2+}$, can be assigned to the second MLCT transition band from Pt(I) to π^*(SLUMO of bpy). The value of $\Delta_{CT(1)-CT(2)}$ = 8500 cm^{-1} is in agreement with the absorption spectrum of the parent complexes.

The highest energy strong band at 284 nm is assigned to $\pi(6) \rightarrow \pi(7)$ of coordinated bpy. The broad and weak absorption

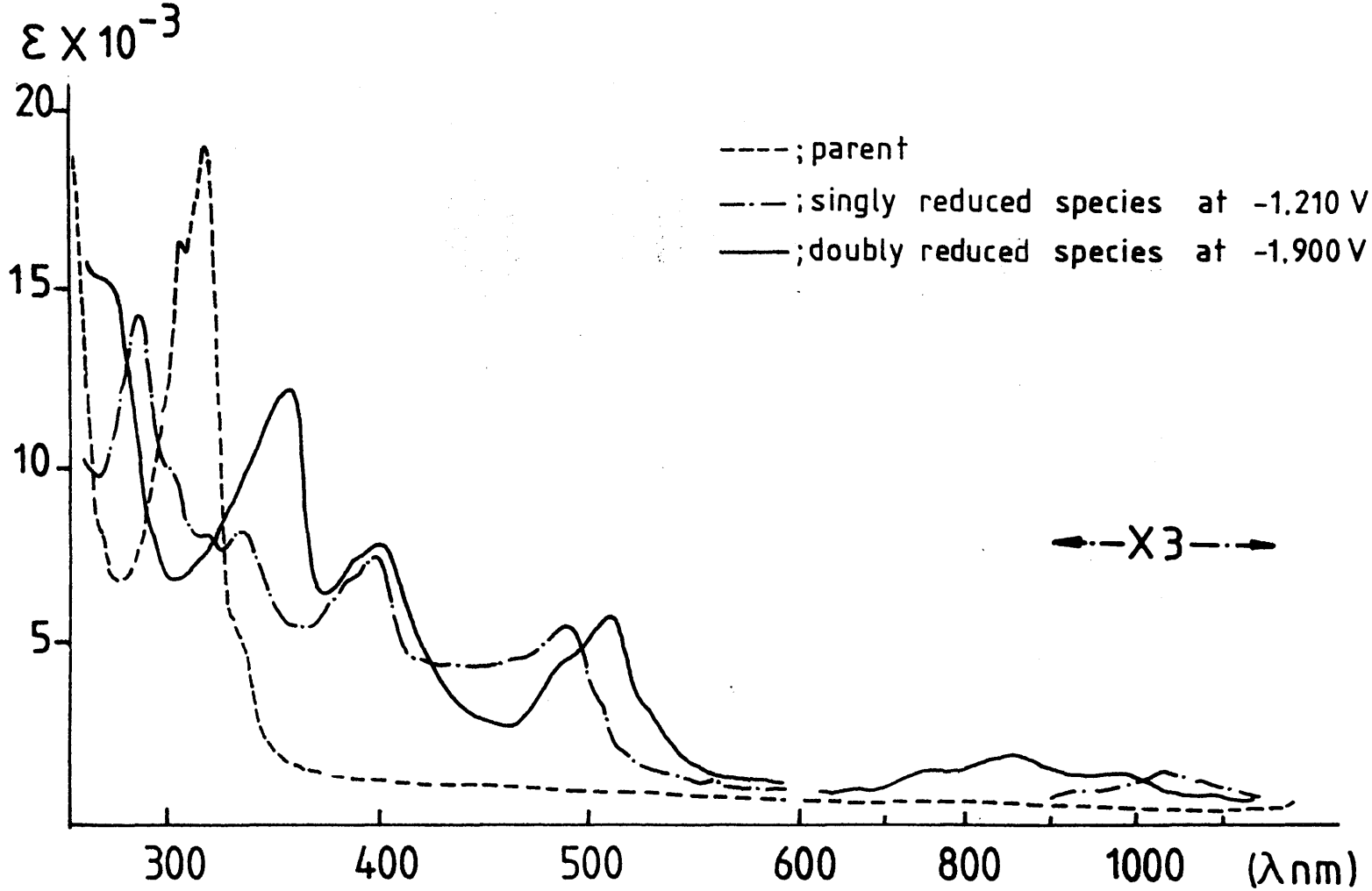

Figure 8.7 Absorption spectra of $[Pt(bpy)(py)_2]^{2+/+/0}$ in DMF at room temperature.

band which appears at around 1100 nm is tentatively assigned to a d → d transition of the platinum metal. The main absorption bands of the singly reduced $[PtLL']^{2+}$ complexes are collected in Table 8.7.

The M[Pt(I)] → L(bpyMe-H) CT transition band appears at considerably longer wavelength in $[Pt(bpyMe\text{-}H)(py)_2]^+$ than in $[Pt(bpy)(py)_2]^+$ (Figure 8.8) because the π*(LUMO) orbital energy of bpyMe-H is lower than that of the bpy ligand. Furthermore, this low energy transition is due to the ortho-metallation which destabilises the d_{xy} orbital. Thus the energy gap between the d and π* (bpyMe-H) orbitals is smaller than the energy gap between the d and π* (bpy) orbitals. Figure 8.9 shows comparative molecular orbital diagrams for $[Pt(I)(bpy)(py)_2]^+$ and $[Pt(I)(bpyMe\text{-}H)(py)_2]^+$.

Charge transfers from d[Pt(I)] to both bpy and bpyMe-H occur in $[Pt(I)(bpyMe\text{-}H)(bpy)]^+$. However, the charge transfer energy differences of each transition between the $[Pt(bpyMe\text{-}H)(py)_2]^+$ and $[Pt(bpy)(py)_2]^+$ are not large (between 646 and 2934 cm^{-1}) and as a result all the absorption bands in the $[Pt(bpyMe\text{-}H)(bpy)]^+$ are broad. The electronic absorption spectra of $[Pt(bpyMe\text{-}H)(bpy)]^+$ and $[Pt(bpy)(Me_2N\text{-}py)_2]^+$ are shown in Figures 8.10 and 8.11.

The electronic absorption spectrum of $[Pt(bpy)(py)_2]^0$ shows both $[bpy]^-$ intraligand π → π* and π* → π* transitions and the M[Pt(I)] → L(py) charge-transfer transition in the region

Table 8.7 The main absorption bands of the $[PtLL']^+$ complexes in DMF. [λnm($\bar{\upsilon}$ cm^{-1})]

compounds	$\pi \rightarrow \pi^*$	MLCT[d $\rightarrow$ π(8)]	MLCT[d $\rightarrow$ py]	MLCT[d $\rightarrow$ π(7)]	d $\rightarrow$ d
$[Pt(bpy)(py)_2]^+$	284(35211)	348(28736)	400(25000)	492(20325)	1094(9141)
$[Pt(bpy)(Me_2N\text{-}py)_2]^+$	287(35017)	344(29070)	404(24752)	492(20325)	1134(8818)
$[Pt(bpyMe\text{-}H)(py)_2]^+$	298(33557)	356(28090)	416(24038)	575(17391)	976(10246)
$[Pt(bpyMe\text{-}H)(bpy)]^+$	290(34483)[a]	357(28011)		535(19802)[a]	1000(10000)[a]

[a]very broad

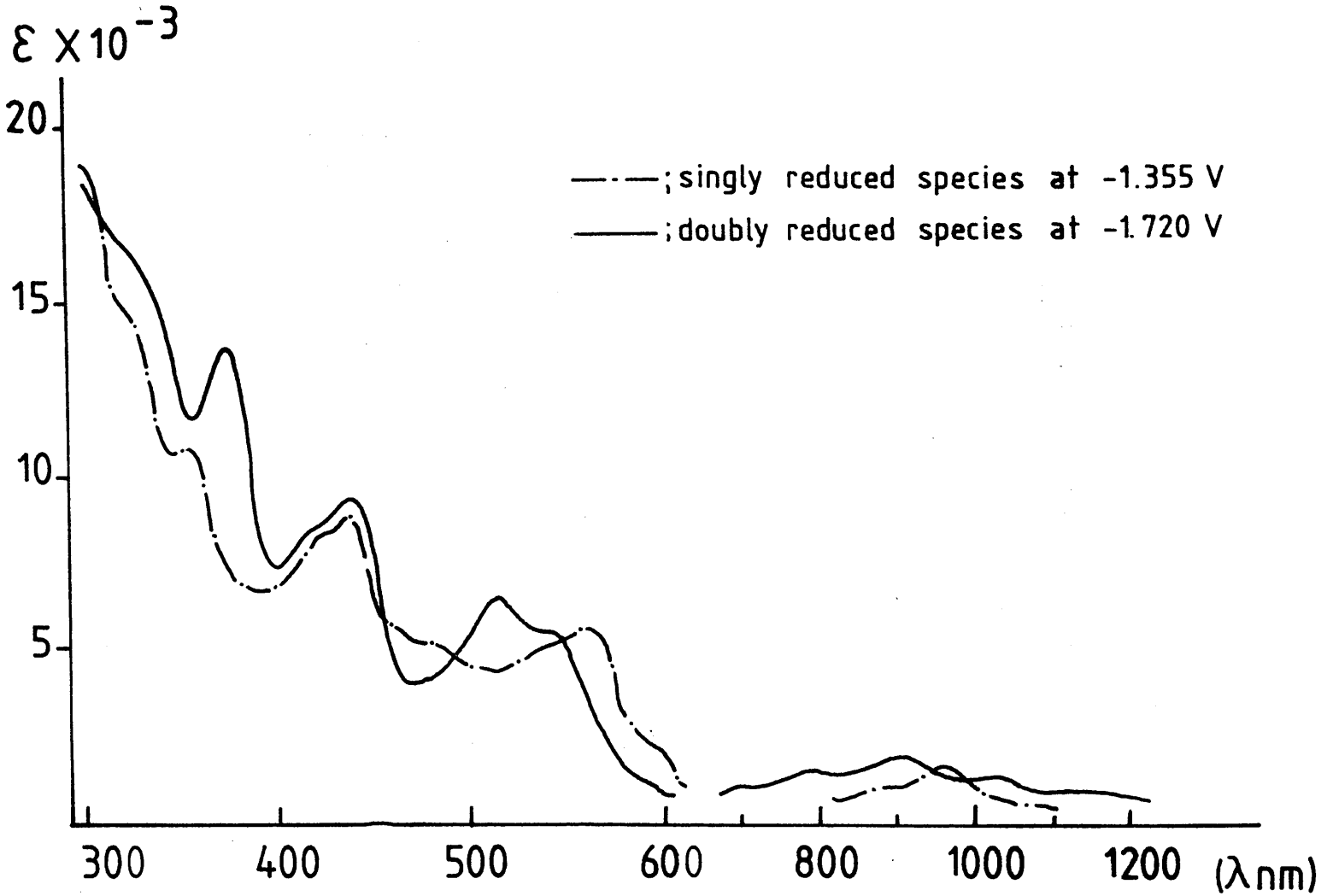

Figure 8.8 Absorption spectra of $[Pt(bpyMe-H)(py)_2]^{+/0}$ in DMF at room temperature.

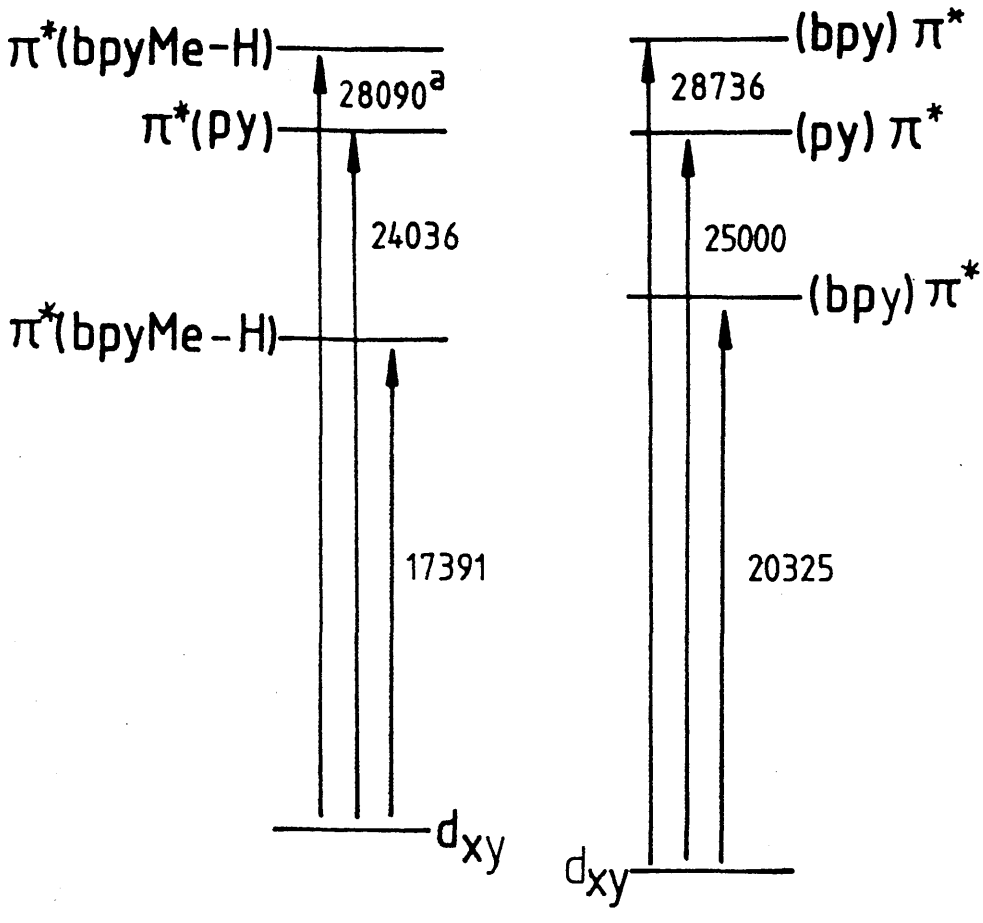

$[Pt(bpyMe-H)(py)_2]^+$ $[Pt(bpy)(py)_2]^+$

Figure 8,9 Comparative molecular orbital diagram for $[Pt(I)(bpy)(py)_2]^+$ and $[Pt(I)(bpyMe-H)(py)_2]^+$

[a] energies cm^{-1}

Figure 8.10. Absorption spectrum of $[Pt(bpy)(Me_2N\text{-}py)_2]^+$ in DMF at room temperature.

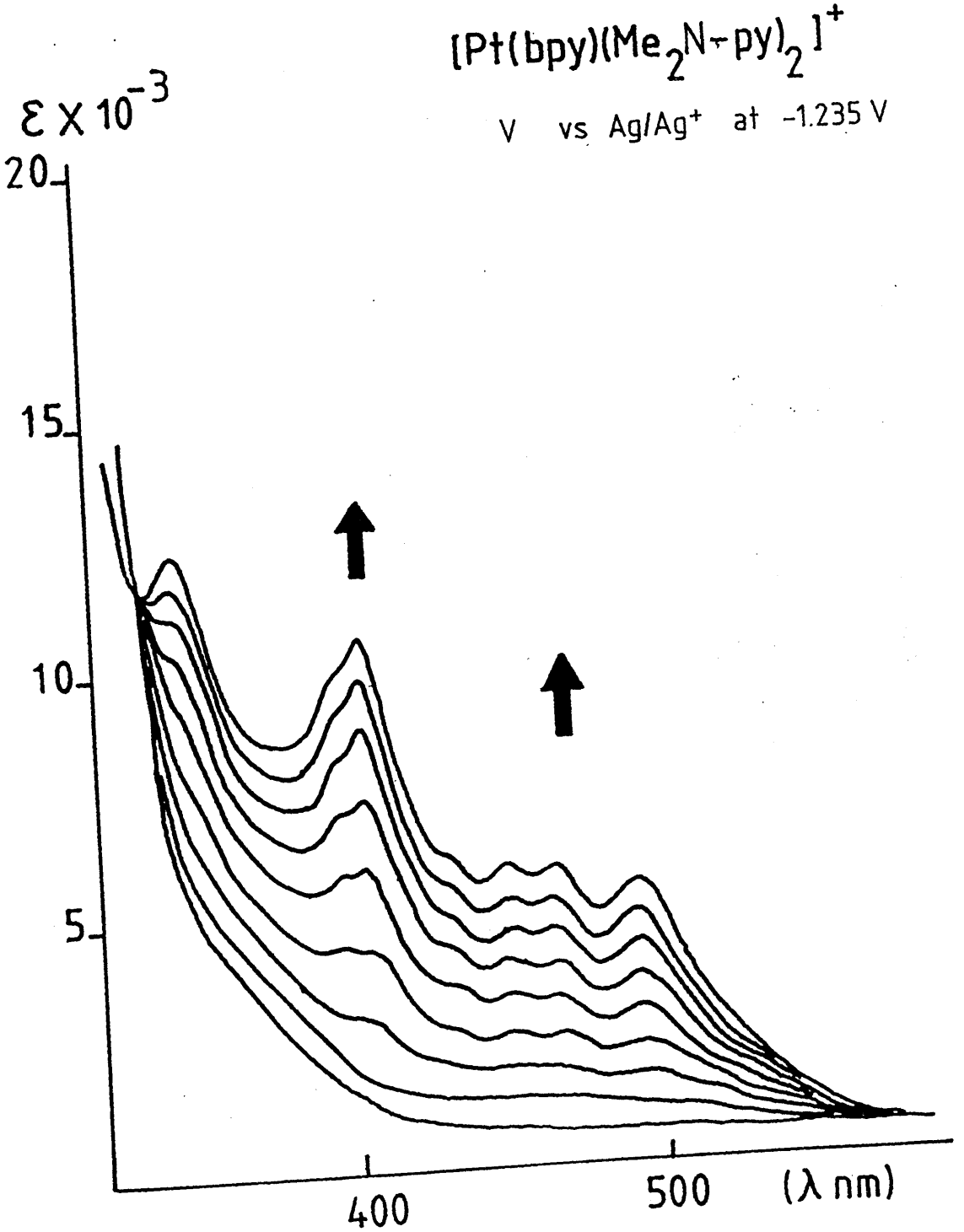

Figure 8.11. Absorption spectrum of $[Pt(bpy)(bpyMe\text{-}H)]^+$ in DMF at room temperature.

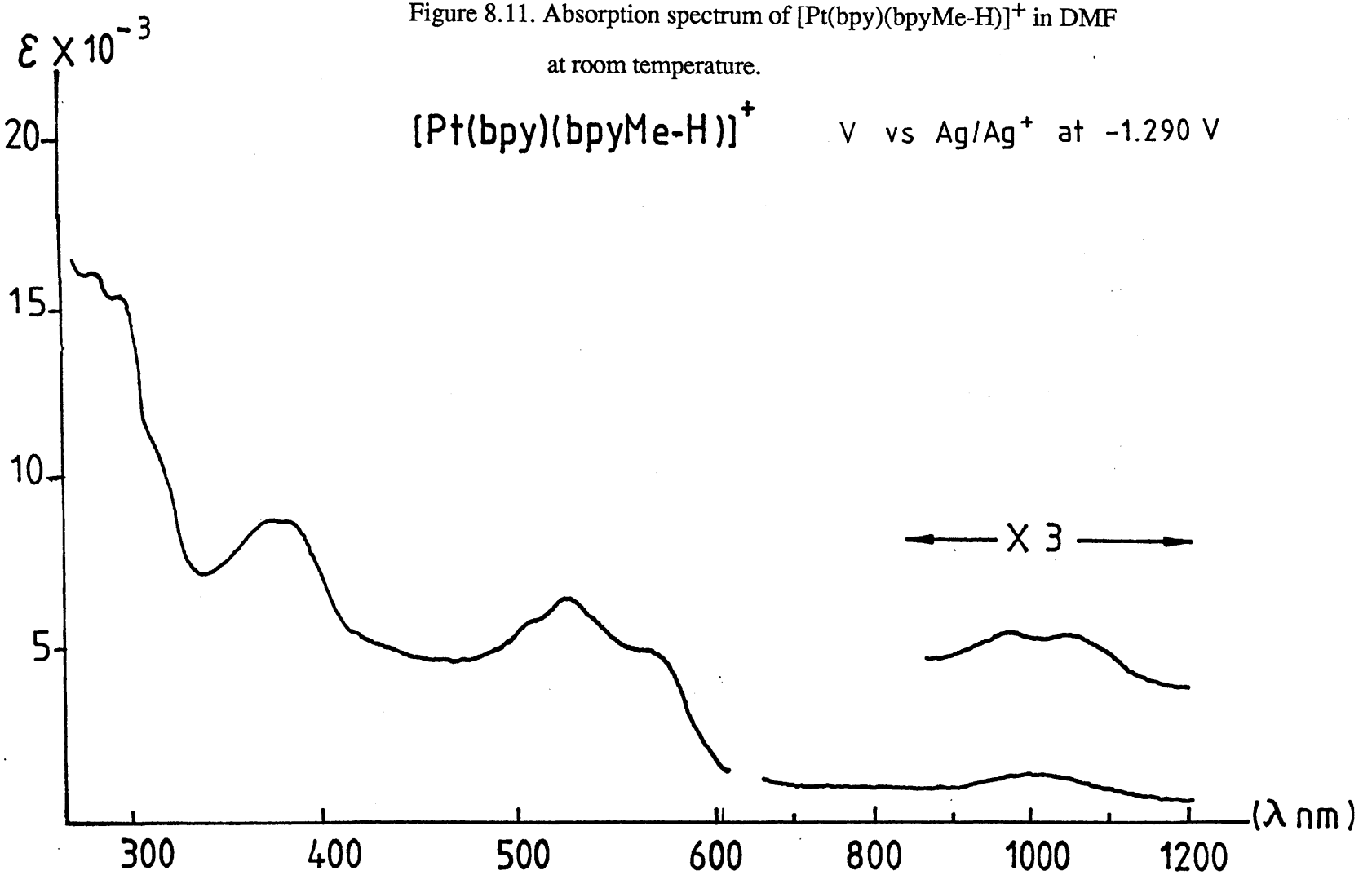

between 300 nm and 1300 nm (Figure 8.7). The high energy band in the near UV region (at 351 nm) is assigned to the intraligand $\pi(6) \rightarrow \pi(7)$ transition of the coordinated $[bpy]^-$ ligand. The band at 481 nm is assigned to the $\pi(7) \rightarrow \pi(10)$ transition of $[bpy]^-$, and the $\pi(7) \rightarrow \pi(8,9)$ transitions of coordinated $[bpy]^-$ appear as predicted at around 900 nm. The strong absorption band at 405 nm is assigned to the M[Pt(I)] $\rightarrow$ L(py) charge-transfer transition.

In the species formed by progressive reduction of $[Pt(bpy)_2]^{2+}$, the strongest absorption band at 313 nm is assigned to the $\pi(6) \rightarrow \pi(7)$ transition of coordinated neutral bpy ligands (Figure 8.12). The intensity loss on going from the parent to $[Pt(bpy)_2]^0$ in the region from 250 - 350 nm is due to the loss of a neutral bipyridine function.

The new band at around 360 nm is assigned to the $\pi(6) \rightarrow \pi(7)$ transition of coordinated $[bpy]^-$, and the extinction coefficient of this band is increased two-fold when the $[Pt(bpy)_2]^0$ species becomes $[Pt(bpy)_2]^-$.

The shoulder at 426 nm in $[Pt(bpy)_2]^0$ is assigned as MLCT (Pt(I) $\rightarrow \pi^*[\pi(7)]$) of the coordinated neutral bpy ligand. The band centred at around 500 nm is assigned to the $\pi(7) \rightarrow \pi(10)$ transition of coordinated $[bpy]^-$. The $[Pt(bpy)_2]^0$ species in this energy region has coexisting $[bpy]^0$ and $[bpy]^-$, and this transition moves to longer wavelength when the species becomes $[Pt(bpy)_2]^-$. The $\pi(7) \rightarrow \pi(8,9)$ transitions of $[bpy]^-$ appear in the near infrared region (at approximately 950 nm). The main bands of $[Pt(bpy)_2]^{0/-1}$ in DMF are shown in Table 8.8.

Figure 8.12 Absorption spectra of $[Pt(bpy)_2]^{2+/0/-}$ in DMF at room temperature.

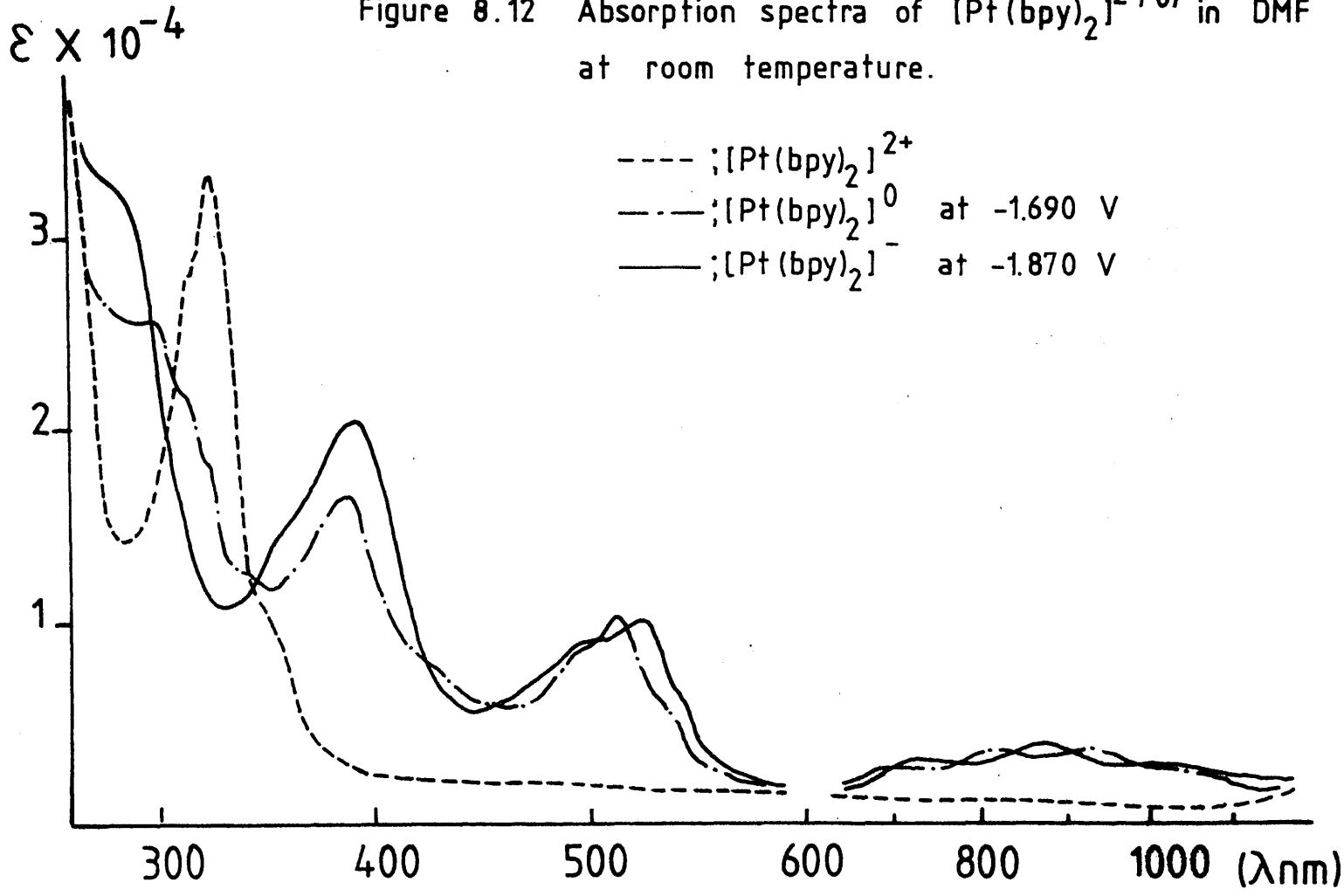

Table 8.8 Absorption bands of the doubly and triply reduced $[PtLL']^{2+}$ complexes in DMF. $[\lambda nm(\tilde{\upsilon}\, cm^{-1})]$

compounds	$\pi \rightarrow \pi^*$ $[\pi(6) \rightarrow \pi(7)]$ of L^-	MLCT(d → py)	MLCT[d → π*(7))]	$\pi^* \rightarrow \pi^*$ $[\pi(7) \rightarrow \pi(10)]$ of L^-	$\pi^* \rightarrow \pi^*$ $[\pi(7) \rightarrow \pi(8.9)]$ of L^-
$[Pt(bpy)(py)_2]^0$	351(28490)	405(24691)		481(20790)	900(11111)
$[Pt(bpy)_2]^0$	359(27855)		426(23474)sh	498(20080)	940(10638)
$[Pt(bpy)_2]^{-1}$	365(27397)			513(19493)	960(10417)
$[Pt(Me_2\text{-}bpy)_2]^0$	352(28409)		417(23980)sh	486(20576)	920(10870)
$[Pt(Me_2\text{-}bpy)_2]^{-1}$	357(28011)			502(19920)	940(10638)
$[Pt(bpyMe\text{-}H)(py)_2]^0$	372(26882)	417(23981)		514(19445)	990(10101)
$[Pt(bpyMe\text{-}H)(bpy)]^0$	377(26525)		429(23310)	516(19380)	1020(9804)
$[Pt(bpyMe\text{-}H)(bpy)]^-$	369(27100)			520(19231)	1000(10000)

In the $[Pt(bpyMe\text{-}H)(bpy)]^{-1}$ (Figure 8.13), the band at 369 nm which is assigned to the intraligand $\pi(6) \rightarrow \pi(7)$ transition of coordinated $[bpy]^-$ appears higher in energy than the corresponding absorption band of $[Pt(bpyMe\text{-}H)(bpy)]^0$, because, as discussed in chapter 8.2.1, the $\pi^*[\pi(7)]$ orbital of bpyMe-H is lower in energy than that of bpy.

8.3.2. Electronic absorption spectra of the reduced organoplatinum complexes.

The absorption spectra of the singly reduced organoplatinum complexes show characteristic intraligand $\pi \rightarrow \pi^*$ and $\pi^* \rightarrow \pi^*$ transitions of the reduced ligands, i.e. $[bpy]^-$ or $[bpym]^-$. The main absorptions are collected in Table 8.9.

The band centered at 495 nm of $[Pt(bpym)(Ph)_2]^-$ is assigned as a $\pi(7) \rightarrow \pi(10)$ transition of the coordinated $[bpym]^-$ ligand (Figure 8.14), and the band centered at 821 nm with a vibrational progression at approximately 1450 cm^{-1} is assigned to the $\pi(7) \rightarrow \pi(9)$ transition of $[bpym]^-$; (the $\pi(7) \rightarrow \pi(8)$ transition is forbidden because it is a u → u transition). The band at 379 nm is assigned to the HOMO → LUMO $[\pi(6) \rightarrow \pi(7)]$ transition of the coordinated $[bpym]^-$ ligand. Similar results are found for the singly reduced binuclear bpym complexes (Figures 8.15)

The absorption spectrum of singly reduced $[Pt(bpy)(Ph)_2]^-$ shows a shoulder at 309 nm, with isosbetic points at 301 nm and

Figure 8.13. Absorption spectrum of $[Pt(bpy)(bpyMe\text{-}H)]^{0/-}$ in DMF at room temperature.

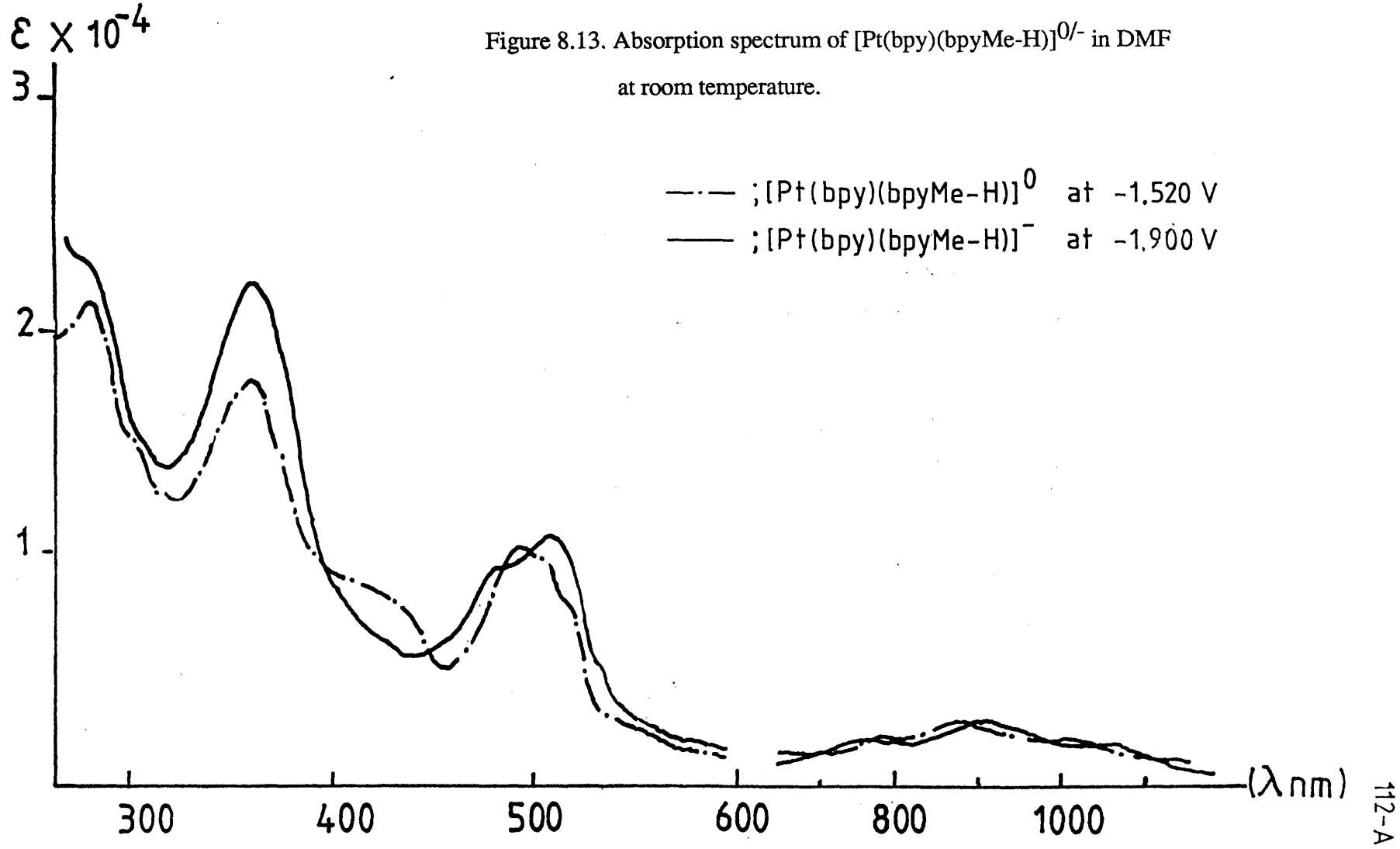

Table 8.9 Absorption bands of the singly reduced organoplatinum complexes in dichloromethane. [λnm ($\bar{\upsilon}$ cm^{-1})]

compounds	$\pi^* \rightarrow$	$\pi^*[\pi(6) \rightarrow \pi(7)]$	$\pi^* \rightarrow$	$\pi^*[\pi(7) \rightarrow \pi(10)]$	$\pi^* \rightarrow \pi^*[\pi(7) \rightarrow \pi(8,9)]$
$[Pt(bpy)(Ph)_2]^-$		367(27248)		520(19231)	965(10363)
$[Pt(Me_2\text{-}bpy)(Ph)_2]^-$		355(28169)		509(19640)	913(10953)
$[Pt(bpym)(Ph)_2]^-$		369(27100)		495(20202)	821(12180)
$\{[(adme)_2Pt]_2(\mu\text{-}bpym)\}^-$		373(26810)		501(19960)	892(11211)
$\{[(p\text{-}tol)_2Pt]_2(\mu\text{-}bpym)\}^-$		376(26596)		507(19724)	912(10965)

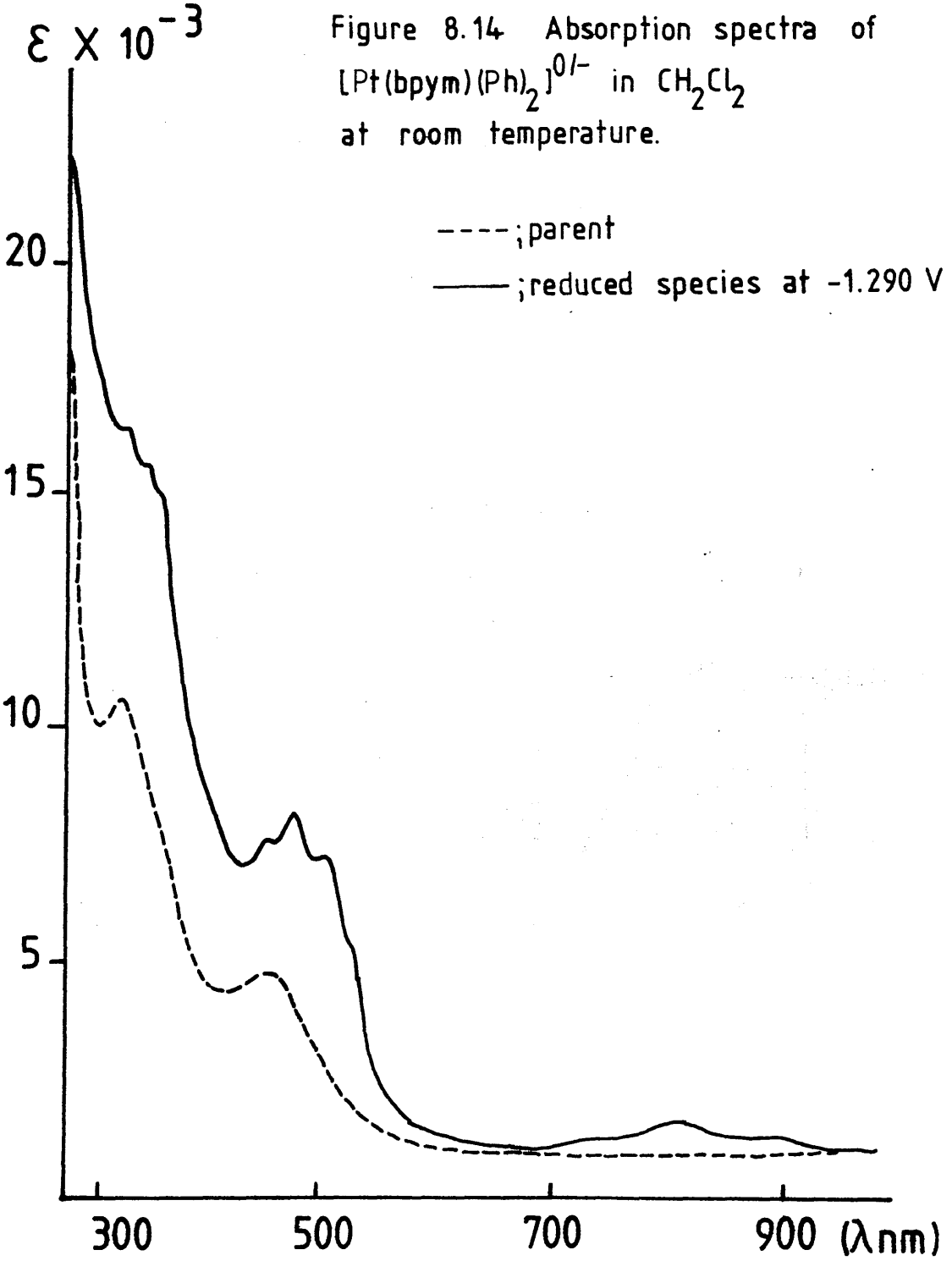

Figure 8.14 Absorption spectra of $[Pt(bpym)(Ph)_2]^{0/-}$ in CH_2Cl_2 at room temperature.

----; parent

——; reduced species at -1.290 V

Figure 8.15
Absorption spectra of $\{[(adme)_2Pt]_2(\mu\text{-bpym})\}^{0/-}$ in CH_2Cl_2 at room temperature

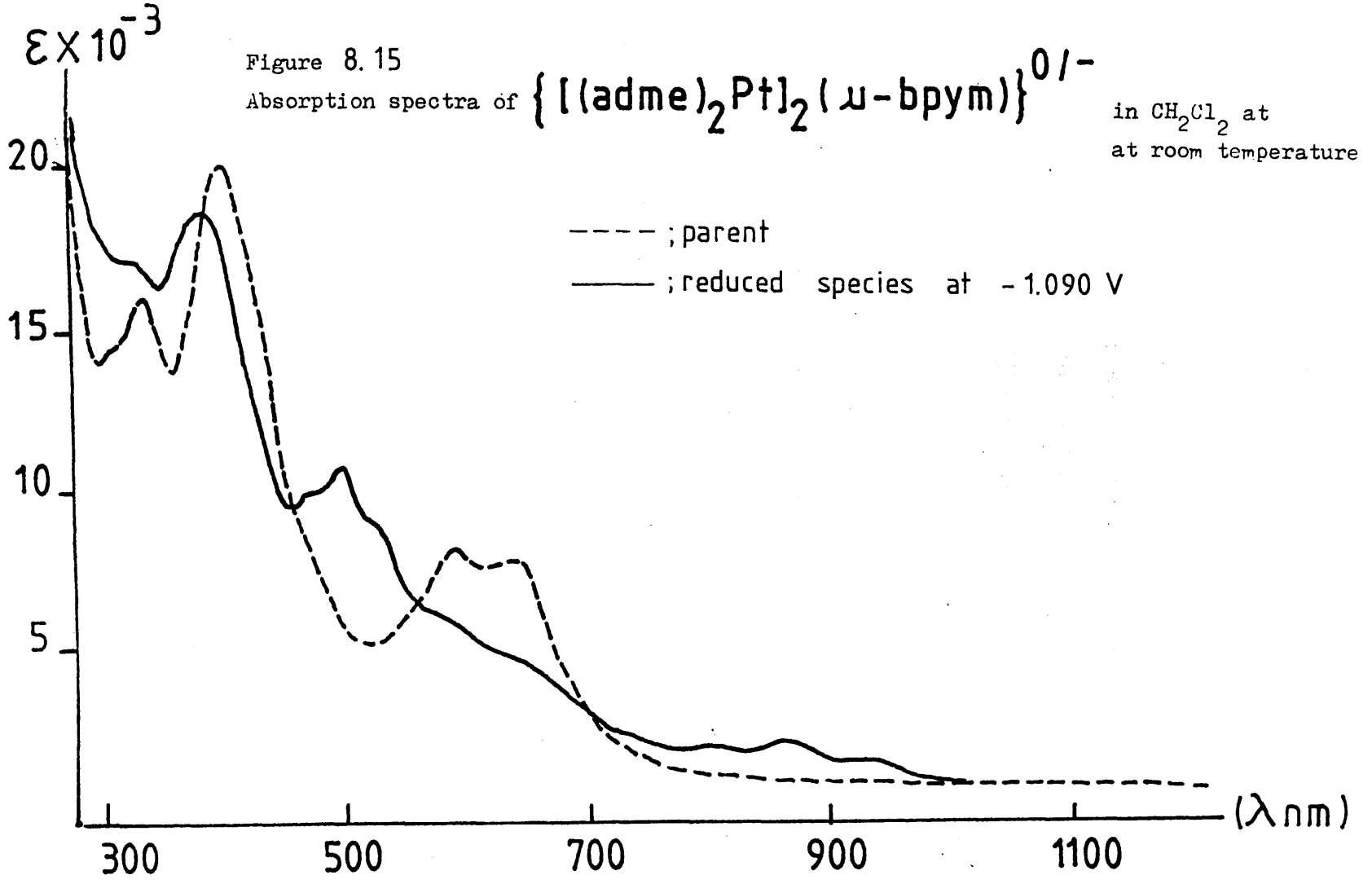

318 nm. This is tentatively assigned to the $L^-[\pi^*(7)] \rightarrow M[Pt(II)]$ charge-transfer transition (Figure 8.16). The d_{xy} orbital is destabilised in organoplatinum complexes and lies at higher energy than that of the $[PtLL']^{2+}$ complexes. When $[Pt(bpy)(Ph)_2]$ becomes reduced, the $\pi^*[\pi(7)]$ orbital of $[bpy]^-$ acts as the HOMO. Hence, we can expect to see the LMCT transition from the $\pi^*([bpy]^-)$ to d[Pt(II)] orbitals. This band is not found in the Pt(II)-$[bpym]^-$ complexes, presumably because of the lower energy of $\pi(7)$.

However, the $L^-(\pi^*$ of bpym$) \rightarrow M[d_{xy}$ of Pt(II)] charge-transfer transition requires higher energy than the $L^-(\pi^*$ of $[bpy]^-) \rightarrow M[d_{xy}$ of Pt(II)] charge-transfer transition because of the lower π^* $[\pi(7)]$ energy. Hence the order of increasing ease of the L^-(ligand π^*) $\rightarrow$ M[Pt(II)] charge-transfer transition is $[Pt(bpym)(Ph)_2]^- < [Pt(bpy)(Ph)_2]^- < [Pt(4,4'\text{-}Me_2\text{-}bpy)(Ph)_2]^-$, corresponding to the order of increasing difficulty of reduction of the free ligands. The electronic absorption spectrum of singly reduced $[Pt(4,4'\text{-}Me_2\text{-}bpy)(Ph)_2]$ is shown in Figure 8.17.

In summary, spectrochemical and electrochemical data agree in showing that the first reduction of species $[PtLL']^{2+}$ is metal based, while that of $LPtR_2$ (R = alkyl or aryl) is based on L. The charge-transfer spectra can be explained in a self-consistent manner, and show such novel features as Pt(I) $\rightarrow$ L and $L^- \rightarrow$ Pt(II) bands.

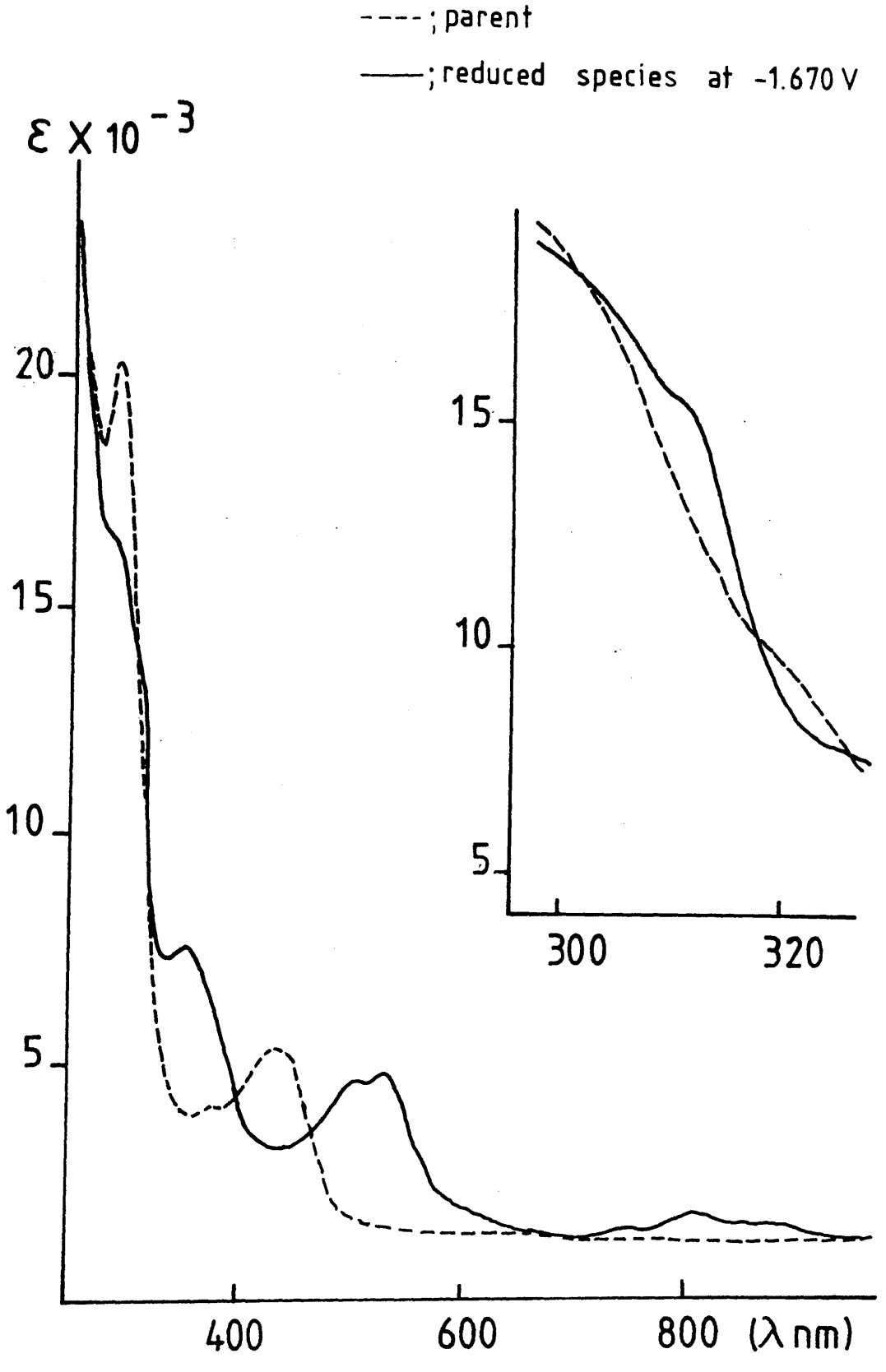

Figure 8.16 Absorption spectra of $[Pt(bpy)(Ph)_2]^{0/-}$ in CH_2Cl_2 at room temperature.

Figure 8.17

Absorption spectra of $[Pt(4,4'\text{-}Me_2\text{-}bpy)(Ph)_2]^{0/-}$ in CH_2Cl_2 at room temperature

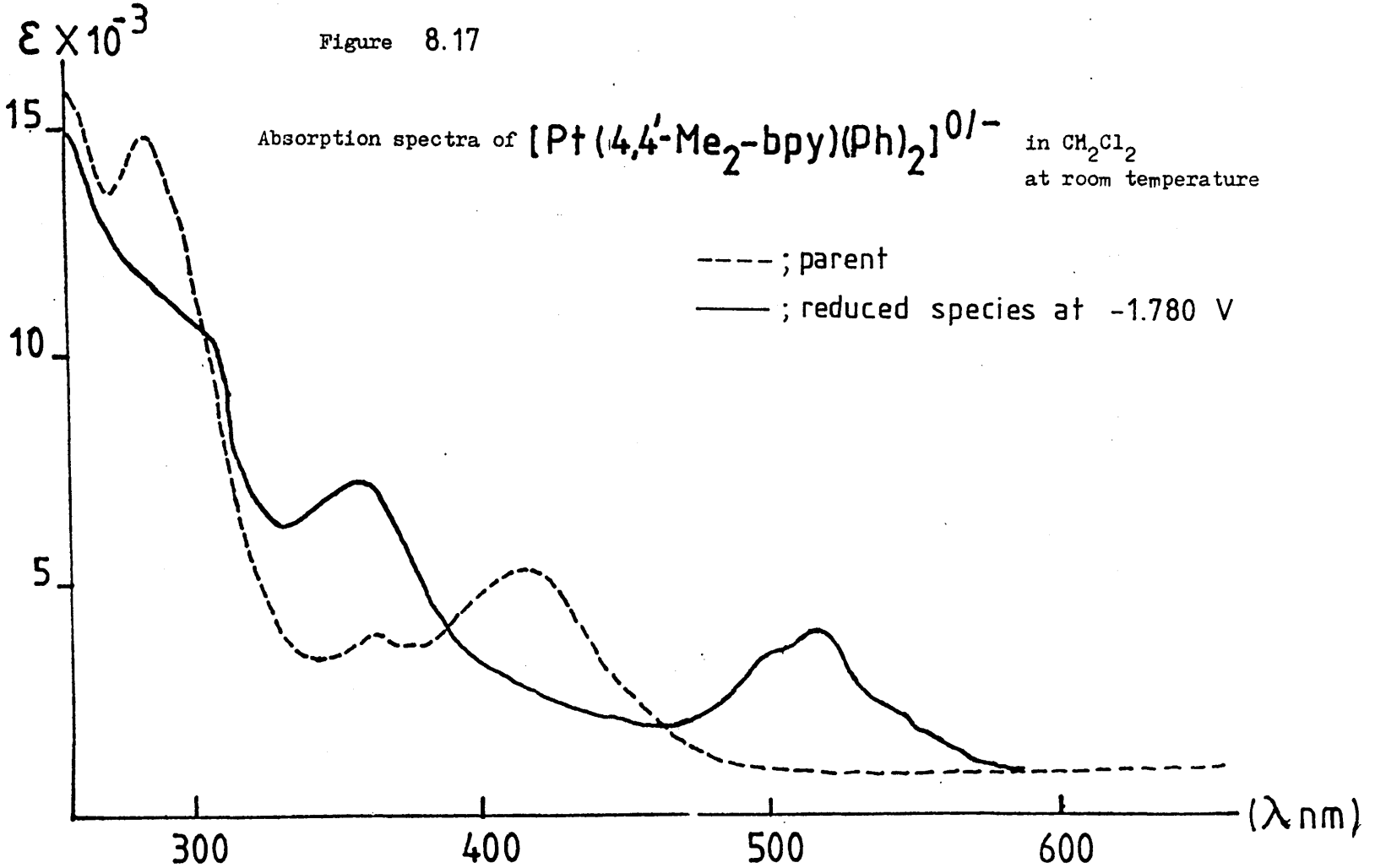

REFERENCES

REFERENCES

1. W.W.Brandt, F.P.Dwyer, and E.C.Gyarfas, *Chem. Rev.*, 1954, 54, 959.
2. F.Blau, *Ber. dt Chem. Ges.*, 1888, 21, 1077.
3. F.Blau, *Monatsh. Chem.*, 1898, 19, 647.
4. D.D.Bly and M.G.Mellon, *Anal. Chem.*, 1963, 35, 1386.
5. A.Werner, *Z. Anorg. Chem.*, 1893, 3, 267.
6. A.Werner, *Ber. dt Chem. Ges.*, 1912, 45, 433.
7. G.H.Walden,Jr., L.P.Hammett, and R.P.Chapman, *J. Am. Chem. Soc.*, 1931, 53, 3908.
8. E.Bielli, P.M.Gidney, R.D.Gillard, and B.T.Heaton, *J. Chem. Soc. Dalton Trans.*, 1974, 2133.
9. G.T.Morgan and F.H.Burstall, *J. Chem. Soc.*, 1934, 965.
10. A.Hazell and A.Mukhopadhyay, *Acta Crystallogr., Sect. B*, 1980, B36, 1647.
11. L.Chassot, E.Müller, and A.von Zelewsky. *Inorg. Chem.*, 1984, 23, 4249.
12. J.Bjerrum, *Chem. Rev.*, 1950, 46, 381.
13. L.A.Summers, 'The Bipyridinium Herbicides,' Academic Press, New York, 1980.
14. N.Sutin and C.Creutz, *Pure App. Chem.*, 1980, 20, 1195.
15. R.J.Fielden, R.F.Homer, and R.L.Jones, *British patent*, 1957, 785,732 [CA., 1958, 52, 6707]
16. L.A.Summers, *Nature (London)*, 1967, 1410.
17. R.F.Homer and T.E.Tomlinson. *J. Chem. Soc.*, 1960, 2498.
18. G.T.Morgan and F.H.Burstall, *J. Chem. Soc.*, 1932, 20.
19. G.T.Morgan and F.H.Burstall, *J. Chem. Soc.*, 1937, 1649.
20. G.T.Morgan and F.H.Burstall, 'Inorganic Chemistry,' Heffers, Cambridge, 1936.

21. J.D.Scott and R.J.Puddephatt, *Inorg. Chim. Acta.*, 1984, 89, L27.

22. M.Bochmann, G.Wilkinson, and G.B.Young; *J. Chem. Soc. Dalton Trans.*, 1980, 1879.

23. V.F.Sutcliffe and G.B.Young, *Polyhedron*, 1984, 3, 87.

24. J.D.Scott and R.J.Puddephatt, *Organometallics*, 1986, 5, 1538.

25. N.Chaudhury and R.J.Puddephatt, *J. Organomet. Chem.*, 1975, 84, 105.

26. W.Kaim and S.Kohlmann, *Inorg. Chem.*, 1986, 25, 3306.

27. W.Kaim and S.Kohlmann, *Inorg. Chem.*, 1987, 26, 68.

28. H.tom Dieck and I.W.Renk, *Chem. Ber.*, 1971, 104, 110.

29. C.Reichardt, 'Solvent Effects in Organic Chemistry,' Verlag Chemie, Weinheim, West Germany and New York, 1979.

30 R.W.Taft and M.J.Kamlet, *Inorg. Chem.*, 1983, 22, 250.

31. D.M.Manuta and A.J.Lees, *Inorg. Chem.*, 1983, 22, 3825.

32. M.J.Blandamer, J.Burgess, and T.Digman, *Transition Met. Chem. (Weinheim, Ger)*, 1985, 10, 275.

33. S.Aoyagui and T.Saji, *J. Electroanal. Chem. Interfacial Electrochem.*, 1975, 58, 401.

34. T.Saji and S.Aoyagui, *J. Electroanal. Chem. Interfacial Electrochem.*, 1975, 63, 31.

35. A.G.Motten, K.W.Hanck, and M.K.DeArmond, *Chem. Phys. Lett.*, 1981, 79, 541.

36. D.E.Morris, K.W.Hanck, and M.K.DeArmond, *J. Am. Chem. Soc.*, 1983, 105, 3032.

37. N.Tanaka, T.Ogata, and S.Niizuma, *Bull. Chem. Soc. Jpn.*, 1973, 46, 3299.

38. Y.Ohsawa, M.K.DeArmond, K.W.Hanck, and C.G.Moreland, *J. Am. Chem. Soc.*, 1985, 107, 5383.

39. S.M.Angel, M.K.DeArmond, R.J.Donohoe, and D.W.Wertz, *J. Phys. Chem.*, 1985, 89, 282.

40. P.G.Bradley, N.Kress, B.A.Hornberger, R.F.Dallinger, and W.H.Woodruff, *J. Am. Chem. Soc.*,1981, 103, 7441.

41. J.M.Winfield, *J.Fluorine Chem.*, 1984, 25, 91.

42. D.D.Bly and M.G.Mellon, *J. Org. Chem.*, 1960, 25, 2945.

43. H.Gilman and S.M.Spatz, *J. Org. Chem.*,1951, 16, 1485.

44. T.Kauffmann, J.Kö̈nig, and A.Woltermann, *Chem. Ber.*, 1976, 109, 3864.

45. F.H.Burstall, *J. Chem. Soc.*, 1938, 1662.

46. E.C.Constable, M.D.Ward, and S.Corr, *Inorg. Chim. Acta*, 1988, 141, 201.

47. D.W.Adamson, *J. Chem. Soc.*, 1949, S144.

48. R.R.Ison, F.M.Franks, and K.S.Soh, *J. Pharm. Pharmacol.*, 1973, 25, 887.

49. F.Krö̈hnke, *Synthesis*, 1976, 1.

50. F.H.Westheimer and O.T.Benfey, *J. Am. Chem. Soc.*, 1956, 78, 5309.

51. B.E.Halcrow and W.O.Kermack, *J. Chem. Soc.*, 1946, 155.

52. J.-M.Lehn, J.-P.Sauvage, J.Simon, R.Ziessel, C.Piccinni-Leopardi, G.Germain, J.-P.Declercq, and M.V.Meerssche; *Nouv. J. Chim.*, 1983, 7, 413.

53. P.E.Fanta, *Synthesis*, 1974, 9.

54. I.C.Calder and W.H.F.Sasse, *Aust. J. Chem.*, 1968, 21, 2951.

55. F.L.Wimmer and S Wimmer, *Transition Met. Chem.*, 1985, 10, 238.

56. C.Eaborn, K.Kunden, and A.Pidcock, *J. Chem. Soc., Dalton Trans.*, 1981, 933.

57. R.A.Palmer and T.S.Piper, *Inorg. Chem.*, 1966, 5, 864.

58. A.London, *J. Chem. Phys.*, 1945, 13, 396.

59. E.T.Stewart, *J. Chem. Soc.*, 1958, 4016.

60. J.P.Maier and D.W.Turner, *Faraday Discuss. Chem. Soc.*, 1972, *54*, 149.

61. Y. Gondo, *J. Chem. Phys.*, 1964, 41, 3928.

62. D.W.Turner, 'Molecular Photoelectron Spectroscopy,' Wiley (London), 1970.

63. C. Mahon and W.L.Reynold, *Inorg. Chem.*, 1967, 6, 1927.

64. E. König and S.Kremer, *Chem. Phys. Lett.*, 1970, 5, 87.

65. O.R.Brown and R.J.Butterfield, *Electrochim. Acta*, 1982, 27, 321.

66. R.F.Homer, G.C.Mees, and T.E.Tomlinson, *J. Sci. Food. Agric.*, 1960, 11, 309.

67. P.D.Sullivan and M.L.Williams, *J. Am. Chem. Soc.*, 1976, 98, 1711.

68. J.E.Derry and T.A.Hamor, *J. Chem. Soc. Chem. Commun.*, 1970, 1284.

69. L.Roullier and E.Laviron, *Electrochim. Acta*, 1978, 23, 773.

70. E.Amouyal, B.Zidler, P.Keller, and A.Moradpour, *Chem. Phys. Lett.*,1980, 74, 314.

71. C.L.Bird and A.T.Kuhn, *Chem. Soc. Rev.*,1981, 10, 49.

72. W.R.Boon, *Chem. Ind.(London)*, 1965, 782.

73. S.König, J.Gross, and W.Schenik, *Liebigs. Ann. Chem.*, 1973, 324.

74. M.Ito and T.Kunawa, *J. Electroanal. Chem. Interfacial Electrochem.*, 1971, 32, 415.

75. S.Ernst and W.Kaim, *J. Am. Chem. Soc.*, 1986, 108, 3578.

76. S.Hünig and J.Groβ, *Tetrahedron Lett.*, 1968, 2599.

77. G.J.Hoijtink, J.van Schooten, E. de Boer, and W.Y.Aalbersberg, *Recl. Trav. Chim. Pays-Bas*, 1954, 73, 355.

78. L.A.Summers, *Adv. Heterocycl. Chem.*, 1978, 22, 1.

79. L.E.Orgel, *J. Chem. Soc.*, 1961, 3638.

80. B.C.Noble, Ph.D thesis, University of Glasgow, 1987.

81. V.Kalyanaraman, C.N.R.Rao, and M.V.George, *J. Chem. Soc.(B)*, 1971, 2406.

82. M.Simic and E.Ebert, *Int. J. Radiat. Phys. Chem.*, 1971, 3, 259.

83. P.S.Braterman and J.-I. Song, *1st Euchem. Inorg. Chem. Seminar*, Dourdan, April, 1988.

84. C.Creutz, *Comments Inorg. Chem.*, 1982, 1, 293.

85. H.Erhard and W.Jaenicke, *J. Electroanal. Chem. interfacial Electrochem.*, 1977, 81, 79.

86. Q.G.Mulazznani, S.Emmi, P.G.Fuochi, M.Venturi, M.Z.Hoffman, and M.G, Simic, *J. Phys. Chem.*, 1979, 83, 1582.

87. E.Müller and K.A.Bruhn, *Chem. Ber.*, 1953, 86. 1122.

88. E.M.Kosower and J.L.Cotter, *J. Am. Chem. Soc.*, 1964, 86, 5524.

89. F.Lelj, N.Russo, and G.Chidichimo, *Chem. Phys. Lett.*, 1980, 69, 530.

90. H.L.Schläfer and G.Gliemann, 'Basic Principle of Ligand Field Theory,' Wiley(London), 1969.

91. S.F.Mason, *Inorg. Chim. Acta. Rev.*, 1968, 2, 89.

92. G.E.Coates and S.I.E.Green, *J. Chem. Soc.*, 1962, 3340.

93. I.M.Brown and S.I.Weissman, *J. Am. Chem. Soc.*, 1963, 85, 2528.

94. G.Wilke and G.Herrman, *Angew. Chem., Int. Ed. Engl.*, 1966, 5, 581

95. M.H.Chisholm, J.C.Huffman, I.P.Rothwell, P.G.Bradley, N.Kress and W.H.Woodruff, *J. Am. Chem. Soc.*, 1981, 103, 4945.

96. N.S.Gill, R.S.Nyholm and P.Pauling, *Nature*, 1958, 182,168.

97. W.M.Reiff, B.Dockum, M.A.Weber, and R.B.Frankel, *Inorg. Chem.*, 1975, 14, 800.

98. R.D.Gillard, R.J.Lancashire, and P.A.Williams, *Transition Met. Chem.*, 1979, 4, 2439.

99. R.R.Ruminski and J.D.Petersen, *Inorg. Chim. Acta*, 1985, 97, 129.

100. C.R.Johnson and R.E.Shepherd, *Inorg. Chem.*, 1983, 22, 2439.

101. A.B.P.Lever and R.J.Crutchley, *Inorg. Chem.*, 1982, 21, 2276.

102. R.J.Butcher, C.J.O'Connor, and E.Sinn, *Inorg. Chem.*, 1979, 18, 492.

103. D.B.Fox, J.R.Hall, and R.A.Plowman, *Aust. J. Chem.*, 1962, 15, 235.

104. T.Ito, N.Tanaka, I.Hanazaki, and S.Nakakura, *Bull. Chem. Soc. Jpn.*, 1969, 42, 702.

105 K.Madeja and E.König, *J. Inorg. Nucl. Chem.*, 1963, 25, 377.

106. P.Krumholz, *Inorg. Chem.*, 1965, 4, 612.

107. P.S.Braterman, A.Harriman, G.A.Heath, and L.J.Yellowlees, *J. Chem. Soc. Dalton Trans.*, 1983, 1801.

108. A.Rusina, A.A.Vlček, and S.Zalis, *Z. Chem.*, 1979, 19, 27.

109. B.Tabner and J.R.Yandle, *J. Chem. Soc. (A)*, 1968, 381.

110. C.L.Honeyburn, *Mol. Phys.*, 1971, 21, 1057.

111. R.Held, F.Dietz, and P.Thomas, *Z. Chem.*, 1972, 12, 304.

112. C.Gooijer, N.H.Velthorst, and C.MacLean, *Mol. Phys.*, 1972, 24, 1361.

113. W.Kaim, J. Am. Chem. Soc., 1982, 104, 3833.

114. S.Ernst, Ph.D thesis, Goethe-Universität, Frankfrut, 1987.

115. A.J.McCaffery, S.F.Mason, and B.J.Norman, *J. Chem. Soc. (A)*, 1969, 1428.

116. W.Kaim, *J. Organomet. Chem.*, 1981, 222, C17.

117. K.Nakamura, *Bull. Chem. Soc. Jpn.*, 1972, 45, 1943.

118. D.Morris, K.W.Hanck, and M.K.DeArmond, J. *Electroanal. Chem. Interfacial Electrochem.*, 1983, 105, 3032.

119. D.E.Morris, Y.Ohsawa, D.P.Segers, M.K.DeArmond, and K.W.Hanck, *Inorg. Chem.*, 1984, 23, 3010.

120. D.P.Rellema, G.Allen, T.J.Meyer, and D.Conrad, *Inorg. Chem.*, 1983, 22, 1617.

121. D.A.Buckingham and A.M.Sargeson, 'Chelating Agents and Metal Chelates,' F.P.Dwyer and D.P.Mellor (Eds), Academic Press, New York, 1960.

122. V.Balzani, F.Boletta, M.T.Gandolfi, and M.Maestri, *Top. Curr. Chem.*, 1978, 75, 1.

123. L.J.Yellowlees, Ph.D thesis, University of Edinburgh, 1982.

124. W.L.Wallace and A.J.Bard, *J. Phys. Chem.*, 1979, 83, 1350.

125. K.K.Cloninger and R.W.Callahan, *Inorg. Chem.*, 1981, 20,1611.

126. R.J.Crutchley and A.B.P.Lever, *J. Am. Chem. Soc.*, 1980, 102, 7128.

127. D.M.Klaasen and G.A.Crosby, *J. Chem. Phys.*, 1968, 48, 1853.

128. G.M.Bryant and J.E.Ferguson, *Aust. J. Chem.*, 1971, 24, 275.

129. C.K.Jørgensen, 'Absorption Spectra and Chemical Bonding in Complexes,' Pergamon Press, Oxford, 1962.

130. E.M.Kober and T.J.Meyer, *Inorg. Chem.*, 1985, 24, 106.

131. B.P.Sullivan, D.J.Salmon, T.J.Meyer, and J.Peedin, *Inorg. Chem.*, 1979, 18, 3369.

132. W.R.McWhinnie and J.D.Miller, *Adv. Inorg. Chem. Radiochem.*, 1969, 12, 135.

133. C.Creutz and N.Sutin, *J. Am. Chem. Soc.*, 1976, 98, 6384.

134. B.Bosnich, *Inorg. Chem.*, 1968, 7, 2397.

135. G.A.Heath, L.J.Yellowlees, and P.S.Braterman, *Chem. Phys. Lett.*, 1982, 92, 646.

136. C.Overton and J.A.Connor, *Polyhedron*, 1982, 1, 53.

137. M.Hunziker and A.Ludi, *J. Am. Chem. Soc.*, 1977, 99, 7370.

138. R.R.Ruminski and J.D.Petersen, *Inorg. Chem.* 1982, 21, 3706.

139. W.Kaim, *Inorg. Chem.*, 1984, 23, 3365.

140. D.E.Richardson and H.Taube, *J. Am. Chem. Soc.*, 1983, 105, 40

141 .H.tom Dieck and E.Kuhl, *Z. Naturforsch.(B)*, 1982, 37(B), 324.

142. R.W.Balk, D.J.Stufkens, and A.Oskam, *Inorg. Chim. Acta*, 1978, 28, 133.

143. A.P.Walker, Ph.D thesis, University of Glasgow,1969.

144. P.S.Braterman, D.W.Milne, and A.P.Walker, *J. Chem. Res.*, 1977, S277, M3301.

145. A.C.Skapski, V.F.Sutcliffe, and G.B.Young, *J. Chem. Soc. Chem. Commun.*, 1985, 609.

146. F.A.Cotton and G.Wilkinson, 'Advanced Inorganic Chemistry,' Wiley (London), 1971.

147. P.M.Gidney, R.D.Gillard, and B.T.Heaton, *J. Chem. Soc. Dalton Trans.*, 1973, 132.

148. D.L.Webb and L.A.Rossiello, *Inorg. Chem.*, 1970, 10, 2213.

149. R.H.Petty and L.J.Wilson, *J. Chem. Soc. Chem. Commun.*, 1978, 483.

150. T.Yamamoto, A.Yamamoto, and S.Ikeda, *J. Am. Chem. Soc.*, 1971, 93, 3350.

151. J.Burgess, *Spectrochim. Acta, Part A*, 1970, 26, 1369.

152. J.Burgess, *J. Organomet. Chem.*, 1969, 19, 218.